1997

Determination of particulate and unburned hydrocarbon emissions from diesel engines fueled with biodiesel

David Yu-Zhang Chang
Iowa State University

INFORMATION TO USERS

This manuscript has been reproduced from the microfilm master. UMI films the text directly from the original or copy submitted. Thus, some thesis and dissertation copies are in typewriter face, while others may be from any type of computer printer.

The quality of this reproduction is dependent upon the quality of the copy submitted. Broken or indistinct print, colored or poor quality illustrations and photographs, print bleedthrough, substandard margins, and improper alignment can adversely affect reproduction.

In the unlikely event that the author did not send UMI a complete manuscript and there are missing pages, these will be noted. Also, if unauthorized copyright material had to be removed, a note will indicate the deletion.

Oversize materials (e.g., maps, drawings, charts) are reproduced by sectioning the original, beginning at the upper left-hand corner and continuing from left to right in equal sections with small overlaps. Each original is also photographed in one exposure and is included in reduced form at the back of the book.

Photographs included in the original manuscript have been reproduced xerographically in this copy. Higher quality 6" x 9" black and white photographic prints are available for any photographs or illustrations appearing in this copy for an additional charge. Contact UMI directly to order.

UMI

A Bell & Howell Information Company
300 North Zeeb Road, Ann Arbor MI 48106-1346 USA
313/761-4700 800/521-0600

Determination of particulate and unburned hydrocarbon emissions from diesel engines fueled with biodiesel

by

David Yu-Zhang Chang

A dissertation submitted to the graduate faculty

in partial fulfillment of the requirement for the degree of

DOCTOR OF PHILOSOPHY

Major: Mechanical Engineering

Major Professor: Jon H. Van Gerpen

Iowa State University

Ames, Iowa

1997

Graduate College

Iowa State University

This is certify that the Doctoral dissertation of

David Yu-Zhang Chang

has met the dissertation requirements of Iowa State University

Signature was redacted for privacy.

Major Professor

Signature was redacted for privacy.

For the Major Program

Signature was redacted for privacy.

For the Graduate College

TABLE OF CONTENTS

LIST OF FIGURES

LIST OF TABLES

ABSTRACT

Methyl esters of soybean oil, known as biodiesel, are receiving increasing attention as an alternative fuel for diesel engines. Biodiesel is a nontoxic, biodegradable, and renewable fuel with the potential to reduce engine exhaust emissions. However, previous results have shown that biodiesel produces a higher fraction of soluble organic material (SOF) in the exhaust particulate matter than petroleum-based diesel fuel although its total particulate emissions were lowered. Also, because biodiesel has a high boiling point and low volatility compared with diesel fuel, its unburned hydrocarbon vapor could be lost by deposition in the hydrocarbon sampling line. This loss could be the source of reported reductions in hydrocarbon emissions from biodiesel-fueled engines. No information about whether the typical measurement temperature for unburned hydrocarbons is suitable for biodiesel hydrocarbon measurement is available. In this project, the formation of SOF in diesel exhaust particulates and the deposition of hydrocarbons in heated sampling lines were studied experimentally and theoretically.

The experimental results showed that biodiesel produced a higher SOF fraction in its total particulates than diesel fuel under virtually all engine operating conditions. The SOF fraction decreased with increasing filter temperature at constant dilution ratio and with increasing dilution ratio at constant filter temperature. Biodiesel injection tests, where a small quantity of neat biodiesel was injected into the exhaust gas showed that most of the unburned biodiesel showed up in the soluble organic fraction of the collected particulates. The response of the heated flame ionization detector did not match the concentration change of unburned biodiesel in the exhaust gas. Based on the predicted results from condensation and multicomponent adsorption models, adsorption of vapor phase hydrocarbons on the carbon particle surface is the primary source of the SOF in the total particulate matter. The condensation process, by itself, can not explain the formation of SOF during the dilution process. Adsorption of hydrocarbons is also shown to take place during transport of the hydrocarbon sample, even at high temperature. At the standard hydrocarbon measurement temperature, adsorption onto the sampling line walls could affect the concentration of

unburned hydrocarbons and biodiesel in the exhaust gas sample. However, when the hydrocarbon sampling line temperature was heated to 250 °C, adsorption did not show significant effect on reducing the hydrocarbon concentration in the exhaust sample.

1. INTRODUCTION

Based on their superiority in fuel economy and low emissions of unburned hydrocarbons (HC) and carbon monoxide (CO), diesel engines have been a popular choice for heavy- and medium-duty power applications. However, diesel engines usually exhaust much larger amounts of particulate matter (PM) than spark ignition engines. Approximately 90% of the diesel particulates are in the size range from 0.0075 to 1.0 μm [1] and have a significant potential health impact if the particles are inhaled and trapped in the bronchial passages and the lung alveoli. The carcinogenic effect related to diesel exhaust particles is now considered to have two components, one is related to the inorganic solid carbon or soot (SOL), and another to the soluble organic fraction (SOF) which is formed from the adsorbed and condensed unburned hydrocarbons on the soot surface when the diesel exhaust gas is emitted into the atmosphere and diluted by the air. Both of them are the result of incomplete combustion of the fuel or lubricating oil. Some recent laboratory research on rats has shown that the solid carbon, or soot, portion of diesel particulates is probably essential for initiation of tumor formation [2, 3]. The associated soluble organic fraction, particularly the polynuclear aromatic hydrocarbons (PAH) and Nitro-PAH, also makes a contribution to the overall carcinogenic effect [4].

Over the past 30 years, especially during the 1980s and 1990s, an explosive growth in internal combustion engine research and development has occurred to address the issue of air pollution. The Environmental Protection Agency (EPA) has issued increasingly stringent diesel engine emission standards to minimize environmental pollution from diesel engines. Figure 1.1 shows the changes of the EPA heavy-duty diesel engine emission standards for oxides of nitrogen (NO_x) and particulate from 1988 to 1999 [5]. The emission standards of CO and HC in this time period are unchanged at 15.5 and 1.3 g/bhp-hr, respectively. Most diesel engines can meet the standards for CO and HC without difficulty. The approaches to diesel engine emission reduction can be classified into four categories: 1) internal control of engine emissions by improving combustion chamber design and piston ring design, and by optimizing air flow in engine cylinder; 2) external control of the exhaust emissions with

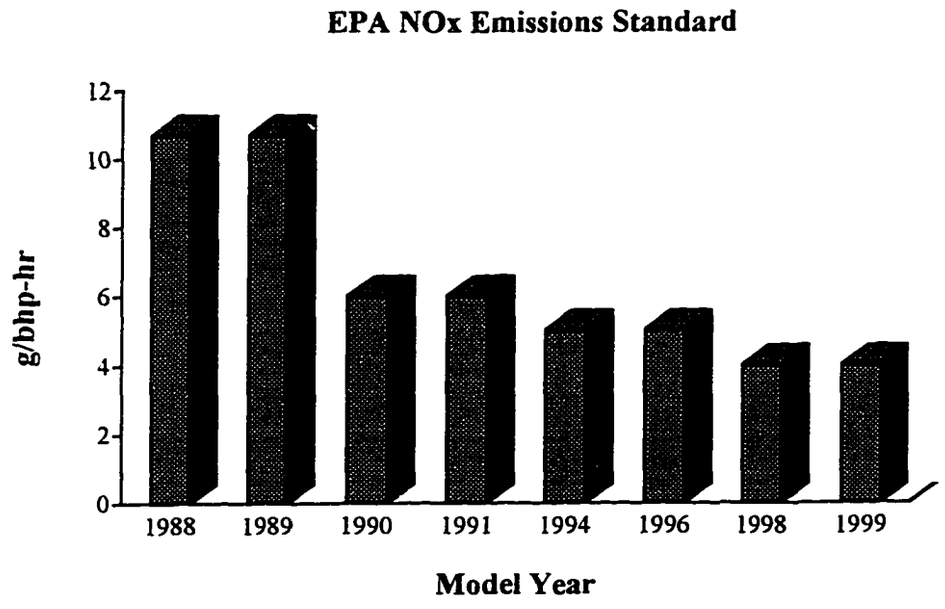

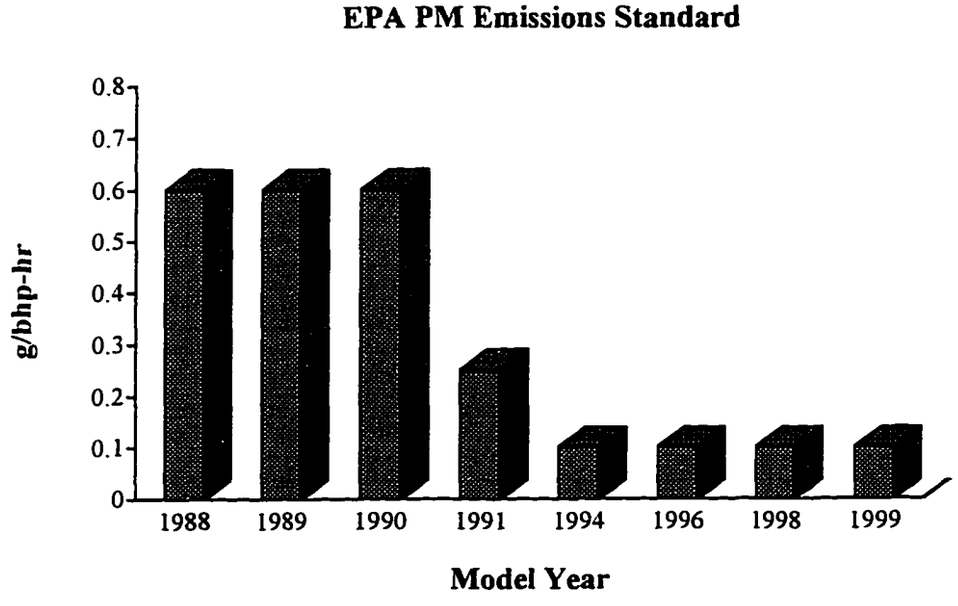

Note: after 1996, new heavy-duty diesel engines used for urban buses must meet a 0.05 g/bhp-hr particulate emissions standard.

Figure 1.1 EPA emissions standards for heavy-duty diesel engines

aftertreatment devices, such as particulate traps, oxidation catalysts, etc.; 3) electronically controlled high pressure fuel injection systems to provide fine and uniform fuel sprays with better matching to the air flow and combustion chamber shape; and 4) improvements in fuel formulations, such as lowering the concentration of sulfur and aromatic compounds in diesel fuel, using alternative fuels (esters of vegetable oils, alcohols, natural gas, etc.) and diesel fuel additives.

Diesel fuel reformulation is one of the most effective methods to control particulate matter emissions. Many alternative diesel fuels have been shown to have better exhaust emissions than traditional diesel fuel. In addition, concerns about the decrease in domestic petroleum reserves and unstable foreign supplies of petroleum, have made the development of alternative fuels increasingly important. Alkyl esters of vegetable oils and animal fats, called *biodiesel*, hold promise as fuel alternatives for diesel engines. A number of researchers have shown that biodiesel has fuel properties and provides engine performance that are very similar to diesel fuel [6, 7, 8, 9]. The primary incentive for using biodiesel is that it is a nontoxic, biodegradable, and renewable fuel. Further advantages over petroleum-based diesel fuel include a high cetane number, low sulfur and aromatics content, low volatility, and oxygen atoms in the fuel molecule. These features of biodiesel lead to its greatest advantage which is its potential for emission reduction including CO, HC, SOL, and PM. Biodiesel also helps to reduce greenhouse gas emissions primarily (CO_2) since the carbon in the fuel was extracted from the atmosphere rather than from fossil reserves, and very little energy is required for fuel production.

However, because some fuel properties (volatility, viscosity, boiling point, etc.), and chemical structure (unsaturated chemical bonds, large molecular size, oxygenation, etc.) of biodiesel are different from diesel fuel, the formation and growth of biodiesel particulates during the measurement process may differ from diesel fuel. The methods used to measure HC emissions and particulates, a heated flame ionization detector (HFID) and a dilution tunnel, respectively, were designed for diesel fuel. These techniques may be not appropriate for biodiesel emission measurement due to its extremely low volatility.

Previous emission research projects on a diesel engine fueled with biodiesel have been done in the Internal Combustion Engine Laboratory at Iowa State University. The results of these projects showed that while the measured HC emissions were lowered when the diesel engine was fueled with biodiesel/diesel fuel blends, the soluble organic fraction (SOF) or hydrocarbon portion of the particulates increased with increasing fraction of biodiesel in the fuel blends compared with the baseline diesel fuel [10, 11]. These emission results of HC and SOF appear to be contradictory. Adsorption and/or condensation of unburned biodiesel in the sampling line of the HFID was suspected to be occurring and could cause a low HC measurement. The same effect in the dilution tunnel would cause the unburned biodiesel to attach to the particulate matter causing high SOF levels. Other researchers have shown that the adsorption process is the major physical phenomenon that governs the formation of SOF on particulates in the dilution tunnel [12, 13, 14].

Very little experimental work has been done to provide information on how the particulate measurement conditions, such as dilution ratio and sample filter temperature affect the biodiesel particulate measurement, and how HC sampling line temperature affects the measurement of HFID for unburned biodiesel. A theoretical study on these problems was also needed to investigate their mechanisms. The objective of this study was to investigate these phenomena. Both experimental and theoretical investigations were part of this study.

The goals of the study were to:

1. investigate the independent effects of dilution tunnel conditions, such as dilution ratio and sample filter temperature, on biodiesel particulate formation during the dilution process.
2. study the effects of HFID sampling line temperature on biodiesel HC emission measurement.
3. develop adsorption and condensation models to predict the biodiesel particulate formation during the dilution process.
4. use the models to study the mechanisms that affect the measurement of biodiesel HC emissions.

This dissertation will include a literature review about diesel engine emissions and emission reduction by biodiesel. A detailed discussion will describe the development of mathematical models to predict the SOF formation during the dilution process and the change of concentration of unburned biodiesel in the HC detector sampling line. The experimental set-up and test procedures also are discussed. Finally, the experiment results and comparisons between the experiments and the computer models will be presented.

2. BACKGROUND

In this chapter, the formation of diesel engine particulate emissions will be described. The first section discusses diesel particulates in general and the second section describes the effects of biodiesel fuel on diesel engine emissions. Finally, the particulate emission measurement process and modeling the formation of the soluble organic fraction in particulates are discussed in detail.

2.1 Diesel Engine Emissions

The combustion process in a diesel engine is unsteady and heterogeneous. A large number of chemical species are contained in diesel engine exhaust gas due to the conditions of high temperature, high pressure, and incomplete combustion. Although their concentrations are low, most of these species are harmful to the environment. The major air pollutants in diesel engine exhaust gas are carbon monoxide (CO), unburned hydrocarbons (HC), oxides of nitrogen (NO_x), and particulate matter (PM) which includes solid carbon (SOL), soluble organic fraction (SOF), and sulfates. Other pollutants found at trace levels are alcohols, aldehydes, ketones, phenols, acids, ethers, etc. The engine crankcase and fuel tank breathers also contribute to engine emissions.

Carbon monoxide emission from diesel engines is controlled primarily by the fuel/air ratio. Under fuel-rich conditions, CO production is the result of incomplete combustion. Carbon monoxide can also be produced by dissociation when the mixture in a diesel engine combustion chamber is fuel-lean. In general, CO emission from diesel engines is very low because they always operate under fuel-lean conditions [15].

The emissions of unburned HC are also the result of incomplete combustion of the hydrocarbon fuel in the diesel engine. Fuel composition can significantly influence the composition and magnitude of the organic emissions. Fuels with high proportions of aromatics and olefins will generate relatively high concentrations of reactive hydrocarbons. The reactive hydrocarbons usually have high potential for oxidant formation in the photochemical smog chemistry.

Due to the heterogeneous nature of diesel combustion, there is a wide distribution of fuel/air ratios within the engine cylinder. Unburned hydrocarbon emissions are attributed to either fuel/air mixtures that are too lean to autoignite or support a propagating flame, or fuel/air mixtures that are too rich to ignite, such as the central core of the fuel spray [15, 16].

Although NO is the dominant oxide of nitrogen formed within the diesel engine cylinder, most NO is further oxidized to NO_2 after the engine exhaust gas is emitted to the atmosphere. Usually, the NO_x emissions from the diesel engine include both NO and NO_2. The results of chemical kinetics calculations show that NO_x emissions are a strong function of burning temperature, oxygen concentration in the combustion zone, and time duration. The highest concentration of NO is obtained for slightly lean mixtures and rapid combustion [15, 16]. Diesel engine NO_x emissions are also dependent on other factors, such as fuel properties (particularly the cetane number) [17, 18, 19, 20, 21], fuel injection system (fuel injection timing and rate) [15, 16, 21], and degree of exhaust gas recirculation [15, 16, 22].

The particulate emissions are one of the major air pollutants emitted from diesel engines. The particulate matter (PM) is defined by the Environmental Protection Agency (EPA) as any diesel exhaust substance that can be collected by filtering the diluted exhaust gas at or below 325 K [23]. The PM consists principally of combustion generated carbonaceous material called solid carbon or soot (SOL). On its surface, some liquid phase materials are formed which are primarily adsorbed and condensed vapor phase unburned hydrocarbons, called the soluble organic fraction (SOF). The SOF is primarily composed of unburned fuel and lubricant along with their partially oxidized products. Sulfate compounds with bound water, typically sulfuric acid, are also formed. The proportion of sulfate in the particulate matter usually is very small, especially when low sulfur diesel fuel is used. The particulates also contain a small quantity of non-carbon ash. Figure 2.1 shows a typical composition of diesel particulates.

The formation of diesel particulates occurs in two stages. First, solid carbon or soot particles are produced in the engine combustion chamber by processes that include nucleation, surface growth, and agglomeration. Second, the soluble organic fraction is formed on the soot particle surface when these particles are exhausted from the engine and diluted with fresh air.

These processes are shown schematically in Figure 2.2. The formation of solid carbon in the diesel combustion chamber takes place in the fuel burning environment at temperatures between 1000 and 2800 K and at pressures between 50 and 100 atm with a very short time period (in the order of milliseconds). Diesel soot particles are formed by the thermal decomposition of the hydrocarbon molecules, followed by agglomeration. The formation process is predicted to occur at carbon/oxygen ratios in the range from 0.5 to 0.8 [24]. Most of the soot is oxidized when it encounters lean zones during the mixing-controlled combustion. The detailed soot particle production in a diesel engine can be divided into two processes: particle generation and particle growth.

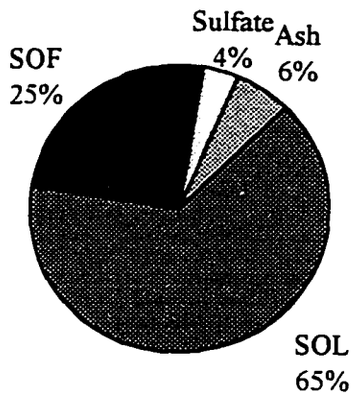

Figure 2.1 Typical diesel particulate composition

During the particle generation or nucleation process, the first condensed phase material arises from the hydrocarbon fuel molecules via their oxidation and/or pyrolysis products. Various unsaturated hydrocarbons, particularly acetylene and its higher analogues ($C_{2n}H_2$), and polycyclic aromatic hydrocarbons (PAH) could be present in these products. Both types of hydrocarbon molecules are considered as the most likely precursors of soot particles in flames. A large number of fine particles will be generated in the region of their formation during the nucleation process.

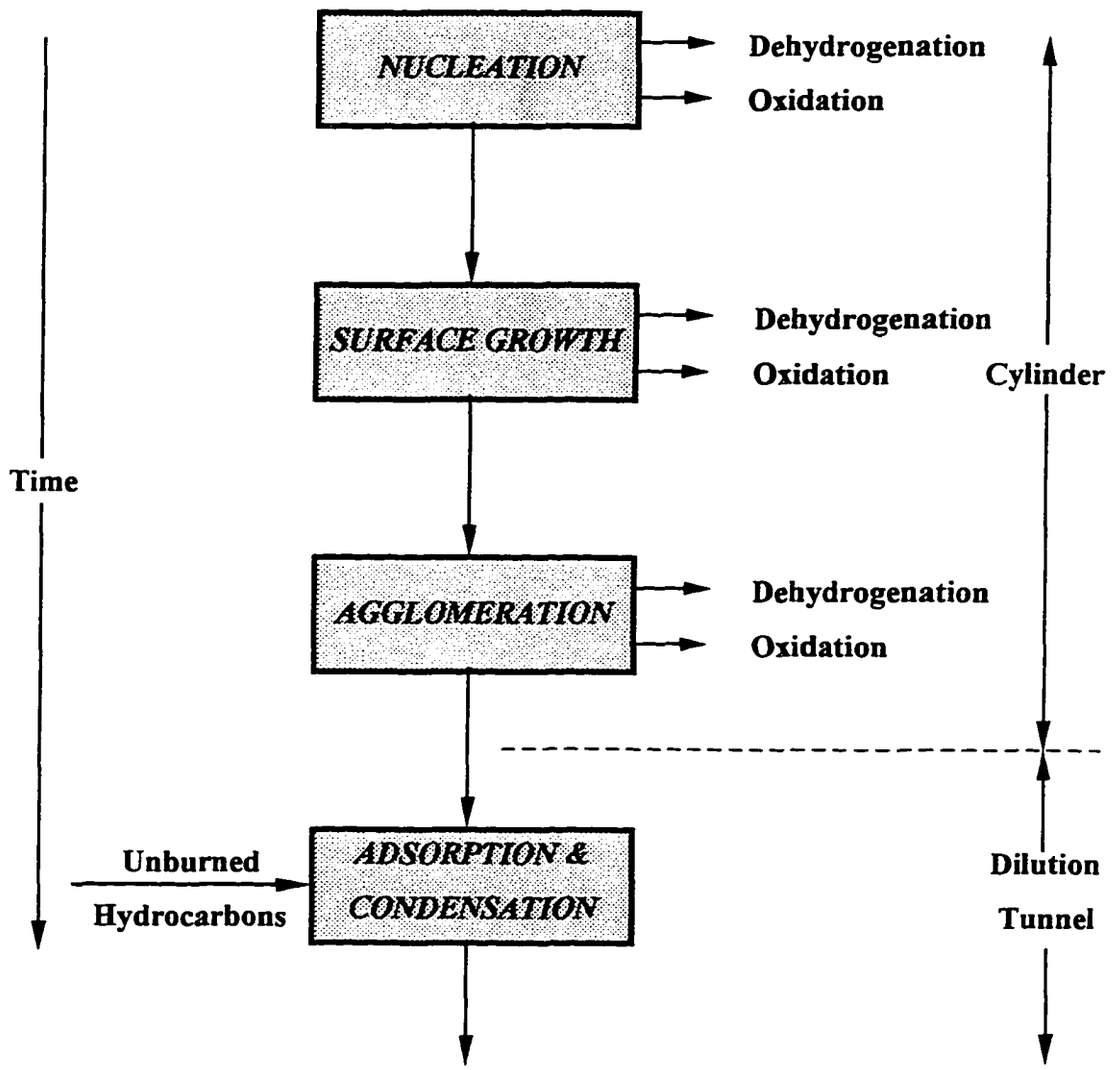

Figure 2.2 Formation of diesel particulates [15]

Following nucleation, these particles experience face growth, coagulation, and aggregation. Surface growth involves the attachment of gas-phase species to the surface of particles and their incorporation into the particulate phase. Although surface growth processes lead to an increase of soot amount, the number of particles remains unchanged. The surface growth stage is followed by processes of collisions and coalescence which take place in the coagulation stage. The number of particles will decrease as their size increases, but the amount of soot stays constant. With collisions of larger particles, these particles are aggregated into chains and clusters [25, 26, 27].

In the processes which take place in the diesel engine combustion chamber, oxidation can occur whenever soot or soot precursors are in the presence of oxidizing species to form gaseous products, such as CO and CO_2.

The final soot concentration will depend on the balance between the processes of formation and oxidation before the soot enters the engine exhaust system. Electron micrographs of diesel soot particles indicate that the carbon may be graphitized to varying degrees, depending on its combustion history. Primary particles, called spheroids, are 0.01 to 0.08 μm in diameter, and are formed from a mixture of graphitic and amorphous carbon [28].

The oxidation of soot particles requires high temperature (above 2000 K) and excess oxygen. When the soot leaves the engine cylinder, the oxidation of soot is very slow. In research conducted by Fujiwara et al. [29], the exhaust soot oxidation process was simulated by passing diesel exhaust gas through a furnace having approximately the same residence time as an exhaust system and measuring the changes in the number and size of the soot particles. Negligible oxidation (about 5%) was observed below 725 K, slight oxidation (about 15%) up to 1070 K, and rapid oxidation for temperatures above 1170 K (70% oxidized at 1475 K). Usually, the temperature in the diesel engine exhaust system is a maximum about 1000 K. Thus, the oxidation of soot particles in the exhaust system can be neglected. The concentration of soot can generally be assumed to be constant when it leaves the engine combustion chamber.

The final process that forms the diesel particulates occurs outside the diesel engine. When the exhaust gas containing soot particles and unburned hydrocarbon vapor is emitted

into the atmosphere, a portion of the unburned hydrocarbons will adsorb and condense on the soot particle surface to form the soluble organic fraction. Figure 2.3 shows a schematic of a typical exhaust particle formed by these processes. During particulate emission measurement, the process occurs in a dilution tunnel that simulates the actual atmospheric dilution process. Previously published simulation studies have shown that physical adsorption governs the formation of SOF during the dilution process [12, 13, 14]. However, with dilution, the temperature of the diluted exhaust gas decreases which decreases the saturation vapor pressure of the unburned hydrocarbons. Condensation may take place if the partial pressure of the unburned hydrocarbons exceeds their saturation vapor pressure.

The process of adsorption is a physical phenomenon that, in this case, involves the adherence of molecules of unburned hydrocarbons to the surfaces of solid carbon by a weak force called the van der Waals force [30, 31]. The extent of adsorption is dependent on the available adsorbent surface (the concentration of solid carbon), the dilution ratio that determines the partial pressure of vapor phase unburned hydrocarbons, and the system temperature. The partial pressure of unburned hydrocarbons is the driving force for the adsorption process. When the dilution ratio is initially increased, the temperature decrease will cause the diesel particulate emissions to increase due to the increase of adsorbed soluble organic fraction on the soot surface. However, at high dilution ratio, because the concentration of unburned hydrocarbons is reduced, the lower partial pressure of unburned hydrocarbons causes the extractable fraction in the particulates to decrease. The sample temperature becomes relatively insensitive to the dilution ratio [32]. High unburned hydrocarbon concentration is the condition where condensation is likely to be significant, and the HCs that are most likely to condense are those with the lowest volatility.

The first step of a particulate analysis procedure generally is to separate the sample into the SOL and SOF portions. Three methods are commonly used for this part of the particulate analysis:

- **Soxhlet Extraction**. This method requires that the weighed sample be extracted with a solvent and results in the separation of the sample into the soluble organic fraction

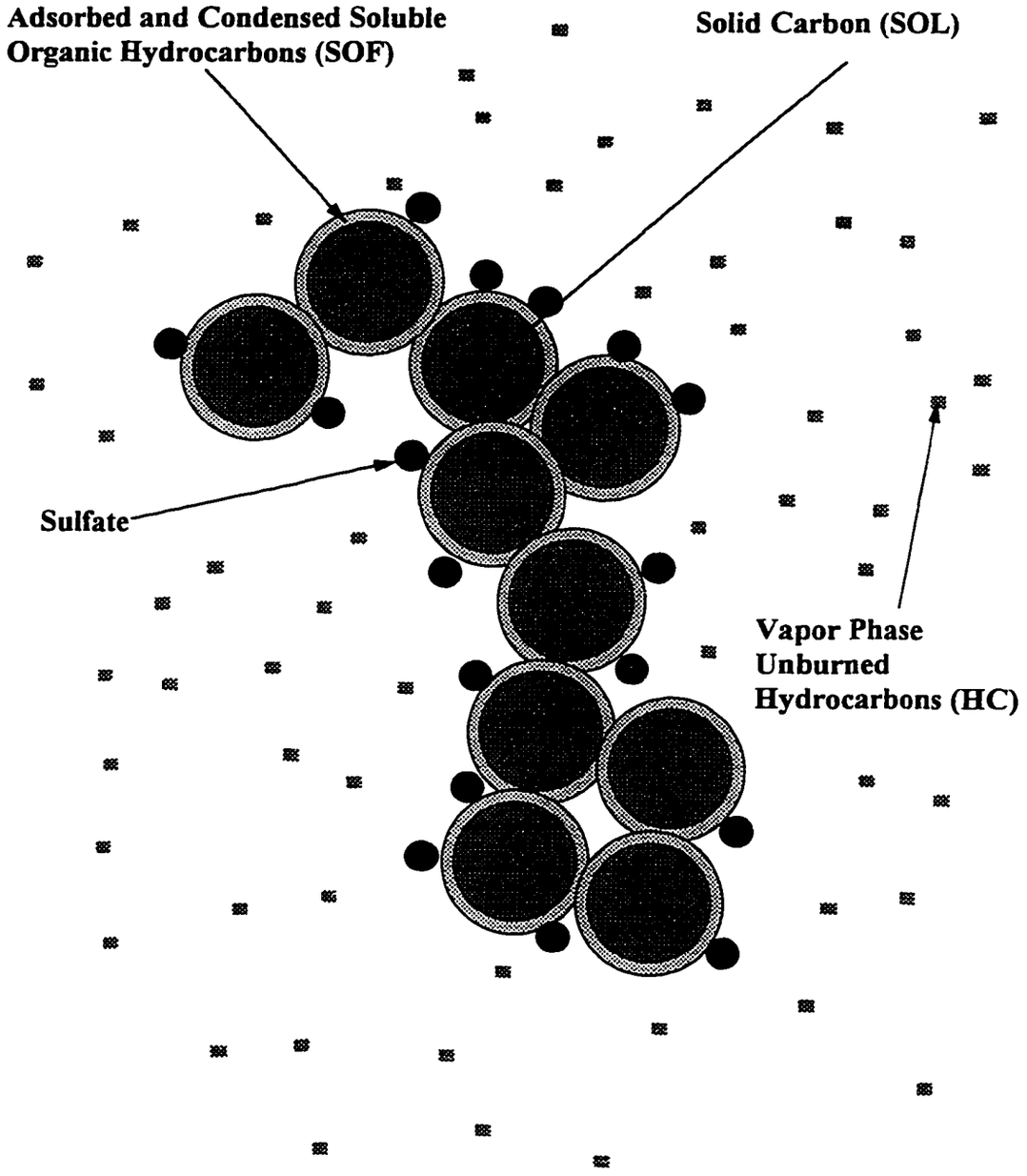

Figure 2.3 Formation of diesel particulate matter

(SOF) and the insoluble fraction (SOL). The extracted mass contains primarily adsorbed and condensed unburned hydrocarbons. The remaining material is sometimes further extracted with water to determine the sulfate fraction. The exact nature of the separation is dependent on the solvent and extraction conditions. A wide variety of solvents have been used for the extraction of particulate matter, such as cyclohexane, benzene-ethanol, methylene chloride, etc. The criteria for the choice of a solvent include its extraction efficiency, purity, volatility, toxicity, cost, and compatibility with subsequent analytical procedures [33, 34, 35].

- **Vacuum Sublimation**. With this method, a weighed particulate sample is heated in a vacuum oven at 200 °C for several hours. The residual that consists primarily of solid carbon and non-volatile ash is weighed. The volatile portion, which contains the adsorbed and condensed unburned hydrocarbons and sulfuric acid, is determined by the difference in the mass of the sample [36, 37].
- **Thermogravimetric Analysis**. In this method, the particulate sample is simultaneously heated and weighed, and the differential weight loss is continuously monitored. The mass volatilized below 600 °C is considered to be the volatile organic fraction [38, 39].

Among the three methods, the solvent extraction method has the advantage of allowing the investigator to look at the chemical composition of the adsorbed and condensed unburned hydrocarbons. It has become the most popular method used for diesel particulate analysis, and is the method recommended by EPA [37, 40]. The Soxhlet extraction method was chosen to analyze the diesel particulate composition in this study.

There are a number of solvents used in the extraction analysis. Benzene and methanol are more effective solvents for extraction of polynuclear aromatic hydrocarbons (PAH) than other commonly used solvents [33, 34]. Polar solvents, such as methanol and methylene chloride are known to be more efficient extraction solvents for polar species than non-polar solvents, such as benzene and cyclohexane. Binary mixtures of polar and non-polar solvents or separate extraction with each solvent have been demonstrated to yield higher levels of soluble organic fraction from airborne particulates than single solvent extraction. The use of binary

solvent extraction, particularly benzene and methanol, has become popular with some researchers [35, 41, 42].

Methylene chloride has been shown to be an efficient solvent for adsorbed and condensed unburned hydrocarbons for particulates and was used as the extraction solvent for this study. Its selection over other available candidates was predicated by a desire to be consistent with EPA procedures for the analysis of diesel particulate matter [35, 43].

Typically 15 to 30 mass percent is extractable in the diesel particulate, but the range of observations is much larger (10 to 90%). Although most of the SOF is formed through incomplete combustion of the hydrocarbon fuel, engine oil may also contribute significantly. The SOF of diesel particulates can be chemically characterized into eight fractions as shown in Table 2.1. Those fractions are generally labeled as: basic, acidic, paraffins, aromatics, transitional, oxygenates, ether insolubles, and hexane insolubles [44, 45].

The basic fraction contains aromatic or aliphatic species with basic functional groups, such as $-NH_2$. Examples of these compounds are the benzacridenes. The acidic fraction contains aliphatic and aromatic species containing acidic functional groups, such as -COOH or phenolic -OH groups. Benzoic acid and the phenols would be examples of this category of compounds.

Table 2.1 Chemical fractions of SOF in diesel particulates [44]

Characterization of SOF	Fractions of SOF
Basic	< 1- 2%
Acidic	3 - 15%
Paraffin	34 -36%
Aromatic	3 -14%
Transitional	< 1 - 6%
Oxygenates	7 - 15%
Ether Insolubles	6 - 25%
Hexane Insolubles	1 - 3%

The paraffin fraction contains the aliphatic straight and branched chain alkanes. Normal-dodecane is an example of this type of compound. Unburned fuel would be a source for high levels of paraffins in diesel particulates.

The aromatic portion of the particulate extractable material will have those compounds that have aromatic structure and no polar functional groups. Alkyl functional groups may be present with a variety of chain lengths expected. An example of the type of compound in this fraction is a polynuclear aromatic, such as benzo(a)pyrene.

The transitional fraction consists of compounds that may be oxygenated but without acidic, basic, or other polar functional groups. Those compounds can be aromatic or aliphatic and have a high probability of containing another type of functional group. The fraction labeled as oxygenates contains those oxygenated compounds that are not acidic or basic, but still have polar functional groups. Aromatic and aliphatic ketones and aldehydes fall into this class of compounds. Examples of these compounds are quinone or α-napthoquinone. The insoluble fraction contains a wide variety of compounds that may include both organic and inorganic compounds [44].

The last major constituent of diesel particulates is sulfate. Sulfur in diesel fuel is converted into SO_2 during the engine combustion process. Approximately 2.5% of the SO_2 is further oxidized into SO_3, and binds with water to form H_2SO_4. This contributes directly to the mass of total particulate matter [46]. Lowering the sulfur content in diesel fuel is one of the most effective ways to reduce particulate emissions. The EPA mandated the use of low sulfur diesel fuel beginning in October, 1993. Modern on-highway diesel fuel contains less than 0.05% sulfur by mass, as opposed to previous diesel fuel which had 0.15 to 0.3% sulfur by mass. The impact of sulfur content on diesel engine particulate emission reduction has been demonstrated by several researchers [46, 47, 48, 49, 50].

2.2 Alternative Fuels - Vegetable Oils and Their Alcohol Esters

The economic development of most nations throughout the world is causing an increase in the demand for energy. With more industrialized nations emerging, the increasing demand for energy has resulted in a continuing reduction in available energy supplies. In

addition, increasingly stringent emission regulations have been issued to reduce the air pollution from engine exhaust. All of these reasons make the search for and study of alternative fuels for internal combustion engines increasingly important. Interest in the development of alternative fuels has grown steadily during the past three decades.

Any alternative fuel for an internal combustion engine should satisfy certain criteria, such as: a minimum of engine modification, no reduction in engine life, not hazardous to human health and the environment during production, transportation, storage, and utilization, and the fuel must be low cost, renewable, abundant, and in stable supply. Ethanol is sometimes mentioned as a candidate alternative fuel for diesel engines. However, the cetane number of ethanol is relatively low which results in a long ignition delay and excessive knock when it is used in diesel engines. In addition, its production cost is high, and specific energy content (energy content per unit mass of fuel) is low. Based on these problems, ethanol is not likely to be a valuable and practical alternative fuel for diesel engines [51].

Research over the past 2 or 3 decades has shown that vegetable oils and their alcohol esters may be a suitable and practical alternative fuel candidate for diesel engines. As early as 1900, Rudolf Diesel, who first developed the diesel engine, demonstrated that the diesel engine was able to use peanut oil as a fuel. While speaking to the Engineering Society of St. Louis, Missouri, in 1912, he said: "The use of vegetable oils for engine fuels may seem insignificant today. But such oils may become in course of time as important as petroleum and the coal tar products of the present time." [52].

There are a number of vegetable oils that may be candidates for alternative fuels for diesel engines, such as soybean oil, sunflower oil, peanut oil, rapeseed oil, olive oil, cottonseed oil, sesame oil, etc. Vegetable oils are naturally occurring triglycerides found in numerous plant varieties. The chemical difference of vegetable oils from typical diesel fuel is that the vegetable oils are composed of triglycerides with fatty acid chains of 16 to 22 carbons in length, while diesel fuel consists of only carbon and hydrogen atoms, which can be arranged in straight or branched chain paraffins, or aromatic configurations. About 94 to 96% of vegetable oils are triglycerides, and the remaining portion contains waxes, sterols, and tocopherols.

The chemical structure of a typical triglyceride is illustrated in Figure 2.4. The *triglyceride* consists of a glycerin molecule with three fatty acid chains attached in place of hydrogen atoms. The structure of the triglycerides in vegetable oils vary with the carbon chain length and number of double bonds of the fatty acid chains. R_1, R_2, and R_3 in the structure of the vegetable oil triglyceride shown in Figure 2.4 represent the hydrocarbon chains of fatty acids, which may be of different chain length and have different numbers of double bonds present. The proportion of the various fatty acids determines the physical and chemical properties of an vegetable oil, such as viscosity, heating value, thermal stability, etc.

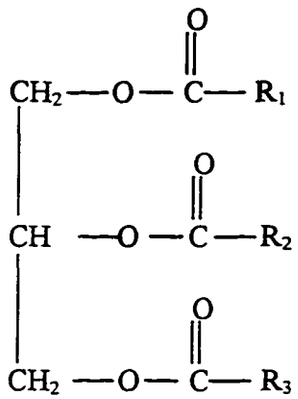

Figure 2.4 Chemical structure of a triglyceride

In most vegetable oils, a small number of the fatty acid molecules have detached from the glycerin base, and are known as *free fatty acids*. The quantity of free fatty acids primarily affects the flash point of a vegetable oil and to some extent its ignition characteristics [53].

The degree of unsaturation (number of carbon-carbon double bonds) determines the oxidative stability as well as the melting temperature of vegetable oils. The double bonds present in unsaturated vegetable oils and their esters are highly susceptible to attack by oxygen molecules and subsequent formation of chemically active hydroperoxides. The extent of oxidation of vegetable oils and their esters is characterized by their *peroxide value*. The

peroxide value can have a significant effect on properties such as the cetane number [54]. Unsaturated compounds in vegetable oils and their esters have much better cold flow properties than saturated oils [53].

Cetane number is one of the most important fuel properties of diesel fuels. It indicates the readiness of a diesel fuel to ignite spontaneously under the temperature and pressure conditions in the combustion chamber of the engine. The higher the cetane number, the shorter the ignition delay. Shorter ignition delay is usually better for diesel engine performance and emissions. The cetane numbers of vegetable oils and their esters increase with increasing chain length of the fatty acids [55].

The heating value is a measure of the energy content of a fuel when it is burned. Generally, the heating values of vegetable oils and their esters are slightly lower than diesel fuel (about 12% lower for neat biodiesel and vegetable oil).

The viscosity of a fuel indicates its resistance to flow. Because vegetable oils have longer carbon chains and larger molecular size than diesel fuel, their viscosity is higher than diesel fuel [56, 57]. No. 2 diesel fuel usually has a viscosity about 2.7 cSt at 40 °C, however, vegetable oils have a viscosity of about 30 cSt, and the viscosity of their esters such as the methyl ester of soybean oil is about 4.1 cSt at the same temperature.

Previous studies on the use of unmodified vegetable oils in diesel engines have characterized their potential as an alternative to or extender for diesel fuel. From an environmental viewpoint, the vegetable oils are desirable because they are entirely renewable, they are biodegradable in the event of spills, and contain only trace amounts of sulfur. Low sulfur levels would significantly reduce the sulfate portion of diesel engine particulate emissions. Short term engine tests with vegetable oils have shown that engine performance, such as power output, torque, thermal efficiency, emissions, etc., are comparable to diesel fuel [58, 59, 60, 61, 62]. However, during the engine tests, unmodified vegetable oils tend to cause severe engine deposits, injector coking, piston ring sticking, and other problems [63, 64, 65, 66]. These problems are believed to be caused by the high viscosity and low volatility of vegetable oils that interfere with the fuel injection process and produce poor fuel atomization and an incomplete combustion process [67]. The low volatility causes the fuel to adhere to the

injector and cylinder walls without vaporizing. The fuel coating the walls may undergo oxidative and thermal polymerization under the high temperature conditions of the combustion process. This polymerization results in deposition on the fuel injector, forming a film that would continue to trap fuel and eventually interfere with the spray. The incomplete combustion may lead to more deposit formation, carbonization of injector tips, ring sticking, and lubricating oil contamination and degradation [68].

The shortcoming of vegetable oils can be improved at least five different ways: dilution, heating, pyrolysis, microemulsion, and transesterification. Dilution of vegetable oil can be accomplished by blending it with diesel fuel or alcohols to the fuel viscosity. Preheating the vegetable oil to a sufficiently high temperature is one of the simplest ways to reduce viscosity, but an extra heating device is required.

Pyrolysis is a chemical process to change the chemical structure of the vegetable oil. The large molecules in the vegetable oil will be cracked or broken into simpler and shorter carbon chain compounds by heating. Many of the shorter chain compounds are straight chain paraffins with high cetane numbers.

A microemulsion is a system consisting of a liquid, dispersed with or without an emulsifier, in an immiscible liquid, usually in droplets smaller than colloidal size. A suitable surfactant is used in the preparation of the mixture to reduce the interfacial tension between the dispersed phase, which is typically aqueous alcohol, and the continuous phase vegetable oil. The microemulsion can provide excellent spray characteristics due to the explosive vaporization of the low-boiling constituents in the tiny droplets. Engine tests have shown that microemulsions can provide an improvement over unmodified vegetable oils in their physical properties, such as viscosity, and the engine performance is similar to diesel fuel [69, 70].

Transesterification is currently used to produce a fuel that has similar properties to diesel fuel. Transesterification can provide a significant reduction in the viscosity of the vegetable oils, and make them suitable for use in a diesel engine without engine modifications [10, 11, 71, 72]. Transesterification is the process of reacting a triglyceride (vegetable oil) with an excess of the stoichiometeric amount of an alcohol in the presence of a catalyst, such as KOH, NaOH or $NaOCH_3$ [72, 73] to produce fatty acid monoesters and the by-product,

glycerin. These monoesters are commonly referred to as *biodiesel*. The chemical reaction is shown in Figure 2.5. The variables that have the greatest influence on the transesterification chemical reaction time and conversion efficiency are concentration, purity of the reactants, ratio of alcohol to oil, temperature, catalyst type, and the stirring rate.

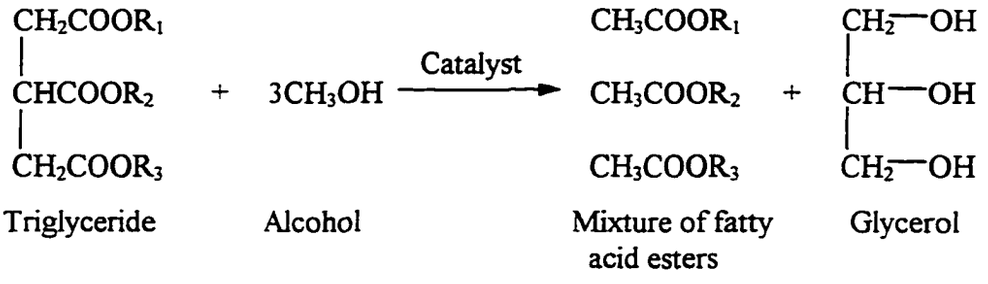

Figure 2.5 Chemical reaction of transesterification

The transesterification reaction improves the physical properties of the vegetable oils in two ways. One is to reduce the molecular weight to approximately one third that of the original triglyceride. Another effect is the conversion of long branched molecules into shorter, straight-chain molecules. With different alcohols, such as methanol, ethanol, or butanol, the product of the alcohol esters is methyl ester, ethyl ester or butyl ester. The methyl esters of soybean oil normally are referred to as *methyl soyate*. These esters have better fuel properties than those of unmodified vegetable oils and are similar to diesel fuel [57, 74]. They usually have lower viscosity, lower cloud point, and about the same heating value as the original oil. Research evaluating engine performance when diesel engines were fueled with various esters of vegetable oils has shown that the engine performance is similar to that of diesel fuel with lower CO, HC, and particulate emissions and slightly higher NO_x emissions [10, 11, 71, 75, 76, 77].

2.3 The Effects of Biodiesels on Diesel Engine Emissions

If an alternative fuel is to compete with a conventional fuel, it must meet today's exhaust emission standards with little or no modifications to the engines or the exhaust system. Many studies have shown that biodiesel has similar fuel properties and engine performance compared with diesel fuel. As noted before, biodiesel is a non-toxic, biodegradable, and renewable fuel. It has a higher cetane number than diesel fuel, no aromatic compounds, essentially no sulfur, and oxygen atoms in the fuel that have the potential to reduce the emissions of CO, HC, and PM. Based on its merits, biodiesel is a potential candidate as an oxygenate and a cetane improvement additive for diesel fuel reformulation to assist the diesel engine industry in meeting its future emission requirements.

The positive benefits of biodiesel on engine emissions have been proven by a number of research studies. Some of these diesel engine emission tests have been conducted in the Internal Combustion Engine Laboratory at Iowa State University. These projects concentrated on biodiesel fuel properties, performance, combustion, and emissions when the diesel engine was fueled with various biodiesels. Chang et al. [10, 11] tested a 4-cylinder, direct injection, turbocharged John Deere 4276T diesel engine with methyl, isopropyl, and winterized methyl esters of soybean oil. The winterized methyl esters were prepared by cooling the biodiesel and removing the crystals of the high freezing point fuel components as they formed. Ester blends with No. 2 diesel fuel (20%, 50%, and 70%, by wt.) showed no change of engine thermal efficiency compared with No. 2 diesel fuel. However, the brake specific fuel consumption was increased due to the lower energy content of the esters (about 12% less than No. 2 diesel fuel). The emissions of PM were reduced by 28% when the 50% isopropyl ester blend were used. The PM emission reduction was primarily due to a significant reduction of the solid carbon portion in the particulates. The SOF portion increased compared with No. 2 diesel fuel. The HC emissions were reduced by 29% by the same fuel blend. The maximum reduction of CO, by 25%, was from the blend of 50% methyl esters of soybean oil. The combustion characteristics of the blends, as indicated by heat release analysis, were similar to No. 2 diesel fuel. Chang et al. [71] also studied the effects of some specially treated biodiesel fuels on diesel engine performance, emissions, and combustion, such as the methyl esters of soybean

oil derived from a genetically modified strain of soybeans, partially transesterified soybean oil, and a synthetic fuel that contained 80% methyl palmitate and 20% methyl stearate. Their results confirmed that biodiesel has a higher cetane number than No. 2 diesel fuel, and that biodiesel with higher amounts of saturated esters has a higher cetane number than the unsaturated esters. Their research also showed that fuel injection timing was advanced slightly when biodiesel was used due to its having slightly higher viscosity than No. 2 diesel fuel. All of the biodiesel fuels that were tested lowered the emissions of CO, HC, and PM emissions compared with No. 2 diesel fuel. They all also showed small increases in NO_x. Although biodiesel particulates showed a higher SOF than No. 2 diesel fuel, the total particulate emissions were lower. The combustion characteristics of biodiesels were similar to the baseline diesel fuel.

Another project that investigated the effects of individual biodiesel compounds on diesel engine emissions was conducted at Iowa State University. Schmidt et al. [78] used the same engine used by Chang to investigate the emission characteristics of blends of five pure esters that are commonly found in soybean oil esters: methyl palmitate, isopropyl palmitate, methyl stearate, isopropyl stearate, and methyl oleate. Two other methyl esters, methyl esters of safflower oil and methyl esters of linseed oil, were also investigated. The largest reduction in particulate emissions were obtained when the diesel engine was fueled with blends of methyl palmitate and No. 2 diesel fuel. The 50% blends of methyl palmitate and isopropyl stearate with No. 2 diesel fuel reduced NO_x emissions by 2 to 3% compared with No. 2 diesel fuel, but blends of the other esters increased NO_x emissions by up to 5%. The SOF in the particulates decreased with increasing unsaturated ester content in the tested fuel. All blends demonstrated a significant reduction in HC emissions, but the unsaturated esters produced 8 to 9% higher HC emissions than the saturated esters.

One of the advantages of biodiesel over diesel fuel is its higher cetane number, and it can be used as a cetane improver for diesel fuel. The cetane number of biodiesel blends increases with increasing biodiesel fraction [10, 11, 71, 78]. Freedman et al. [79] and Harrington [80] have also reported that esters of vegetable oils have high cetane numbers and that saturated esters have higher cetane number than the unsaturated esters. The estimated

cetane number (calculated based on ignition delay data collected in a combustion bomb) of some saturated esters, such as methyl stearate and methyl arachadate, were over 100 [79].

Last et al. [75] tested methyl esters of soybean oil, blended with low sulfur diesel, in a Navistar T444E diesel engine. Their tests with the SAE 13-mode steady state test using biodiesel blends in diesel fuel between 10% and 100% showed substantial improvements in total particulate emissions. The reduction of particulate emissions was from 24.1% to 37.5% for various biodiesel blends using standard fuel injection timing. The emission of CO was reduced by at least 6.9%, and HC was reduced by 28%. However, the emission of NO_x was increased from 3.5% to 28% as the percentage of biodiesel in the fuel blends was increased. Under light-load engine conditions, the biodiesel blends showed a slight disadvantage on the particulate emissions due to increased SOF.

Graboski et al. [77] tested a 1991 DDC Series 50 diesel engine using the EPA Heavy-Duty transient test with 20%, 35%, 65%, and 100% methyl soyate blends. The results indicated that the emissions of CO, HC, and PM were reduced by 47%, 44%, and 66%, respectively, and NO_x emissions were increased by 11% when the engine was fueled with neat biodiesel, compared with No. 2 diesel fuel. The engine efficiency was found to be the same for biodiesel and its blends as for diesel fuel.

McDonald et al. [76] evaluated the emissions and engine performance of neat methyl soyate and a 30% blend with low sulfur No. 2 diesel fuel in a Caterpillar 3304 PCNA engine. They tested the fuels using the ISO 8178-C1 8-mode off-highway test procedure and the heavy-duty and light-duty transient test cycles, and found that the peak brake power decreased 9% and the brake specific fuel consumption increased 13% to 14% for neat biodiesel due to its lower energy content compared with No. 2 diesel fuel. The neat biodiesel and the 30% blend increased the volatile organic fraction of the particulates compared with the reference diesel fuel, but greatly decreased the solid carbon portion. The emissions of CO and HC were also reduced with biodiesel. When an oxidation catalyst was used, these emissions were decreased further.

Alfuso et al. [81] found that, at the same fuel injection timing, methyl esters of rapeseed oil caused a rise in NO_x emissions, a decrease in HC and CO emissions, and a strong

reduction in smoke. The biodiesel particulate emissions were higher than for the diesel fuel in transient test cycles. Alfuso found that emissions of NO_x, HC, and CO from biodiesel may be reduced, with only a small effect on particulate, by the adoption of EGR in the presence of an exhaust oxidation catalyst.

Choi et al. [82] used a single cylinder Caterpillar 3400 diesel engine to study the effects of fuel injection pressures on engine emission when 20% and 40% methyl soyate blends were used under high and low load conditions. At high load conditions, they observed a large reduction in particulate emissions with a slight increase in NO_x with the biodiesel blends. The particulate emission reduction increased with increasing fraction of biodiesel in the fuel blends. However, at low loads, the particulate emissions were higher than for diesel fuel. They also reported that the percentage of SOF in the particulates increased with biodiesel blends under both engine conditions.

2.4 Measurement of Unburned Hydrocarbon Emissions

Although almost all biodiesel emission tests indicate that the unburned hydrocarbon emissions are reduced compared with diesel fuel, it is not clear whether the results are due to the use of biodiesel fuels, or due to other causes such as the adsorption and condensation of HC on the sampling line wall and the filter, or to an incorrect response of the heated flame ionization detector (HFID) to unburned biodiesel.

The HFID is designed to measure the total HC concentration in the exhaust gas from internal combustion engines. The detection method is based on flame ionization, and is very sensitive. The hydrocarbon sensor is a burner where a regulated flow of engine exhaust gas sample passes through a flame sustained by regulated flows of a fuel gas and air. A complex ionization process occurs when the hydrocarbon compounds of the exhaust sample enter the flame, and electrons and positive ions are produced. Polarized electrodes collect these ions, causing a current that is proportional to the rate at which carbon atoms enter the burner, and results in a measurement of the concentration of hydrocarbons in the original exhaust sample. A heated sampling line is used to carry the sample gas from the engine exhaust manifold to the

detector and the detector is enclosed in a temperature-controlled oven to prevent condensation and adsorption of vapor phase unburned hydrocarbons.

The response of the HFID is dependent on the molecular structure of the hydrocarbon. It can determine the number of carbon atoms originating in all HC compounds in petroleum based fuels although the actual response depends on the individual HC species. These compounds include paraffins (alkanes), olefins (alkenes), aromatics, etc. However, the presence of other atoms in the HC molecule, such as oxygen, can suppress the ionization current from the exhaust sample. Table 2.2 illustrates the typical responses of a flame ionization detector to different molecular structures [16].

Table 2.2 Responses of FID to different molecular structure [16] (normalized with respect to methane)

Molecular Structure	Relative Response
Alkanes	1
Alkenes	1.3
Alkynes	0.95
Aromatics	1
Carbonyl radical (CO^-)	0
Oxygen in primary alcohol	-0.6

The methyl esters in biodiesel contain a carboxyl group that has two oxygen atoms. This carboxyl group may interfere with the correct response of the HFID during HC emission measurement. This phenomenon has been suspected to be the cause of low HC emissions for biodiesel found by some researchers [11, 71, 78].

Another possible factor that could cause low HC emissions for biodiesel is adsorption and condensation in the sampling line and within the FID's filter. Figure 2.6 shows a diagram of the HFID system used to measure the HC emissions. The standard operating temperature of the HFID and its sampling line is 465 K for diesel fuel measurements. Because

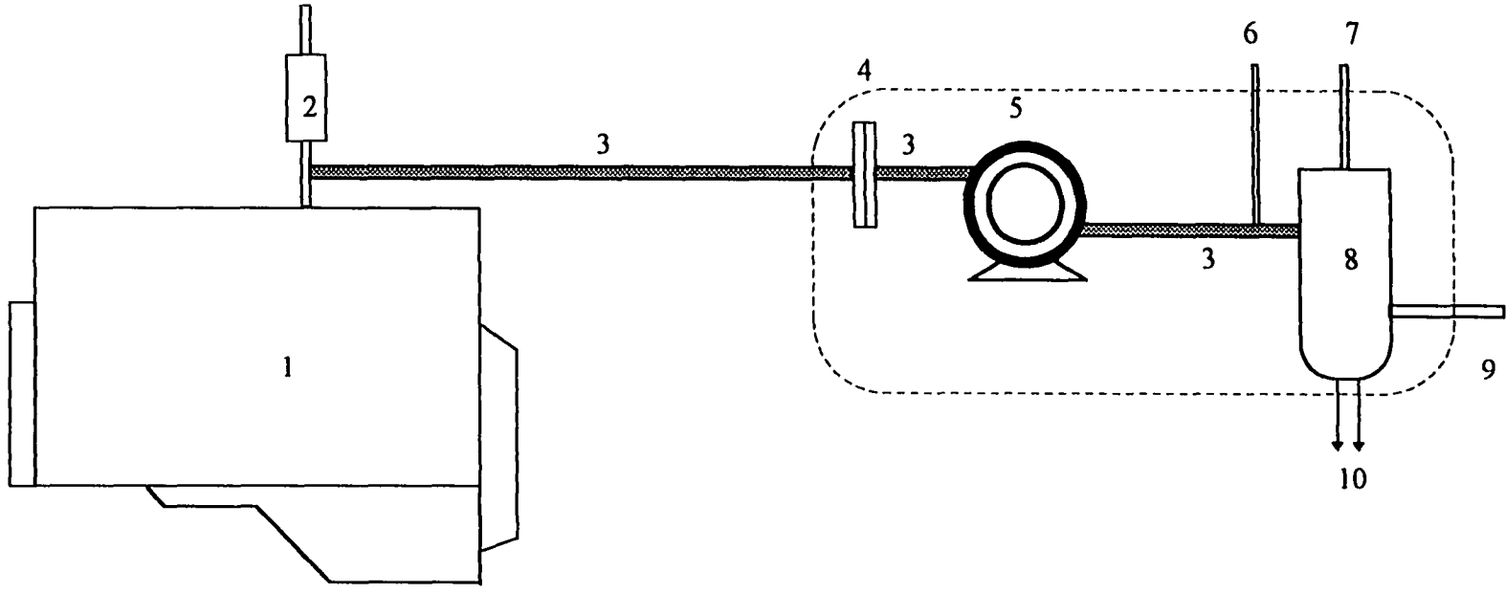

1. Diesel Engine.
2. Exhaust Pipe.
3. Heated HC Sampling Pipe.
4. Filter.
5. Sampling Pump.
6. Fuel Line.
7. Air Line.
8. Burner.
9. Exhaust Port of Burner.
10. Signal Output.

Figure 2.6 Schematic diagram of HC sampling system of HFID

of its particularly low volatility, unburned biodiesel is more likely to be deposited in the sampling line and the filter before it reaches the HC detector.

Abbass et al. [83] studied the effect of exhaust gas temperature on the HC emission measurement by setting the temperatures of the engine exhaust pipe and sampling line at 180, 50, and 2 °C. They found that the HC concentration at 50 °C was approximately two thirds that at 180 °C, but this decreased to approximately one third of the 180 °C HC concentration at 2 °C. The measurement of HC concentration was found to be a strong function of the sampling temperature.

In general, the esters of vegetable oil show fuel properties and engine performance which are very similar to diesel fuel and much better than the unmodified vegetable oils. Biodiesels have higher cetane number, lower emissions of CO, HC, and PM than diesel fuel, but the NO_x emissions are slightly higher than for diesel fuel. Biodiesel is a potential low emission alternative fuel for diesel engines.

2.5 Measurement of Particulate Emissions

The definition of particulate matter by EPA is any diesel exhaust substance that can be collected by filtering diluted exhaust gas at or below 325 K (52 °C) [23]. The measurement of diesel particulate matter requires a special measurement system based on specifications contained in the Code of Federal Regulations [23]. A schematic of the measurement system is shown in Figure 2.7. It consists of a primary dilution tunnel, a heat exchanger, a positive displacement pump (PDP), and a constant volume sampler (CVS). This whole system is called a positive displacement pump-constant volume sampler, or PDP-CVS. During the particulate emission test, the entire exhaust gas of the diesel engine is supplied to the dilution tunnel. This type of tunnel is termed a "full-flow" dilution tunnel. Another type of dilution tunnel, called a "partial-flow" dilution tunnel, allows only a fraction of the diesel engine exhaust gas into the dilution tunnel. The advantage of the partial-flow dilution tunnel is that it is small in size and does not require a large capacity dilution air source.

The dilution tunnel is intended to simulate the mixing of engine exhaust gas with the atmosphere when it is emitted from the engine, where some of the unburned hydrocarbons will

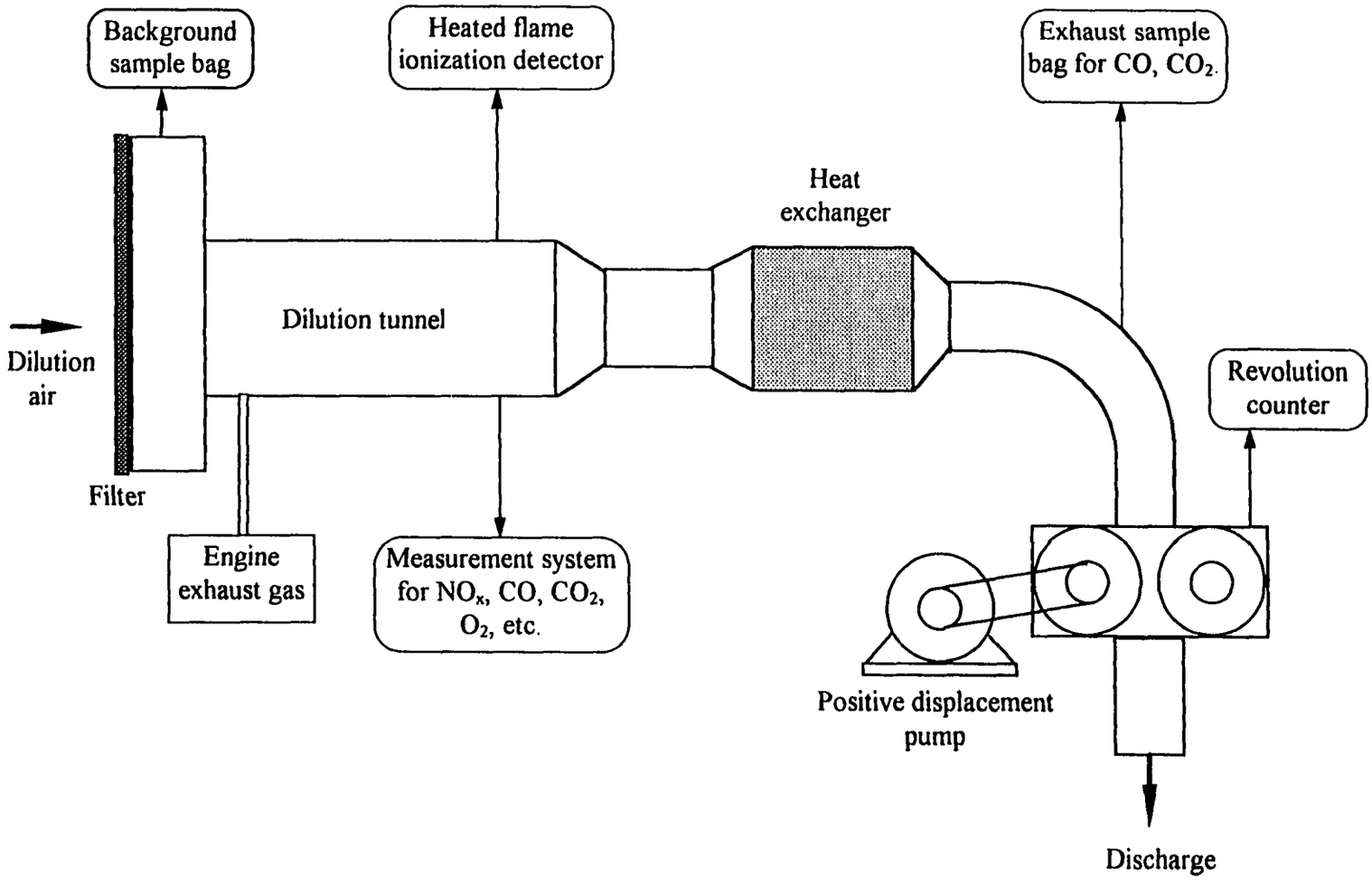

Figure 2.7 EPA specified exhaust emission measurement system [23]

adsorb and condense onto the soot particle surface. The total mass of these adsorbed and condensed hydrocarbons is the soluble organic fraction (SOF) of the particulates. With the dilution tunnel, the quantity, chemical characteristics, and biological characteristics of the SOF can be studied as well as the dynamics of the atmospheric dilution process.

In the particulate measurement system, the CVS system will draw a constant mass flow rate of diluted exhaust gas from the dilution tunnel. During transient engine tests, the exhaust gas flow rate and its temperature will be highly variable when it enters the dilution tunnel. However, the large heat exchanger can bring the diluted exhaust gas to an almost constant temperature. Because the PDP is drawing a constant volume flow rate of diluted exhaust gas, and the pressure in the dilution tunnel does not vary significantly, the mass flow rate of the sample gas is also constant. This technique ensures that the particulate measurements taken during a transient cycle test are properly weighted with respect to the different conditions of the test cycle.

A filter is used to collect the engine particulate sample by passing a measured portion of the diluted exhaust gas through it. Many experiments have shown that Teflon-coated fiberglass filters are the best candidates for diesel particulate measurement [84, 85]. The sample flow rate must be a constant mass fraction of the total diluted exhaust gas flow rate so that the collected particulate sample represents the particulate emissions emitted by the engine during the test. To prevent the loss of any unburned hydrocarbons that might adsorb or condense on the surface of the heat exchanger, the particulate sample must be taken upstream of the heat exchanger.

It is clear that the EPA required PDP-CVS system is very expensive. Some researchers have simplified the EPA standard dilution tunnel and developed their own systems. There are a number of examples of successful simplified dilution tunnels [86, 87, 88, 89, 90]. Some of them were full-flow type dilution tunnels, and some draw a constant fraction of the total exhaust gas into the dilution tunnel. The dilution tunnel used in this study is a simplified, full-flow device.

The quantity of particulate matter collected with sample filters depends on the conditions of the dilution tunnel, such as the dilution ratio, the sample filter temperature, etc.

The *dilution ratio* is the ratio of diluted exhaust gas mass flow rate to the raw exhaust mass flow rate. The temperature of the diluted exhaust gas is a function of its dilution ratio. With the assumptions of adiabatic dilution and constant specific heats, the minimum dilution ratios were calculated to be 3.5:1 and 10:1 to bring raw exhaust gases at 400 K and 600 K to the diluted exhaust temperature to 325 K [91].

When the temperature at the particulate sample filters is kept constant, the particulate concentration will drop with lower dilution ratio because the temperature of the diluted exhaust will be higher. On the other hand, if the dilution ratio is high enough (greater than 100:1), the particulate concentration will decrease with increasing dilution ratio because of the low concentration of vapor phase unburned hydrocarbons. The change of particulate mass is primarily attributable to the change of its soluble portion. MacDonald et al. [92] used a mini-dilution tunnel to study the individual effects of dilution ratio and particulate sample filter temperature on diesel engine particulate measurement. A 0.5-L single cylinder diesel engine was used to generate the particulates under steady state conditions. When the temperature of the sample filter was increased from 35 °C to 100 °C while the dilution ratio was maintained at 10.8:1, the particulate concentration was decreased by 13%. When the filter temperature was held constant at 52 °C and the dilution ratio was increased from 5:1 to 100:1, the collected particulate mass was decreased approximately 26%. These changes in the total particulate mass were shown to be due to the changes in the soluble fraction in the particulates.

Frisch et al. [93] also investigated the effect of dilution ratio on diesel particulate emissions using a Caterpillar 3208 DI diesel engine and a partial flow dilution tunnel. The dilution ratio was increased from 1:1 to 50:1. They reported that the measured total particulate concentration increased as the dilution ratio was increased. The fuel properties, such as distillation temperature, API gravity, and aromatic content, also had a significant effect on the soluble organic fraction level.

2.6 Modeling Particulate Emissions during the Dilution Process

As discussed in Section 2.1, the soluble portion of the particulates is formed during the exhaust gas dilution process. The SOF can have a significant effect on the collected amount of

total particulates and is dependent on dilution variables such as dilution ratio and sample temperature. The possible mechanisms affecting the formation of SOF are condensation, diffusion, and adsorption. Plee et al. [14] studied the three possible processes theoretically. First, the Clausius-Clapeyron equation was used to simulate the formation of SOF by condensation processes. By definition, condensation will occur if the vapor pressures (P_{HC}) of the gas phase hydrocarbons exceed their saturated vapor pressure (P_{sat}). Plee used the ratio of P_{HC}/P_{sat} to estimate the fraction of unburned hydrocarbon which was present on the soot particle surface at a given dilution ratio and filter temperature. In the condensation model, the fraction of unburned hydrocarbons in the particulates was a function of the saturation ratio, P_{HC}/P_{sat}, and the ratio was a function of the diluted exhaust gas temperature, the initial unburned hydrocarbon concentration, and the boiling point of the hydrocarbons. They assumed that the concentration of HC was 13 ppm (as hexane), and three typical compounds which could be represent in the SOF were used, the final, 50%, and initial boiling point of the extracted substance, where they corresponded to the 90% boiling point of the lubricating oil (811K), the initial boiling point of the lubricating oil (672 K), and final boiling point of the fuel (612 K), respectively. The results of the simulation showed that condensation was favored by low dilution ratio, low filter temperature (which was a result of high dilution ratio), high unburned hydrocarbon concentration, and compounds with high boiling point. By comparing with their previous experimental results [92], the predicted results from the condensation mechanism failed to predict the experimentally observed trends with varying filter temperature and dilution ratio.

The second mechanism examined by Plee et al. [14] was mass diffusion. Both transport of unburned hydrocarbons to the soot particle surface (inter-phase diffusion) and penetration of the hydrocarbon vapor into the solid carbon particles (intra-phase diffusion) were considered. The phenomenon of diffusion could take place as long as a concentration gradient was present. Plee et al. simulated the diffusion process with Fick's Law, and found that the quantity of hydrocarbon absorbed on the carbon particle surface by diffusion increased with filter temperature. These results conflicted with their previous experimental results, where the quantity of SOF was decreased with increasing filter temperature.

Therefore, Plee concluded that the diffusion mechanism also did not control the formation of SOF in the particulates.

The last mechanism that Plee investigated was adsorption. The adsorption process could occur at saturation ratios less than unity. Only physical adsorption was assumed, and the Langmuir isotherm model was used in their study. The Langmuir isotherm equation is based on the kinetic equilibrium between adsorption and desorption. Because they did not have enough information to compute the rate coefficient of adsorption (K) and the adsorption energy (E) of the SOF, the values of K and E were chosen arbitrarily. The results predicted by the model indicated that the adsorption fraction of the SOF decreased nonlinearly and did not drop off sharply with increasing filter temperature. The fraction of adsorbed SOF also decreased when the dilution ratio was increased. For both cases, the adsorption simulation gave the same trends as the experimental results. Plee et al. [14] concluded that the adsorption of unburned hydrocarbon vapor on the solid carbon surface appeared to be the dominant mechanism during the SOF formation process. However, both condensation and adsorption might be important under conditions of high hydrocarbon concentrations.

Clerc et al. [13] used the BET adsorption isotherm equation to model the formation of SOF in diesel particulates. The BET isotherm can simulate the multilayer adsorption process which is closer to the actual formation process of SOF than the Langmuir isotherm equation. To complete the prediction of SOF formation, Clerc et al. assumed that the SOF consisted of heptadecane only which represented the 50% boiling point of the vapor phase unburned hydrocarbon emissions from the Caterpillar 3208 diesel engine used in their study. Clerc also assumed that only physical adsorption controlled the SOF formation. The concentration of unburned hydrocarbons (the adsorbate in the adsorption system) was determined with a HFID and the concentration of solid carbon particles (the adsorbent) was found based on raw exhaust opacity using the Beer-Lambert Law, and was assumed not to change during the dilution process. The predicted results showed a consistent trend with that from the experiment and with the results from Plee's study [14]. The model-predicted SOF concentration was within 35% and the total particulate concentration was within 25% of measured values.

The BET adsorption isotherm equation was also used to predict the SOF formation in diesel particulates for raw exhaust gas by Johnson [12]. Because the unburned hydrocarbon emissions and the adsorbed SOF consist of various hydrocarbon compounds, the IAS (Ideal Adsorbed Solution) theory was applied to predict multicomponent adsorption in Johnson's model. The IAS model needs single component adsorption data to complete the prediction, so the BET isotherm and Langmuir isotherm equations are used to provide this information. In the IAS multicomponent adsorption model, the adsorbed SOF is assumed to be an ideal liquid and the unburned hydrocarbons in vapor phase are assumed to be an ideal gas mixture. The concentrations of solid carbon and gaseous HC which were the adsorbate and adsorbent in the adsorption system were determined from the results of engine experiments. The adsorption energy of the unburned hydrocarbons was calculated as a function of carbon number in the straight-chain hydrocarbons. The composition of the unburned hydrocarbons was measured with gas chromatography monitored by a flame ionization detector (FID). The measured carbon distribution was from C_1 to C_{40}, and n-alkanes were assumed to represent those components in the hydrocarbons. Based on these assumptions and experiment information, the predicted adsorption of the BET-IAS model showed a strong function of carbon number in the hydrocarbons. However, the predicted amount of adsorbed hydrocarbon was very small. This was possibly due to the high temperature applied on the adsorption system because the adsorption was predicted for hot undiluted exhaust gas.

The adsorption mechanism has also been used by other researchers to investigate the diesel particulate formation during the dilution process and the effects of dilution ratios and filter temperature on the SOF formation [94, 95].

Despite the fact that formation models for the total particulates produced during the exhaust gas dilution process have been reported, there are few models that predict biodiesel particulate formation in the dilution tunnel and study the effects of HC sampling line conditions on biodiesel unburned hydrocarbon emission measurement. During this project, both experimental and theoretical studies were conducted to investigate the effects of dilution tunnel conditions on the biodiesel particulate formation and the effects of HC sampling line conditions on biodiesel HC emission measurement.

3. MODEL DEVELOPMENT FOR CONDENSATION AND ADSORPTION OF UNBURNED HYDROCARBONS

Although diesel engine total particulate and unburned hydrocarbon emissions can be measured with a dilution tunnel and a heated flame ionization detector (HFID), respectively, predictive models can be used to interpret the measurements and to explain unexpected results. This can save considerable time and expense.

When the incomplete combustion products, such as solid carbon (SOL) and unburned hydrocarbons (HC), leave the combustion chamber and enter the exhaust system and dilution tunnel, the concentration of solid carbon will be frozen because the temperature is too low for carbon oxidation. However, during the dilution process, some of the vapor phase unburned hydrocarbons will collect on the surface of the carbon particles to form the soluble organic fraction (SOF). There are two possible mechanisms, condensation and adsorption, that control the amount of SOF formed on the particulates during the dilution process. These processes can be modeled to predict the formation of SOF and total particulate emissions. The extent that each of these two physical processes participates depends on the unburned hydrocarbon concentration, the diluted exhaust gas temperature, the pressure, and the properties of the unburned hydrocarbons. The concentration of unburned hydrocarbons in the heated sampling line of the HFID is also dependent on these two mechanisms. The condensed and adsorbed HC may deposit on the sampling line wall or on the carbon particle surface and be collected by the filter in the HFID so that the HC concentration is lowered by the time when the sample gas arrives at the burner of the HFID. In this chapter, these two mechanisms will be discussed in detail, and the corresponding models will be developed. A model for the condensation process will be developed first, followed by the adsorption process.

3.1 Condensation Process

The physical phenomenon of condensation takes place when the partial pressure of unburned hydrocarbons (P_{HC}) in the diluted and raw exhaust gases exceeds its saturation vapor pressure (P_{sat}). Khatri et al. [96] have suggested that condensation of unburned

hydrocarbons in the vapor phase may be responsible for the presence of significant organic extractable on the carbon particle surface. Their results showed that moderate dilution ratios (between 5 and 50) allowed for the highest saturation ratio of P_{HC} to P_{sat}. Thus, the strongest driving force for condensation occurs in roughly the same dilution ratio range used by a typical dilution tunnel system (between 5 and 10). The vapor pressure of the unburned hydrocarbons depends on the dilution ratio, while its saturation vapor pressure is a function of temperature. The HC partial pressure can be expressed as a function of its initial concentration, the atmospheric pressure, and the dilution ratio.

3.1.1 Model of unburned hydrocarbon vapor condensation

A criterion used to determine whether or not condensation will occur is the saturation ratio, P_{HC}/P_{sat}, where P_{HC} is the vapor pressure of the unburned hydrocarbons in the engine exhaust gas (either diluted or in the raw exhaust gases) and P_{sat} is the saturation vapor pressure of the unburned hydrocarbons at a given temperature. The saturation vapor pressure is a function of saturation temperature and the substance. Therefore, the quantity of the condensed unburned hydrocarbons not only depends on their temperature, but also on whether their vapor pressure exceeds the corresponding saturation vapor pressure. Thus, the amount of condensed hydrocarbons is dependent on the concentration of vapor phase hydrocarbons in the exhaust gas.

The condensation of unburned hydrocarbons can be simulated by calculating their saturation vapor pressure and partial pressure in the exhaust gas. The partial pressure of the unburned hydrocarbons can be determined by assuming that their behavior is the same as an ideal gas. Because the concentration of unburned hydrocarbons from a diesel engine is very low (about 300 ppm as C_1 in the raw exhaust gas for the engine used in this study), the partial pressures of the individual hydrocarbon compounds are also very low. The assumption of ideal gas behavior is appropriate for the unburned hydrocarbon vapor, especially after the dilution process.

The total unburned hydrocarbon vapor pressure in the diluted exhaust gas is expressed as,

$$P_{HC} = \frac{y_{HC}}{\overline{DR}} P_{atm} \qquad (3\text{-}1)$$

where P_{HC} = the total unburned hydrocarbon pressure in the diluted exhaust gas.

P_{atm} = the pressure in the dilution tunnel. Assumed equal to atmospheric pressure.

y_{HC} = the molar fraction of total unburned hydrocarbons in the raw exhaust gas that was measured with the HFID during the engine emission test.

$\overline{DR}$ = the molar dilution ratio (mole ratio of diluted exhaust to undiluted exhaust).

The total unburned hydrocarbon emissions from the diesel engine consists of various C-H and C-H-O species. When the term "hydrocarbon" is used in this dissertation, the oxygenated hydrocarbons, such as esters and aldehydes, that are also present in the exhaust are assumed to be included. For diesel fuel, the distribution of unburned hydrocarbons is from C_1 to C_{40} [97, 98]. The higher carbon number species may originate with the lubricating oil. The composition of the HC emissions from biodiesel or its blends with diesel fuel also shows a wide range of carbon numbers. Because the actual composition of the unburned hydrocarbons is very complex and is not known, some assumptions about the composition of the unburned hydrocarbon emissions must be made.

- The composition of the unburned hydrocarbon from diesel fuel is assumed to consist of n-dodecane only. Normal-dodecane is a commonly used surrogate for diesel fuel. This assumption is also consistent with the common assumption that the average composition of the exhaust HC is equal to the average composition of the fuel.
- The composition of unburned hydrocarbons from neat biodiesel is the same as the composition of biodiesel. The composition of the neat biodiesel used in this study is shown in Table 3.1.
- For various biodiesel blends (biodiesel and diesel fuel), their unburned hydrocarbon emission compositions have the same composition as the corresponding fuel. Fosseen [99] has reported that the biodiesel was the primary composition that caused the increase of soluble fraction in the particulate matter when he ran a 6V-71N

Table 3.1 Composition of neat biodiesel (%)

Composition		Fraction by mass	Fraction by mole
Methyl palmitate	$C_{17}H_{34}O_2$	10.95	11.83
Methyl stearate	$C_{19}H_{38}O_2$	3.70	3.62
Methyl oleate	$C_{19}H_{36}O_2$	21.91	21.59
Methyl linoleate	$C_{19}H_{34}O_2$	55.01	54.59
Methyl linolenate	$C_{19}H_{32}O_2$	8.43	8.37

certification engine fueled with 20% biodiesel blend to study the composition of the SOF. The assumed unburned hydrocarbon compositions of the various possible tested blends are shown in Table 3.2.

More accurate data about the carbon number distribution of the HC emissions of various fuels could be obtained by analyzing the composition of the SOF with high pressure liquid chromatography (HPLC). However, this equipment was not available for this study.

The partial pressure of each unburned hydrocarbon compound in the diluted exhaust gas can be written as:

Table 3.2 Composition of unburned hydrocarbon (% by mass)

Fuel		Diesel	20% biodiesel	50% biodiesel	100% biodiesel
n-Dodecane	$C_{12}H_{26}$	100.00	80.00	50.00	0.00
Methyl palmitate	$C_{17}H_{34}O_2$	0.00	2.37	5.92	10.95
Methyl stearate	$C_{19}H_{38}O_2$	0.00	0.72	1.81	3.70
Methyl oleate	$C_{19}H_{36}O_2$	0.00	4.32	10.80	21.91
Methyl linoleate	$C_{19}H_{34}O_2$	0.00	10.92	27.30	55.01
Methyl linolenate	$C_{19}H_{32}O_2$	0.00	1.67	4.19	8.43

$$P_i = \frac{y_i y_{HC}}{DR} P_{atm} \qquad (i = 1, 2, \ldots\ldots, N) \qquad (3\text{-}2)$$

where P_i = the partial pressure of each species in the diluted exhaust gas.

y_i = the molar fraction of each unburned hydrocarbon species of the total HC emissions shown in Table 3.1 for the different fuels.

Then, the saturation ratio, R_i, of the unburned hydrocarbon partial pressure to its saturation pressure for each individual species is,

$$R_i = \frac{P_i}{P_{sat,i}} = \frac{y_i y_{HC}}{DR} \times \frac{P_{atm}}{P_{sat,i}} \qquad (i = 1, 2, \ldots\ldots, N) \qquad (3\text{-}3)$$

where $P_{sat,\,i}$ = the saturation vapor pressure of each individual HC component.

As soon as the saturation ratio exceeds unity, the condensation of unburned hydrocarbon vapor takes place. An expression for the fraction of the total amount of an unburned hydrocarbon species that is condensed at a given condition specified by the dilution ratio, temperature, and initial HC concentration, can be developed as follows.

The fraction of condensed HC, F_i, on the particle surface is:

$$F_i = \frac{y_{dil,i} - y_{sat,i}}{y_{dil,i}} \qquad (i = 1, 2, \ldots\ldots, N) \qquad (3\text{-}4)$$

where $y_{dil,\,i}$ = the molar fraction of the individual unburned hydrocarbon species in the diluted exhaust gas.

$$y_{dil,i} = \frac{y_i y_{HC}}{DR} \qquad (i = 1, 2, \ldots\ldots, N) \qquad (3\text{-}5)$$

$y_{sat,\,i}$ = the saturation molar fraction of the individual unburned hydrocarbon species.

The term, $y_{sat,i}$, can be calculated from equations (3-3) and (3-5) when the saturation ratio R_i is equal to one. At the saturation state ($R_i = 1$)

$$y_{dil,i} = y_{sat,i} = \frac{y_i y_{HC}}{\overline{DR}} \qquad (i = 1, 2, \ldots\ldots, N)$$

Substituting this relation into equation (3-3) gives:

$$y_{sat,i} = \frac{P_{sat,i}}{P_{atm}} \tag{3-6}$$

After substituting this expression into equation (3-4), the fraction that is condensed of each unburned hydrocarbon species in the diluted exhaust gas is:

$$F_i = 1 - \frac{\overline{DR}}{y_i y_{HC}} \times \frac{P_{sat,i}}{P_{atm}} = 1 - \frac{1}{R_i} \tag{3-7}$$

The absolute quantity of each condensed unburned hydrocarbon can be determined as:

$$\dot{m}_i = F_i \times y_{dil,i} \frac{\dot{m}_{dil}}{MW_{dil}} MW_i \tag{3-8}$$

where $\dot{m}_i$ = the mass condensation rate of the individual HC species.

$\dot{m}_{dil}$ = the mass flow rate of the diluted exhaust gas.

MW_i = the molecular weight of the individual HC species.

MW_{dil} = the molecular weight of the diluted exhaust gas which is assumed to be the same as the molecular weight of air (28.97 g/mole).

The total condensed unburned hydrocarbon rate, $\dot{m}$, is determined as:

$$\dot{m} = \sum_{i=1}^{N} \dot{m}_i \tag{3-9}$$

Equation (3-7) also shows that condensation of unburned hydrocarbon vapor occurs if the species partial pressure is higher than its saturation pressure. The units used in this study will be grams of each HC compound per kg of exhaust gas emitted from the engine (undiluted).

To use either the condensation model, equation (3-8), or to calculate the saturation ratio, equation (3-3), the properties of the unburned hydrocarbons are required. This is particularly true of the saturation pressure, which is needed to predict the amount of condensed unburned hydrocarbon vapor on the particle surface.

3.1.2 Saturation vapor pressure of unburned hydrocarbons

An expression that can be used to calculate the saturation vapor pressure is the Clausius-Clapeyron equation that assumes a constant enthalpy of vaporization:

$$P_{sat} = P_{atm} \exp\left[\frac{-h_{fg}}{R}\left(\frac{1}{T} - \frac{1}{T_b}\right)\right] \tag{3-10}$$

where P_{sat} = the saturation vapor pressure of unburned hydrocarbons.

P_{atm} = the atmospheric pressure.

T = the saturation temperature of unburned hydrocarbons.

T_b = the boiling point of unburned hydrocarbons at atmospheric pressure (P_{atm}).

R = the gas constant.

h_{fg} = the enthalpy of vaporization of unburned hydrocarbons.

However, the enthalpy of vaporization of any liquid depends on state variables, such as temperature,

$$h_{fg} = h\{T, P_{sat(T)}\} \tag{3-11}$$

The Clausius-Clapeyron equation in this form will not give the exact value for the enthalpy of vaporization because of the assumption of a constant enthalpy of vaporization. Fortunately, there are many empirically-based equations that have been developed to describe the relationship between saturation pressure and temperature. Some of these equations are correlations whose parameters are adjusted by fitting experimental vapor pressure data, and some are prediction equations that have the same form as the correlation relationships. However, their parameters are predicted from other data, such as the normal boiling temperature, critical constants, etc.

The study of saturation pressure and its equations begin with Dalton in about 1800 [100]. He may be the first person to have accurately measured saturation pressure, and he produced a linear equation relating the saturation pressure and the absolute temperature. Clapeyron developed his equation for a change of state in 1834, and Clausius integrated it for gaseous transitions in 1850. During the following time period, much experimental work was done, and many new equations were developed. Because of simplifying assumptions implicit in the Clausius-Clapyron equation, a series of semiempirical equations has been proposed which modified the Clausius-Clapeyron equation in different ways. A few of these saturation pressure equations are shown in Table 3-3. One of the most frequently used equations is that developed by Antoine [101]. It has the form:

$$\log P_{sat} = A - \frac{B}{T + C} \qquad (3\text{-}12)$$

where A, B, and C are constants characteristic of the substance. The Antoine equation accurately represents the behavior of most substances over a limited temperature range.

The correlations shown in Table 3.3 were obtained to fit experimental data within a specific temperature range. Although published data is available for esters, it is usually between 150 and 240 °C. When the correlations are used for a lower temperature range, such as from 30 to 80 °C which are the typical temperatures in a dilution tunnel, their predictions for the saturation pressure deviate severely for some esters. However, the saturation pressure

Table 3.3 Selected saturation pressure equations

Equation	Developer	Date
$\log P = A + BT$	Dalton [102]	1800
$\log P = C\log(A + BT)$	Young [102]	1820
$\log P = AT/(B + CT)$	Roche [102]	1830
$\ln P = -\Delta H/RT + A$	Clausius-Clapeyron [102]	1850
$\log P = A + B/T + C\log T$	Dupre-Rankine [102]	1866
$\log P = A - B/(T + C)$	Antoine [101]	1888
$\ln P = A_0/T + A_{ln}\ln T + A_1 + DP/T^2$	Frost-Kalkwarf [103]	
$\ln P = A_0/T + A_{ln}\ln T + A_1 + A_7T^6$	Riedel [103]	
$\ln P = A_0/T + A_1 + A_2T - A_3T^2$	Cragoe [104]	
$\log P = A + B/T + C\log T + DT + ET^2$	Yaws [105]	1994

of most of n-alkanes and esters show a linear relationship between $\log_{10}(P_{sat})$ and $1/T$ as shown in Figure 3.1. The relationship between P_{sat} and T can be expressed in the following form (which can be viewed as a version of the Antoine equation) [106]:

$$\log_{10}(P_{sat}) = \frac{\alpha}{T} + \beta \qquad (3\text{-}13)$$

where α and β are correlation constants.

The linear relationship between $\log_{10}(P_{sat})$ and $1/T$ can be easily determined by performing a linear regression on the experimental data. Figure 3.1 shows the regression lines for the esters as well as for n-dodecane, the species used to represent the unburned hydrocarbons from diesel fuel. These relations were used in this study to predict the saturation pressures. The detailed regression process and the original saturation pressure data are discussed in Appendix A.

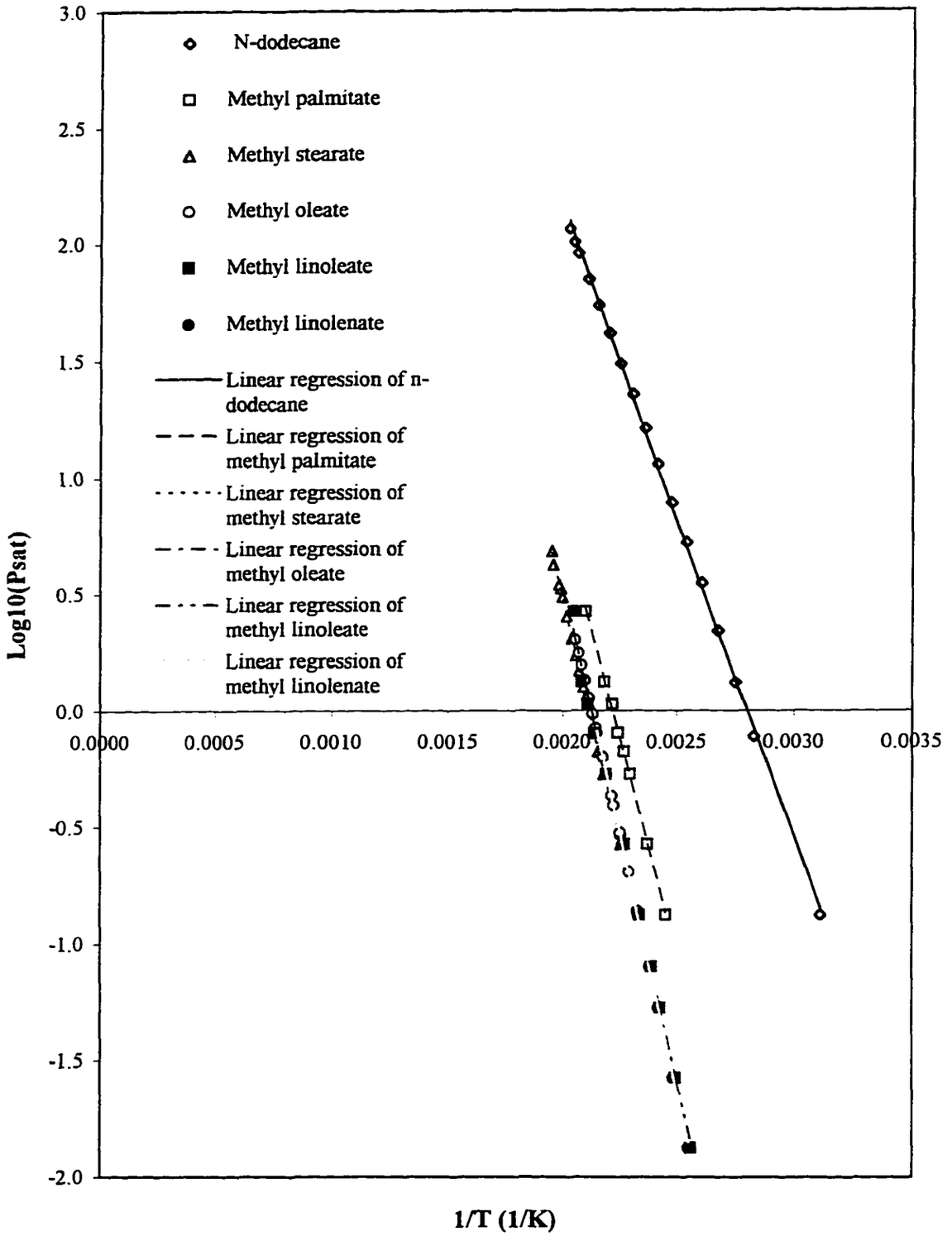

Figure 3.1 Relationship between saturation pressure and temperature [106, 107, 108, 109]

3.1.3 Application of the condensation model

The developed condensation model is ready for the prediction of the soluble fraction formation on the carbon particle surface. A FORTRAN program was written that incorporates the condensation model. This program first calculates the saturation ratio of each hydrocarbon specie. If the saturation ratio of a species is greater than one, its condensation will take place and its condensed molar fraction is calculated. Based on the information of the total diluted exhaust gas flow rate and the fraction of each hydrocarbon in the diluted exhaust gas, the amount of each condensed hydrocarbon can be determined. The total quantity of condensed hydrocarbons is the sum of each condensed hydrocarbon.

To use this model to predict the quantity of condensed unburned hydrocarbons on the carbon particle surface during the exhaust gas dilution process, certain input data are required: the concentration of total unburned hydrocarbons in the raw exhaust gas, the dilution ratio, the pressure, and the temperature in the dilution tunnel. The input data for HC concentration were measured with the HFID during the engine emission experiment. The HC concentrations for the fuels and engine operating conditions measured during the experiment will be discussed in Chapter 5. The dilution ratio and temperature can be selected as the input variables. When different dilution ratios or temperatures are input, the effects of each of them on the hydrocarbon condensation can be investigated.

The condensation model can predict both the total amount of condensed unburned hydrocarbons and the condensed quantity of each HC compound in units of g/kg exhaust gas. When the condensation model is used to study the concentration change of the unburned hydrocarbons in the HC sampling line, the dilution ratio is set equal to one which corresponds to the raw exhaust gas case. Different HC sampling temperatures can be input to this model to investigate whether or not HC condensation takes place in the HC sampling line.

3.2 Adsorption Process

Adsorption of unburned hydrocarbons on the carbon particle surface is another possible mechanism that contributes to the formation of soluble fraction HC during the engine exhaust gas dilution and during the exhaust gas sample transport in the HC sampling line. This

physical phenomenon takes place even at saturation ratios less than unity. The word *adsorption* is believed to have been first used by Kayser to describe his observations of the condensation of gases on free surfaces in 1881 [110]. When two phases, at least one of them gaseous, contact, the composition of these phases close to the phase boundary will differ from the composition observed in regions distant from that boundary. This will occur even though the phases are in equilibrium. The increase in concentration in the region where the phases are in mutual contact is called adsorption. It is obvious that adsorption is a surface phenomenon. The solid substance upon whose surfaces adsorption occurs is termed the *adsorbent*. Since adsorption occurs on surfaces, a substance that qualifies as a good adsorbent must have a large surface area on a per-unit-mass basis. The adsorbed substance is called the *adsorbate*. There may be one or more adsorbates in a given adsorption situation.

As mentioned before, there are many species in the diesel engine exhaust gas. However, usually only the particles of solid carbon (soot) and the vapor phase unburned hydrocarbons participate in the adsorption process to form the particulate emissions. The carbon particles serve as the adsorbent and the unburned hydrocarbons act as the adsorbate that will adsorb on the surface of the carbon particle.

3.2.1 Classification of adsorption

Adsorption is the process which governs the interaction of a vapor or gas with a solid surface, and it occurs due to attractive forces present on the surface of the solid. Adsorption can be further divided into two processes, physical adsorption (commonly referred to as physisorption) and chemical adsorption (referred to as chemisorption) [111].

Physical adsorption involves a relatively weak attractive force, the van der Waals force, and is based on dispersion or polar interactions between the surface and the adsorbed molecule. This is a long-range and weak interaction that can be divided into three parts: dipole-dipole interactions between polar molecules, dipole-induced-dipole interactions, and finally induced-dipole-induced-dipole or dispersion interactions [111].

The amount of energy released when a molecule is physically adsorbed on a surface is of the order of the enthalpy of condensation of the adsorbate. This energy is generally

absorbed as vibration of the lattice and dissipated as heat. The released energy is insufficient to lead to bond breaking, and so in physical adsorption the molecule retains its identity. Physical adsorption is highly reversible, does not change the chemical nature of the adsorbate, has a low activation energy, and may involve more than one layer of adsorbate (multilayer). Physical adsorption is negligible for adsorbates above their critical temperature. There is a difference between physical adsorption and condensation in that the interaction at the surface provides thermodynamics favorable to adsorption at pressures below saturation, and at temperatures which may be above the normal boiling point of the adsorbate.

In chemical adsorption, the molecules stick to the surface as the result of the formation of a new chemical, usually through a covalent bond. The energy of attachment is much greater than for physical adsorption, and typical values are in the region of 200 kJ/mol [111]. Because it involves a chemical reaction, chemical adsorption is a very selective, irreversible process in which the chemical nature of the adsorbate is changed. Chemical adsorption only occurs when the adsorbate can come into direct contact with the adsorbent, therefore only a single monolayer can be chemically adsorbed onto a surface.

Generally, the distinction between physical adsorption and chemical adsorption of gases on solid adsorbents does not present difficulties. The distinction can be summarized as [112]:

- Energy of adsorption – small in the case of physical adsorption, large in the case of chemical adsorption (the same order as the enthalpy change of the relevant chemical reaction).
- Reversibility – the adsorbed substance can be reversibly removed from the surface when physical adsorption is involved. However, the removal of a chemically adsorbed layer is very difficult and is irreversible.
- Thickness of adsorbed layer – in the case of physical adsorption, under suitable conditions of temperature and pressure, adsorbed layers are formed having thicknesses of several diameters of the adsorbate molecule. In chemical adsorption only monolayers are formed.

During the dilution process of the engine exhaust gas in a dilution tunnel and the transport process in a HC sampling line, chemical adsorption does not occur to a significant extent due to the relatively low temperature. Therefore, in this study, only the theory of physical adsorption will be discussed in detail, and the adsorption model of unburned hydrocarbons will be developed based on the theory of physical adsorption.

3.2.2 Model of unburned hydrocarbon vapor adsorption

As discussed previously, the diesel particulate matter primarily consists of two portions, the solid carbon portion and the soluble organic fraction. The concentration of carbon particles is usually constant by the time they enter the engine exhaust system, especially during the dilution process, because the temperatures in the exhaust system and in the dilution tunnel are too low to oxidize the carbon particles. The final mass of total particulates is governed by the amount of soluble organic fraction that forms on the surface of the carbon particles. Adsorption is one of the possible mechanisms that control the total particulate emissions during the dilution process. The purpose of developing an adsorption model is to predict the total particulate emissions when the exhaust gas is diluted in a dilution tunnel for a diesel engine fueled with different fuels. In addition, the adsorption model can also be used to investigate the HC concentration change when the engine exhaust gas sample is transported in a HC sampling line at different temperatures because HC adsorption may take place in the HC sampling line and cause incorrect HC measurement.

Adsorption theories are an attempt to describe the process of adsorption in terms of physically meaningful variables. Variables include the concentrations of HC and carbon particles, the dilution ratio, the temperature and pressure in the dilution tunnel, and the fuel properties.

Because the unburned hydrocarbons in diesel exhaust gas consist of various C-H and C-H-O species, the actual adsorption processes occurring in the dilution tunnel and the HC sampling line are multicomponent adsorption. To predict the adsorption process with multiple components, multicomponent adsorption theory should be applied. However, prediction of the unburned hydrocarbon adsorption on the diesel particulates is a difficult task due to the large

number of organic compounds present in diesel exhaust gas [113]. The difficulty is increased because of possible variations in the chemical character of the hydrocarbon emissions with engine operating conditions [114]. To simplify the composition of the unburned hydrocarbons in order to predict the adsorption with multicomponent adsorption theory, the assumed unburned hydrocarbon composition used previously for the condensation model, shown in Table 3.2, is also applied for the adsorption model.

There are some established approaches to predicting multicomponent adsorption. One of them, called Ideal Adsorption Solution theory (IAS) developed by Mayers [115] can be used to predict multicomponent adsorption by analogy with liquid-vapor equilibrium over a saturated liquid mixture. Another method to treat the multicomponent adsorption is the application of the theory of volume filling of micropores. The adsorption system may also be solved using statistical thermodynamics. Some commonly used multicomponent adsorption models are the extended Langmuir equation [110], extended Langmuir-Freundlich equation [110], vacancy solution theory [116], and potential theory [117]. Because the IAS theory was used as the basis for the adsorption model used to predict the formation of soluble organic fraction on the carbon particle surface, it will be discussed in more detail in the following section.

3.2.2.1 Ideal Adsorbed Solution theory

The Ideal Adsorbed Solution (IAS) theory was developed by Mayers and Prausnits [115] in 1965 for gas mixture adsorption, and was extended to multicomponent liquid-phase adsorption by Radke and Prausnitz [118] in 1972. It is a general theory capable of predicting multicomponent adsorption equilibrium from the pure-component adsorption isotherm data of the individual adsorbates.

The adsorption isotherm is an assumption that the adsorption system temperature is constant when the adsorption occurs. During particulate emission measurement, the exhaust gas of the diesel engine is diluted in the dilution tunnel. Although the partial pressure of each unburned hydrocarbon species depends on its concentration and the dilution ratio, the temperature at the particulate sample filters will be kept constant. Therefore, the adsorption of

unburned hydrocarbons on the carbon particle surface can be modeled as an adsorption isotherm. The same situation is true in the HFID sampling line.

The fundamental equations of IAS theory are analogous to the equations used to describe conventional gas and liquid systems and are assumed to be applicable to the gas and adsorbed phases, respectively. For example, the adsorbed liquid phase is assumed to be an ideal solution. Raoult's Law for the ideal solution states is expressed as,

$$Py_i = P_{vap}x_i \qquad i = 1, 2, \ldots\ldots, N \tag{3-14}$$

where P = the total equilibrium vapor pressure of the mixture gas.

x_i = the molar fraction of the ith component in the adsorbed phase.

P_{vap} = the vapor pressure of component i.

The analog of Raoult's Law for the adsorption system is,

$$Py_i = P_i^o x_i \qquad i = 1, 2, \ldots\ldots, N \tag{3-15}$$

where P_i^o = a hypothetical pressure of the ith adsorbate in its pure-component adsorption that yields a spreading pressure, π.

y_i = the molar fraction of the ith component in the gas phase.

x_i = the molar fraction of the ith component in the adsorbed phase.

$P_i^o(\pi)$ can be thought of as the pure adsorbate vapor pressure for component i at the temperature T and the spreading pressure π of the mixture. The spreading pressure is a measure of the change of the Gibbs free energy of the adsorption interface due to adsorption, and is referred to as the adsorbate's adsorption potential.

Based on the IAS theory, when the spreading pressures of each component in the adsorption system are equal, the multicomponent adsorbates are in equilibrium with one another. The vapor phase of the multicomponent adsorption system is assumed to be an ideal gas and the ideal gas equation follows:

$$P_i V = n_i RT \tag{3-16}$$

Based on the ideal gas equation, the analogous adsorption equation is,

$$\pi_i A = n_i RT \tag{3-17}$$

where π_i = the spreading pressure of a single component.

A = the surface area of the adsorbent.

n_i = the number of adsorbed moles of component *i* that is governed by an adsorption isotherm.

The relationship between π_i and P_i^o can be found with Gibbs' adsorption theorem, where the spreading pressure at P_i^o is calculated from Gibbs' integral over the region $P = 0$ to $P = P_i^o$.

$$\pi_i(P_i^o) = \frac{RT}{A}\int_0^{P_i^o} \frac{n_i^o(P_i^o)}{P_i^o} d\,P_i^o \qquad i = 1, 2, \ldots\ldots, N \tag{3-18}$$

where n_i^o and P_i^o are the equilibrium adsorbed phase concentration and the pressure of the vapor phase in the pure component adsorption of the *i*th adsorbate, respectively. One more assumption for the IAS model for the adsorbed phase is that there is no change in the specific adsorption area (adsorption area per mole of adsorbate) upon mixing the various adsorbates.

Under the equilibrium conditions between the vapor and adsorbed phases, the chemical potential of any adsorbate in the two phases is the same at constant temperature and spreading pressure, thus equation (3-18) will consist of N - 1 equations, $\pi_1(P_1^o) = \pi_2(P_2^o) = \ldots\ldots = \pi_N(P_N^o)$. Another equation is needed before the multicomponent adsorption problem can be solved for the individual P_i^o. Because the specific adsorption area is inversely proportional to the adsorbed phase concentration, one relationship can be built as,

$$\frac{1}{n_t} = \sum_{i=1}^{N} \frac{x_i}{n_i^o} \tag{3-19}$$

where n_t is the total adsorbed adsorbate on the solid surface. The amount of adsorption of the ith adsorbate, n_i, is determined as,

$$n_i = n_t x_i \tag{3-20}$$

The Nth equation used to solve for the N values of P_i^o is,

$$\sum_{i=1}^{N} x_i = 1 \tag{3-21}$$

The N equations consist of the system of equations describing the multicomponent adsorption equilibrium between the vapor and the adsorbed phases. The molar fractions of the adsorbed phase, x_i, can also be determined from Raoult's Law,

$$x_i = \frac{P y_i}{P_i^o} \tag{3-22}$$

The steps required to solve for the multicomponent adsorption of unburned hydrocarbons during the dilution process can be summarized as following:

- A suitable pure component adsorption isotherm equation is required to determine the value of n_i^o that is the adsorbed quantity of each HC component in the single-component case.
- The total pressure of the diluted exhaust gas, P, and the composition of the vapor phase unburned hydrocarbons, y_i, that is a function of the dilution ratio, must be specified for the adsorption system.

- N -1 equations are obtained from the condition of the same spreading pressure with this form,

$$\pi_i(P_i^o) = \pi_{i+1}(P_{i+1}^o) \qquad (i = 1, 2, \ldots\ldots, N\text{-}1)$$

- The Nth equation is found with the requirement of,

$$\sum_{i=1}^{N} x_i = 1$$

which is based on Raoult's Law.

- The N unknowns, $P_1^o, P_2^o, \ldots\ldots, P_N^o$, are solved from these N equations. The individual and total adsorbed moles can determined using equations (3-20) and (3-19), respectively.

The Gibbs' integration, equation (3-18), can be performed only when a pure component adsorption isotherm equation is assigned. The pure component adsorption isotherm model will be discussed in the following section.

3.2.2.2 Model of pure component adsorption isotherm

A number of theoretical models exist to describe the relationship between the amount of a single adsorbate adsorbed on a solid surface and the adsorbate concentration in the bulk phase. Since the adsorption process and the analysis are usually carried out at constant temperature, the relationships are referred to as isotherms. Because the adsorption process occurs at a constant temperature condition when the engine exhaust gas is diluted in the dilution tunnel and the HC sample is transported in the heated HC sampling line of the HFID, an adsorption isotherm is assumed to be appropriate to describe these processes.

The simplest adsorption case involves one adsorbate (single-component) in the adsorption system. Some adsorption models used for the single-component adsorption isotherm will be reviewed first.

- **The Freundlich adsorption isotherm**

An empirical equation for the adsorption isotherm relating the quantity of adsorbed adsorbate to the gas phase pressure was proposed by Boedecker [112] in 1895 with this form,

$$\theta = K_F P^{1/n} \tag{3-23}$$

where θ = the fraction of the first molecular layer filled by adsorbate.

K_F = the Freundlich constant.

P = the gas phase pressure.

n = constant.

This adsorption isotherm is one of the earliest attempts to make an analytical study of adsorption. Due to efforts by Freundlich [119] to popularize its application, the equation has become known as the Freundlich adsorption isotherm. Although it is simple, this adsorption model does not always accurately predict adsorption for a wide range of pressures. It has been widely used as an empirical equation for qualitative research [112].

- **The Langmuir adsorption isotherm**

The first theoretical approach to the study of adsorption was undertaken by Langmuir [120]. He proposed that there were a definite number of sites on the adsorbent surface, and only one adsorbate molecule could be adsorbed at each of these sites. Langmuir made the assumptions that the interactions between the adsorbed molecules in the adsorbed layer and the homogeneous adsorbent surface can be neglected and that only one mono-molecular adsorption layer can be formed on the surface of the adsorbent. By using the kinetic equilibrium approach, the Langmuir adsorption isotherm equation had the form,

$$\theta = \frac{kP}{1 + kP} \tag{3-24}$$

where k = the equilibrium constant.

P = the gas phase pressure.

The adsorption initially shows a linear relation between the gas phase pressure and the adsorption fraction. When the adsorbate partial pressure in the gas phase is sufficiently high, that is, $kP >> 1$, the fractional coverage will approach one, and the adsorbent surface becomes saturated with a mono-molecular adsorbate layer.

- **The BET adsorption isotherm**

The Langmuir isotherm is not representative of all isotherms. Brunauer [121] divided the adsorption isotherm into five types as shown in Figure 3.2 that illustrates the relationship between adsorbed mole number (n^s) and the saturation ratio (P/P_{sat}). Type I is the Langmuir isotherm type, characterized by a monotonic approach to a limiting adsorption that presumably corresponds to a complete monolayer. The flat region in the type I adsorption isotherm, where the pressure ratio P/P_{sat} approaches one, has never been observed for physical adsorption. This type is observed in chemical adsorption at pressure ratios (P/P_{sat}) far below one. Type II is common in the situation of physical adsorption and corresponds to multilayer adsorption. Type III is relatively rare and is characteristic of an energy of adsorption equal to or less than the enthalpy of vaporization of the adsorbate. The pressure ratio $P/P_{sat} = 1$ is approached by adsorptions of type II and III asymptotically, and adsorption on powdered samples has shown this behavior experimentally. An adsorption isotherm of type IV suggests that the adsorption causes the formation of two surface layers. Type V is found in the adsorption of water vapor on an activated carbon surface. Both types IV and V are considered to reflect capillary condensation phenomena in that they level off before the saturation pressure is reached and may show hysteresis effects [122].

The type II adsorption isotherm has became of considerable practical importance due to its popularity in physical adsorption research on high energy, powdered solids. In 1938, Brunauer, Emmett, and Teller developed a multilayer

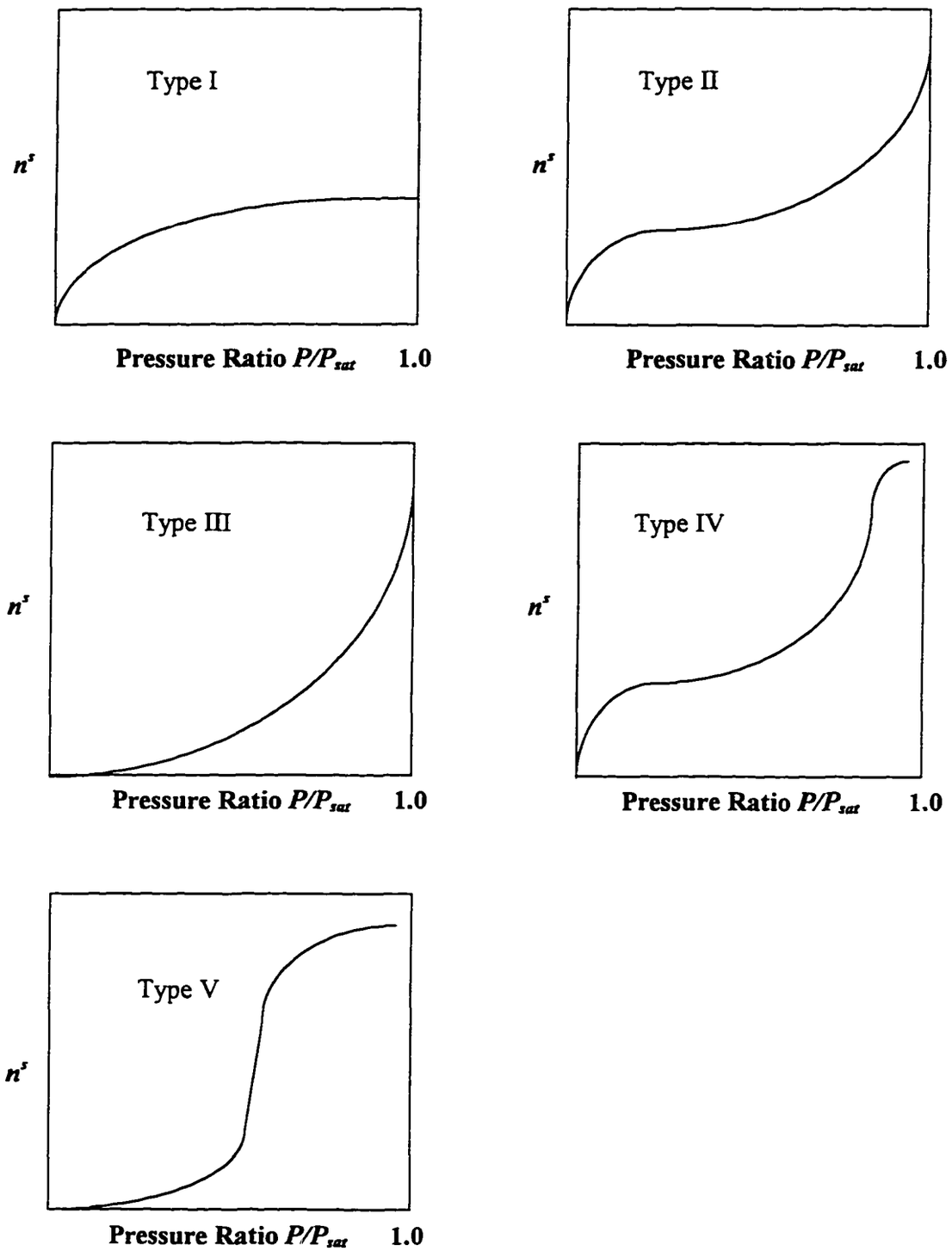

Figure 3.2 Five types of adsorption isotherm [121]

adsorption theory that was to extend Langmuir's approach to multilayer adsorption, and their model has come to be known as the BET adsorption isotherm equation [123]. The assumptions of their theory were that the Langmuir equation could be applied to each adsorption layer, and that an adsorbate molecule encountering an occupied site on the adsorbent surface did not leave the site immediately, but formed a short-lived layer. With a vapor pressure increase, the number of free sites on the adsorbent surface decreases as the pressure ratio P/P_{sat} approaches one. The number of active sites occupied by single adsorbate molecules decreases in the same way because double, triple, and more adsorption layers are formed.

By using the kinetic equilibrium, the final BET isotherm equation is,

$$\theta = \frac{cx}{(1-x)[1+(c-1)x]} \tag{3-25}$$

where $x = P/P_{sat}$.

$c = k_1/k_2$.

k_1 = the adsorption equilibrium constant for the first adsorbed layer.

k_2 = the adsorption equilibrium constant for the higher adsorbed layers.

Usually, k_1 is much greater than k_2.

There are other commonly used adsorption isotherm models, such as the Harkins-Jura equation [124, 125], potential theory [110], etc. In addition, the isotherm models can be derived using thermodynamic approaches [110] and statistical methods [126].

Among these models of adsorption isotherms, the Langmuir and BET isotherms are the most important models within the engineering and chemistry areas. Both have been applied to model hydrocarbon adsorption in diesel exhaust [12, 13, 14, 94]. Because the Langmuir isotherm only treats the adsorption as a monolayer process, it is not suitable to model the adsorption process occurring during the exhaust gas dilution process. The adsorption of unburned hydrocarbons on the carbon particle surface is a multilayer process. If an adsorption equation that has the capacity to predict the multilayer adsorption process is

used in the model of unburned hydrocarbon adsorption, the adsorption model will better predict the quantity of adsorbed unburned hydrocarbon. Therefore, the BET isotherm was selected as the equation to calculate the single component adsorption for the IAS multicomponent adsorption model. The BET adsorption isotherm will be discussed in more detail in the following section.

3.2.2.3 Multilayer adsorption isotherm - BET model

When a vapor is adsorbed at a given temperature that is below its critical temperature, its adsorption is not limited to the formation of a single adsorption layer. Because of the influence of the adsorbent, the van der Waals force field on the surface of the monolayer is stronger than the force field between molecules of the vapor so that for the higher adsorption layers, molecules may be deposited at a given site at lower pressure P than the saturation pressure P_{sat}. The second and higher layers may even be formed before the formation of the first one has been filled due to the favorable configuration entropy term [127].

When adsorption of a vapor becomes infinitely high, the adsorption can be characterized as condensation at the saturation vapor pressure. The typical multilayer adsorption shows the same adsorption trend as Type II in Figure 3.2. With increasing the vapor pressure, as P tends to P_{sat}, the adsorption should increase further. Under this condition, the adsorption layer grows thicker. When $P = P_{sat}$, vapor condensation occurs. Then, the adsorption becomes multilayer, and the isotherm passes through a point of inflection.

The flat region of the Type I adsorption isotherm (the Langmuir isotherm) shown in Figure 3.2 has never been observed as pressures approach P_{sat} [122]. The Langmuir isotherm disregards the possibility that an initial overlayer may act as a substrate for further adsorption to give a multilayer adsorbate. Brunauer, Emmett, and Teller [123] developed their multilayer adsorption theory to extend Langmuir's approach to multilayer adsorption. For the BET adsorption isotherm model, some essential assumptions are made that are also used for the Langmuir isotherm [110]:

- Adsorption of adsorbate molecules occurs at well-defined localized sites.

- On the adsorbent surface, there are a definite number of active sites, S, at each of which only one adsorbate molecule may be adsorbed, and all the adsorption sites are energetically identical.
- Interactions between neighboring adsorbed adsorbate molecules can be neglected.
- The adsorbent surface is homogeneous.

The BET model considers the adsorption process in terms of kinetic theory and applies the Langmuir equation to each layer. The model has the added postulate that the energy of adsorption for the first layer of adsorbed adsorbate would have some special value, E_a, that is the adsorption energy of the adsorbate, and the energy of adsorption for additional layers would equal to the energy of vaporization of the adsorbate, E_v. Actually, the adsorption energies of the second and higher layers are not equal, but the differences are usually much smaller than that between the first and second layers. A further assumption is that adsorption and desorption can only take place on the exposed surfaces. Once a layer is covered by the next layer, it no longer interacts with the vapor phase [123]. Figure 3.3 illustrates the way the adsorbent surface is covered by the adsorbate.

The condition for adsorption equilibrium is taken to be that the rates of adsorption and desorption become equal. For the first layer,

$$a_1 P S_0 = b_1 S_1 \tag{3-26}$$

where a_1 and b_1 are the rate constants of adsorption and desorption, respectively.

The equation for the second layer is,

$$a_2 P S_1 = b_2 S_2 \tag{3-27}$$

where a_2 and b_2 are the rate constants for the second layer.

In general, for all other succeeding layers,

$$a_i P S_{i-1} = b_i S_i \tag{3-28}$$

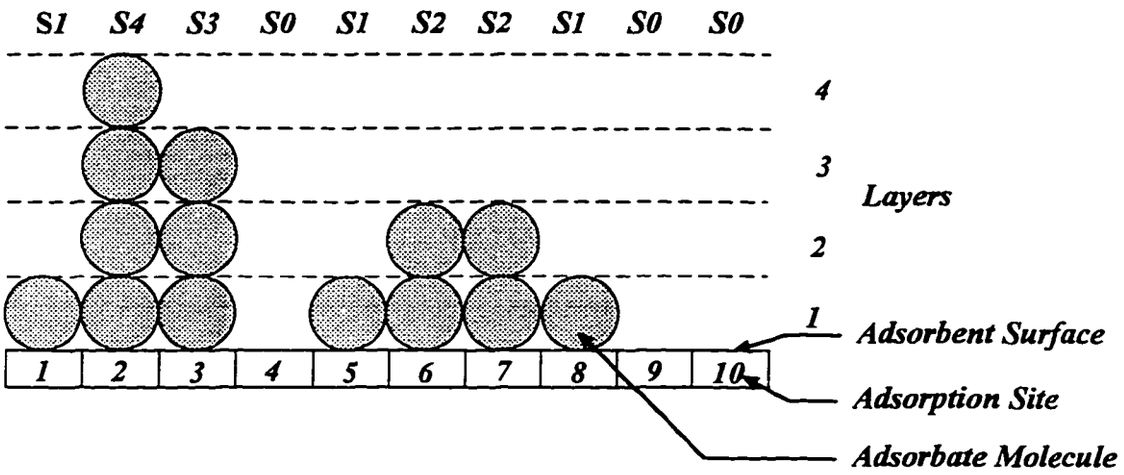

Characteristics of the adsorbent surface:

Total available adsorption sites (total monolayer site number) $S = \sum_{i=0}^{4} S_i = 10$.

Bare site number $S_0 = 3$.

Site number covered by monolayer adsorbate $S_1 = 3$.

Site number covered by two layer adsorbates $S_2 = 2$.

Site number covered by three layer adsorbates $S_3 = 1$.

Site number covered by four layer adsorbates $S_4 = 1$.

Total number of adsorbed molecules $S_{tot} = \sum_{i=0}^{4} i\, S_i = 14$.

Degree of surface coverage $\theta = \frac{S_{tot}}{S} = 1.4$.

Figure 3.3 Adsorption process for BET isotherm model [127]

where i = 2 to ∞.

By assuming that all layers except the first layer behave similarly, the rate constants, $a_2 = a_3 = \ldots\ldots = a_i = a$ and $b_2 = b_3 = \ldots\ldots = b_i = b$.

The last equation can be expressed in terms of S_o as,

$$S_i = \frac{a_i}{b_i} P S_{i-1} = (\frac{a}{b})^{i-1} \frac{a_1}{b_1} P^i S_o \qquad (3\text{-}29)$$

Let $a/b = x'$, and $a_1/b_1 = cx'$, where c is related to the adsorption and desorption rate constants for different adsorbed layers. With these definitions, a new expression for equation (3-29) is,

$$S_i = c(x'P)^i S_o \qquad (3\text{-}30)$$

Because a monolayer site contributes one molecule, a bilayer holds two molecules, and so on, the total volume of material adsorbed, v, at a given condition is proportional to the total number of molecules adsorbed,

$$v \propto S_1 + 2S_2 + 3S_3 + \ldots\ldots = \sum_{i=1}^{\infty} iS_i \qquad (3\text{-}31)$$

When an adsorption equilibrium is reached, the monolayer volume coverage with the adsorbed adsorbate is,

$$v_m \propto S_1 + S_2 + S_3 + \ldots\ldots = \sum_{i=0}^{\infty} S_i \qquad (3\text{-}32)$$

The adsorption fraction, θ, is defined as the ratio of the total amount adsorbed, n or the adsorbed volume v, to the amount adsorbed at monolayer coverage of the adsorbent, n_m or

v_m. So, the adsorption fraction can be determined as the ratio of the number of adsorbed adsorbate molecules to the number of adsorbed molecules necessary for a complete monolayer. The number of adsorbate molecules adsorbed for the monolayer coverage is equal to the number of adsorption sites present on the adsorbent surface. The total number of adsorbed molecules will be the sum of the number of adsorption sites available on each layer multiplied by the number of layers below that layer. This can be visualized as a stack of adsorbed adsorbate molecules on each of the adsorption sites.

$$\theta = \frac{v}{v_m} = \frac{n}{n_m} = \frac{S}{S_o} = \frac{\sum_{i=1}^{\infty} i S_i}{\sum_{i=0}^{\infty} S_i} \tag{3-33}$$

Substituting equations (3-30), (3-31), and (3-32) into equation (3-33) gives,

$$\theta = \frac{\sum_{i=1}^{\infty} i S_i}{\sum_{i=0}^{\infty} S_i} = \frac{c S_o \sum_{i=1}^{\infty} i (x' P)^i}{S_o + c S_o \sum_{i=1}^{\infty} (x' P)^i} \tag{3-34}$$

Since $\sum_{i=1}^{\infty} i y^i = \frac{y}{(1-y)^2}$ and $\sum_{i=1}^{\infty} y^i = \frac{y}{1-y}$, if y is substituted for $x'P$, and these two expressions are substituted into equation (3-34), the summations can be eliminated from the expression for θ.

$$\theta = \frac{c S_0 \frac{x' P}{(1-x' P)^2}}{S_0 (1 + c \frac{x' P}{1 - x' P})} \tag{3-35}$$

which rearranges to,

$$\theta = \frac{cx'P}{(1-x'P)[1+(c-1)x'P]} \tag{3-36}$$

Finally, when the adsorbate in the vapor phase and the adsorbed adsorbate layer which is deeply and uniformly buried are in equilibrium, the condition for equilibrium is,

$$aSP = bS, \text{ or } P = b/a,$$

where S is the total number of sites. When an equilibrium applies at the surface of the bulk adsorbed adsorbate that is in the liquid state, regardless of whether or not the surface is deeply buried under it, the equilibrium pressure, P, can be identified as the saturation vapor pressure of the adsorbate, P_{sat}. The ratio of $x' = a/b$ can written as,

$$x' = \frac{a}{b} = \frac{1}{P_{sat}} \tag{3-37}$$

After introducing this relation into equation (3-36), the BET isotherm equation is obtained,

$$\theta = \frac{cx}{(1-x)[1+(c-1)x]} \tag{3-38}$$

where θ = the adsorption fraction that is the ratio of the total amount adsorbed hydrocarbon to the amount adsorbed at monolayer coverage of the hydrocarbon.

$x = \frac{P}{P_{sat}}$.

P = the partial pressure of the adsorbate or of each vapor phase HC species.

P_{sat} = the saturation pressure of each vapor phase HC species.

The term, c, in the BET isotherm model is related to the adsorbate's adsorption and vaporization energies, and is defined as,

$$c = \frac{a_1 b}{b_1 a} \tag{3-39}$$

The adsorption and desorption rate constants for the first and other layers can be expressed as,

$$a_1 = a_{1o} \exp(\frac{E_a}{RT}) \tag{3-40}$$

$$b_1 = b_{1o} \exp(\frac{E_d}{RT}) \tag{3-41}$$

$$a = a_o \exp(\frac{E_v}{RT}) \tag{3-42}$$

$$b = b_o \exp(\frac{E_f}{RT}) \tag{3-43}$$

where a_{1o} and b_{1o} = the forward and backward rate constants for the first adsorbed layer.

a_o and b_o = the forward and backward rate constants for the higher adsorbed layers.

E_a and E_d = energies of adsorption and desorption, respectively.

E_v and E_f = energies of evaporation and condensation, respectively.

R = the gas constant.

These relations can be combined with equation (3-39) to give:

$$c = \frac{a_{1o} b_o}{b_{1o} a_o} \exp(\frac{\Delta E_{ads} - \Delta E_{vap}}{RT}) \tag{3-44}$$

where $\Delta E_{ads} = E_a - E_d$, the adsorption energy of the adsorbate.

$\Delta E_{vap} = E_v - E_f$, the vaporization energy of the adsorbate.

The group containing a_{1o}, b_{1o}, a_o, and b_o is usually approximately equal to one [12].

The BET equation (3-36) reveals the relationship between the amount of adsorbed vapor on the adsorbent surface, the partial pressure of the adsorbate, and the local temperature through P_{sat} and c. Additionally, the adsorption process is influenced by the physical and chemical characteristics of the adsorbent and the adsorbate as reflected in the parameters n_m, c, and P_{sat}. Therefore, the BET adsorption model will be useful in relating the SOF concentration to the diluted diesel exhaust gas temperature, the unburned hydrocarbon concentration, the carbon particle concentration, and the properties of the unburned hydrocarbons.

The Gibbs' integration that is used to predict the multicomponent adsorption for the engine exhaust gas discussed in section 3.2.2.1 can be performed with the BET isotherm equation. By substituting equation (3-38) into equation (3-18), the spreading pressure of each component in the unburned hydrocarbons is:

$$\pi_i = \frac{RT}{A} n_{m,i} \ln\left[\frac{P_{sat,i} + P_i^o (c_i - 1)}{P_{sat,i} - P_i^o}\right] \qquad (3\text{-}45)$$

Because the IAS model was not dependent on the single-component adsorption isotherm equation, it is reasonable to perform IAS analysis with the multilayer BET isotherm equation. Some researchers have used the IAS theory with different pure-component adsorption isotherms to predict multicomponent adsorption. The IAS model has been used to predict the adsorption isotherm for two component systems, such as methane-ethane mixtures, ethylene-carbon dioxide mixtures on activated carbon, and mixtures of carbon monoxide-oxygen and propane-propylene on silica gel [115]. The predicted isotherms showed excellent agreement with experimental data. Valenzuela and Myers [128] used IAS theory with the Toth equation and the UNILAN equation, which are single component adsorption isotherm equations, to predict mixture adsorption, and published their results as a handbook of

adsorption of gas mixtures. Johnson [12] also used the IAS model to investigate the adsorption of hydrocarbons in diesel engine exhaust gas. So, the IAS theory is perhaps the most widely tested and used multicomponent adsorption model.

However, to perform the prediction of unburned hydrocarbon adsorption on the carbon particle surface, the following data are required to be input to the adsorption model:

- T = the adsorption system temperature.
- P = the partial pressure of the individual HC component in the diluted exhaust gas.
- P_{sat} = the saturation pressure of the individual HC component in the diluted exhaust gas.
- A_m = the area occupied by an adsorbed HC molecule.
- E_{ads} = the adsorption energy.
- E_{vap} = the vaporization energy.
- n_m = the monolayer capacity of the individual HC component.

The other information required for the adsorption model are the concentrations of the carbon particles that serve as the adsorbent and the unburned hydrocarbons that act as the adsorbate in the adsorption system, and the dilution ratio. These concentrations were measured during the engine emission tests. The determination of the partial and saturation pressures of each HC component in the exhaust gas was discussed in the section describing the condensation model. The remaining parameters such as the adsorption energy, the vaporization energy, the area occupied by an adsorbed HC molecule, and the monolayer capacity of each individual HC component will be described in the following sections.

3.2.2.4 Energies of adsorption and vaporization of unburned hydrocarbons

When the amount of each unburned hydrocarbon compound adsorbed on the carbon particle surface is predicted by using the BET adsorption isotherm model, the energies of adsorption and vaporization are required. The energy of vaporization, also called the enthalpy of vaporization, is a fundamental quantity characterizing the energy of the vapor-liquid equilibrium. Thermodynamically, it is defined as the difference between the enthalpies of the vapor and liquid phases at a given temperature and the corresponding saturation vapor

pressure, P_{sat}. From the molecular point of view, the enthalpy of vaporization may be regarded as the energy required to overcome the forces binding the molecules in a liquid and subsequently do the work of expansion against the saturation vapor pressure to the volume of the saturated vapor. From a practical view, the enthalpy of vaporization represents the amount of heat that must be supplied to transform a substance from the liquid to the gas phase at the equilibrium saturation vapor pressure.

The enthalpy of vaporization is dependent on temperature. As the liquid temperature increases, its enthalpy of vaporization will be decreased. This physical property can be estimated with empirical correlations. One approximate calculation of the energy of vaporization is the Trouton equation [129],

$$\Delta E_{vap} = 21 T_b \tag{3-46}$$

where T_b is the boiling point of the substance. A more accurate equation was given by Kistiakowsky [129],

$$\Delta E_{vap} = 8.75 T_b - 4.571(\log T_b^2) \tag{3-47}$$

The energy of adsorption is the energy released upon the adsorption of an adsorbate by an adsorbent. Adsorption is an exothermic process. The general magnitude of the heat evolved serves as a clue to the nature of the forces involved and may be used to distinguish between physical adsorption and chemical adsorption. The adsorption energy is a function of coverage. With increasing coverage, the adsorption energy will decrease which means that the most favorable adsorption sites are filled first [130]. The adsorption energy is also a function of temperature. Avigul and Kiselev [131] showed that the energy of adsorption of n-alkanes on graphite was decreased by 5 to 10% when the temperature rose from 20 to 100 °C. In addition, the energy of adsorption is dependent on the chemical structure of adsorbates. For a given carbon number, the following order of energy can observed: alkanes > aromatics > olefins.

However, the energy of adsorption of unburned hydrocarbons, especially unburned hydrocarbons of biodiesel, has not been studied in detail. The energy of adsorption of the unburned hydrocarbons used in this study is based on research results which involved activated carbon in the adsorption systems. The adsorbates in these adsorption systems are usually alkane hydrocarbons.

The energy of adsorption of n-decane ($C_{10}H_{22}$) and dihydromyrcene ($C_{10}H_{18}$) on a fully reinforcing carbon black, Spheron 6, were measured by Schaeffer et al. [130]. They also summarized results of the heat of adsorption of other n-alkanes, such as ethane (C_2H_6), propane (C_3H_8), n-butane (C_4H_{10}), and n-pentane (C_5H_{12}), and obtained a equation that described the relationship between the energy of adsorption and the carbon number in n-alkanes.

$$\Delta E_{ads} - \Delta E_{evp} = 1.27 + 0.15n \quad \text{kcal/mole} \tag{3-48}$$

where n is the carbon number in the n-alkane molecules.

Based on the experimental results, Avgul and Kiselev [131] found that the energy of adsorption of n-alkanes increased linearly with increasing number of carbons in the molecules. Avgul and Kiselev developed the following relation between the energy of adsorption and the carbon number at 20 °C,

$$\Delta E_{ads} = 1.0 + 1.60n \quad \text{kcal/mole} \tag{3-49}$$

They also found a relationship between the energy of adsorption and the carbon number based on the dependence of the adsorption potential energy which represented a force of attraction and repulsion between an adsorbed n-alkane molecule and the carbon atoms in a graphite plane. Their model gave the following equation:

$$\Delta E_{ads} = 0.85 + 1.88n \quad \text{kcal/mole} \tag{3-50}$$

Among these correlations, Schaeffer's function, equation (3-48), has been applied in diesel unburned hydrocarbon adsorption by other researchers [12]. It also gives the difference between the energies of adsorption and vaporization. The results predicted by Avgul and Kiselev's equation (3-50) were slightly higher than their experimental results. This may be due to only flat-lying orientations being used in the model. On the other hand, the carbon black used their experiment was a highly crystalline form which was graphitized at 3000 °C. Diesel soot shows a poorly ordered surface with fewer optimum orientation sites available during adsorption. So, the correlation will give a higher energy of adsorption for diesel soot. Therefore, Schaeffer's correlation was chosen as the equation to calculate the energy difference between the adsorption and vaporization of unburned hydrocarbons in this study.

Because data or correlations for the adsorption energy of esters were not found in the literature, the correlation of adsorption energy for n-alkanes, Schaeffer's correlation, is also used to predict the energy of adsorption for the esters in this study.

3.2.2.5 Molecule size of unburned hydrocarbons

To find the monolayer capacity of the unburned hydrocarbons, their molecular size should be determined first which dictates the area occupied by a single adsorbed unburned hydrocarbon molecule. There are several methods that can be used to find the area occupied by an adsorbed molecule. If the volume of the adsorbed molecule is assumed to approximate a sphere, the projected area of this sphere can be used to estimate the molecule area where its diameter is calculated from the liquid density assuming close packing of the spheres. Another method used to determine the molecule area is based on the BET adsorption isotherm which requires measurement of the amount adsorbed on an adsorbent of known surface area. The crossectional area of the molecule can also be estimated based on its critical constants [132]. McClellan et al. [132] reviewed the available literature and took the average of up to 36 independent measurements for 106 compounds to obtain the values. They compared the results obtained from the liquid density and the BET isotherm methods, and found that the areas measured by the BET adsorption isotherm were higher than those from the liquid density method. This may be because the adsorbing molecules were not spherical, and tended

to move toward a state with lowest potential energy by assuming a flat orientation relative to the surface. McClellan also recommended an estimate of molecule area based on the density of the adsorbed material if a shape and packing of molecules can be assumed. Based on the assumption of spherical shape and hexagonal close packing, the following equation can be used to find the area for different molecules.

$$A_m = 1.091\left(\frac{MW}{N_{AV}\rho}\right)^{2/3} \tag{3-51}$$

where A_m = the cross section area of the molecule.

MW = the molecular weight.

N_{AV} = Avagadro number, $N_{AV} = 6.02205 \times 10^{23}$ mol^{-1}.

ρ = the density of the adsorbate in liquid state, g/cm^3.

The calculated crossectional areas of the unburned hydrocarbon molecules are included in Appendix B.

3.2.2.6 Monolayer capacity of unburned hydrocarbons

Because the adsorption isotherm models usually calculate the fraction of adsorption on the carbon particle surface, the monolayer capacity of the unburned hydrocarbons must be known. This depends on their molecule size and on the surface area of the unburned hydrocarbon molecules. Barris [95] used a surface area analyzer based on the BET isotherm for the adsorption of nitrogen on diesel carbon particles to determine the particle's specific surface area that was approximately 90 m^2/g. When he did the analysis, he assumed the density of the primary diesel carbon particle was 2 g/cm^3, and that the particles were spheres. With these conditions, the diesel carbon particle diameter was about 0.033 μm. The results from Vuk et al. [28] were in good agreement with this calculation based on electron microscopy measurements. When the diesel carbon particles were treated as spheres and their geometric surface area used as the area available for adsorption [12], the diesel soot specific surface area was 100 m^2/g which is close to the 90 m^2/g determined by Barris. Johnson [12]

also used the specific surface area of 90 m^2/g for diesel soot to model the adsorption of unburned hydrocarbon on the carbon particle surface. Based on these results, the value of 90 m^2/g for the specific surface area of the diesel carbon particle was used in this model. Because there is no published data about the carbon particle size from the products of ester combustion, the same specific surface area as diesel fuel was used for the esters contained in the biodiesel.

To calculate the adsorption conventionally, the carbon particle concentration in the engine exhaust gas was calculated, per kilogram of exhaust gas. The adsorbent or the carbon particle surface area concentration, can be determined from the following equation,

$$A_p = A_s \times m_c \tag{3-52}$$

where A_p = the carbon particle surface area concentration, m^2/kg exhaust gas.

A_s = the adsorbent specific surface area, m^2/g.

m_c = the concentration of carbon particle in engine exhaust gas, g/kg exhaust gas.

The monolayer capacity can be determined as,

$$n_m = \frac{A_p}{A_m N_{AV}} \tag{3-53}$$

This relationship assumes that the site area for the adsorbate includes an extra amount which accounts for the area left uncovered due to packing constraints.

3.2.2.7 The density of the liquid unburned hydrocarbons

The density of the liquid phase unburned hydrocarbons is needed to estimate the crossectional area of the HC molecules. Because the density is a strong function of temperature for liquid substances, its change should be considered when the formation of liquid phase unburned hydrocarbons is modeled. Several different methods are available to

calculate the liquid phase density at various temperatures. The Goldhammer method [133] gives one formula as,

$$\rho = MW\,\rho_b\left(\frac{1-T_r}{1-T_{br}}\right)^n \tag{3-54}$$

where ρ = the density.

MW = the molecular weight.

ρ_b = the molar density at the normal boiling point.

$T_r = T/T_c$, and T_c = critical temperature.

$T_{br} = T_b/T_c$, and T_b = boiling point.

n = a constant that depends on the chemical class that is shown in Appendix C.

Because the equation requires information about critical data, and it is difficult to find critical data for esters, other method was used in this study, called Grain's method [133]. Grain modified the Goldhammer method by approximating $T_c \approx 3/2T_b$. Then, equation (3-54) becomes,

$$\rho = MW\,\rho_b\left(3-2\frac{T}{T_b}\right)^n \tag{3-55}$$

The term, ρ_b, is the inverse of the molar volume, V_b. The molar volume can be calculated by summing incremental values for every atom, chemical structure, and bond in the compounds. The detailed calculation procedure is shown in Appendix C.

3.2.3 Application of the adsorption model

As discussed earlier, the adsorption model requires input data to predict the quantity of adsorbed SOF on the carbon particle surface during the exhaust gas dilution process. The general input information is:

- The concentration of the carbon particles in the raw engine exhaust gas serving as the adsorbent in the adsorption system, g/kg exhaust gas.
- The concentration of the unburned hydrocarbons in the raw engine exhaust gas serving as the adsorbate in the adsorption system, ppm as C_1.

Both of these quantities are determined during the engine emission experiment. They change with the engine operating conditions and the fuels used in the diesel engine. Detailed information on these concentrations can be found in Chapter 5.

- The pressure of the exhaust gas in the dilution tunnel (assumed as the atmospheric pressure, P_{atm} = 101.325 kPa).
- The temperature of the diluted exhaust gas, K.
- The dilution ratio.

The last two inputs served as the variables in the model to investigate the effects of the particulate filter temperature and the dilution ratio on the formation of SOF on the carbon particle surface during the dilution process. A FORTRAN program was written based on the multicomponent adsorption model. Other parameters, such as the partial pressure of each component in the diluted HC sample, the density of the liquid phase HC, and the monolayer capacity of the adsorbed HC. are calculated in the program according to the input information. The output of the model is the total adsorbed SOF and the adsorbed quantity of each component in the unburned hydrocarbons during the exhaust gas dilution process.

When the model is applied to the process of unburned hydrocarbon sample transport in the heated sampling line, the dilution ratio is set equal to one because no dilution air is added to the raw exhaust gas. The pressure in the HC sampling line is assumed to be the same as atmospheric pressure. Because the engine exhaust gas consists of several compounds, such as CO_2, CO, NO_x, HC, N_2, O_2, etc., one mixture molecular weight was needed to represent the exhaust gas molecular weight. The molecular weight of the exhaust gas was determined by assuming complete combustion at the proper equivalence ratio. The detailed derivation of the exhaust gas molecular weight is shown in Appendix D.

4. EXPERIMENTAL APPARATUS AND TEST PROCEDURE

In this chapter, the equipment used in this study, such as the engine, particulate measurement system, and emission analyzers, will be discussed. The fuels and test procedure will also be described in detail.

4.1 Diesel Engine Test Setup

A John Deere model 4276T, four-cylinder, four-stroke, turbocharged, direct injection diesel engine was used in this study. The basic engine specifications are illustrated in Table 4.1. The combustion system of the diesel engine is a bowl-in-piston and medium-swirl type. It is equipped with a distributor type fuel pump. The fuel injectors have four 0.305 mm diameter holes with an opening pressure of 250 bar. The diesel engine was connected to a 150 HP General Electric model TLC2544 direct current dynamometer.

Eleven thermocouples were mounted on the engine to monitor the temperatures of the inlet air, fuel, oil, coolant, and exhaust gas during the engine tests. In addition, another nine thermocouples were installed in the particulate measurement system and in the lab to measure and control the temperatures of the particulate sample system. There were three pressure probes on the engine to measure the engine's turbocharger boost pressure, exhaust back pressure, and the lubricating oil pressure with Bourdon pressure gages.

Table 4.1 Specifications of John Deere 4276T diesel engine

Bore	106.5 mm
Stroke	127.0 mm
Connecting rod length	202.9 mm
Compression ratio	16.8:1
Maximum power	57.1 kW @ 2100 rpm
Peak torque	305.0 Nm @ 1300 rpm
Firing order	1-3-4-2

The volume flow rate of air into the engine was determined using a Meriam laminar flow element with a Baratron differential pressure transducer to measure the pressure drop. The engine inlet air was drawn from another lab where the temperature was controlled at 293 K, but the humidity was not controlled. The fuel mass flow rate was measured using an electronic scale with a stopwatch. A heat exchanger and an electric heater were used to control the fuel temperature to 313 K.

4.2 Particulate Measurement System

The particulate measurement system consisted of two dilution tunnels, the dilution air sources, the particulate sampling system, the filter weighing chamber, and the extraction system. Each part of the system will be discussed in this section.

4.2.1 Dilution tunnel

Diesel engine particulate emissions are measured with a special measurement system based on specifications contained in the Code of Federal Regulations [23]. The measurement system requirements of the EPA have been discussed in Chapter 2.

The dilution tunnel used in this study was a simplified full-flow dilution tunnel. Since the test objective was not to try to determine whether or not the engine met EPA emission standards, an EPA type measurement system was not essential. The details of the design and validation tests were discussed in Bemett Murray's M.S. thesis [90]. Figure 4.1 shows the particulate measurement system including the primary and secondary dilution tunnels. The primary dilution tunnel was used to dilute the engine exhaust gas with compressed air, and the secondary tunnel was employed to mix a portion of the diluted exhaust gas with additional air.

The primary tunnel was built of standard galvanized spiral tubing in 1989. The material of the dilution tunnel was not ideal since it did not have a perfectly smooth interior. A rough interior increases the potential for particulate deposition, and could cause problems with particulates being reentrained into the stream during a later test. However, no abnormal phenomena were observed during the previous tests or this experiment.

The primary dilution tunnel was 0.305 meters in diameter and the distance between the

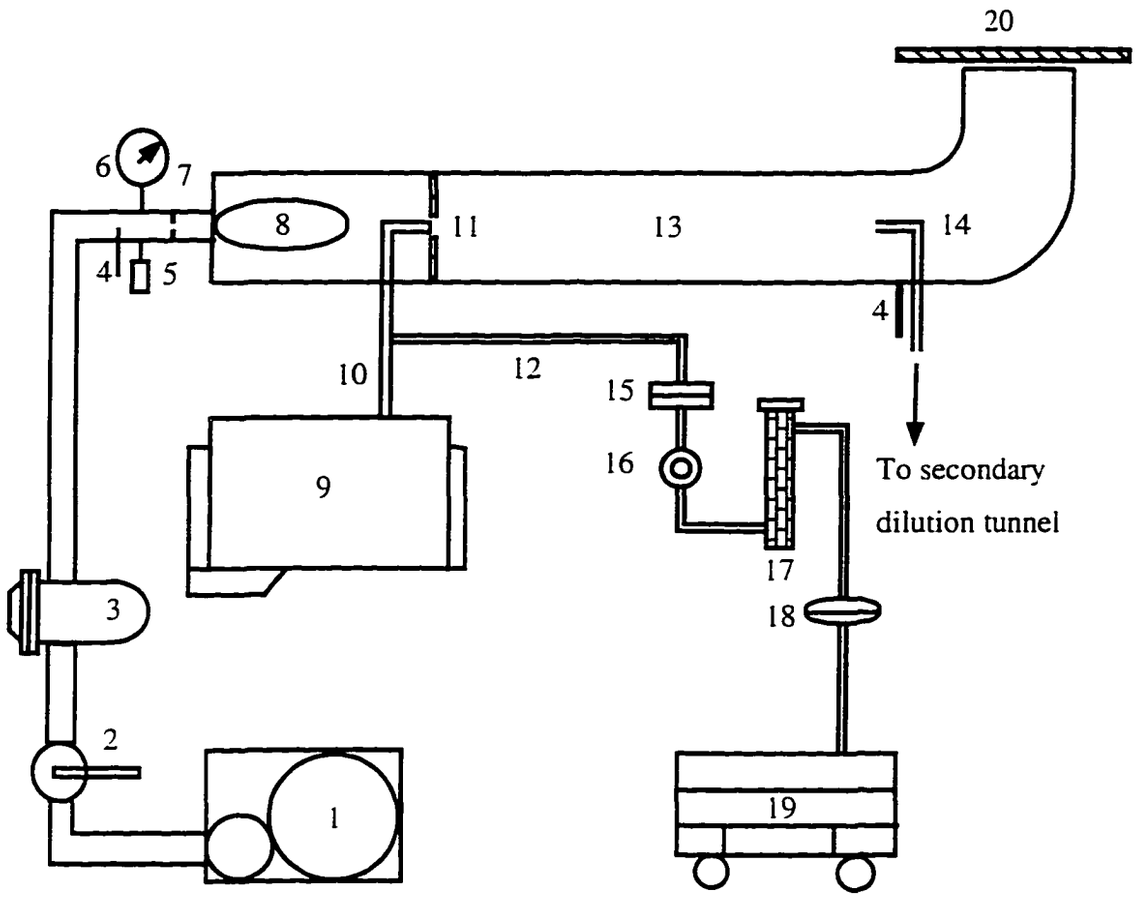

1. Centac II air compressor
2. Ball valve
3. Air filter
4. Thermocouple
5. Pressure transducer
6. Pressure gage
7. Orifice
8. Muffler
9. Diesel engine
10. Exhaust pipe
11. Mixing orifice
12. Gaseous emission sampling tube
13. Primary dilution tunnel
14. Particulate sampling probe
15. First filter
16. Sampling pump
17. Desiccant dryer
18. Secondary filter
19. Emission cart
20. Laboratory exhaust fan

Figure 4.1 Dilution system of particulate measurement

introduction of the engine exhaust gas and the particulate sample probe was 3.05 meters which corresponded to 10 dilution tunnel diameters. The distance provided sufficient time for mixing of the engine exhaust gas with the dilution air before the diluted exhaust gas was sampled by the particulate sampling system. The dimensions of the dilution tunnel were chosen so that a turbulent flow could be developed to ensure complete mixing of the exhaust gas and the dilution air, and the Reynolds number was higher than 1.0×10^5 inside the tunnel. That complete mixing occurs has been confirmed several times [90, 134].

A 90° elbow of 60 cm length exhaust pipe introduced the exhaust gas into the primary dilution tunnel. The elbow faced downstream of the dilution air and was used to direct the exhaust gas into the center of the dilution tunnel to ensure even mixing of the exhaust gas with the dilution air. A 20 cm diameter orifice was installed in the dilution tunnel at the point of entry of the exhaust gas to increase the flow velocity and turbulence of the dilution air. A high volume ceiling exhaust fan was located at the dilution tunnel exit which was turned on to ventilate the laboratory whenever the dilution tunnel was operated.

To eliminate the effects of changes in ambient temperature, the whole primary dilution tunnel was insulated so that no heat transfer occurred during the dilution process. The temperature change of the exhaust gas was caused only by the dilution. In addition, the engine exhaust pipe was also insulated between the turbocharger and the inlet port of the dilution tunnel.

To provide a wide range of dilution ratio during the engine tests, a secondary partial flow dilution tunnel was used as shown in Figure 4.2. The secondary dilution tunnel, made of aluminum, was 11.43 cm in diameter. A stainless steel particulate sample transporting pipe which faced upstream in the primary dilution tunnel was used to introduce the diluted exhaust gas into the secondary dilution tunnel. The length between the inlet plane and the exit plane of the tube was 53.0 cm. The length of the secondary dilution tunnel from the exit plane of the transporting pipe to the primary particulate sample filter was 12.7 cm. The secondary dilution tunnel had two functions during the particulate emission measurement, one was to increase the range of dilution ratio which could now reach over 100:1, and another was to increase the residence time of the diluted exhaust gas before it reached the particulate sample filters.

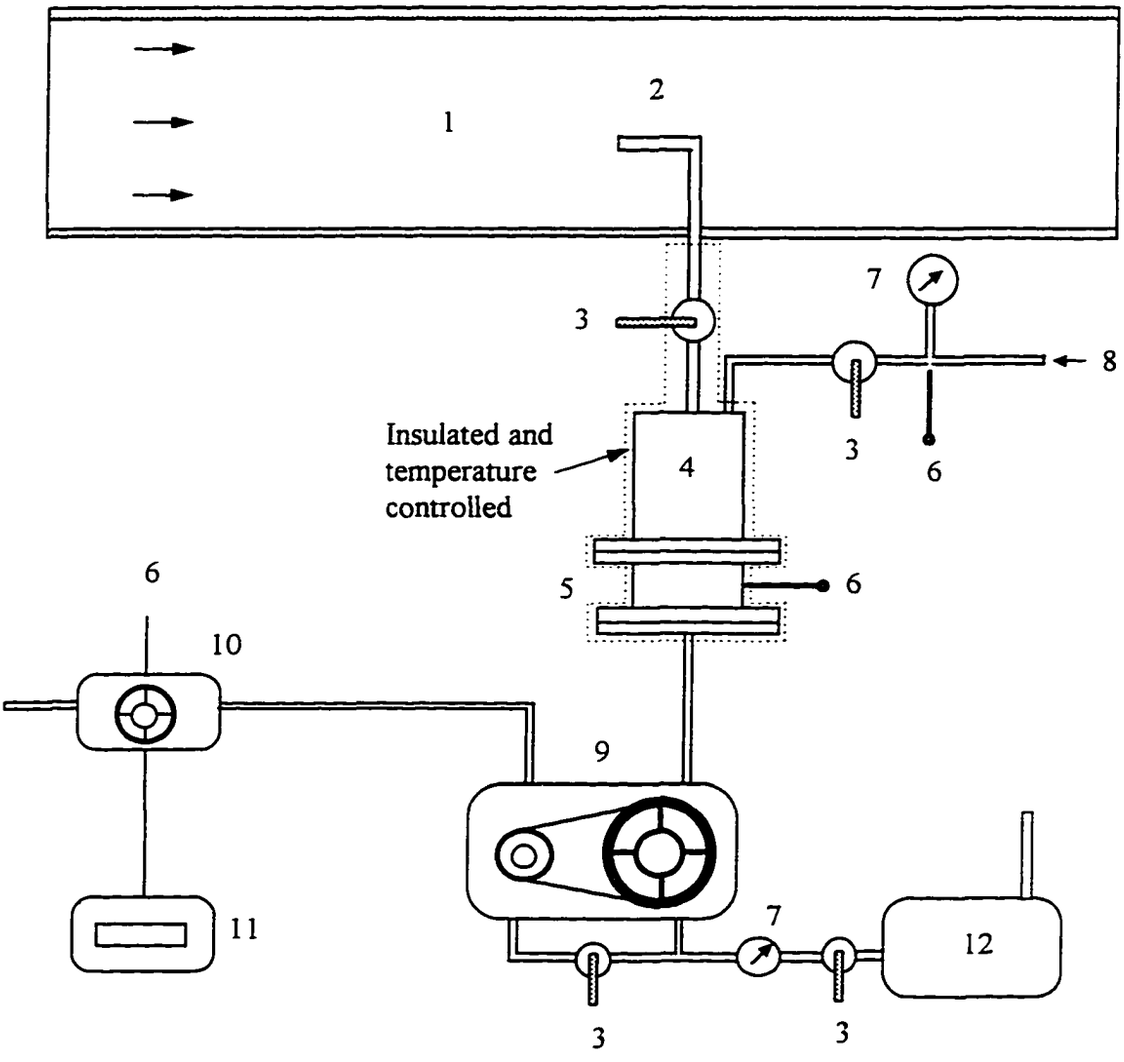

1. Primary dilution tunnel
2. Particulate sampling probe
3. Ball valve
4. Secondary dilution tunnel
5. Filter holder
6. Thermocouple
7. Pressure gage
8. Secondary dilution air
9. Sample pump
10. ROOTS meter
11. Frequency counter
12. Vacuum pump

Figure 4.2 Secondary dilution tunnel and particulate sample system

The temperature of the particulate sample was controlled with three heating tapes around the secondary dilution tunnel and the sample transporting pipe. The three heating tapes could be turned on or off individually to maintain the controlled temperature. The temperature control system consisted of temperature controllers, solid state relays, thermocouples, and heating tapes. The desired temperature could be controlled within $\pm$ 1.5 °C.

4.2.2 Dilution air system

The dilution air for the primary dilution tunnel was provided by an Ingersoll-Rand Centac II two-stage air compressor that developed an outlet gauge pressure of 620 kPa. The controller of the air compressor maintained the pressure within $\pm$ 7 kPa of the set point. The compressed air was introduced into the primary dilution tunnel through a 5 cm diameter pipe and the flow rate of dilution air was controlled by a ball valve as shown in Figure 4.1. A standard in-line air filter and a smooth-edged orifice were installed downstream from the valve. A Viatran model 141 pressure transducer and a thermocouple were located between the air filter and the orifice. The dilution air flow rate was determined by measuring the pressure and temperature of the compressed air on the upstream side of the orifice and using a calibration equation. The dilution air mass flow rate could be determined with equation (4-1). The calibration equation can be found in reference [90].

$$\dot{m}_{pd} = -0.195 + 0.0705\left(\frac{P_{por}}{\sqrt{T_{por}}}\right) - 0.806 \times 10^{-4}\left(\frac{P_{por}}{\sqrt{T_{por}}}\right)^2 \qquad (4\text{-}1)$$

where $\dot{m}_{pd}$ = mass flow rate of primary dilution air (kg/s).

P_{por} = absolute static pressure upstream of the orifice (kPa).

T_{por} = temperature upstream of the orifice (K).

The in-line air filter was installed to ensure that particles present in the dilution air did not enter the dilution tunnel. A test was conducted to determine the significance of particulates in the dilution air [134]. The test results showed that without an air filter, the filter

weight increase due to the particulates in the dilution air was only a small fraction of the engine exhaust particulates. When the air filter was used, the quantity of particulates in the dilution air was much lower than was observed without the air filter and the filter weight increase caused by the particulates from the air could be neglected.

An air-exhaust muffler was fitted to the end of the compressed air line to reduce the noise which was produced by the uncontrolled expansion of the dilution air when it entered the dilution tunnel. The dilution ratio, defined as the ratio of diluted exhaust mass flow rate to the raw exhaust gas mass flow rate, could be varied widely. The maximum dilution air mass flow rate that could be achieved was 0.74 kg/s. The mass flow rate of the engine exhaust gas varied between 0.058 kg/s for light-load at 1400 rpm to 0.066 kg/s for full-load at 1400 rpm engine conditions. Therefore, the maximum dilution ratios for these two engine conditions were 13.8:1 and 12.3:1, respectively.

The secondary dilution air system could provide additional air to the diluted exhaust gas sample that came from the primary dilution tunnel. The dilution air was from the Physical Plant of Iowa State University. An oil removal filter, an air pressure regulator, and a smooth-edged orifice were located in the air supply line. The mass flow rate of the secondary dilution air could be determined by measuring the pressure and temperature upstream of the choked orifice with a pressure gage and a thermocouple. The pressure gage was a HEISE high accuracy gage with a resolution of 0.7 kPa. The secondary dilution air system was calibrated during an earlier study. The following equation was used to calculate the mass flow rate of the secondary dilution air [135].

$$\dot{m}_{sd} = 4.2608 \times 10^{-4} + 0.64435\left(\frac{P_{sor}}{\sqrt{T_{sor}}}\right) \qquad (4\text{-}2)$$

where $\dot{m}_{sd}$ = mass flow rate of secondary dilution air (kg/min.).

P_{sor} = absolute static pressure at the orifice (bar).

T_{sor} = temperature at the orifice (K).

4.2.3 Particulate sampling system

The particulate sampling system consisted of ball valves, a filter holder, a sampling pump, a Roots-type gas flow meter with a frequency counter, a by-pass valve, a vacuum gage and a vacuum pump as shown in Figure 4.2. The ball valve in the particulate sampling pipe was opened when the experiment started, and closed at the end of the test to keep the diluted exhaust gas out of the system between tests. The filter holder was used to support a primary and a backup filter. The distance between these two filters was 8.9 cm, and a thermocouple was mounted between them to monitor the temperature in the filter holder during sampling. This thermocouple was also used to provide information to control the temperature of the particulate filter. A second thermocouple was located at the inlet of the gas meter so that the density of the sample flow could be computed with this temperature.

The electronic counter attached to the Roots gas flow meter was capable of displaying the total amount of gas that had passed though the sampling system during the test. The flow rate was adjusted manually to keep the particulate sample flow constant during the test. This was necessary because the sample flow rate would drop as the filters became loaded with particulates. The vacuum pump was used to test the system for leaks. The leak test procedure was described in reference [134].

The filters used to collect the particulate sample in this project were 110 mm Pallflex T60A20 filters. The particulate sample volume flow rate was chosen to be 3.3×10^{-3} m^3/s (7 $ft^3/min.$) in order to collect enough particulate matter on the filters to minimize the impact of errors in filter weighing.

4.2.4 Particulate weighing chamber

A temperature and humidity controlled weighing chamber was used to weigh and store the filters during the study. Compressed air was passed through an oil removal filter and diffused into the chamber to control the humidity. The air was bubbled through water if an increase in humidity was required. To satisfy the EPA's requirements for temperature and humidity in the weighing chamber, the temperature in the chamber was maintained within $\pm$ 2 K of 296 K, and the relative humidity of the chamber was maintained within $\pm$ 3% of 50%

[23]. Figures 4.3 and 4.4 illustrate the recorded data of temperature and relative humidity for a 60-day period. The average values of temperature and relative humidity were 295.80 K and 49.92%, respectively.

A Mettler model AE240 analytical balance with a reproducibility of 20 micrograms and a readability of 10 micrograms was placed inside the weighing chamber. There were also two shelves in the weighing chamber. One of them was covered with metal screen to eliminate any electrostatic charge on the filter surface.

4.2.5 Soluble hydrocarbon extractor and solvent

The particulate filters were Soxhlet extracted with methylene chloride in a fume hood. There were two Pyrex Soxhlet extractors using 125 ml flasks at the bottom, and Alihn type condensers at the top. During each extraction, a particulate filter was contained in an 80 × 25 mm extraction thimble. Two Electromantle heaters heated the flasks and maintained a constant solvent temperature. The solvent used in this test was methylene chloride (CH_2Cl_2) which is the most common solvent for particulate analysis. The effects of this solvent on diesel fuel, biodiesel, and engine oil were discussed in reference [128].

4.2.6 Equipment for measuring gaseous emissions

The gaseous emission sampling system was shown in Figure 4.1. A portion of the engine exhaust gas was drawn directly from the engine exhaust pipe with a vacuum pump. A filter system was located in the sampling line to remove solid particles from the sample gas to protect the emission analysis equipment from damage. The exhaust sample provided to the CO, NO_x, CO_2, and O_2 emission analyzers was a dry gas because the sample was passed through an ice bath to remove the water vapor. However, the sample to the heated flame ionization detector (HFID) was a wet gas. The unburned hydrocarbons in the exhaust gas were determined with a Beckman model 402 heated flame ionization detector. The temperatures of the sampling line and the oven in the detector were set to 465 K during normal tests. Because the power for the heating system of the sampling line and the oven was limited, the maximum temperatures that could be reached were about 475 K. To obtain the

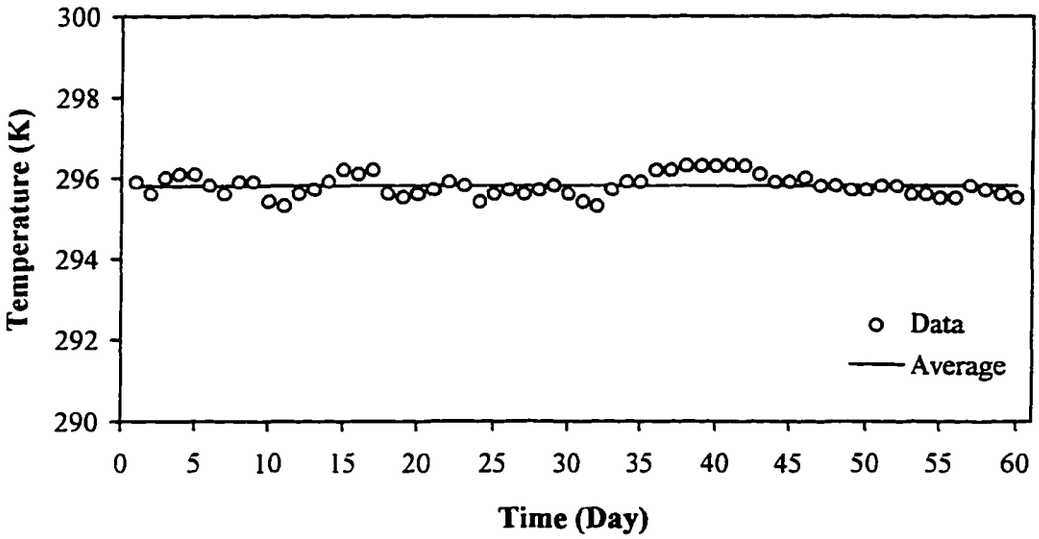

Figure 4.3 Temperature in the weighing chamber during the test

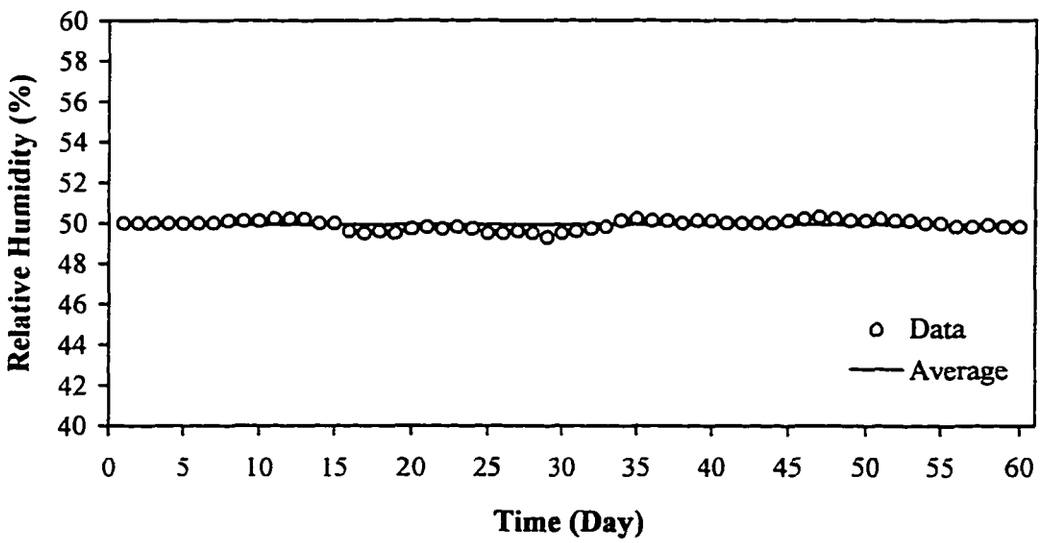

Figure 4.4 Relative humidity in the weighing chamber during the test

higher temperatures used in this study, a new heated sampling line with a larger power supply was used, and its temperature could be set as high as about 580 K. An extra 500 W heating element was placed in the HFID oven chamber to increase the heating power. The temperatures of the sampling system and the oven were adjusted automatically by controlling the power to these two heating systems. The concentrations of CO and CO_2 were measured with two Beckman model 864 infrared analyzers. The concentrations of total oxides of nitrogen and oxygen in the exhaust gas were determined with a Beckman model 955 NO/NO_x analyzer and a Beckman model 7003 polarigraphic oxygen monitor, respectively.

4.3 Fuels

Two fuels were selected as the base fuels in this study, methyl esters of soybean oil (MS) and low sulfur No. 2 diesel fuel (D2). The soy methyl esters were sold as biodiesel by NOPEC Corporation (Lakeland, FL). The specification of the biodiesel is shown in Table 4.2.

The No. 2 diesel fuel was a commercially available diesel fuel. Its properties are shown in Table 4.3. Additional properties of the biodiesel are also illustrated in this table. The fuel properties shown in Table 4.3 were analyzed by Phoenix Chemical Laboratory, Inc. (Chicago, IL).

Besides the two baseline fuels, the fuels actually used in this study were blends of the No. 2 diesel fuel and the biodiesel. These fuel blends included 20% and 50% of biodiesel mixed with No. 2 diesel fuel, by mass.

4.4 Experimental Procedure

This study was divided into four stages. The first test investigated the effects of dilution conditions on biodiesel particulate emissions, and the second investigated the effects of HFID sampling line conditions on the HC emissions of biodiesel. The last two tests focused on the effects of unburned biodiesel on the particulate and HC emissions under various dilution conditions and HC sampling line temperatures by injecting a small amount of biodiesel into the diesel engine exhaust manifold. These studies were carried out at two different engine

Table 4.2 Specification of biodiesel[a]

Property	Test Method	Results	NBB[b] Limits
Flash point, °C	ASTM D93	141	100 min.
Water and sediment, Vol%	ASTM D1796	0.00	0.050 max.
Carbon residue	ASTM D4530	0.02	0.050 max.
Sulfated ash, wt%	ASTM D874	0.001	0.020 max.
Viscosity, cSt 40 °C	ASTM D445	4.4	1.9 - 6.5
sulfur, wt%	ASTM D2622	0.01	0.05 max.
Cloud point, °C	ASTM D2500	0	By customer
Pour point winter, °C	ASTM D97	-3	-5 max.
Copper strip corrosion	ASTM D130	1	No. 3b
Acid number, mg KOH/mg	ASTM D664	0.23	0.80 max.
Free glycerin, wt%	GC[c]	0.006	0.020 max.
Total glycerin, wt%	GC	0.215	0.240 max.

[a]Information provided by NOPEC Corporation.
[b]National Biodiesel Board.
[c]Gas chromatography.

conditions for all fuels, 100% of maximum torque at 1400 rpm and 20% of maximum torque at 1400 rpm. Both engine conditions were run at steady state only.

At the beginning of each test, all emission equipment was calibrated with zero and span gases. The zero gas usually was compressed air, and the span gases were different for each analyzer. All emission equipment was warmed up for at least 24 hours before each test.

4.4.1 Particulate matter tests

For the particulate matter tests, the particulate sample filters were weighed with the Mettler micro-balance after the sample filters were allowed to equilibrate in the weighing chamber for 48 hours. During the experiment, six filters were used as reference filters to check the repeatability of the micro-balance. Before any sample filters were weighed, two reference filters were weighed first to make sure the balance and the weighing chamber were working

Table 4.3 Fuel properties of No. 2 diesel and biodiesel fuels

	No. 2 diesel	Biodiesel
Cetane Number	44.9	55.0
Carbon, wt%	86.53	77.81
Hydrogen, wt%	13.18	12.39
C/H Ratio	6.565	-
Sulfur, wt%	0.045	<0.005
Gross Heating Value, MJ/kg	45.56	39.84
Net Heating Value, MJ/kg	42.77	37.21
Hydrocarbon Type, FIA		
Paraffins, vol.%	62.5	-
Olefins, vol.%	2.2	-
Aromatics, vol.%	35.3	-

properly. EPA regulations require the reference filters to be changed at least once per month, so two of the six filters were kept in the weighing chamber at any given time period. Table 4.4 shows the statistical data for the reference filter weights. The variations could be neglected due to the small coefficients of variation of these reference filters. To check the reproducibility of the measurement, each filter was usually weighed two times. The final weight of the filter was the average of the two readings.

Before starting the engine, the primary dilution air was run through the dilution tunnel and the particulate sampling system was operated for at least 10 minutes to keep the surfaces of the tunnel and the sampling system free of deposits that could remain from previous tests.

When the engine was started, its speed and load were set at 1400 rpm and 100% of rated load, and it ran for 30 minutes as a warm-up. To start the test, a pair of particulate sample filters were placed in the filter holder, and the particulate sampling system was turned on. The temperature controllers were set to the desired temperature, and the power to the heating tapes on the filter holder was also turned on at the same time. When the engine

Table 4.4 Statistical data for the reference filters

	Filter 1	Filter 2	Filter 3	Filter 4	Filter 5	Filter 6
Min. weight, mg	341.80	343.16	314.08	350.11	317.66	311.11
Max. weight, mg	341.95	343.27	314.21	350.19	317.74	311.20
No. of weighing	24	24	24	24	24	24
Mean weight, mg	341.88	343.21	314.15	350.14	317.69	311.15
S.D.[a], mg	0.06	0.04	0.05	0.02	0.03	0.03
C.V.[b], %	0.02	0.01	0.02	0.01	0.01	0.01

[a]Standard deviation.
[b]Coefficient of variation.

reached its equilibrium operating condition as indicated by stable coolant and oil temperatures, and the temperature at the particulate filters came to the desired value, a fresh pair of particulate sampling filters were placed in the filter holder. Then the particulate sampling system was restarted. A stopwatch was also started at this time, and the weight of the fuel supply tank was recorded.

The electronic counter in the particulate sampling system shown in Figure 4.2 displayed the instantaneous particulate sample flow rate. During the test, the particulate sampling pump bypass valve was manually adjusted to maintain the particulate sample flow rate within 3% of 0.198 m^3/min. (7.00 ft^3/min.). Other data, such as the temperatures and pressures from the engine and dilution system, engine torque and speed, etc., were also manually recorded.

At the end of the tests, the particulate sampling pump was shut off, and the test duration, the final weight of the fuel supply tank, and the total volume of particulate sample gas that passed through the sampling system were recorded. The sampling filters were removed from the filter holder, and placed in the weighing chamber for stabilization. The condition of the dilution tunnel was then brought to another state according to the test matrix. After the new dilution condition was reached, a new test began. When the fuel was changed, the engine was run for one hour at the full-load condition to clear all previous fuel out of the

engine fuel system. At the end of each test day, the engine was run with diesel fuel for 10 minutes so that any non-diesel fuel did not remain in the engine.

The loaded particulate sampling filters were weighed twice after having equilibrated in the weighing chamber for 24 to 48 hours. The difference between the final weight and the weight before sampling was considered to be the total particulate mass.

4.4.2 Unburned hydrocarbon emission tests

Before any test was started, the HC detector was turned on to warm-up, and the temperatures of the detector oven and the HC sampling line were set to the required value. The warm-up usually took at least 24 hours before the detector was used. The diesel engine warm-up procedure was the same as that described in last section. After both the engine and the detector reached their stable conditions, the HC detector was calibrated with zero and span gases. Then, the computer program that was used to collect the emission data with a RTI-820 data acquisition board was started. The HC, CO, CO_2, NO_x, and O_2 emission data were collected at one second intervals for 6 minutes. After the emission data were taken, the temperatures of the HC sampling line and the HC detector oven were set to a new value. Because the temperature change in the detector oven and the HC sampling line between two HC emission tests was small, usually only 20 °C, the equipment and sampling line could reach the new conditions quickly. A 20 minute warm-up time period was used to condition them when the measurement conditions were changed. After the new equilibrium operating conditions were reached, the HC detector was recalibrated with the zero and span gases, and the new measurement was started.

4.4.3 Biodiesel injection tests

The last test was to inject a small quantity of biodiesel into the engine exhaust manifold to study the effects of unburned biodiesel on the soluble organic fraction in the particulates and on the vapor phase unburned hydrocarbon emissions. In this test, the diesel engine was fueled with No. 2 diesel fuel only. A nozzle with a small injection hole of less than 0.5 mm diameter was inserted into the engine exhaust manifold before the turbocharger

turbine. Because the temperature of the exhaust gas was high, 745 K at full-load and 475 K at 20% of full-load (1400 rpm), it was expected that the injected biodiesel could be vaporized quickly when it was injected into the exhaust manifold. The turbocharger should also provide excellent mixing of the injected biodiesel and the exhaust gas. The injected biodiesel was provided at a mass flow rate of about 5% of the engine fuel flow rate.

After the engine and the measurement equipment reached stable conditions, the biodiesel injection pump was turned on for 5 minutes to allow the biodiesel injection to reach steady state. Then, the particulate or HC emissions were measured following the same test procedures discussed in Sections 4.4.1 or 4.4.2. The biodiesel injection pressure was controlled between 13.8 kPa (2.0 Psi) and 20.7 kPa (3.0 Psi) depending on different engine conditions. A one-gallon biodiesel fuel tank was placed on an electronic scale to measure the weight change during the injection test. The weight difference during the test period was the biodiesel mass that was injected into the engine exhaust manifold. The time of each test was also recorded with a stopwatch. The average biodiesel injection rate was the weight difference of the biodiesel fuel tank divided by the time.

4.5 Test Matrix

At least three sets of data were collected for each test, each engine condition, and each fuel so that the repeatability of the tests could be investigated. All engine tests were conducted with an engine speed at 1400 rpm. The conditions for all of the engine tests are shown below.

For particulate emission tests:

- **Constant dilution ratio at 15:1 without biodiesel injection**

  Filter temperature: 45 to 80 °C at 100% of full-load.

  30 to 80 °C at 20% of full-load.

- **Constant filter temperature at 52 °C without biodiesel injection**

  Dilution ratio: 20:1 to 200:1 at 100% of full-load.

  5:1 to 100:1 at 20% of full-load.

- **Constant dilution ratio at 15:1 with biodiesel injection**

  Filter temperature: 52 to 80 °C at 100% of full-load.

30 to 80 °C at 20% of full-load.

- **Constant filter temperature at 52 °C with biodiesel injection**

  Dilution ratio: 20:1 to 100:1 at 100% of full-load.

  No test at 20% of full-load.

  For unburned hydrocarbon emission tests:

- **Without biodiesel injection**

  HC sampling line temperature: 90 to 300 °C at 100% of full-load.

  90 to 300 °C at 20% of full-load.

- **With biodiesel injection**

  HC sampling line temperature: 90 to 300 °C at 100% of full-load.

  90 to 300 °C at 20% of full-load.

After the tests with biodiesel injection and with constant particulate sampling filter temperature, a mass balance on the injected biodiesel was computed. The results showed that a portion of the biodiesel was not vaporized when it was injected into the exhaust manifold at the 20% of full-load engine condition. It may have deposited on the engine exhaust manifold surface, and fuel leaking from the engine exhaust system was noted during this test. Therefore, the test with biodiesel injection was not continued for the light-load engine at the constant filter temperature condition.

Because this study was based on one variable variation at a time, such as dilution ratio varied with a constant filter temperature at 52 °C, or filter temperature varied with a constant dilution ratio at 15:1, the trends observed should be considered as variations about the baseline condition. This baseline condition was chosen because it represents currently accepted practice for dilution tunnel operation. Combinations of filter temperature and dilution ratio not investigated here may give different trends.

4.6 Data Analysis

The particulates that were sampled from the diluted engine exhaust gas contained solid carbon and sulfate compounds as well as adsorbed and condensed hydrocarbons commonly termed the soluble organic fraction (SOF). To characterize the amount of soluble material, the

particulate filters were extracted with methylene chloride to determine the proportion of SOF in the particulates.

After each loaded filter was stabilized in the weighing chamber for 48 hours, it was put in an extraction thimble, and the filter and thimble were weighed together. Then, the thimble with the filter was placed in a Pyrex Soxhlet extractor. One hundred ml of methylene chloride was poured into a flask at the bottom of the Soxhlet tube. After the power for the solvent heater was turned on, and cooling water was passed through the top condenser, the extraction process was started. Each filter was extracted for from 60 to 70 cycles.

The thimble with the extracted filter was placed in a heated chamber for one hour after the last cycle was finished. The temperature in the chamber was kept at about 315 K which was just above the boiling point of methylene chloride to evaporate the solvent quickly and completely. The thimble was then placed in the weighing chamber for another 48 hours. At the end of that period, it was weighed. The difference in the weight before extraction and after extraction was considered to be the mass of SOF.

To compare the emission levels and engine performance, and to use the data for the simulation study, the measured emission levels were converted to the units of g/kW hr and g/kg exhaust gas. This requires the development of a balanced chemical equation for the combustion reaction that is discussed in Appendix A. This equation requires a chemically correct expression for the fuel blends. Determination of the average molecular weight and heating values of the biodiesel blends were discussed in reference [134]. The humidity and dry-wet basis correction also were described in reference [134].

All experiment schedules were based on block design principle statistically. The fuel and the dilution tunnel conditions or HC sampling line temperature formed a factorial treatment and blocked by different engine test days. Statistical analyses were performed on the emission data for each dilution tunnel or HC sampling line condition test using analysis of variance and multiple comparison method. Least significant difference (LSD) was used to determine whether or not there was a significant difference between each pair of fuels within a dilution tunnel or HC sampling line condition test. A significance level of 0.05 was used for all analysis of variance.

5. RESULTS AND DISCUSSION

In this chapter, the experimental results will be discussed first. This will be followed by the predictions of the formation of soluble organic fraction (SOF) in the particulate matter during the dilution process and the effects of HC sampling conditions on the unburned hydrocarbon concentration in the HC sampling line. The effects of dilution tunnel conditions, HFID sampling line conditions, fuels, and engine operating conditions on the formation of vapor and liquid phase unburned hydrocarbons will be analyzed in detail. In particular, the SOF and HC levels from experiment and predictions based on the condensation and adsorption models are compared also.

5.1 Results from Experiment

The effects of dilution tunnel conditions, HC analyzer sampling line conditions, fuels, and engine operating conditions on the formation of vapor and liquid unburned hydrocarbons were investigated at two steady state engine conditions in this study. The influence of each factor on both phases of unburned hydrocarbon emission will be analyzed in this section. All experimental results plotted in this study are the average of three tests for each fuel. These results were also analyzed statistically with the method of least significant difference to determine whether or not there was a significant difference between each pair of fuels within a given condition.

5.1.1 Formation of soluble organic fraction during the dilution process

The dilution tunnel conditions, such as dilution ratio and filter temperature, have a significant effect on diesel particulate formation when the engine exhaust gas is diluted in the tunnel. Actually, the dilution ratio and filter temperature interact together. When the dilution ratio is increased, the temperature at the particulate sampling filter will be lowered, but the partial pressure of hydrocarbon vapor is decreased also. To investigate the independent effect of each dilution tunnel condition on the total particulate formation during the dilution process, the dilution ratio and filter temperature were varied individually.

The effects of the dilution tunnel conditions on the total particulate matter formation were studied at two steady state engine conditions, 20% and 100% of full-load at 1400 rpm. When the diesel engine was run at 20% of full-load condition, its unburned hydrocarbon concentration was higher than at the full-load engine conditions. The high unburned hydrocarbon concentration in the engine exhaust gas would be expected to cause a difference in the SOF formed on the carbon particle surface during the dilution process.

5.1.1.1 Effects of dilution ratio on the formation of soluble organic fraction

Dilution ratio was defined in this study as the ratio of the mass flow rate of diluted engine exhaust gas to the mass flow rate of raw engine exhaust gas. When the dilution ratio was varied, the concentrations of both the solid carbon particles and the unburned hydrocarbons were changed which could influence the formation of total particulate matter. The primary process affecting the total particulate matter during the dilution process was the formation of soluble organic fraction which involves the deposition of adsorbed and condensed hydrocarbons on the surface of the carbon particles. The amount of solid carbon present in the tunnel is expected to be constant during the dilution process since the temperature in the dilution tunnel is too low for oxidation. All experiments relating to the influence of the dilution tunnel conditions on the formation of particulate matter were conducted under steady state engine operating conditions. Four fuels, No. 2 diesel, and 20%, 50%, and 100% biodiesel blends with No. 2 diesel fuel, were tested in this study, and the No. 2 diesel fuel served as the baseline for the purpose of comparison.

When the effect of dilution ratio on the formation of particulate matter was investigated, the temperature at the particulate sample filters was held constant at 52 °C (325 K). Figure 5.1 shows the observed relationship between the dilution ratio and the total particulate matter mass concentration for the full-load operating condition at 1400 rpm. The unit of particulate concentration used in this plot is mg of particulate per kilogram of raw exhaust gas and it will be used throughout this study. Each data point shown on this plot represents the average of three measurements.

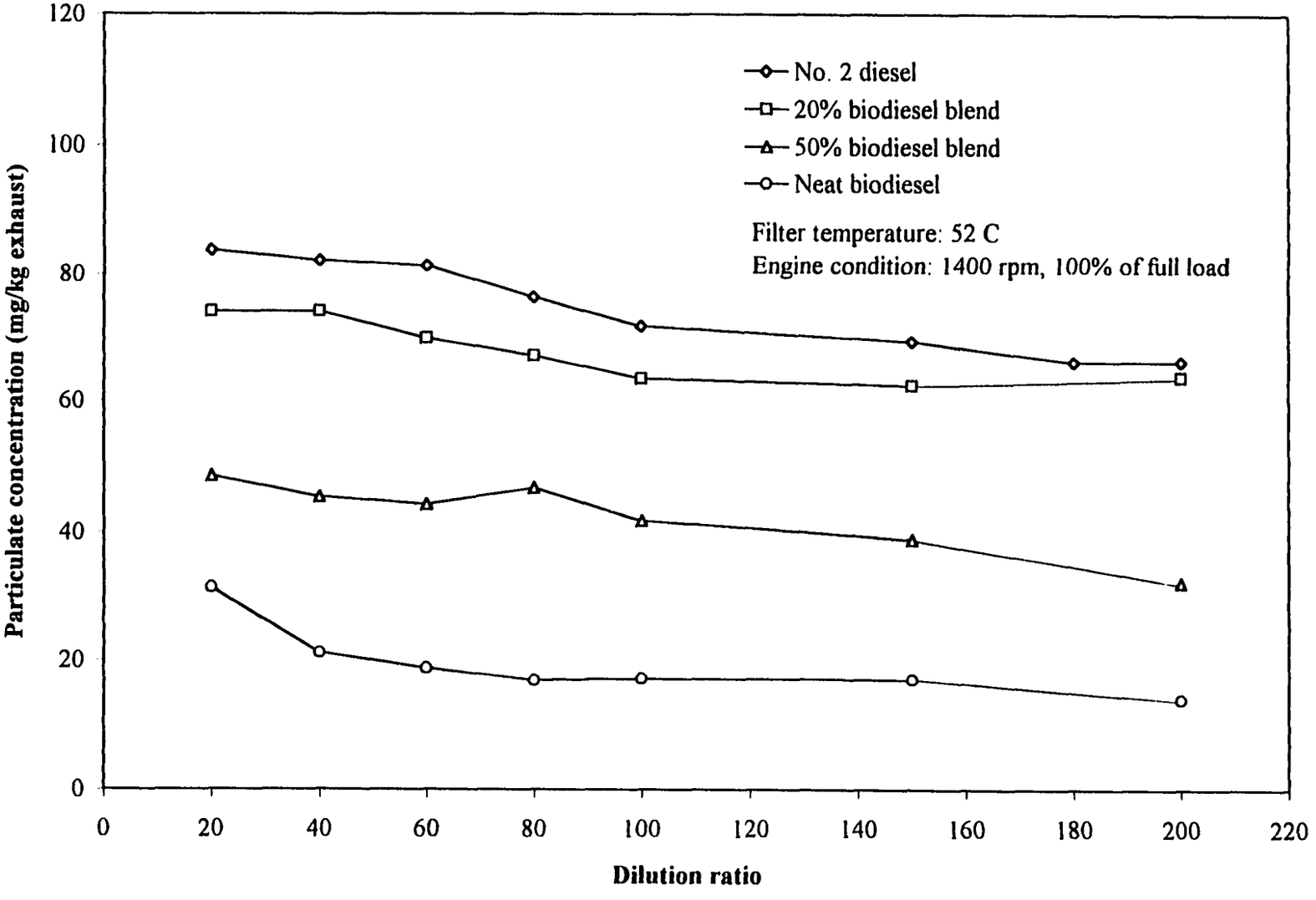

Figure 5.1 Effects of dilution ratio on total particulate emission at full-load engine condition

The dilution ratio was varied from 20:1 to 200:1 at this engine condition. The minimum dilution ratio was restricted by the filter temperature. Because the primary and secondary dilution tunnels were insulated on their outside surfaces, the smallest dilution ratio achievable at the full-load engine operating condition, while maintaining a filter temperature of 52 °C, was 15:1.

Figure 5.1 shows that the concentration of total particulate matter was reduced with increasing dilution ratio for the full-load engine conditions for each fuel. At each dilution ratio, the particulate emissions from the biodiesel blends were significantly lower than for No. 2 diesel fuel which is consistent with biodiesel emission tests reported by other researchers except between the No. 2 diesel fuel and the 20% biodiesel blend. The decrease of total particulate matter concentration with dilution ratio at the full-load engine condition was greatest at low dilution ratios and small or non-existent at high dilution ratios.

As discussed earlier, the formation of soluble organic fraction was a result of the adsorption and condensation unburned hydrocarbons on the surface of solid carbon particles. The total mass of carbon particles was nearly constant after the engine exhaust gas left the engine. Figure 5.2 illustrates the total mass of solid carbon at the same engine test condition, but measured at different times. The results of the carbon particle emission for the No. 2 diesel fuel and the 20% biodiesel blend revealed a relatively large variation compared with other two fuels. The carbon particle concentration was determined by using solvent extraction to determine the SOF and then subtracting this from the total PM. This process can introduce considerable variability. However, the average of the carbon particle emission with the fuel blends of 20%, 50%, and 100% biodiesel showed that these blends lowered the carbon particle emissions by 14.5%, 45.6%, and 81.6% compared with No. 2 diesel fuel, respectively.

Figures 5.3 and 5.4 show the soluble organic fraction as a percentage of the total particulate mass and as an actual mass, respectively, when the dilution ratio was varied. The soluble organic fraction from the biodiesel blends was significantly higher than for the No. 2 diesel fuel at low dilution ratios although the difference is much more pronounced for SOF as a fraction of the total PM than for the actual mass. A higher SOF fraction in the total particulates was observed when the fraction of biodiesel in the fuel blends was increased.

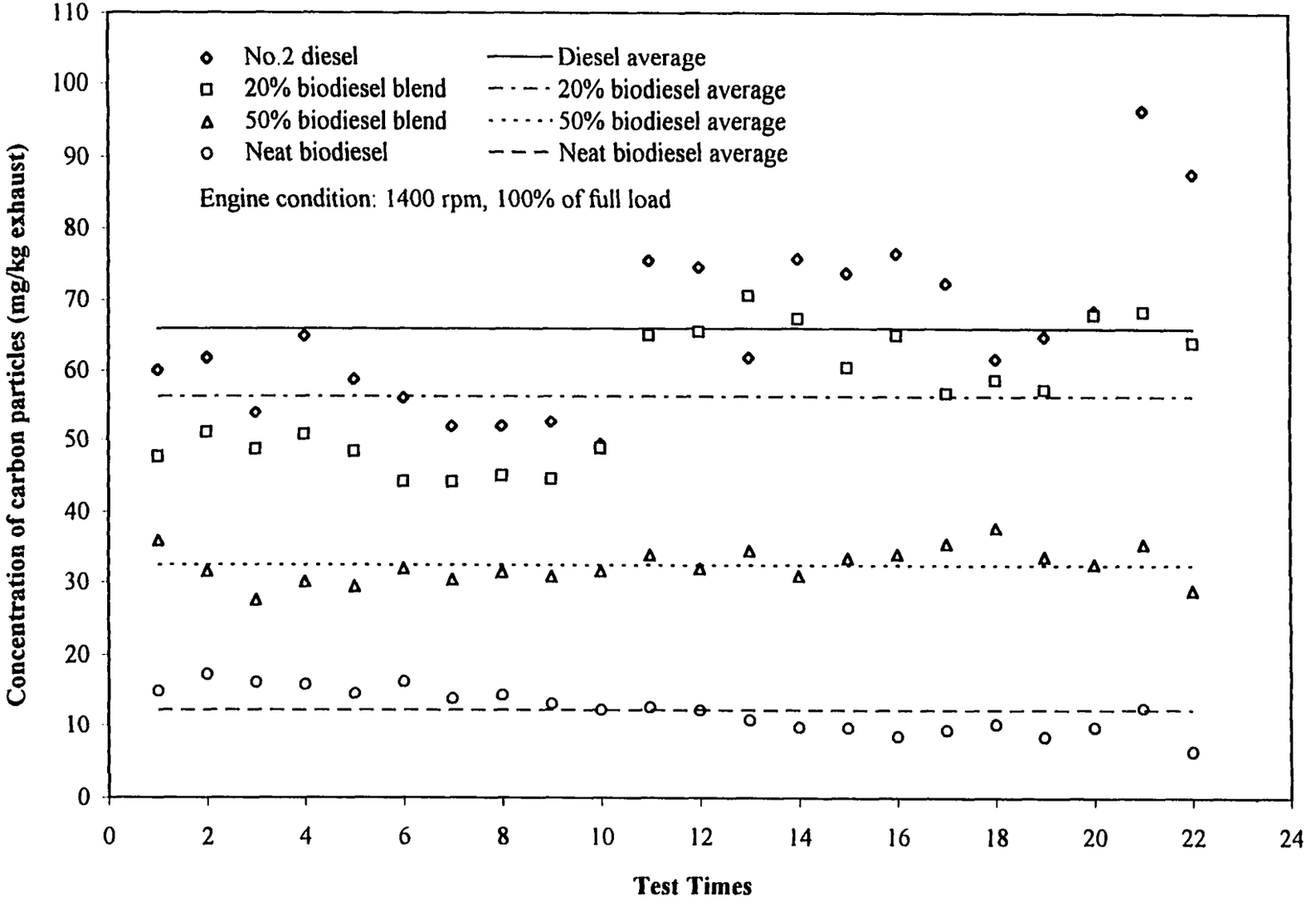

Figure 5.2 Concentration of carbon particles in engine exhaust gas at full-load engine condition

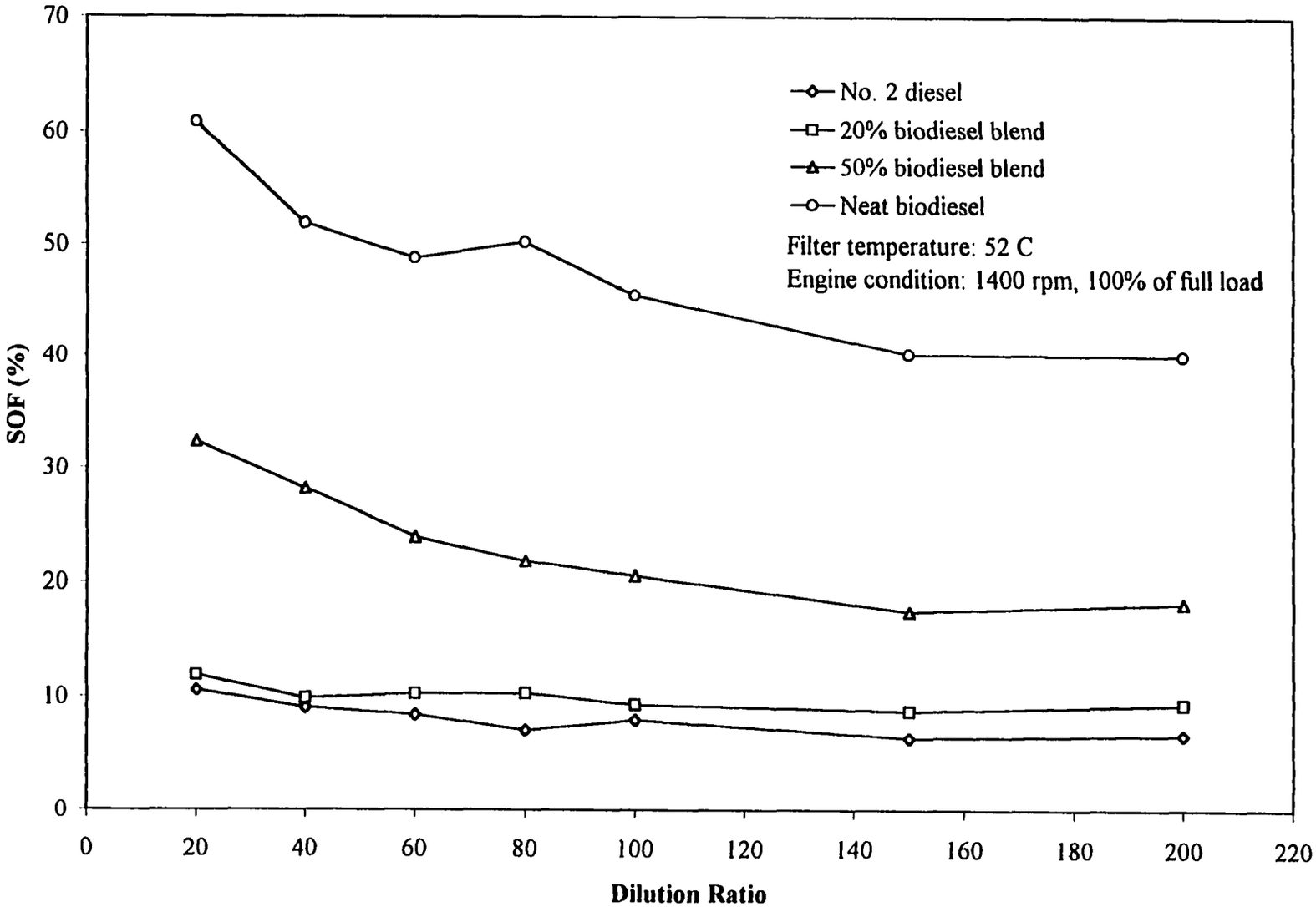

Figure 5.3 Effects of dilution ratio on the SOF in total particulate matter at full-load engine condition

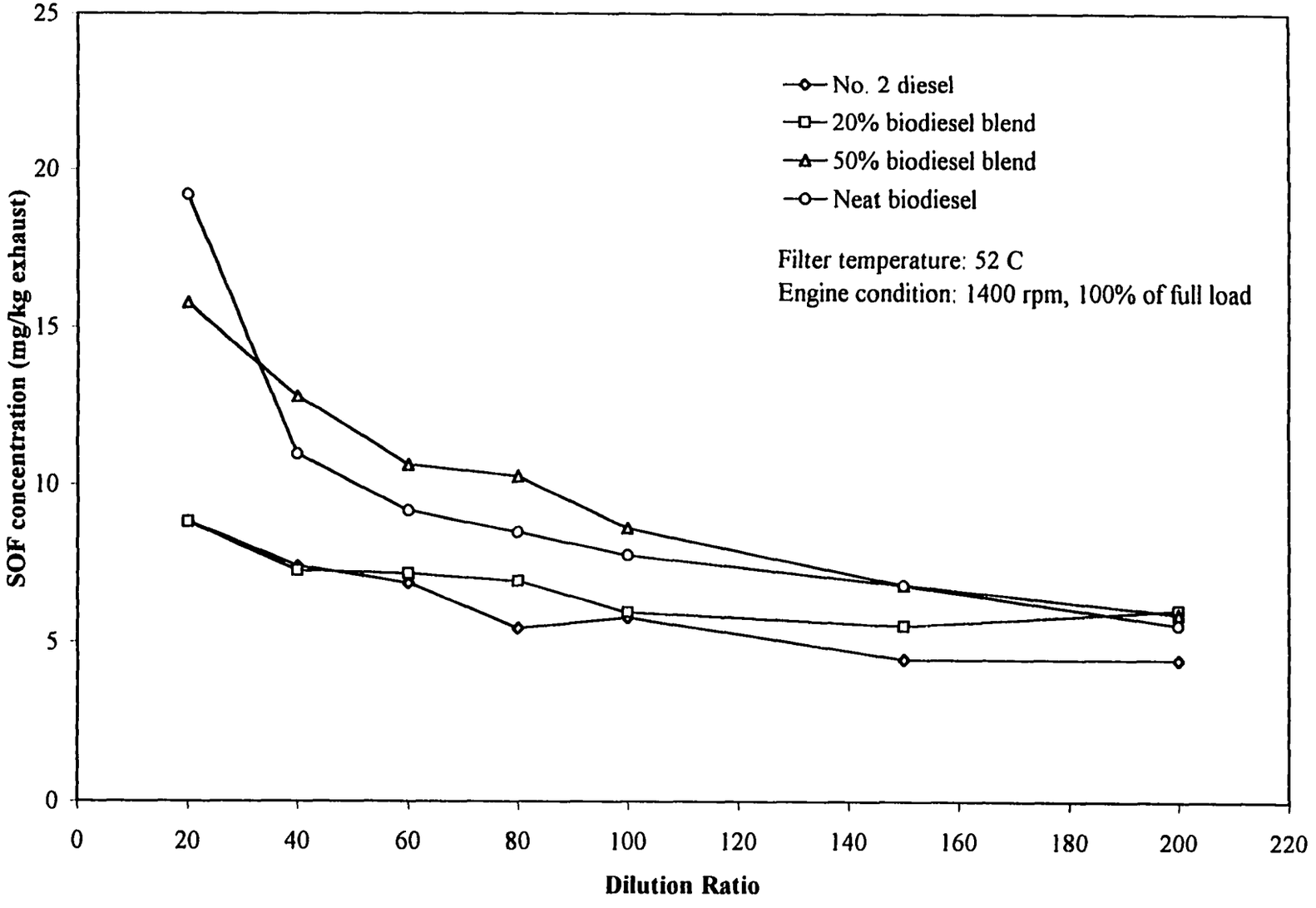

Figure 5.4 Effects of dilution ratio on the SOF concentration at full-load engine condition

These results also show that the amount of unburned hydrocarbons that are adsorbed and condensed on the carbon particle surface will vary when the engine exhaust gas is diluted. When the dilution ratio was higher than 80:1, the SOF masses of No. 2 diesel fuel and neat biodiesel did not show statistical difference. The formation of SOF is strongly dependent on fuel properties, such as volatility, boiling point, etc. Biodiesel is a fuel with higher boiling point and lower volatility than No. 2 diesel fuel. When unburned biodiesel is diluted in the dilution tunnel, it should be more likely to condense and adsorb on the carbon particle surface.

The concentration of the total particulate matter of biodiesel blends gave opposite results when the diesel engine was run at 20% of the full-load operating condition compared with full-load engine condition. Figures 5.5 through 5.7 show the changes of total particulates and SOF for different dilution ratios at 20% of full-load. At this partial load engine condition, the dilution ratio was varied from 6.5:1 to 100:1. The concentrations of total particulate matter for all the fuels were generally decreased with increasing dilution ratio. A rapid change of the total particulate concentration at low dilution ratios was observed. The change was the largest for fuel blends with the high biodiesel fraction. The neat biodiesel gave a 50% difference between dilution ratios of 6.5:1 and 20:1. When the dilution ratio was increased beyond 60:1, the change of total particulate concentration was small which was not statistically significant for all fuels. The final total particulate mass was governed by the formation of soluble organic fraction on the carbon particle surface. As shown in Figure 5.6, over 60% of the total particulate mass consisted of SOF at the 20% of full-load engine condition. The percentage of SOF in the total particulate matter depended on the dilution ratio. At low dilution ratio, almost 90% of the particulate mass was from SOF for diesel fuel, and 95% of the neat biodiesel particulate matter mass was SOF.

The total mass of solid carbon revealed an irregular change from test to test at the same engine condition as shown in Figure 5.8. This probably is due to the uncertainty in the determination of SOF because the carbon mass is determined by subtraction. When the SOF is high, the carbon mass may be so small that slight errors in the SOF percentage can cause large percentage errors in the carbon particle fraction.

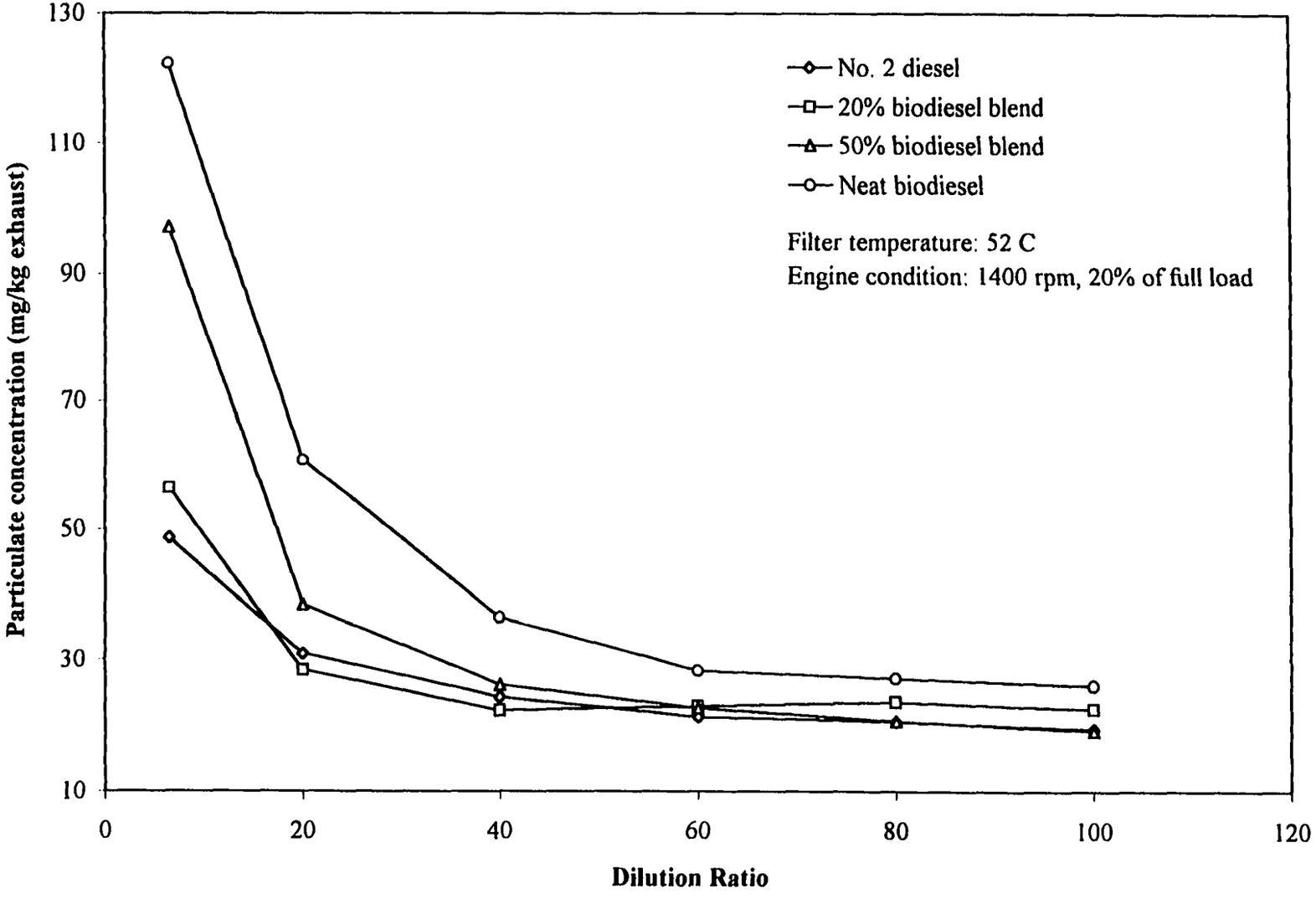

Figure 5.5 Effect of dilution ratio on total particulate emissions at light-load engine condition

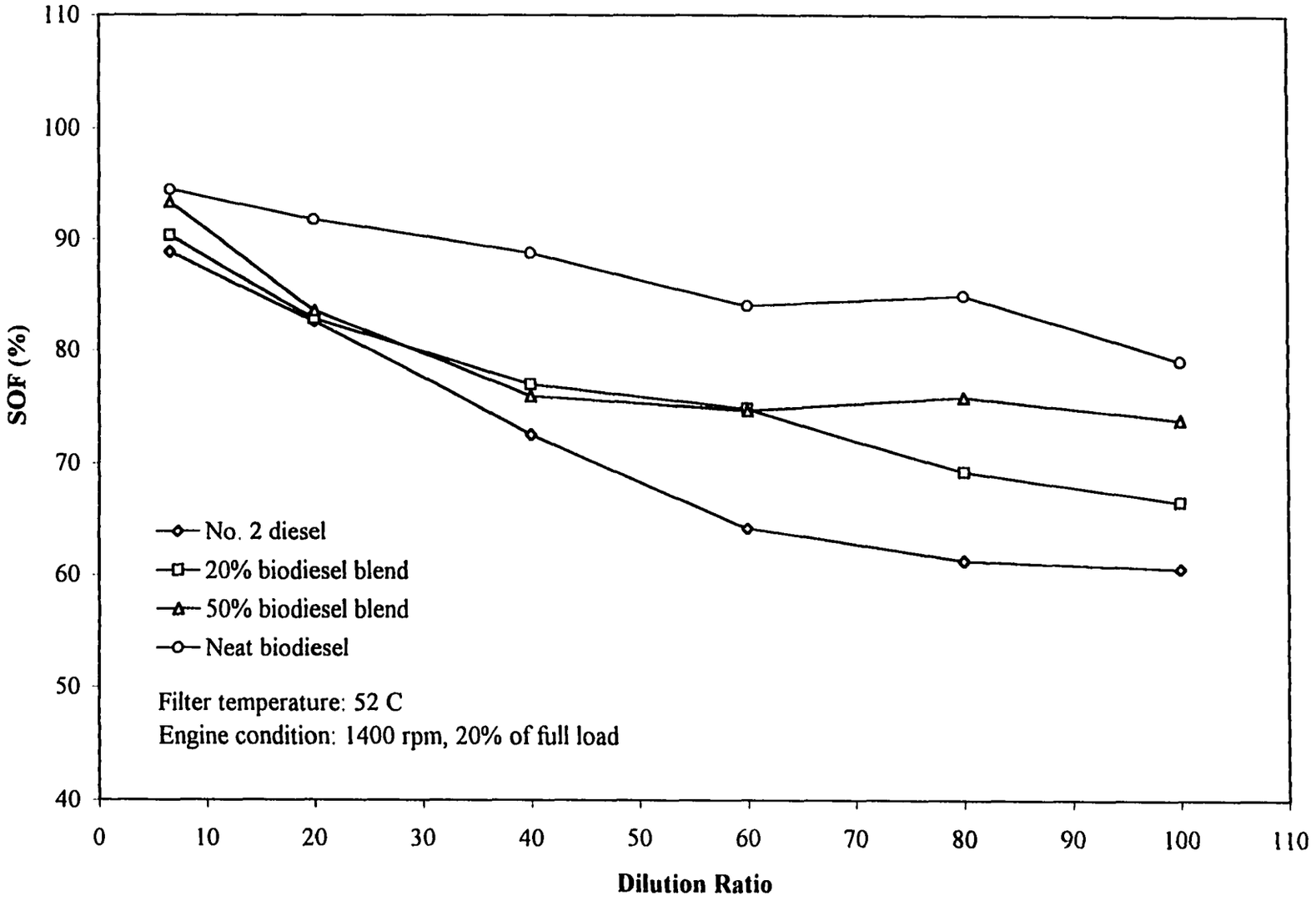

Figure 5.6 Effect of dilution ratio on SOF in total particulate matter at light-load engine condition

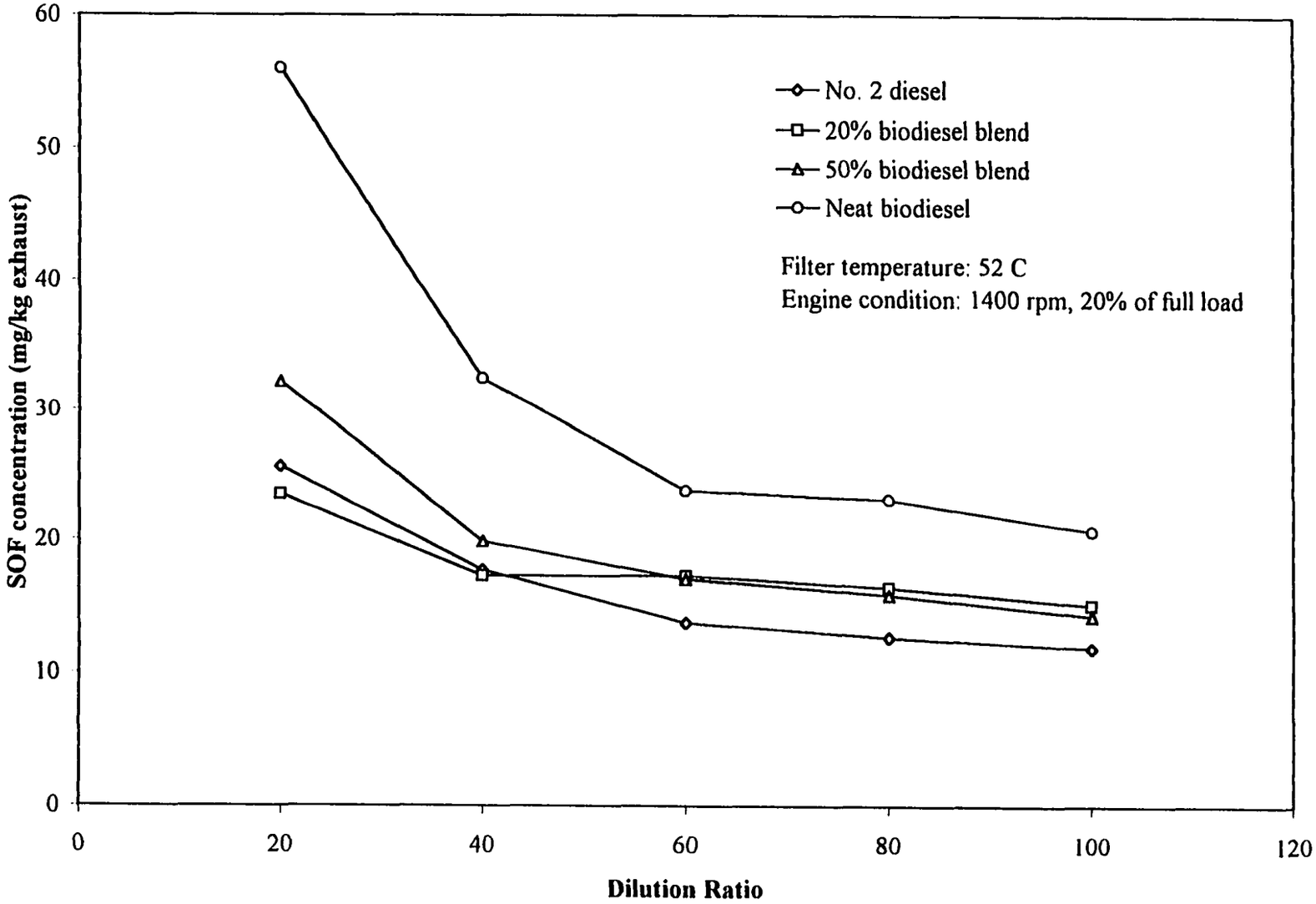

Figure 5.7 Effect of dilution ratio on the SOF concentration at light-load engine condition

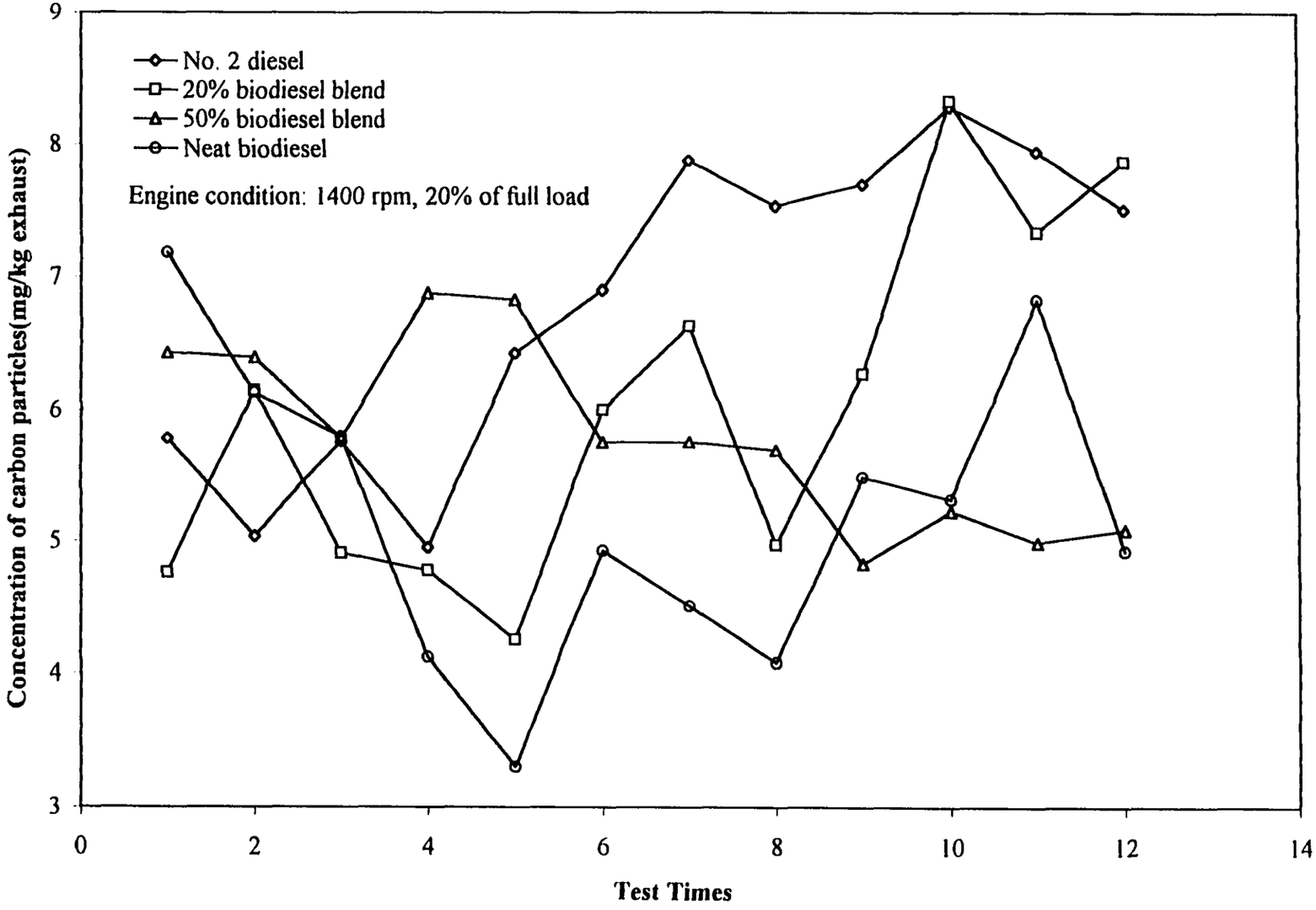

Figure 5.8 Concentration of carbon particles in engine exhaust at light-load engine condition

These experimental results show that, due to its low volatility, biodiesel and its blends produced a large fraction of soluble organic fraction in the total particulate matter compared with No. 2 diesel fuel. The adsorbed and condensed unburned hydrocarbons constituted most of the particulate matter increased as the dilution ratio was decreased.

5.1.1.2 Effects of filter temperature on the formation of soluble organic fraction

The effects of filter temperature on the total particulate matter was studied when the dilution ratio was kept constant at 15:1. The range of filter temperature variation was limited by the engine operating conditions. The filter temperature range for the full-load condition was from 47 to 80 °C, and from 30 to 80 °C for the 20% of full-load engine condition.

The total particulate concentration decreased when the particulate sampling filter temperature was increased at the full-load engine condition illustrated in Figure 5.9. The largest change in the particulate concentration occurred at low filter temperature. The effect of filter temperature on the total particulate mass was much greater for biodiesel than for No. 2 diesel fuel. The reduction of total particulate concentration with filter temperature increase was due to the reduction of the soluble organic fraction in the particulates. Figures 5.10 and 5.11 show the relationship between the SOF as a percentage of the total particulate mass and as an actual mass and the filter temperature for the four fuels. The neat biodiesel and its blends produced a significantly higher fraction of SOF in the total particulates than the baseline diesel fuel. Because the solid carbon mass for each fuel was nearly constant, as was shown in Figure 5.2, the lower particulate mass shows that more unburned hydrocarbons remained in the vapor phase at high filter temperature.

As noted earlier, both the total particulate concentration and the SOF fraction from the biodiesel blends were higher than No. 2 diesel fuel at the 20% of full-load engine condition. They showed a decreasing trend when the particulate sampling filter temperature was raised, as shown in Figures 5.12 through 5.14., due to less SOF being captured on the filter. However, when the filter temperature was higher than 70 °C, the changes of the total particulate matter and the SOF were not statistically significant for these fuels.

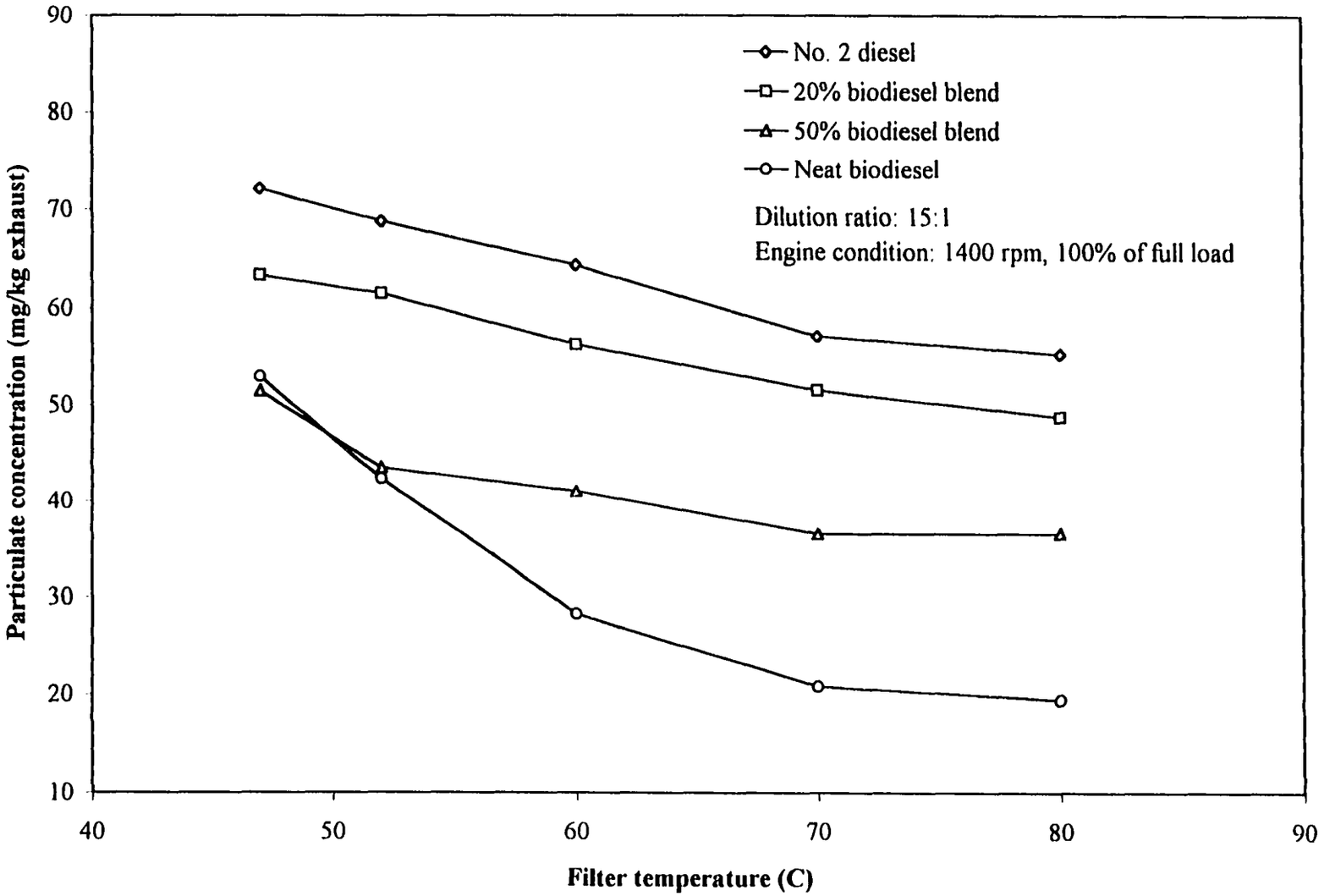

Figure 5.9 Effects of filter temperature on total particulate emissions at full-load engine condition

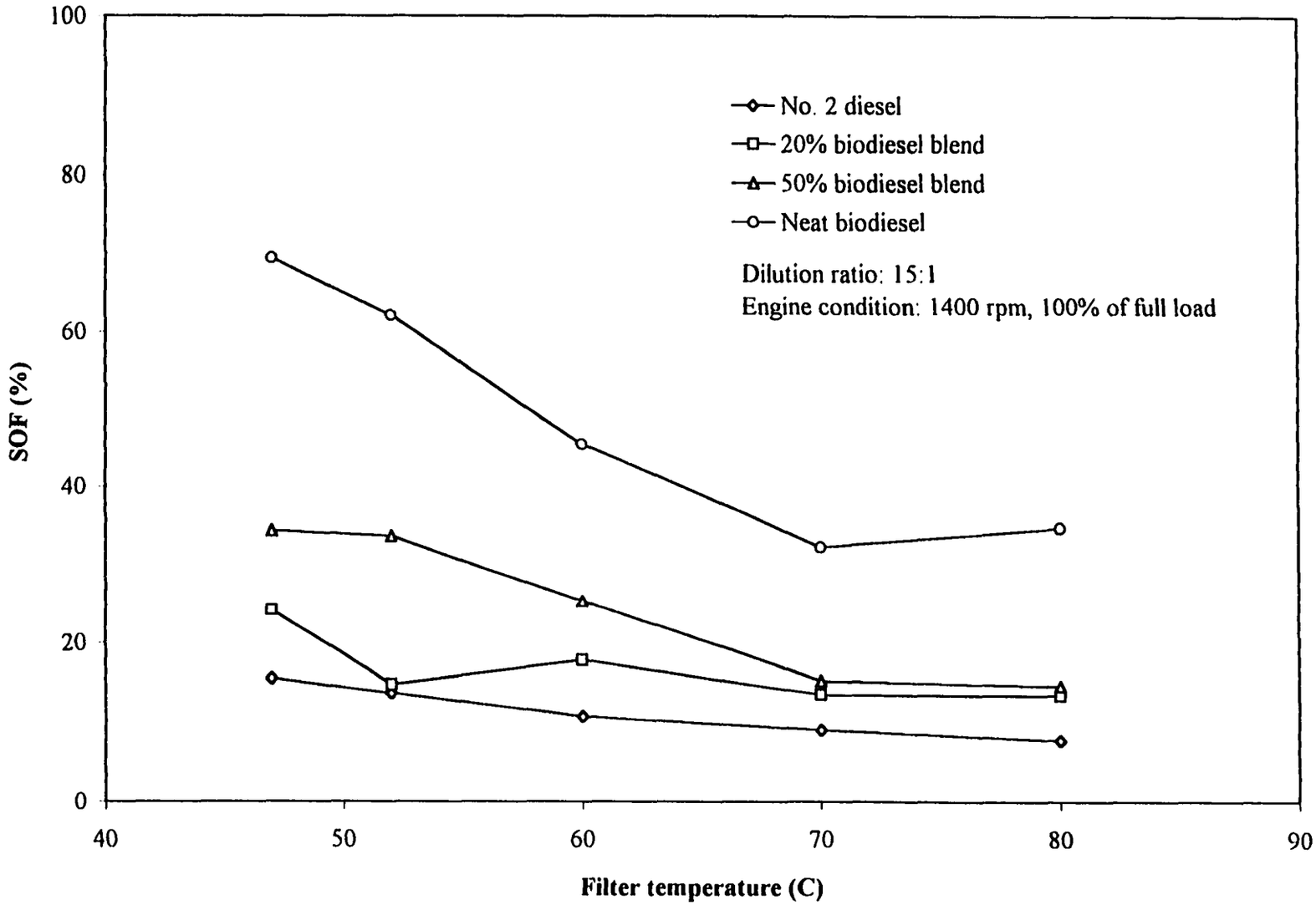

Figure 5.10 Effects of filter temperature on SOF in the total particulate matter at full-load engine condition

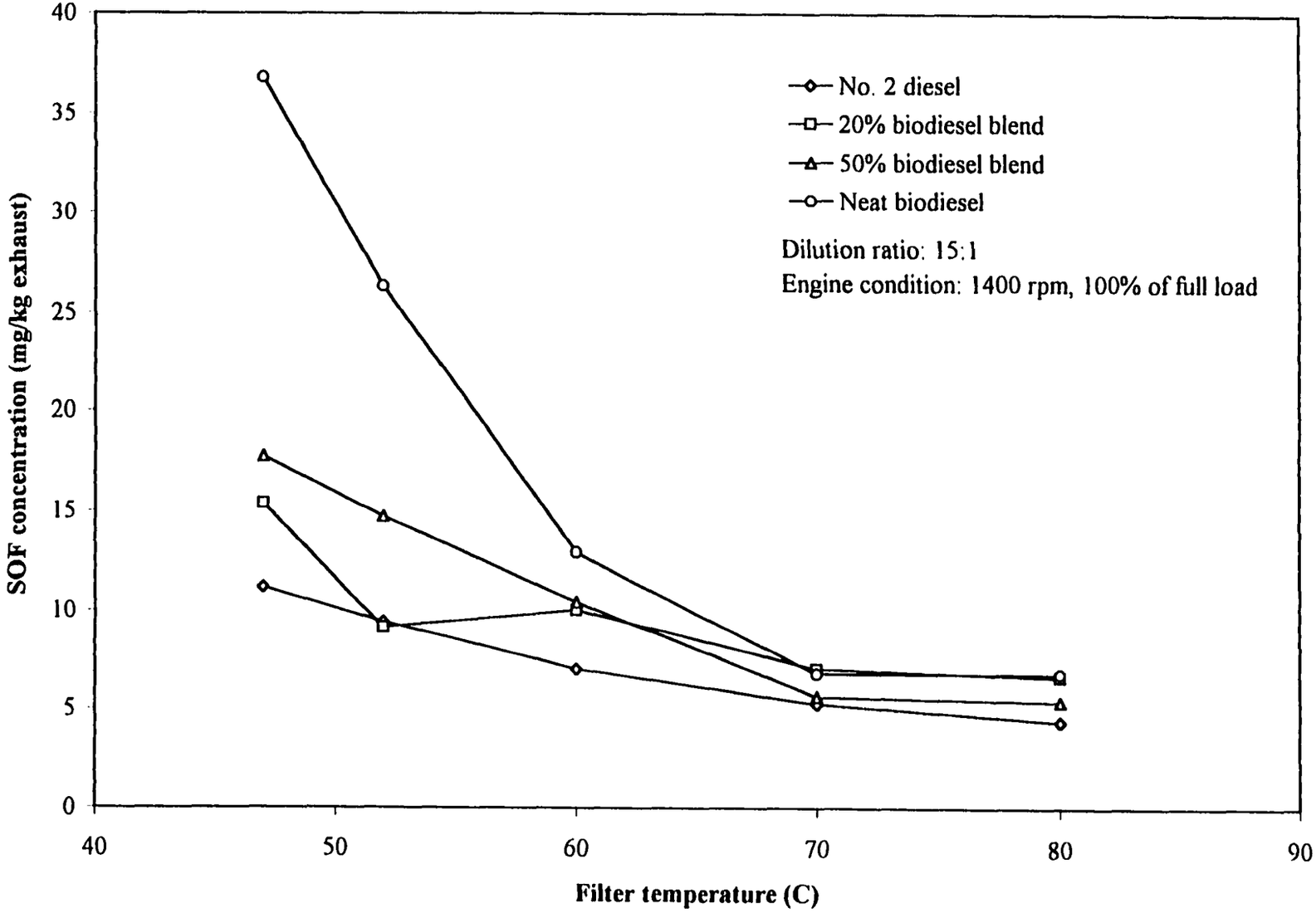

Figure 5.11 Effects of filter temperature on the SOF concentration at full-load engine condition

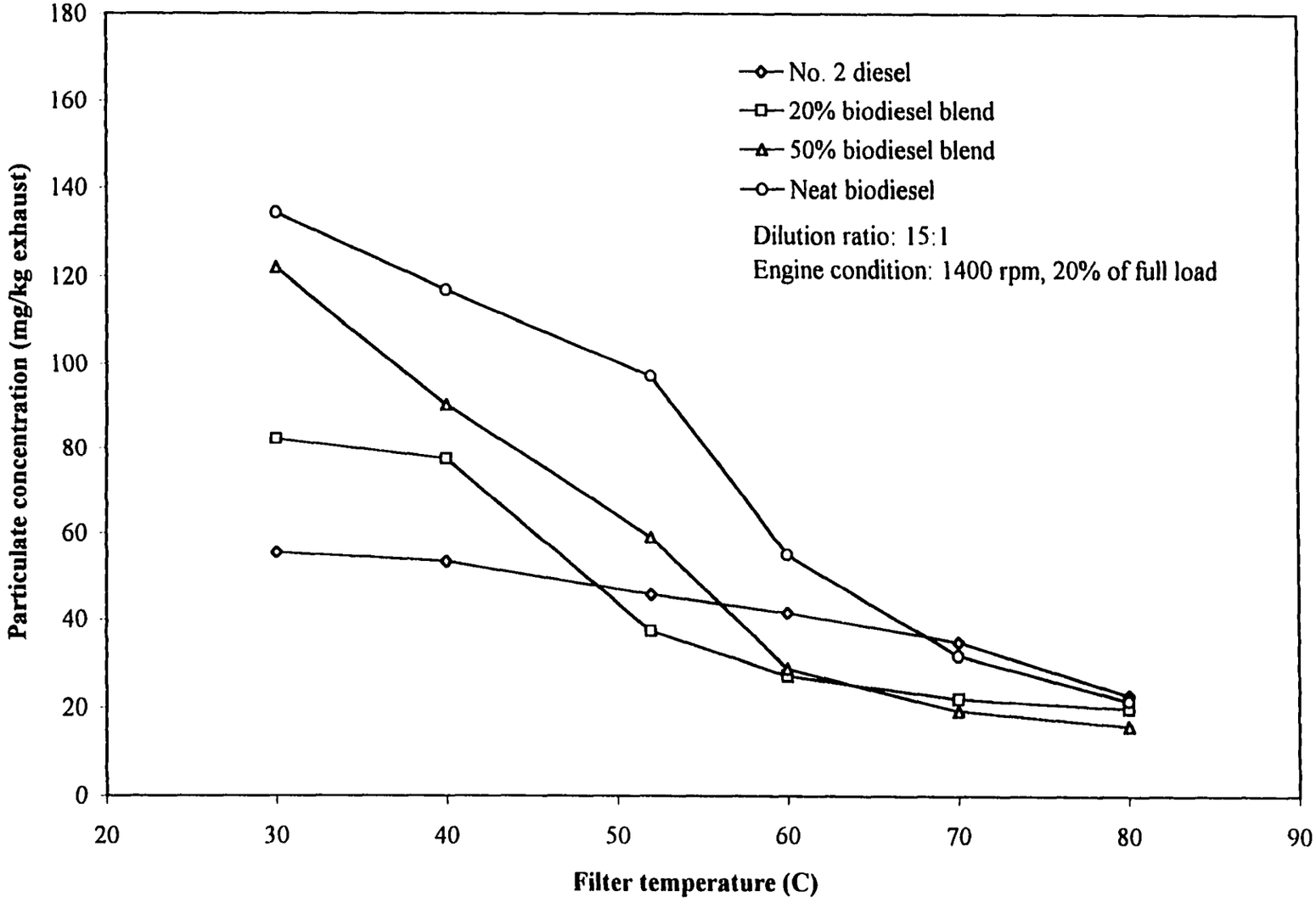

Figure 5.12 Effects of filter temperature on total particulate emissions at light-load engine condition

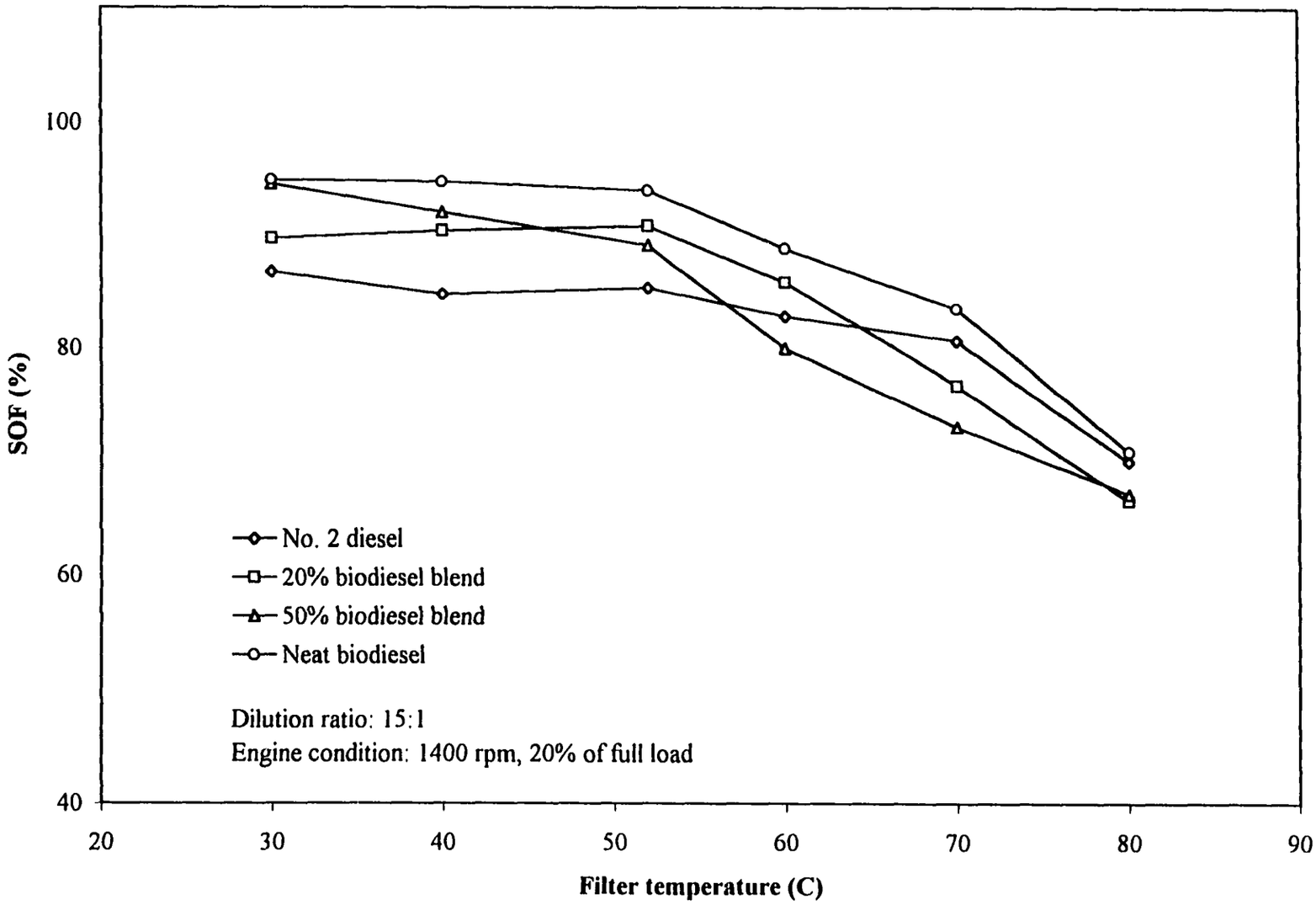

Figure 5.13 Effects of filter temperature on SOF in total particulate matter at light-load engine condition

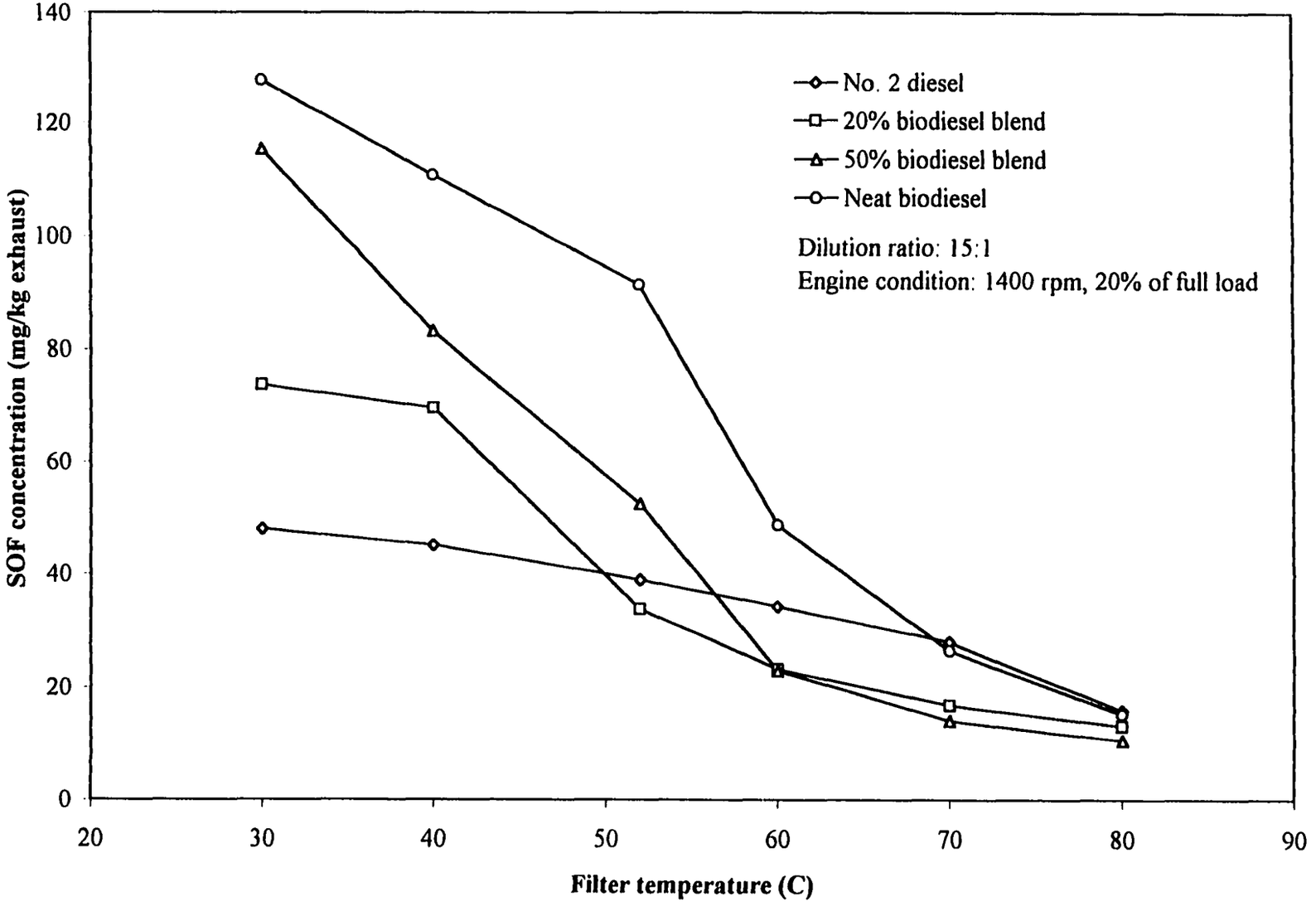

Figure 5.14 Effects of filter temperature on the SOF concentration at light-load engine condition

The results of the independent effects of dilution ratio and filter temperature on the particulate matter mass were in general agreement with other studies [92]. The total particulate mass changes were primarily due to changes in the soluble organic fraction of the particulates. The quantity of SOF in the particulates dropped rapidly when the filter temperature or dilution ratio was increased. These changes were similar for both engine operating conditions.

5.1.1.3 Effects of fuel on the formation of soluble organic fraction

One of the most important factors that controls the formation of the total particulate matter during the dilution process is fuel properties. Because biodiesel has a higher boiling point and lower volatility than No. 2 diesel fuel, it is more likely to adsorb and condense than diesel fuel. Although neat biodiesel and its blends lowered the total particulate emissions, compared with No. 2 diesel fuel, at the full-load engine condition, they produced a higher level of SOF. As the content of biodiesel in the blends increases, the difference of the SOF fraction between the biodiesel blends and diesel fuel becomes more significant as was shown in Figures 5.1, 5.2, 5.9, and 5.10. At the full-load engine condition, neat biodiesel gave the maximum SOF fraction for two dilution tunnel conditions, 60.9% and 69.6%, at a dilution ratio of 20:1 with a constant filter temperature of 52 °C and a filter temperature 47 °C with a constant dilution ratio of 15:1, respectively. Diesel fuel produced a soluble fraction of only 10.5% and 15.5% of the total particulate mass under the same dilution tunnel conditions. With a constant filter temperature of 52 °C, the neat biodiesel had a 34.3% change in SOF between dilution ratios 20:1 and 200:1, while the SOF difference was 49.9% when the filter temperature changed from 47 to 80 °C with a constant dilution ratio of 15:1. For corresponding conditions, the diesel fuel showed differences of 35.4% and 49.2%, respectively. So, the sensitivity of both diesel fuel and biodiesel to the dilution tunnel conditions, such as dilution ratio and sampling filter temperature, was nearly the same. However, the absolute quantity of SOF from the biodiesel was more than for diesel fuel.

5.1.1.4 Effects of engine operating condition on formation of soluble organic fraction

As discussed earlier, the concentration of total particulate matter produced by the diesel engine was higher at the 20% of full-load engine operating condition than at 100% of full-load at the same engine speed of 1400 rpm. However, the total particulate emissions responded differently to biodiesel at the different engine operating conditions. At the full-load engine condition, biodiesel blends could significantly lower the total particulate emissions compared with No. 2 diesel fuel. However, at the partial load engine condition, biodiesel blends generated a higher level of total particulate matter than No. 2 diesel fuel. The change was mainly caused by the increased formation of soluble organic fraction at light-loads. Although the total mass of carbon particles in the exhaust gas at the part load engine condition was lower than at the full-load condition, the concentration of unburned hydrocarbons was higher at light-load than at full-load as shown in Figure 5.15. The high unburned hydrocarbon concentration would increase the saturation ratio of vapor phase unburned hydrocarbon in the diluted exhaust gas. The saturation ratio is one of the forces that causes adsorption and condensation to take place to form liquid phase soluble fraction on the particle surface.

5.1.2 Effects of HC sampling line temperature on vapor phase HC emissions

The unburned hydrocarbons from diesel engine exhaust gas consist of a wide variety of hydrocarbon components. Almost all of the unburned hydrocarbons are in the vapor phase when the exhaust gas leaves the engine combustion chamber. When the exhaust gas moves along the exhaust pipe and is emitted into the atmosphere, more and more unburned hydrocarbons in the vapor phase will be converted to liquid phase because of the lower temperature. The condensed unburned hydrocarbons will form the soluble organic fraction on the surface of solid carbon particles. When diesel engine HC emissions are measured, the sample of engine exhaust gas is transported from the engine exhaust pipe to the HC analyzer with a heated sampling line. If there is no heating device used to keep the sampling line at a high temperature, some of the vapor phase HC will adsorb and condense on the sampling line wall and on the carbon particles collected by the filter in the HC analyzer. This loss of HC will

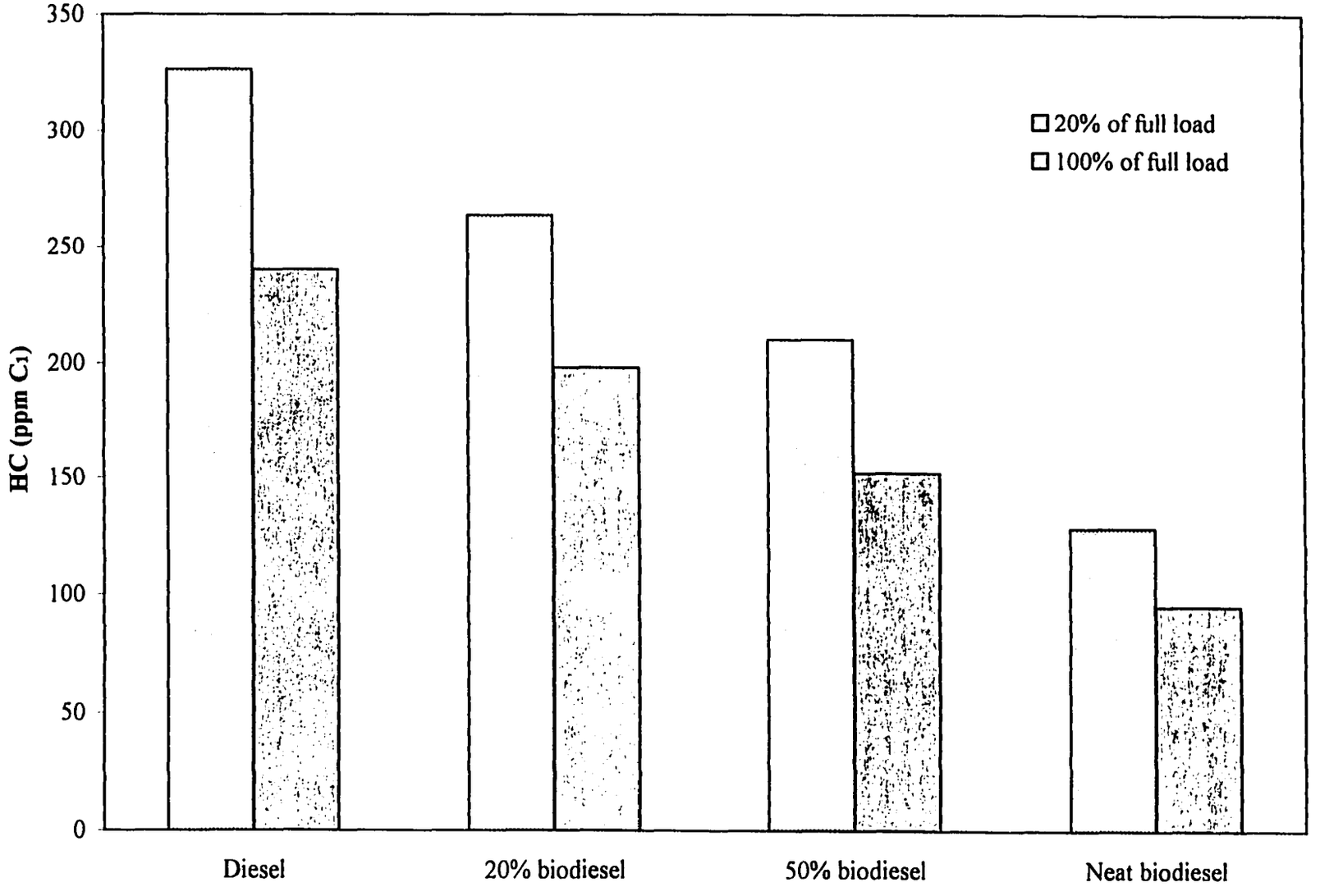

Figure 5.15 HC concentration at different engine operating conditions

cause the concentration of unburned hydrocarbons in the exhaust gas to be lowered when it reaches the HC analyzer, and the measured HC emissions will not be correct. To prevent the problems of condensation and adsorption from occurring during the HC sampling process, the standard procedure for HC emission measurement is to set the temperature of the HC sampling line and the detector oven at 190 °C. Because biodiesel has a lower volatility and a higher boiling point than No. 2 diesel fuel, the EPA-required sample temperature may be not suitable for biodiesel HC measurement. The objective of this part of the project was to investigate the effects of HC sampling line and detector oven temperature on the measured HC concentration.

Figures 5.16 and 5.17 show the concentrations of unburned hydrocarbons in the vapor phase as the sampling line temperature was varied at 100% and 20% of full-load engine operating conditions, respectively. Both figures show that the concentrations of HC increased as the sampling line temperature increased. The HC concentration was more strongly affected at low sampling line temperature than at high temperature.

The HC concentration *changes* within different temperature ranges for the two engine conditions are shown in Figures 5.18 and 5.19, respectively. The changes are based on the HC concentrations at 90, 200, and 300 °C. The temperature at 200 °C was selected as the dividing point because it was close to the sampling line temperature for the standard HC measurement. The HC concentration from 90 to 200 °C presented a large variation over that temperature range. When the sampling line temperature was increased from 200 to 300 °C, the HC concentration changes became small. It appears that few of the unburned hydrocarbon species will condense above 200 °C.

As shown in Figures 5.18 and 5.19, diesel fuel showed a larger change of HC concentration for the tested temperature range than biodiesel blends. With increasing fraction of biodiesel in the fuel blends, the absolute HC emissions and HC concentration change between 90 and 300 °C were decreased. The same trends were also shown for the temperature range between 90 and 200 °C. However, at the higher temperature range, although the HC emissions from the biodiesel blends were lower than for diesel fuel, the changes of their HC concentrations within the sampling line temperature range were slightly larger than for diesel

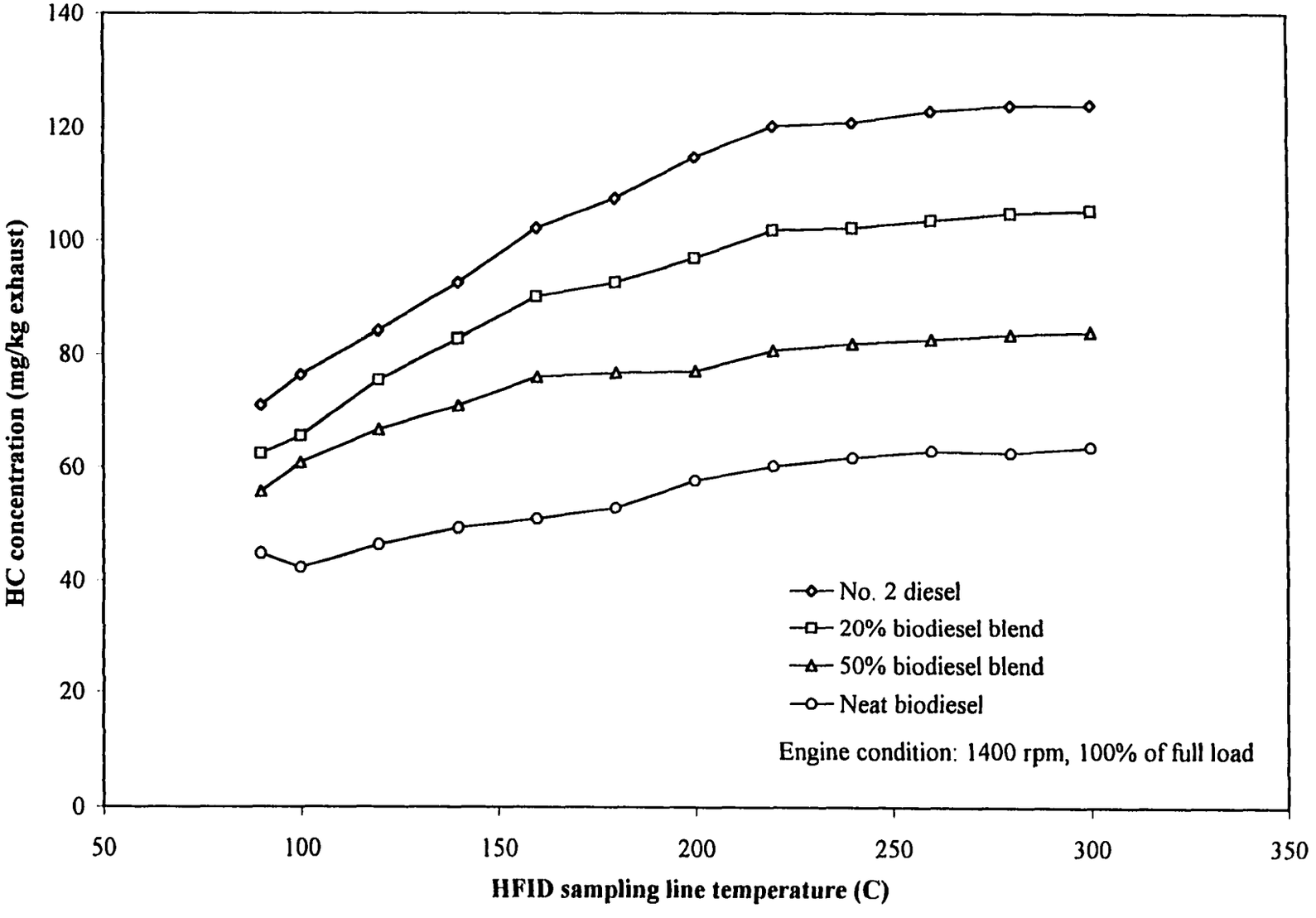

Figure 5.16 HC emissions at full-load engine condition

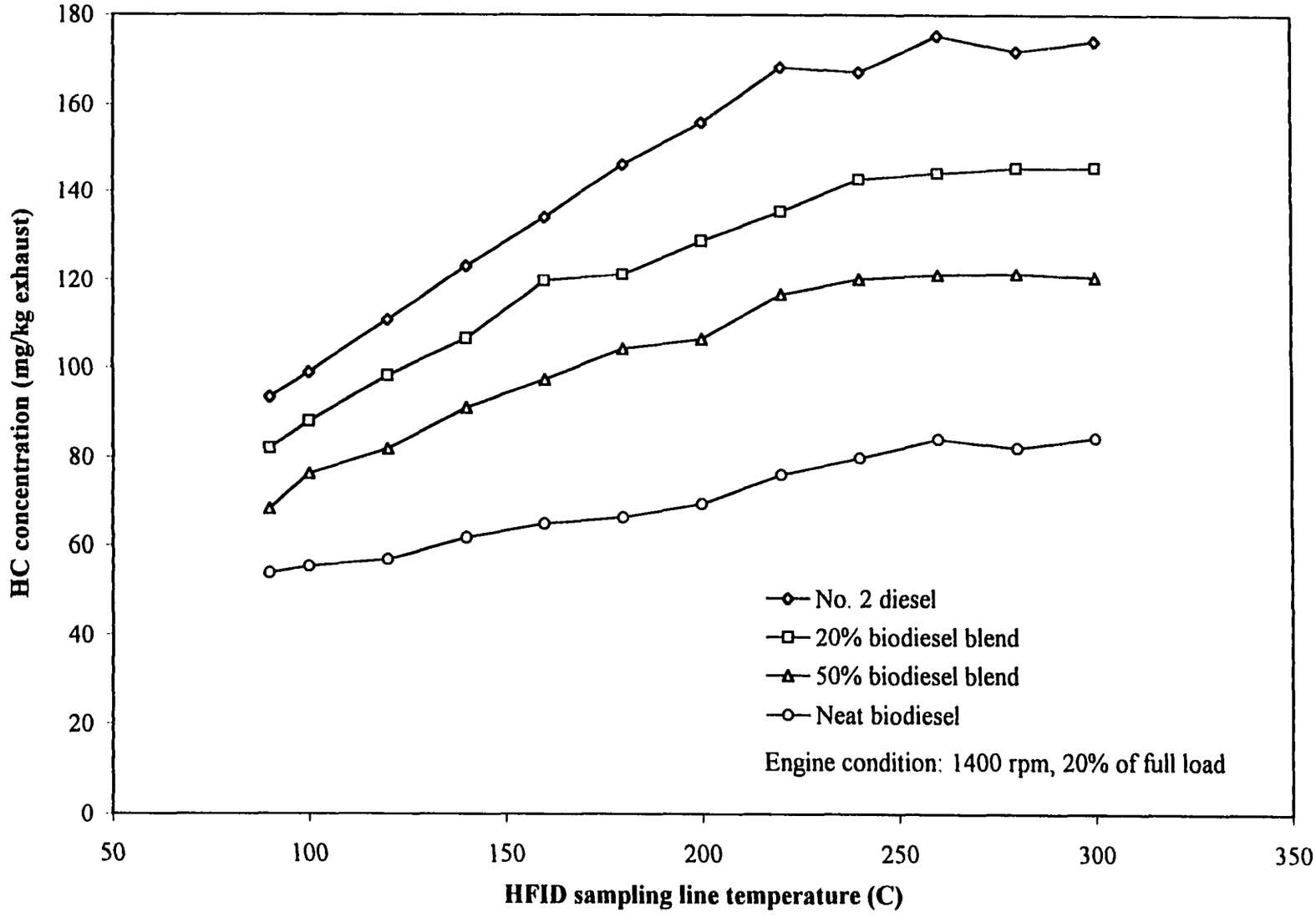

Figure 5.17 HC emissions at light-load engine condition

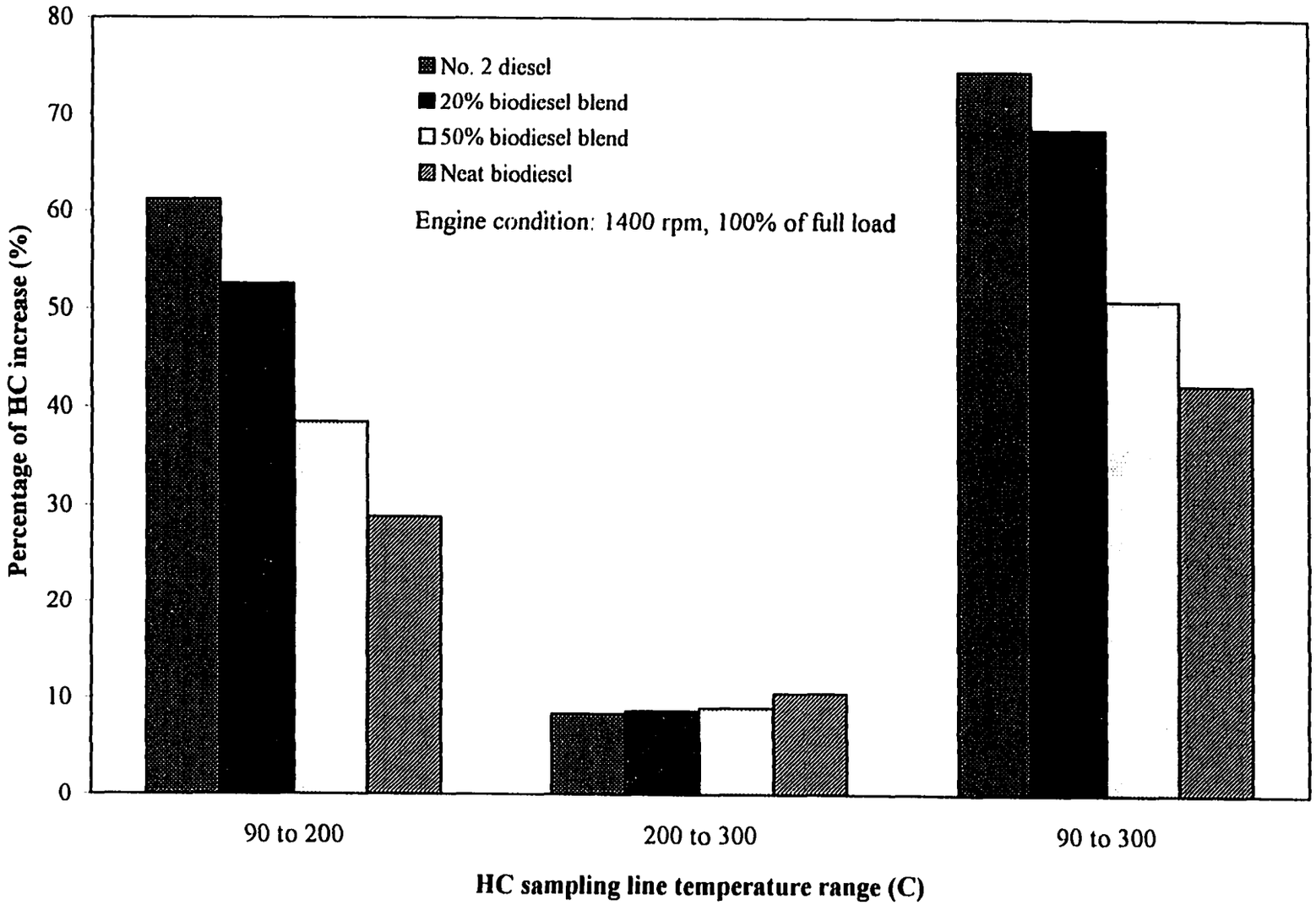

Figure 5.18 Change in HC concentration with sampling line temperature at full-load engine condition

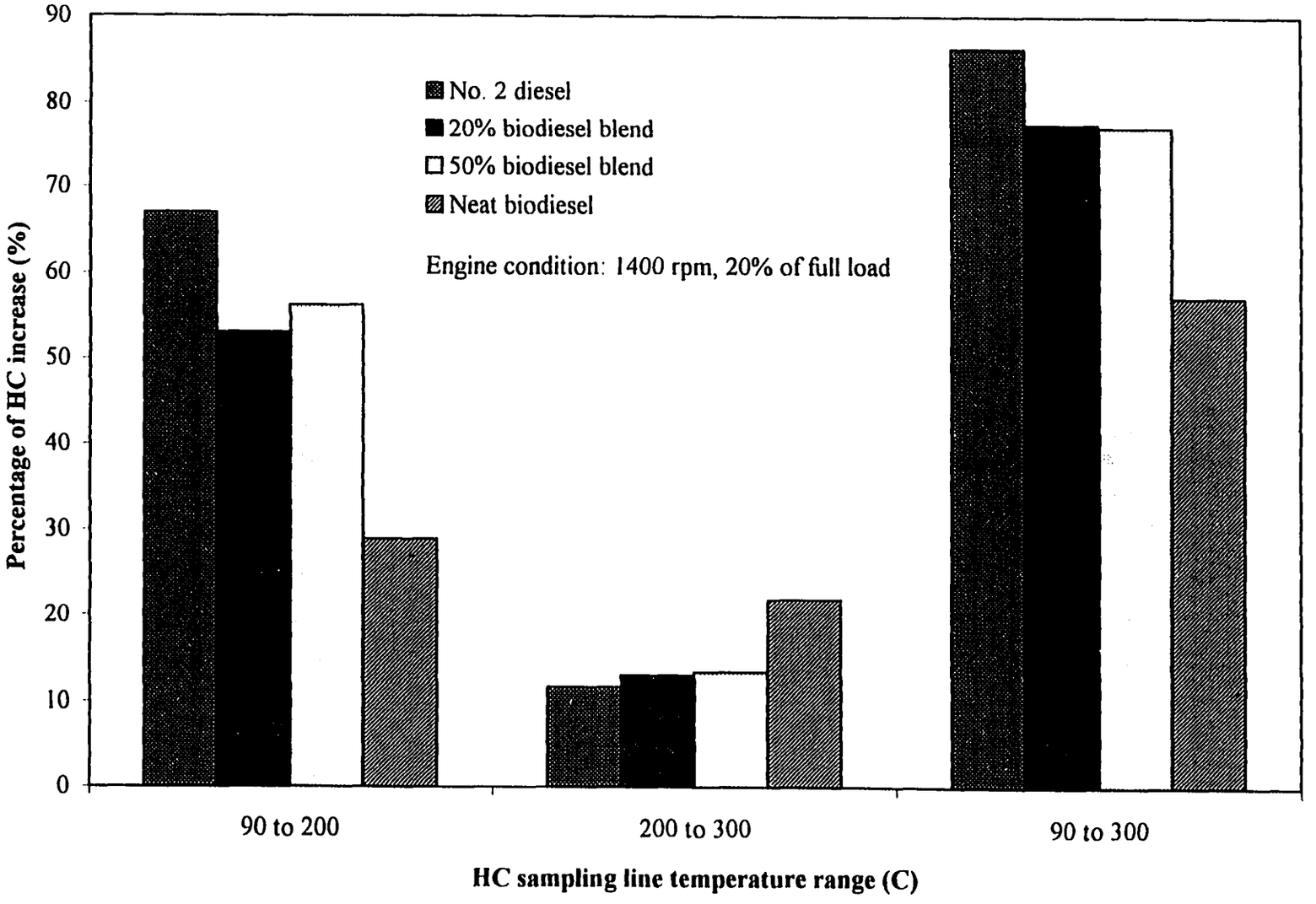

Figure 5.19 Change in HC concentration with sampling line temperature at light-load engine condition

fuel. When the HC sampling line temperature increased from 200 to 300 °C, the HC concentration of the neat biodiesel was increased by 10.5% and No. 2 diesel fuel by 8.3% at the full-load condition, while the increases of the HC concentration at the part load operating condition were 21.9% and 11.7% for the neat biodiesel and the No. 2 diesel fuel, respectively.

Based on the experimental results, the unburned hydrocarbon concentration in the raw exhaust gas is seen to be a strong function of the sampling temperature. Due to its fuel properties, most of the unburned hydrocarbons from No. 2 diesel fuel were in the vapor phase when the HC sampling line temperature was above 190 °C. However, the HC concentration from biodiesel shows a slightly large variation with the sample temperature when the HC sampling temperature was above 190 °C compared with No. 2 diesel fuel. At the high sampling temperature, more biodiesel that might have deposited on the walls of the sampling line is staying in the vapor phase.

5.1.3 Results of SOF formation during dilution process with biodiesel injection

To better understand the SOF formation from unburned biodiesel during the engine exhaust gas dilution process and the HC concentration variation when HC passes through the heated sample line, a small quantity of neat biodiesel was injected into the engine exhaust manifold to simulate the passage of unburned fuel through the engine. Because the exhaust gas temperature was relatively low, the injected biodiesel would not be burned. It was expected that most of the injected biodiesel would be vaporized and mixed with the engine exhaust gas. During this experiment, the diesel engine was only fueled with No. 2 diesel fuel. Because the concentrations of unburned hydrocarbons and carbon particles from No. 2 diesel fuel were measured in advance and assumed constant at a given engine operating condition, the injected biodiesel could be tracked by measuring the vapor phase unburned hydrocarbons with the heated flame ionization detector (HFID) and the liquid phase soluble organic fraction from the particulate measurement. The mass flow rate of injected biodiesel was controlled and recorded accurately during the engine tests. Therefore, the total mass from the measured increase in vapor phase HC and the increase in liquid phase SOF should equal the quantity of injected biodiesel.

5.1.3.1 Mass balance between the injected biodiesel and measured HC and SOF

To correctly study the distribution of unburned biodiesel to the vapor and liquid phases, the mass balance between the quantity of injected biodiesel and the sum of the measured increase in the vapor phase unburned hydrocarbons and the adsorbed and condensed hydrocarbons on the surface of carbon particles was determined. The quantity of injected biodiesel was measured directly as a mass flow rate, and the mass flow rates of vapor phase HC and liquid SOF were calculated based on the measured concentrations of HC and SOF, the exhaust gas flow rate, the dilution air flow rate, the temperature, and the pressure.

Figures 5.20 and 5.21 show the results of the mass balance for two dilution tunnel conditions: varying filter temperature with a constant dilution ratio of 15:1, and varying dilution ratio with a constant filter temperature of 52 °C, at the full-load engine operating condition. When the dilution ratio was less than 60:1 at constant filter temperature, the amount of measured SOF was greater than 100% of the injected biodiesel which means the quantity of liquid phase unburned biodiesel collected from the particulates was larger than the input biodiesel. It should be noted that the HC and SOF levels described here were the incremental amounts beyond the normal levels found with diesel fuel. When the filter temperature was lower than 70 °C with a constant dilution ratio of 15:1, the recovered mass of injected biodiesel from the SOF in the total particulates was also larger than 100%. More unburned biodiesel showed up in the SOF than the injected quantity of biodiesel. The unbalance phenomenon may have been caused by the injection device and the fuel properties of biodiesel. The pressure difference before and after the biodiesel injector was not high enough to produce a fine spray. Some of the injected biodiesel may have been liquid droplets of a large size. Because biodiesel is a low volatility fuel with a high boiling point, it is very difficult to vaporize. When the biodiesel was injected into the engine exhaust system, a portion of biodiesel was vaporized. However, some may have stayed in the liquid phase. The large size droplets could not move and mix with the exhaust gas well. They may have settled and deposited on the surfaces of the engine exhaust manifold and pipe. At a later time, with more energy being obtained from the hot exhaust system surface, the deposited biodiesel may have left the surface and been measured. The measurements of particulate and HC were not taken

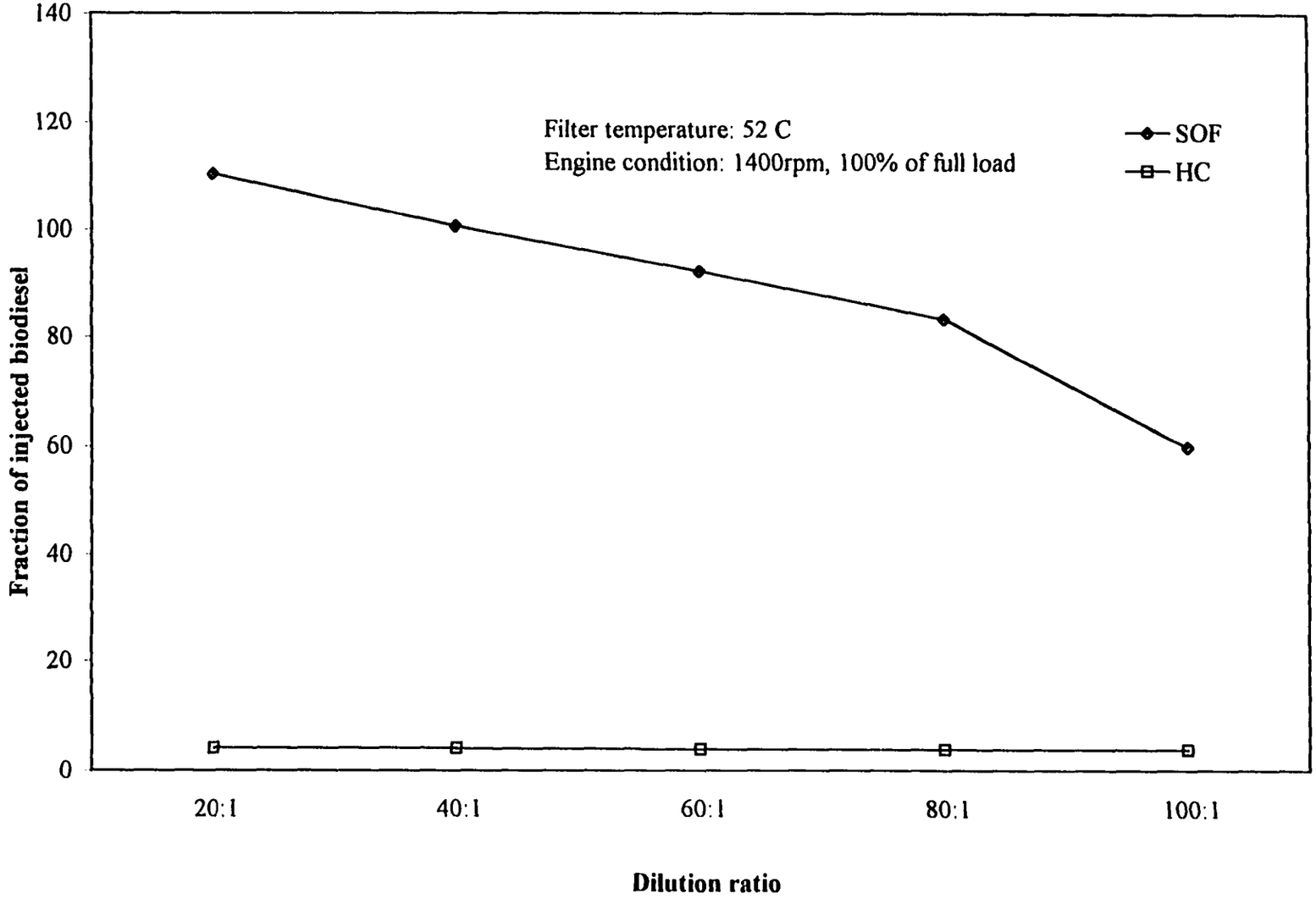

Figure 5.20 Recovery of injected biodiesel on SOF and HC for constant filter temperature

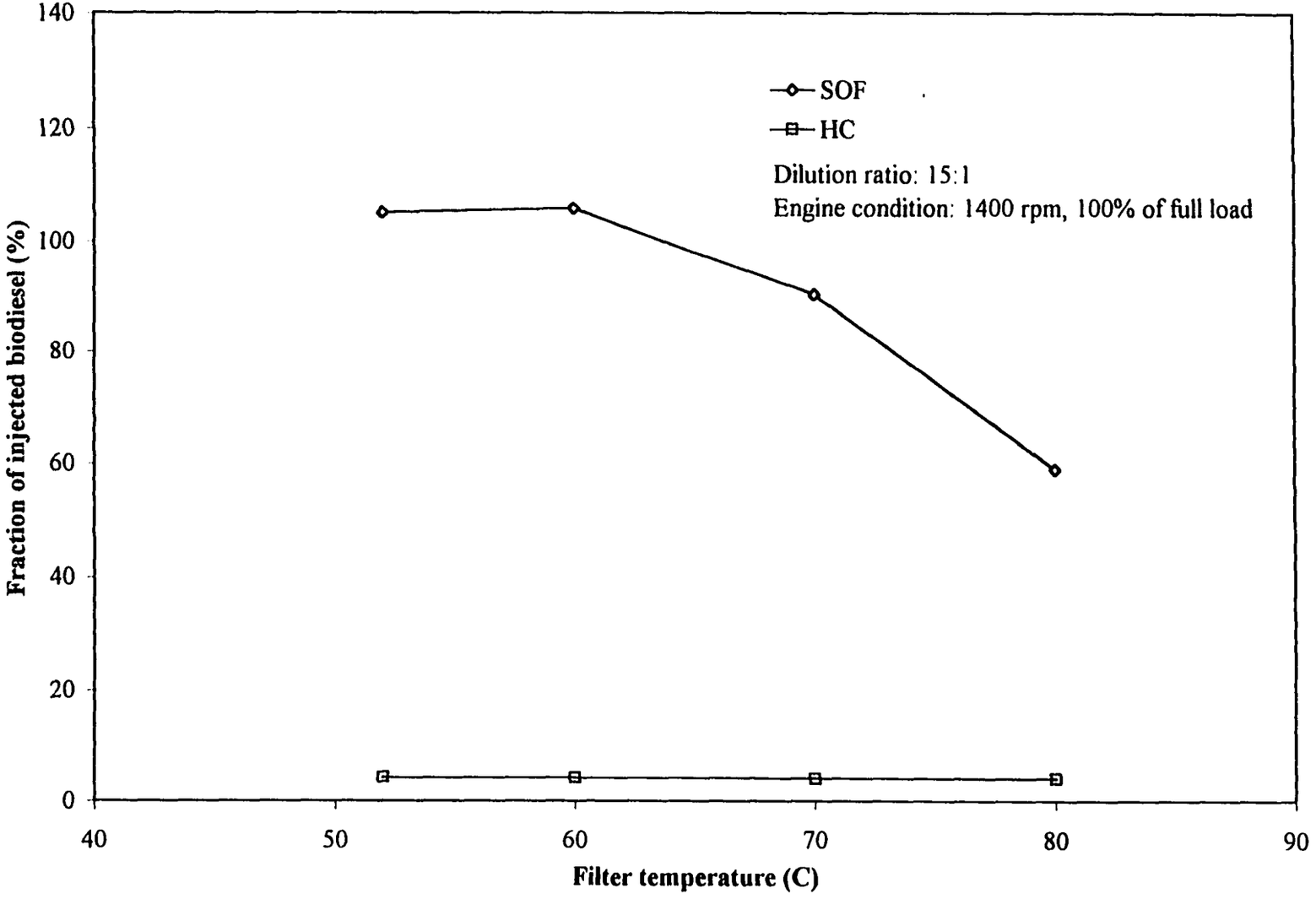

Figure 5.21 Recovery of injected biodiesel on SOF and HC for constant dilution ratio at full-load engine condition

until the injected biodiesel reached a stable state. At this time, the concentration of vapor phase unburned biodiesel in the engine exhaust system was the sum of the vaporized deposit and the currently injected biodiesel. When the particulate sample was taken, the quantity of soluble organic fraction may have been larger than the injected biodiesel.

Figure 5.22 shows the results of the mass balance for varying filter temperature with a constant dilution ratio of 15:1 at the 20% of full-load engine operating condition. At this condition, the situation was even worse than for the full-load engine condition. Even when the filter temperature was as high as 80 °C, the unburned biodiesel in the SOF was larger than 100%. This may have been because the engine exhaust gas temperature was much lower at the partial load engine condition than at the full-load engine condition. More unburned biodiesel could have been deposited on the surface of the engine exhaust system, and vaporized later. Some unburned biodiesel was observed to be leaking from the connector between the turbocharger and the exhaust pipe. Due to the leak, no more engine tests were conducted with biodiesel injection at the light-load condition.

5.1.3.2 Effects of unburned biodiesel on the formation of the soluble organic fraction

Although the mass balance based on the injected biodiesel showed that additional, unaccounted-for mass was entering the system, the trend of unburned biodiesel distribution in the liquid and vapor phase unburned biodiesel could still be investigated using these experimental data. The dilution ratio was found to have the same effect on the formation of the total particulates and soluble organic fraction in the particulates as at the normal conditions when the filter temperature was constant at 52 °C. When the dilution ratio was increased, the quantities of total particulates and SOF were reduced as shown in Figures 5.23 and 5.24. The difference in the SOF of the particulates between the dilution ratios 20:1 and 100:1 with biodiesel injection was 43.4% compared with 13.3% change without biodiesel injection. When the concentration of unburned biodiesel was increased, the quantity of soluble fraction in the total particulate mass was increased significantly. Based on the observation, nearly all of the unburned biodiesel contributed to the soluble fraction on the carbon particle

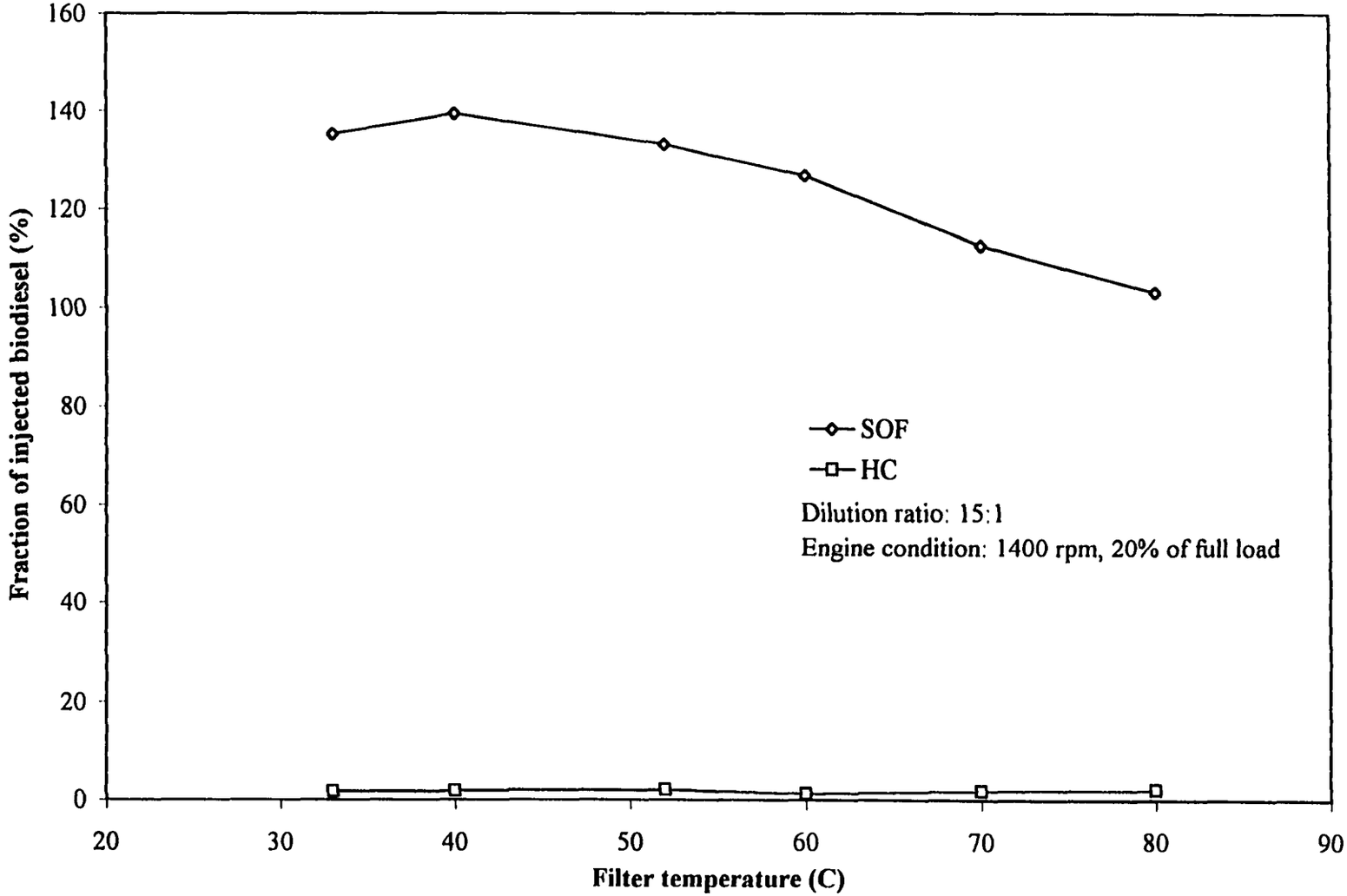

Figure 5.22 Recovery of injected biodiesel on SOF and HC for constant dilution ratio at light-load engine condition

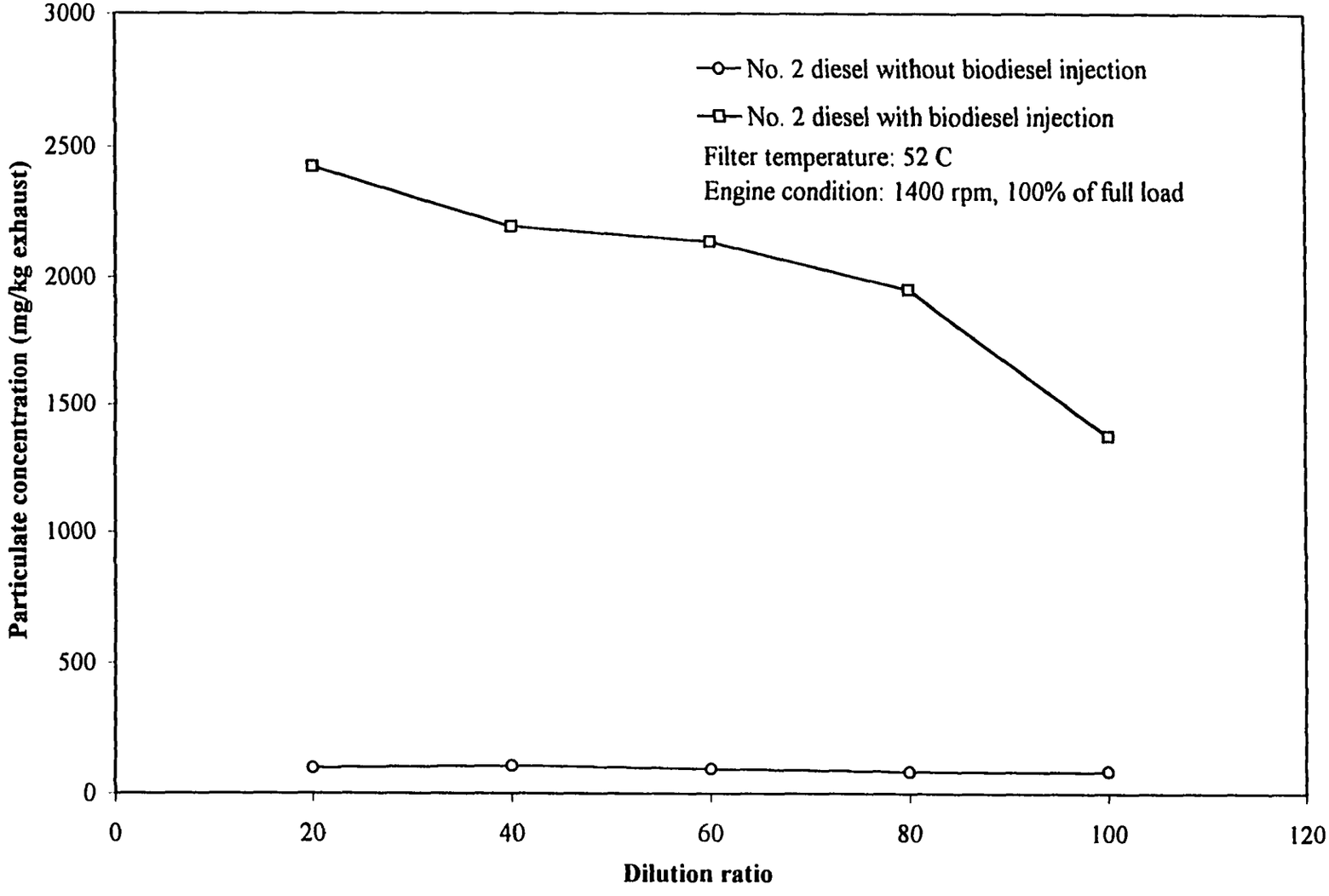

Figure 5.23 Effects of dilution ratio on total particulate emissions with biodiesel injection at full-load engine condition

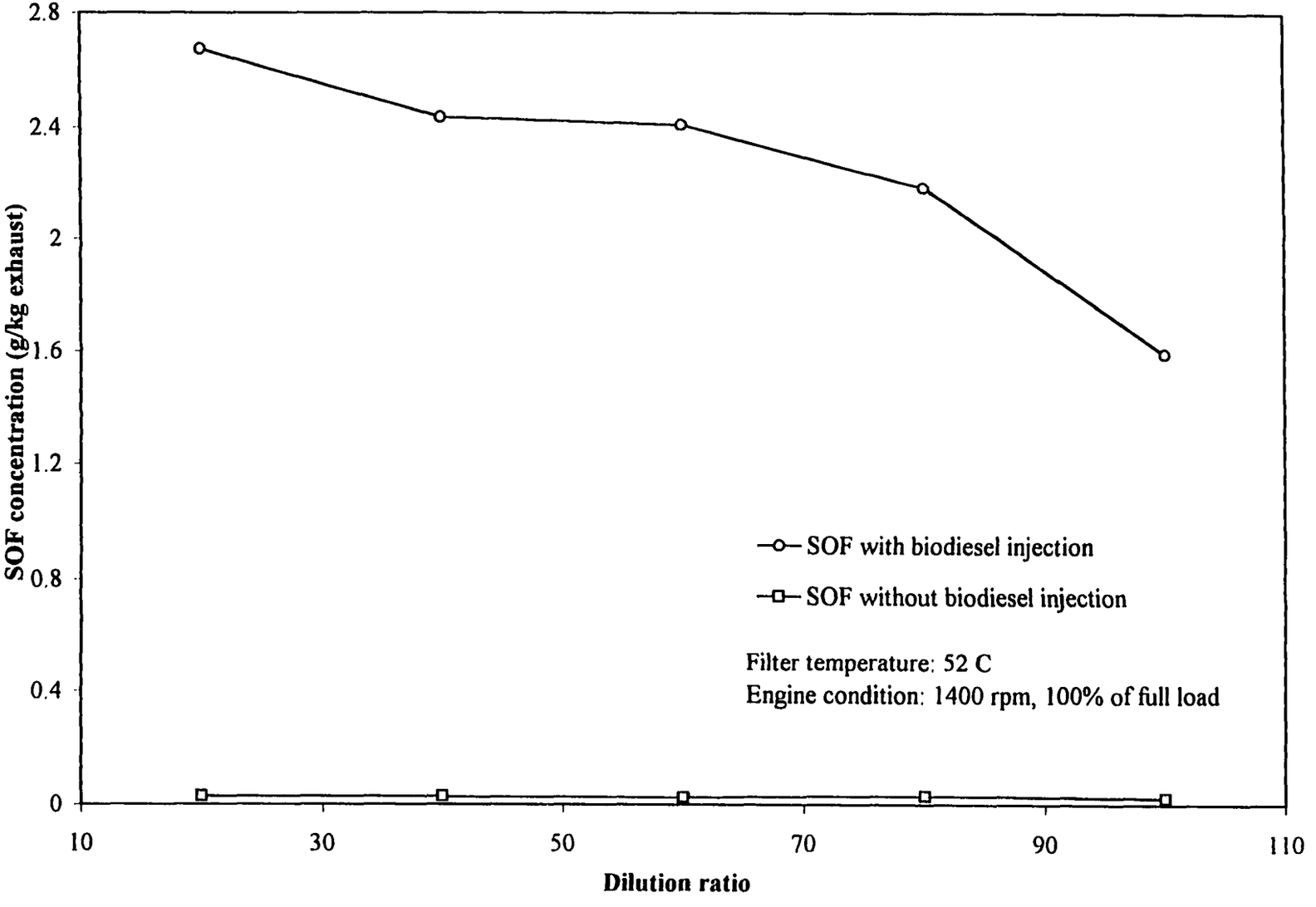

Figure 5.24 Effects of dilution ratio on SOF formation in injected biodiesel at full-load engine condition

surface during the engine exhaust gas dilution process. Only a small fraction was in the vapor phase as shown in Figures 5.20 and 5.21.

When the dilution ratio was kept constant at 15:1, the total particulates and SOF were reduced as the filter temperature increased as illustrated in Figures 5.25 and 5.26. The concentration of SOF showed a large reduction with increasing temperature. A 48.4% reduction of SOF between the filter temperatures of 52 and 80 °C was observed when the injected biodiesel was added in the exhaust gas, while the SOF formation variation was only 7.8% for the same temperature range at the normal unburned hydrocarbon level for diesel fuel.

Based on Figures 5.20 to 5.22, nearly all of the injected unburned biodiesel showed up in the SOF, and only a small proportion was traced to the vapor phase unburned hydrocarbons. When the biodiesel was injected into the engine exhaust gas, the injected biodiesel found in the vapor phase (measured at 200 °C) was only 4.1% at full-load engine condition and 1.8% at the partial load condition. However, the quantity of injected biodiesel recovered in the SOF was at least 59% for the two dilution tunnel conditions. The high conversion to SOF with biodiesel injection is probably due to the low temperature in the dilution tunnel and the high partial pressure of the unburned biodiesel.

At the light-load engine condition, only the experiment with constant dilution ratio was conducted. The results of total particulates and SOF with high unburned biodiesel concentration showed the same trend as that at the full-load engine condition.

5.1.3.3 Effects of unburned biodiesel on vapor phase HC emissions

As discussed earlier, only a small fraction of the injected biodiesel was present in the vapor phase unburned hydrocarbons. Figures 5.27 and 5.28 show the unburned hydrocarbon concentration as the HC sampling line temperature was changed with and without biodiesel injection under different engine operating conditions. As the HC sampling line temperature increased, the unburned hydrocarbon concentrations also increased. However, at low HC sampling line temperature, the HC concentrations with and without the injected biodiesel added did not change at the 20% of full-load engine operating condition. The increase of the

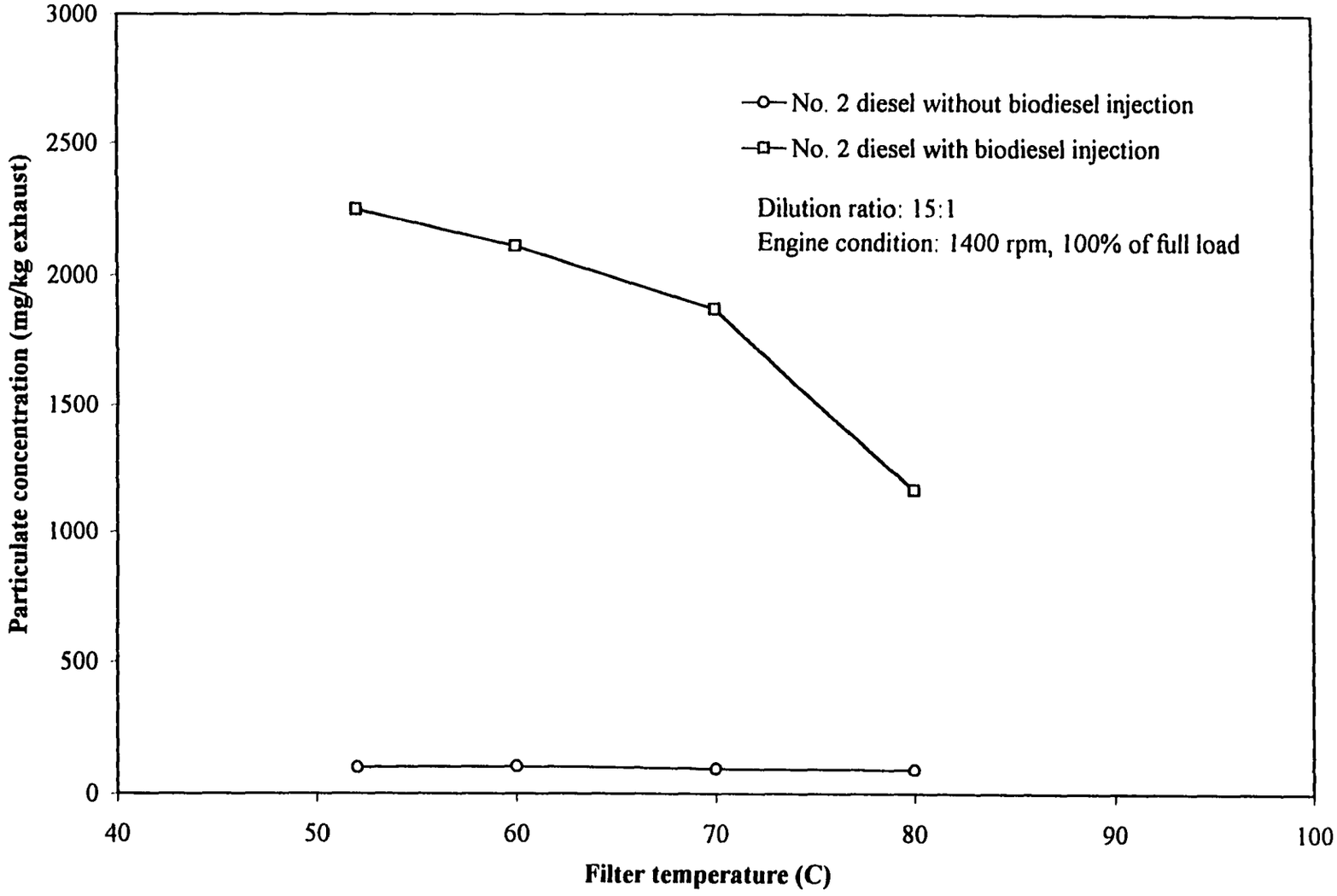

Figure 5.25 Effects of filter temperature on particulate emissions with biodiesel injection at full-load engine condition

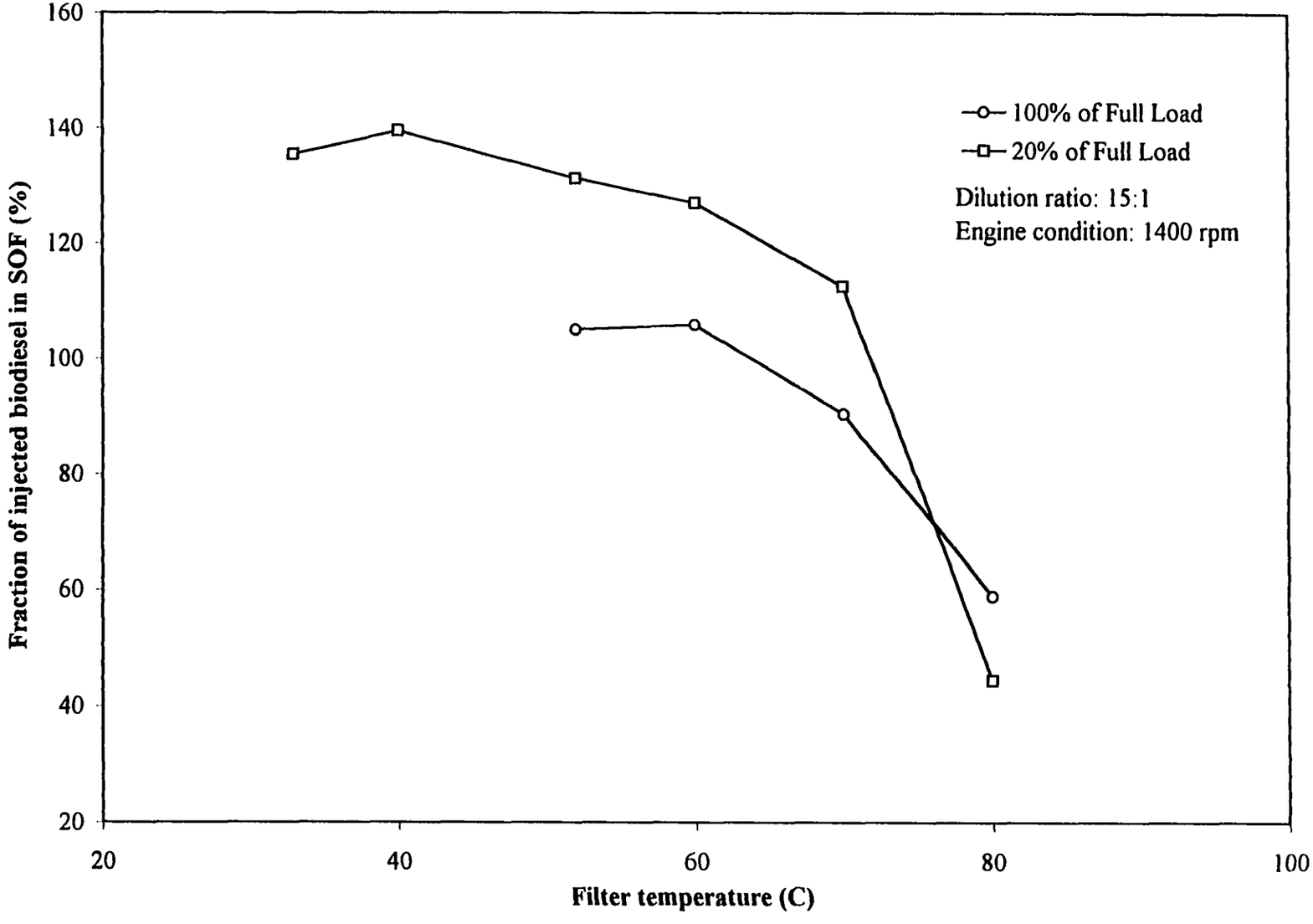

Figure 5.26 Effects of filter temperature on SOF formed from injected biodiesel at different engine conditions

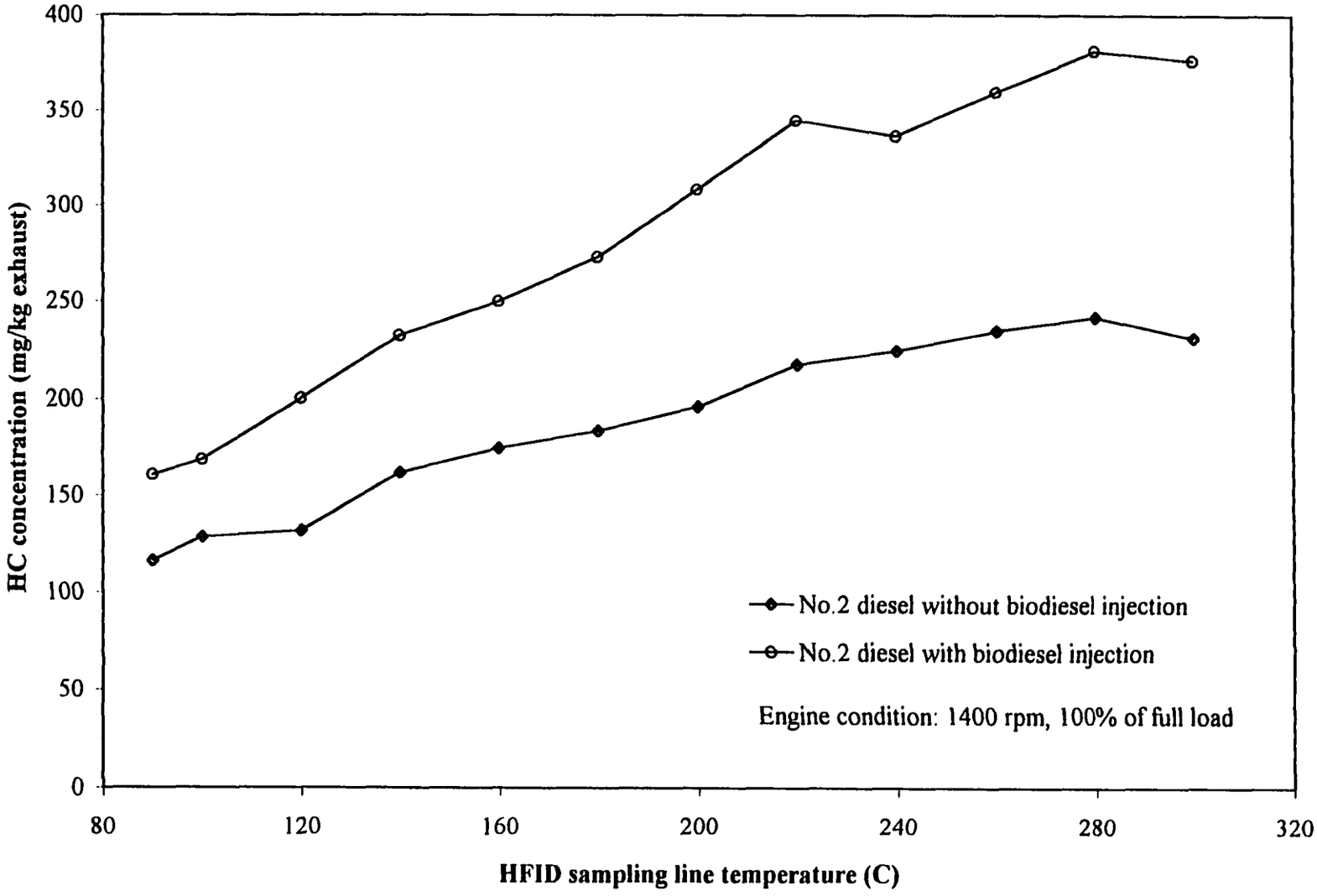

Figure 5.27 HC emissions with and without biodiesel injection at full-load engine condition

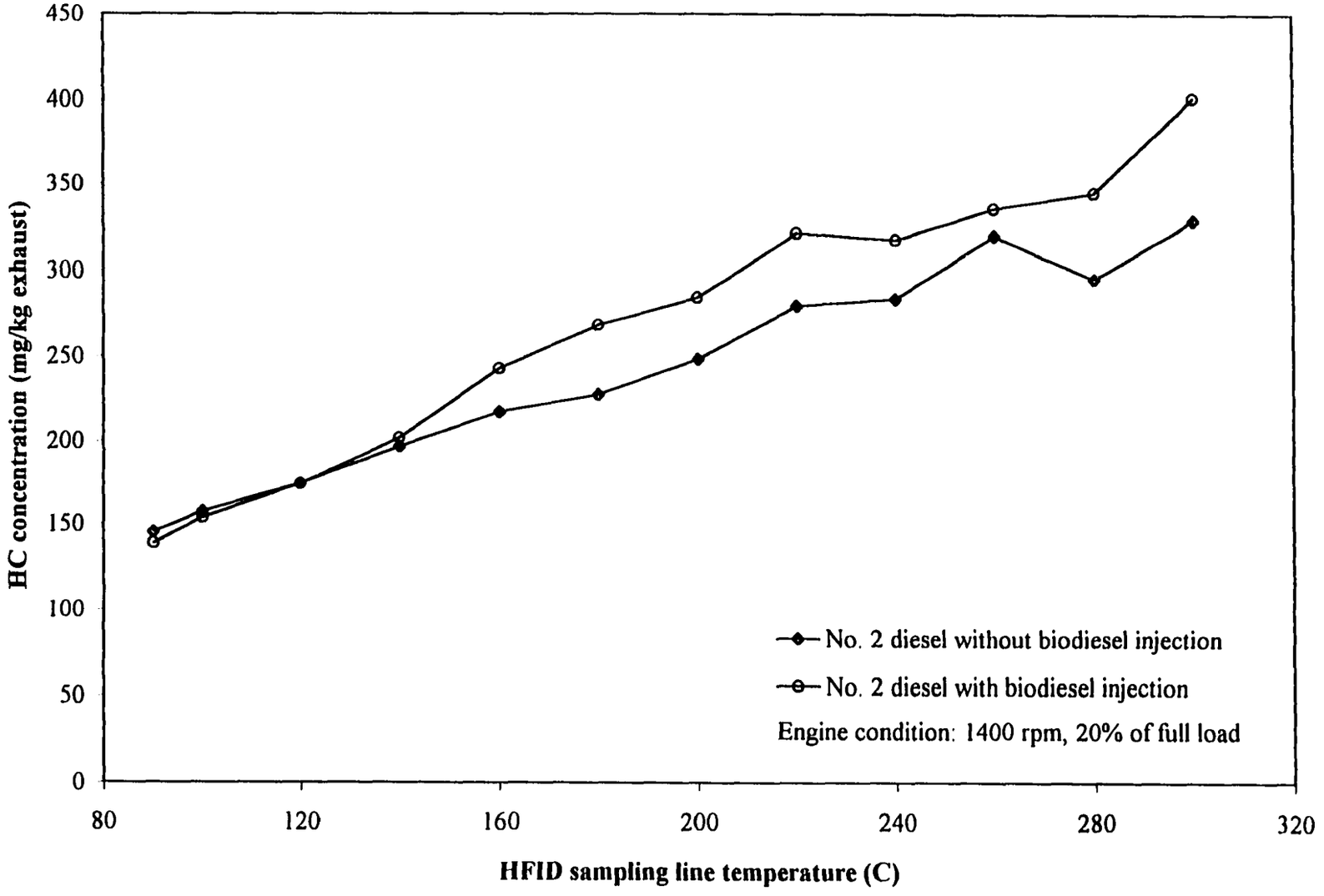

Figure 5.28 HC emissions with and without biodiesel injection at light-load condition

HC emissions at the full-load engine condition was larger than that at the light-load condition. At the HC sampling line temperature of 300 °C, the HC concentration with biodiesel injection was 62.8% higher than with no biodiesel injection at the full-load engine condition, and 21.9% higher at the partial load condition. The fraction of the injected biodiesel present as vapor phase unburned hydrocarbon was also increased as the sampling line temperature increased as shown in Figure 5.29. However, the maximum recovery rate was only 5.5% of the injected biodiesel at 300 °C at the full-load engine condition.

When biodiesel was injected into the engine exhaust system at an average injection rate of 0.17 g/s, the unburned hydrocarbon concentration in the engine exhaust gas should have reached 859 ppm as C_6 (including the baseline diesel HC concentration) at the full-load engine condition if all the injected biodiesel was vaporized. However, the flame ionization detector only reached a HC concentration of 95 ppm as C_6. When the sampling line temperature was increased to 300 °C, the HC concentration in the exhaust gas measured with the HFID was still only 116 ppm as C_6. At the 20% of full-load engine condition, the biodiesel injection rate was set to about 0.11 g/s which was equal to a HC concentration in the engine exhaust gas of 701 ppm as C_6 (including the diesel HC concentration). The reactions of the HC detector were 67 and 95 ppm as C_6 at the sampling line temperatures of 200 and 300 °C, respectively.

During the engine tests, when the neat biodiesel was injected into the engine exhaust gas, an obvious increase of blue smoke was observed at the exit of the dilution tunnel. This means that the content of liquid droplets of unburned biodiesel in the exhaust gas was increased significantly. However, the HC detector did not show much increase of HC concentration. The measured unburned hydrocarbon concentration did not match the actual HC content in the engine exhaust gas. Perhaps, these biodiesel droplets were too large to pass the particle filter in the detector. The HC concentration of the exhaust gas sample reaching the analyzer was much lower than its true value. Moreover, these biodiesel droplets would easily attach to the carbon particle surface during the exhaust gas dilution process. In addition, some researchers [16] have reported that the response of a flame ionization detector was different for different molecular structure. Biodiesel is an oxidized fuel. It contains about 10% (by mass) oxygen in its molecule and has some double bond compounds. This may cause the

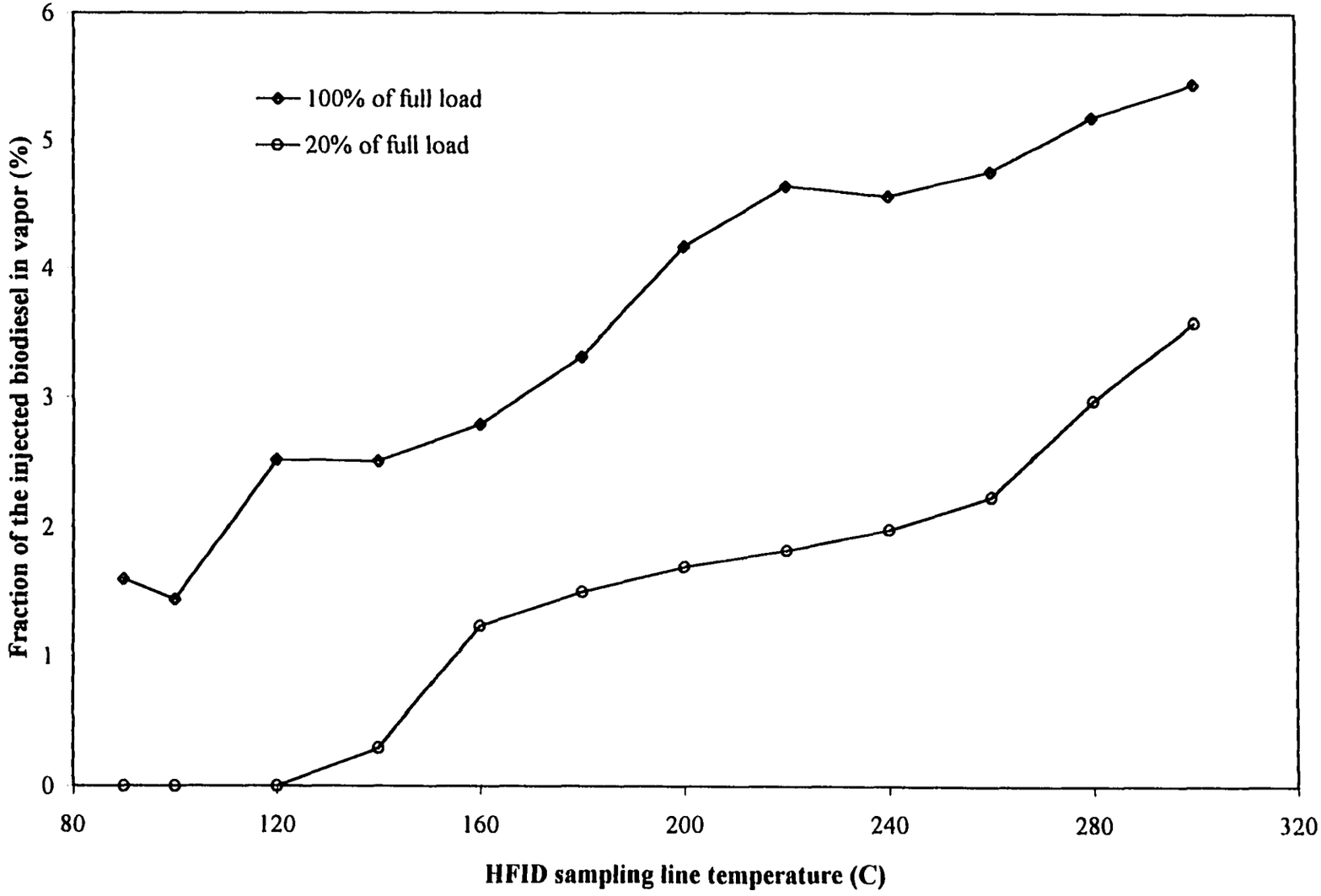

Figure 5.29 Recovered fraction of injected biodiesel as HC vapor-phase

incorrect reaction of HC detector on the unburned biodiesel. More research is needed to study the reaction of a traditional HC detector to biodiesel.

5.2 Results from Model Prediction

A predictive model can help to increase the understanding of the formation of the liquid soluble organic fraction on the particulate surface and allow simulation of the formation process. Mathematical models for condensation and adsorption have been developed to predict the quantity of SOF in the particulates based on dilution tunnel variables such as the dilution ratio, the filter temperature, the solid carbon concentration, the vapor phase HC concentration, etc. The models were also used to study the concentration variation of the vapor phase unburned hydrocarbons in the HC sampling line at different temperatures. When these models were developed, the condensation and adsorption processes were assumed to be at an equilibrium state. The processes of condensation and adsorption of unburned hydrocarbon vapor can be divided into two stages: the condensation and adsorption and the mass diffusion of the hydrocarbons. When the process of condensation or adsorption removes the adsorbates (unburned hydrocarbon vapor) from the adjacent vapor phase, a concentration gradient is created and more adsorbate moves in to fill the void. The process of mass diffusion replaces the hydrocarbons removed from the surrounding boundary layer and this operation continues until an equilibrium state is reached between the unburned hydrocarbons in the bulk flow and the liquid phase soluble fraction on the particle surface. An important concern in determining the kinetics of vapor adsorption or condensation is the mass transfer rate of unburned hydrocarbons from the bulk flow of the diluted exhaust gas to the surface of the carbon particle. The mass transfer rate will be discussed in the following section.

5.2.1 Mass transfer by diffusion from bulk diluted exhaust to carbon particle surface

Mass transfer by diffusion is caused by a concentration gradient. The similarity between convection heat transfer and diffusion mass transfer is well known. A mass transfer coefficient that is similar to a heat transfer coefficient can be determined by assuming

negligible viscous dissipation, chemical reaction, and low mass transfer rate. The detailed mass transfer rate calculation is discussed in Appendix E.

An assumption used during the model development was that the adsorption and condensation take place at equilibrium. Based on the assumptions and calculations discussed in Appendix E, the change in concentration of unburned hydrocarbons as a function of time during the adsorption process is shown in Figure 5.30. After about 0.0025 second, the unburned hydrocarbon concentration is close to an equilibrium condition. However, the residence time is about 0.25 second when the engine exhaust gas enters the dilution tunnel at the full-load engine condition with the dilution air flow rate for a dilution ratio of 15:1. The assumption of equilibrium adsorption used in this study appears to be justified.

5.2.2 Predicted results of SOF formation during the dilution process

The condensation and adsorption models were developed based on the physical mechanisms that control the formation of SOF during the engine exhaust gas dilution process. The quantity of SOF formed during the dilution process was simulated using these two models at different dilution tunnel conditions and engine operating conditions. The accuracy of the models was then assessed by comparing the predicted results with the experimental results at the same conditions.

5.2.2.1 Prediction of SOF formation based on condensation model

5.2.2.1.1 Effects of dilution ratio on SOF formation due to condensation. When the prediction of SOF formation was performed, some information about the initial composition of the system was needed as input. Table 5.1 shows the information provided as input to the condensation and adsorption models. The concentration of HC was measured with the heated flame ionization detector at 190 °C, and the concentration of solid carbon was determined from the particulate samples based on the engine tests discussed previously. The composition of the unburned hydrocarbons in the engine exhaust gas was assumed to be the same as the fuel composition which was shown in Table 3.2.

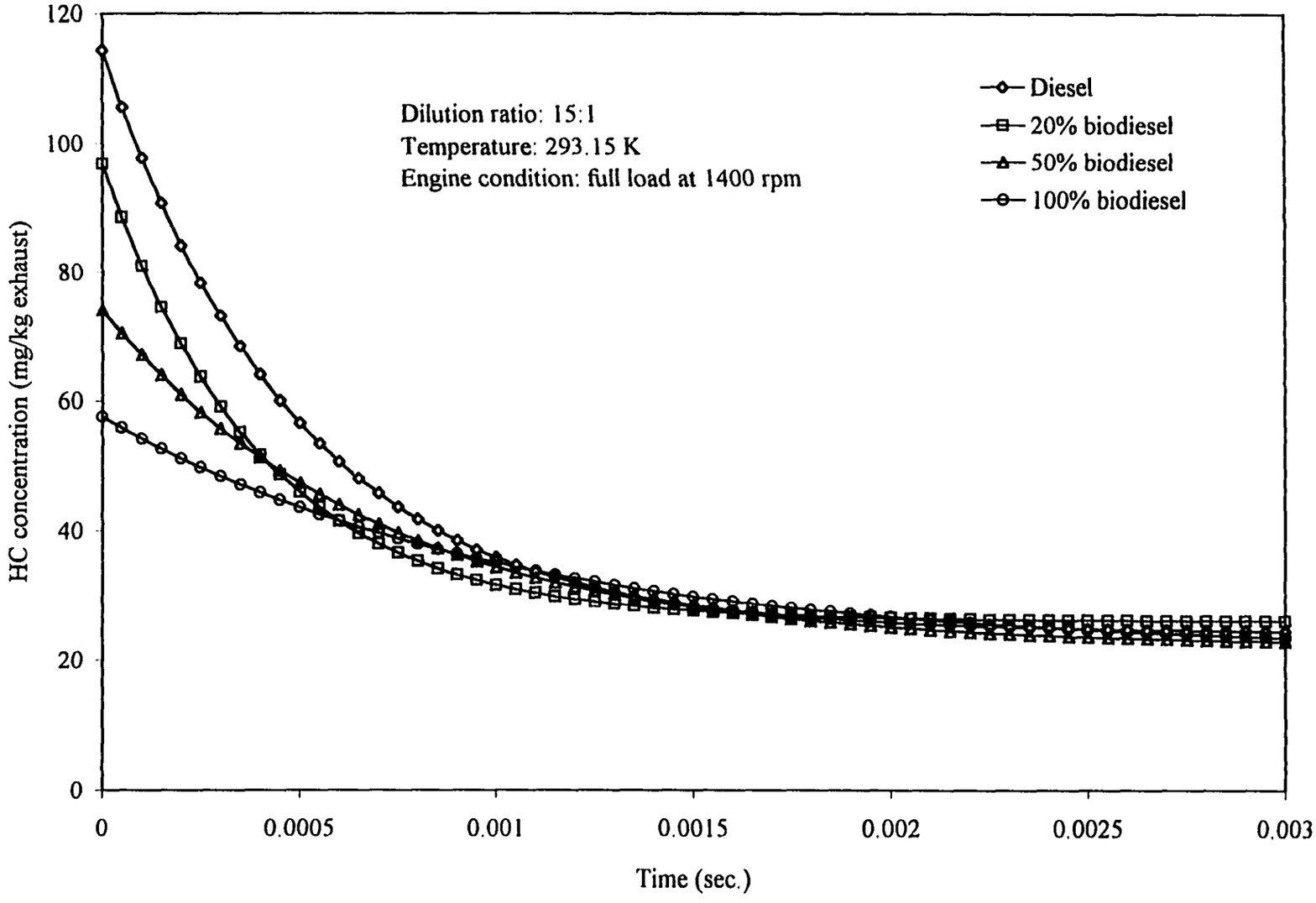

Figure 5.30 Time required to reach adsorption equilibrium

Table 5.1 Input information for model predictions

Fuel	Engine condition	Solid carbon concentration mg/kg exhaust gas	HC concentration ppm as C_1
No. 2 diesel	100% of full-load	65.9	239.7
20% biodiesel	"	56.4	198.2
50% biodiesel	"	33.5	152.1
100% biodiesel	"	13.5	94.9
No. 2 diesel	20% of full-load	6.8	326.7
20% biodiesel	"	6.0	263.6
50% biodiesel	"	5.8	210.1
100% biodiesel	"	5.2	128.6

Figures 5.31 and 5.32 show the comparison between the results of the experiments and the predictions of the condensation model at a constant filter temperature of 325 K, when the dilution ratio was varied for two engine operating conditions. The quantity of condensed hydrocarbons on the carbon particle surface calculated by the condensation model was most significant for small dilution ratios. As the fraction of biodiesel in the fuel blends was increased, the condensed HC became larger at a given dilution ratio. However, when the dilution ratio was greater than 15:1, no condensation of unburned hydrocarbons took place for any of the fuels at the constant filter temperature of 325 K. The No. 2 diesel fuel, represented by n-dodecane, did not show any condensed HC for any dilution ratio. These results indicate that, based on the condensation model, there should be no soluble organic fraction formed on the particle surface when the dilution ratio is greater than 15:1 and the filter temperature is kept at 325 K. However, the experimental results show that a significant amount of SOF is formed at a dilution ratio of 20:1 for each fuel. Even when the dilution ratio was equal to 200:1, there was still some SOF that formed on the particulates as shown in Figures 5.31 and 5.32.

The condensation model predicts a sharp reduction in the quantity of condensed HC as the dilution ratio is increased. However, the results of the total particulate measurement did

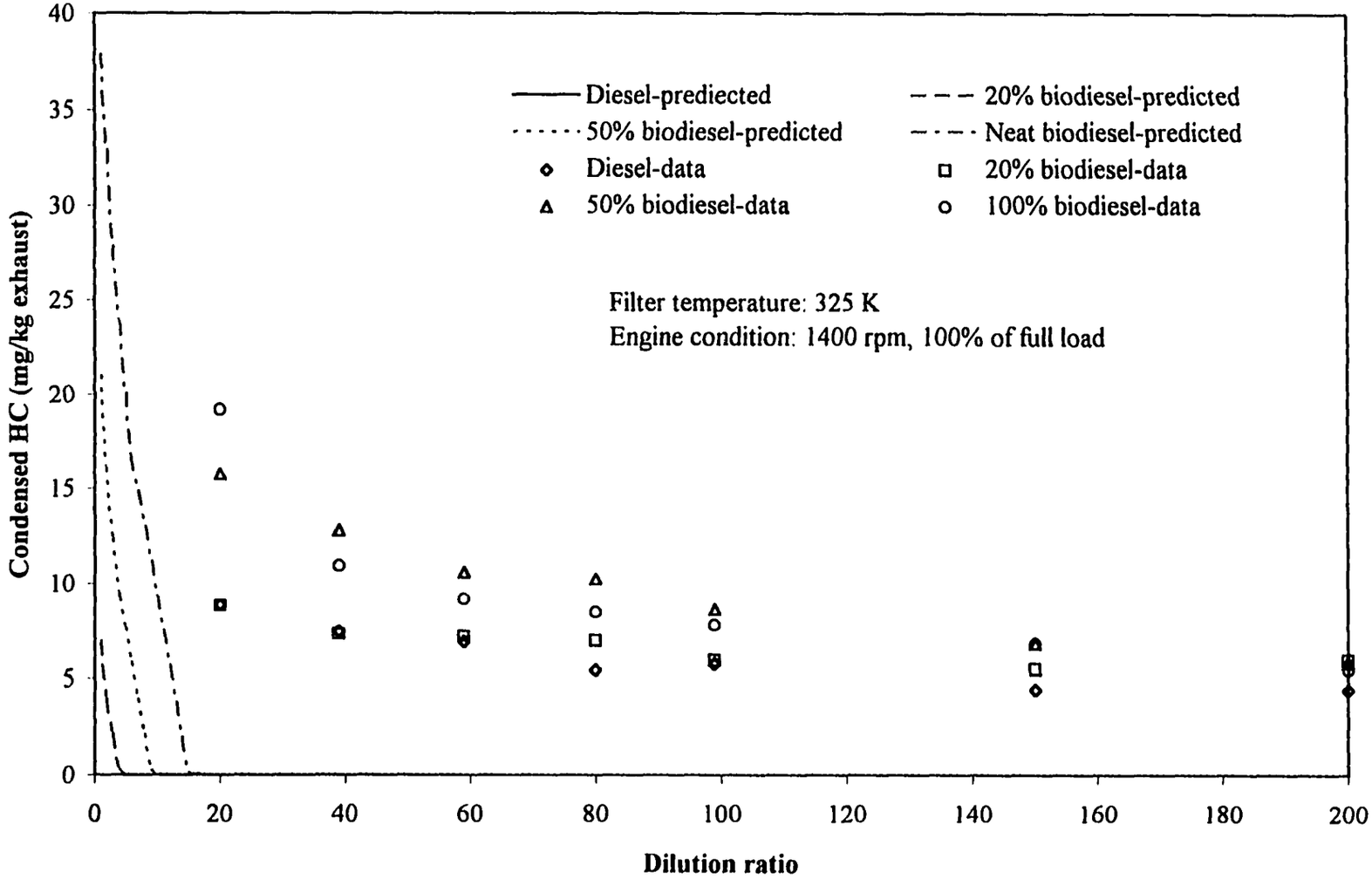

Figure 5.31 Comparison of SOF formation between condensation model and experimental data at constant filter temperature and full-load engine condition

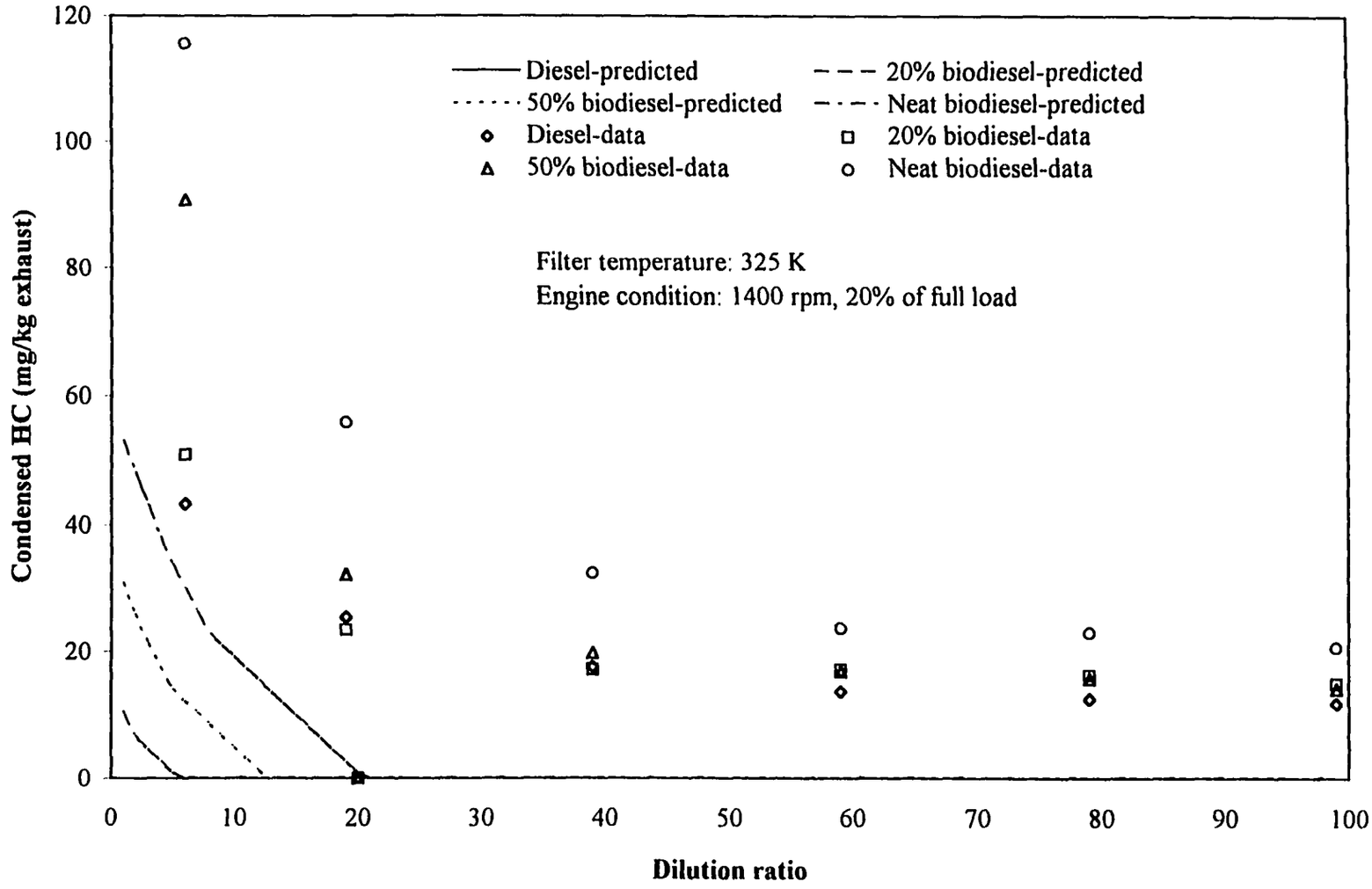

Figure 5.32 Comparison of SOF formation between condensation model and experimental data at constant filter temperature and light-load engine condition

not reflect this dilution effect. The simple condensation model could not, by itself, accurately predict the experimentally observed trends of SOF formation with varying dilution ratio.

5.2.2.1.2 Effects of filter temperature on SOF formation due to condensation. The predicted effects of filter temperature on the SOF formation with a constant dilution ratio of 15:1 using the condensation model are shown in Figures 5.33 and 5.34 for the 100% and 20% of full-load engine conditions. No condensation was expected for n-dodecane when the filter temperature was changed because its saturation pressure is relatively high and the saturation ratio is less than one. However, condensation of the biodiesel blends was possible at filter temperatures less than 312, 320, and 326 K as shown in Figure 5.33 for 20%, 50%, and 100% biodiesel blends, respectively. Although some condensation of unburned fuel was predicted by the condensation model for neat biodiesel at a filter temperature of 320 K, the predicted quantity was much lower than that measured during the experiment. A significant amount of soluble fraction on the total particulates was observed during the experiment even at high filter temperature. It is obvious that the condensation phenomenon alone can not accurately describe the formation of SOF during the dilution process.

At the 20% of full-load engine operating condition, more condensed hydrocarbons can be found than at the 100% of full-load engine condition based on the calculation of the condensation model. This was due to the higher concentration of unburned hydrocarbons in the exhaust gas which increased their partial pressures. The predicted results from the condensation model for both varying dilution ratio and filter temperature were similar to those of Plee [14].

Based on the comparison between the results of the model predictions and the experiments, it can be concluded that the condensation mechanism incorrectly estimates the magnitude of the condensed SOF on the carbon particle surface. As was shown in Figures 5.31 to 5.34, nearly all of the vapor phase hydrocarbon condensation occurs at low filter temperature, whereas no HC condensation is expected at temperatures and dilution ratios in excess of 330 K and 20:1, respectively, which is not in agreement with the experimental observations.

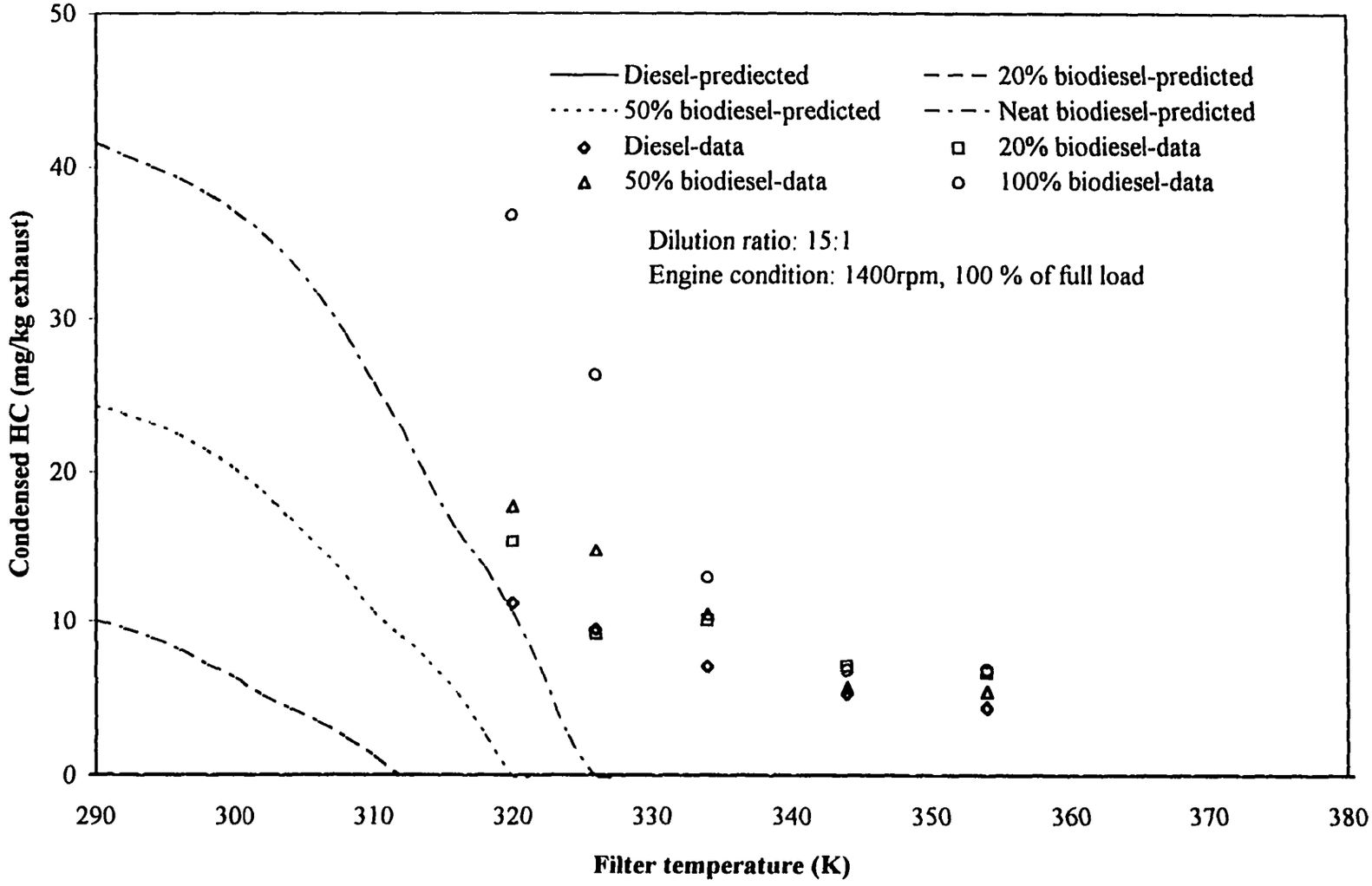

Figure 5.33 Comparison of SOF condensation between condensation model and experimental data at constant dilution ratio and full-load engine condition

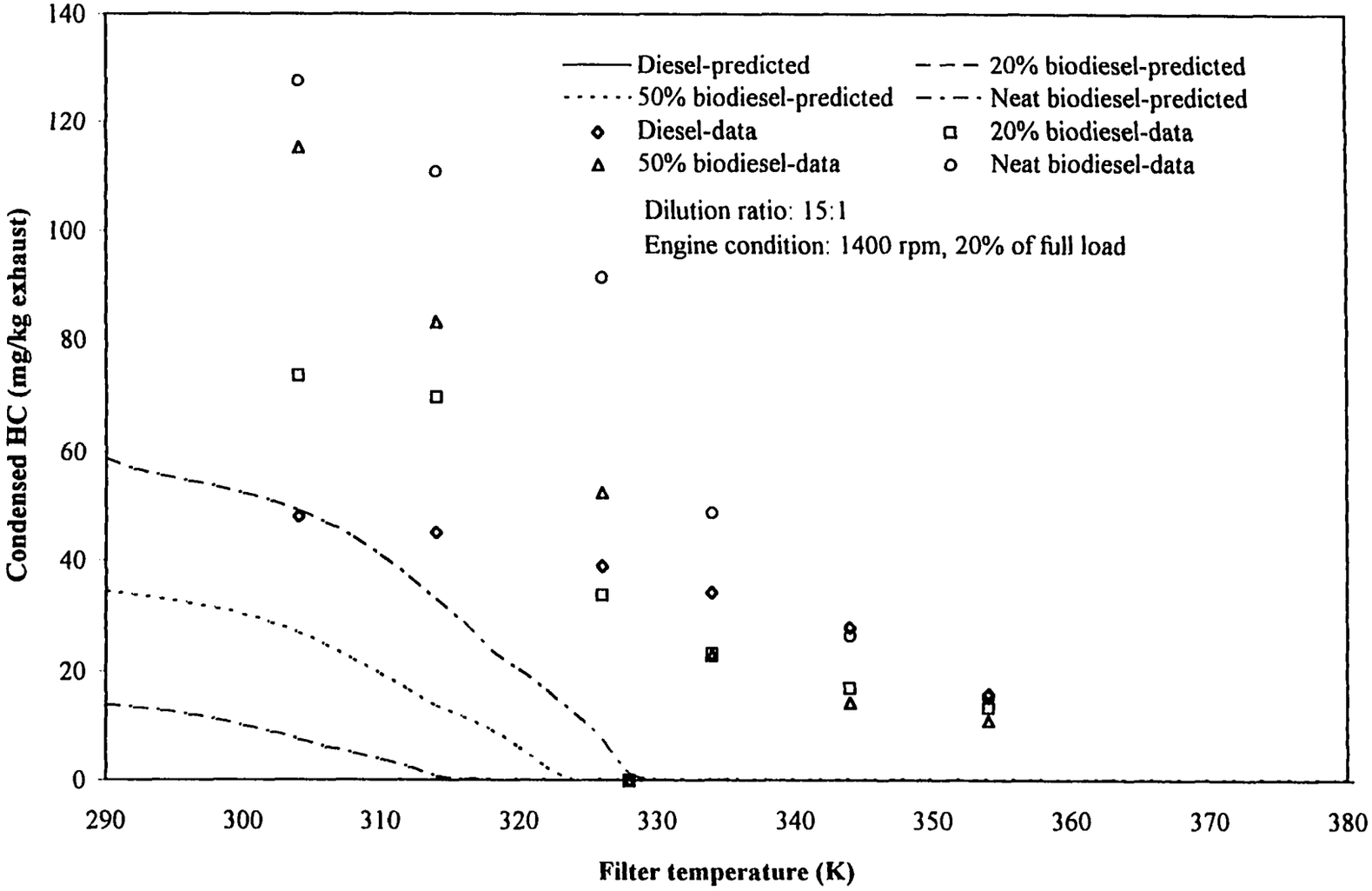

Figure 5.34 Comparison of SOF condensation between condensation model and experimental data at constant dilution ratio and light-load engine condition

5.2.2.1.3 Effects of fuel components on SOF formation during the dilution process. The occurrence of condensation is determined by the saturation ratio of the individual hydrocarbons in the dilution system. When the saturation ratio of each vapor component in the exhaust gas is larger than unity, condensation is predicted to take place and liquid phase unburned hydrocarbons will be formed on the carbon particle surface. The saturation ratio is a function of the hydrocarbon properties, such as boiling point, saturation vapor pressure, temperature, etc. Figures 5.35 to 5.38 show more detailed information about the saturation ratio of each component in the fuels as the dilution ratio is varied and Figures 5.39 to 5.42 show the saturation ratio as the filter temperature is varied. Because diesel fuel was assumed to have the same chemical structure as n-dodecane which boils at a temperature far below that of the biodiesel components, its saturation ratio was usually far below its saturation line for all dilution ratios and filter temperatures. Because the fractions of methyl oleate and methyl linoleate in biodiesel were relatively high, 21.6% and 54.6% by mole, respectively, and since these esters have a higher boiling point and a lower volatility than diesel fuel, their saturation ratios were the first to reach unity as the amount of biodiesel in the blends increased. Similar trends were observed for both dilution ratio and filter temperature variations based on the calculated results. When the engine was run at the part load condition, similar condensation results were obtained.

5.2.2.2 Prediction of SOF formation based on adsorption model

Adsorption is the other mechanism that governs SOF formation during the engine exhaust gas dilution process discussed earlier. The adsorption process can occur at saturation ratios of less than unity. The adsorption model was developed based on adsorption isotherm theory with the capability to predict multicomponent adsorption. The accuracy of the predictions of the adsorbed quantity of unburned hydrocarbons on the carbon particle surface during the dilution process can be determined by comparing the adsorbed quantity predicted by the model with the adsorbed quantity measured during the engine tests at the same conditions. The quantity of adsorbed unburned hydrocarbons were predicted with the same unburned hydrocarbon composition shown in Table 3.2 and the same input information used

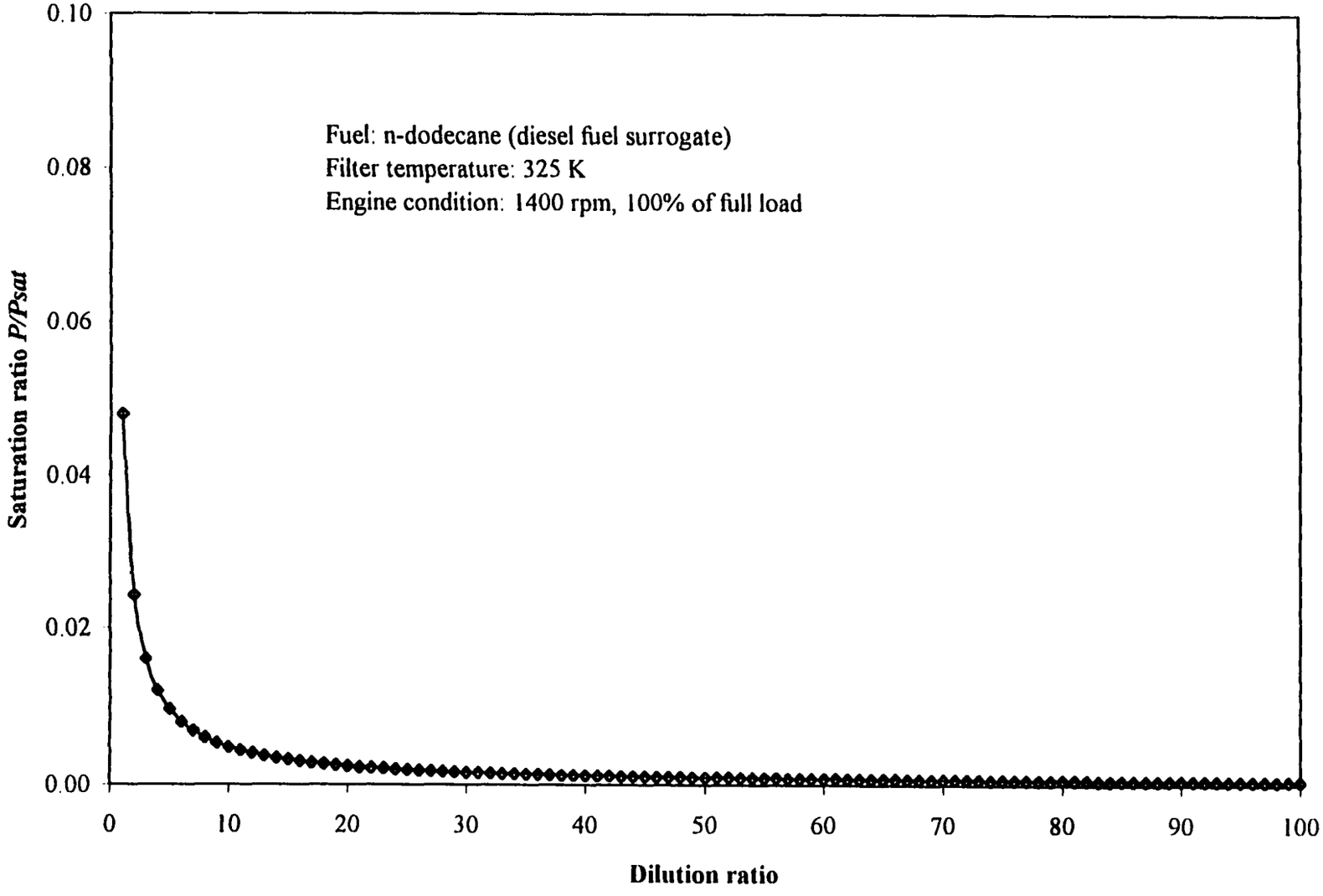

Figure 5.35 Effects of dilution ratio on saturation ratio of n-dodecane at full-load engine condition

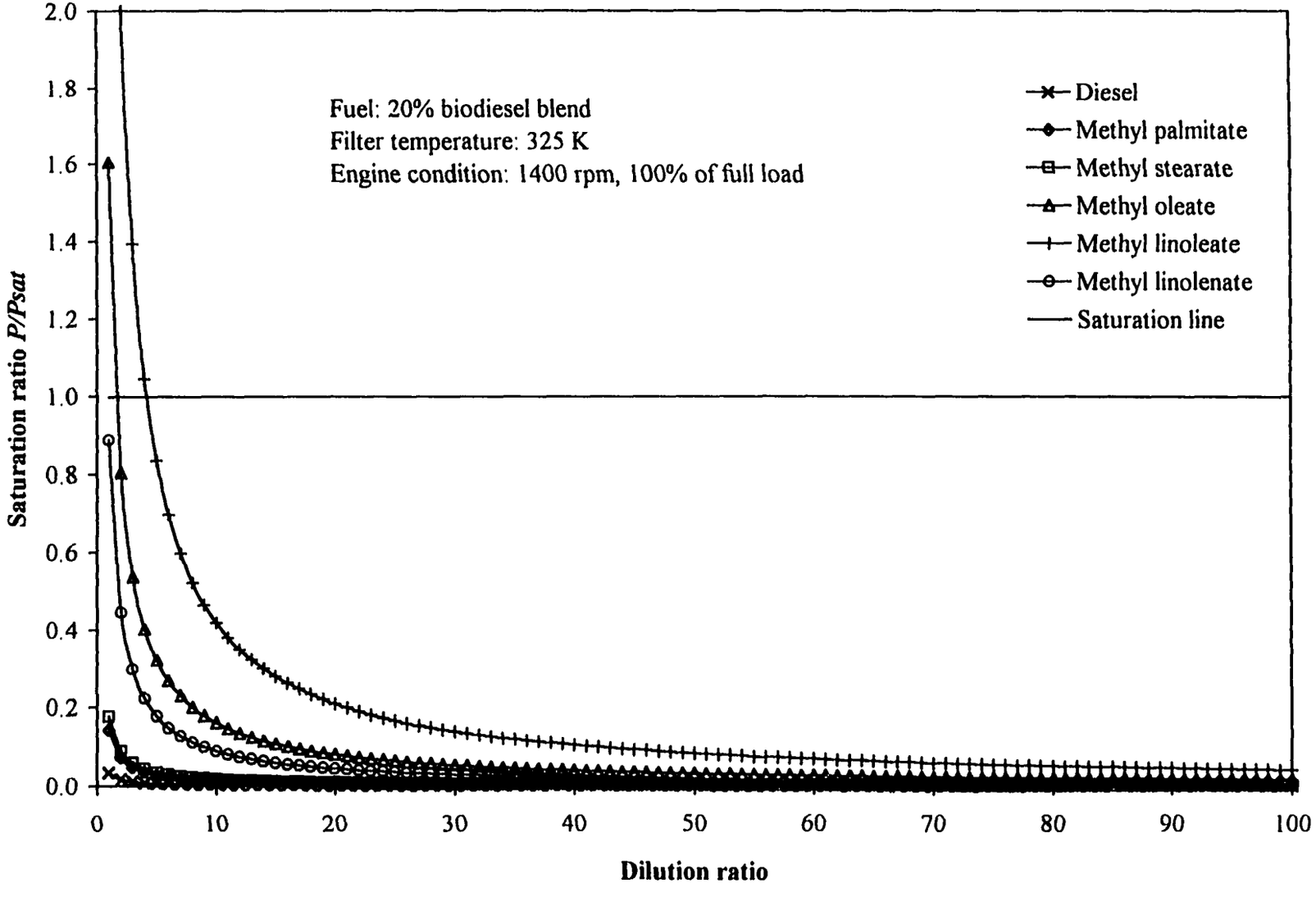

Figure 5.36 Effects of dilution ratio on saturation ratio of 20% biodiesel blend at full-load engine condition

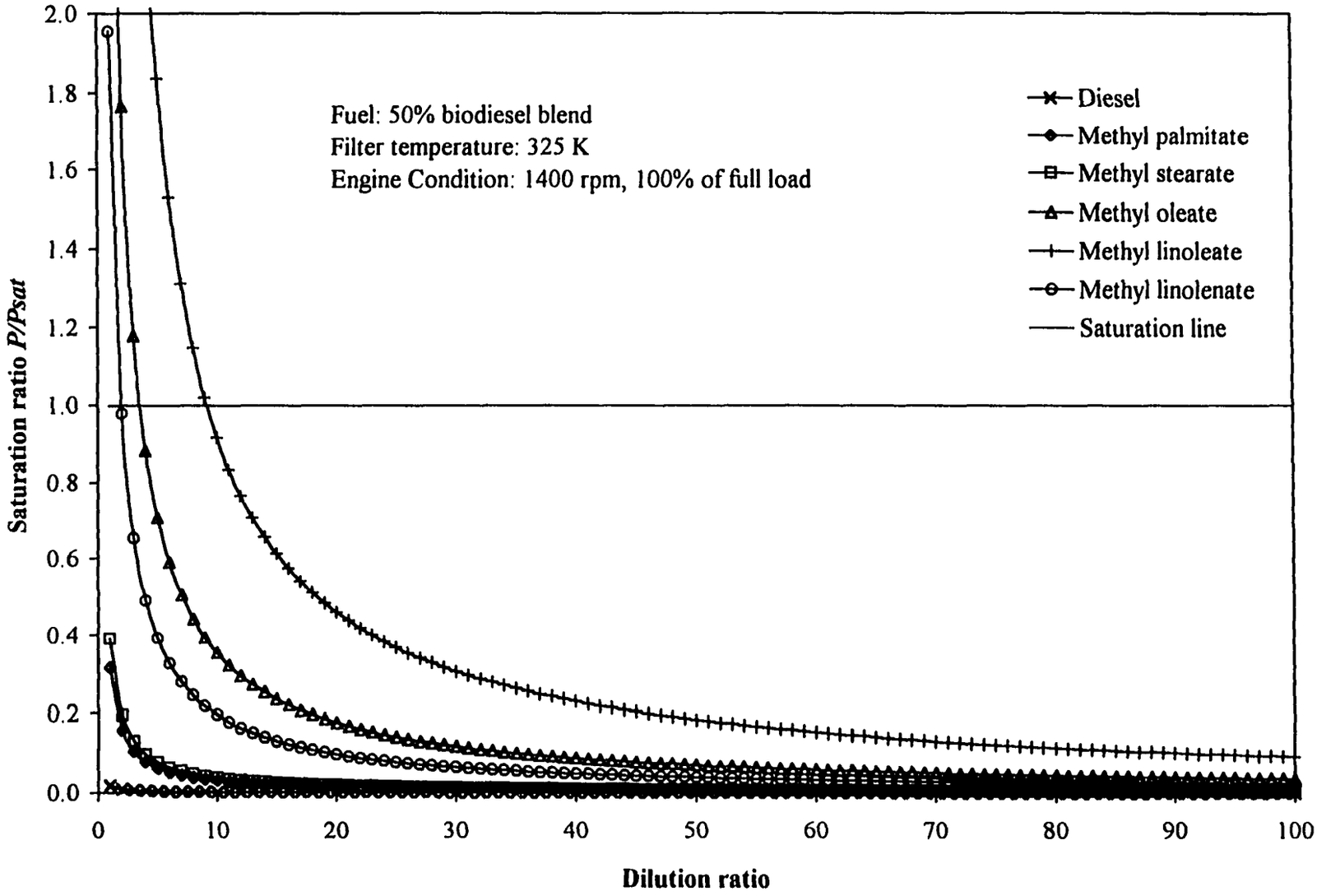

Figure 5.37 Effects of dilution ratio on saturation ratio of 50% biodiesel blend at full-load engine condition

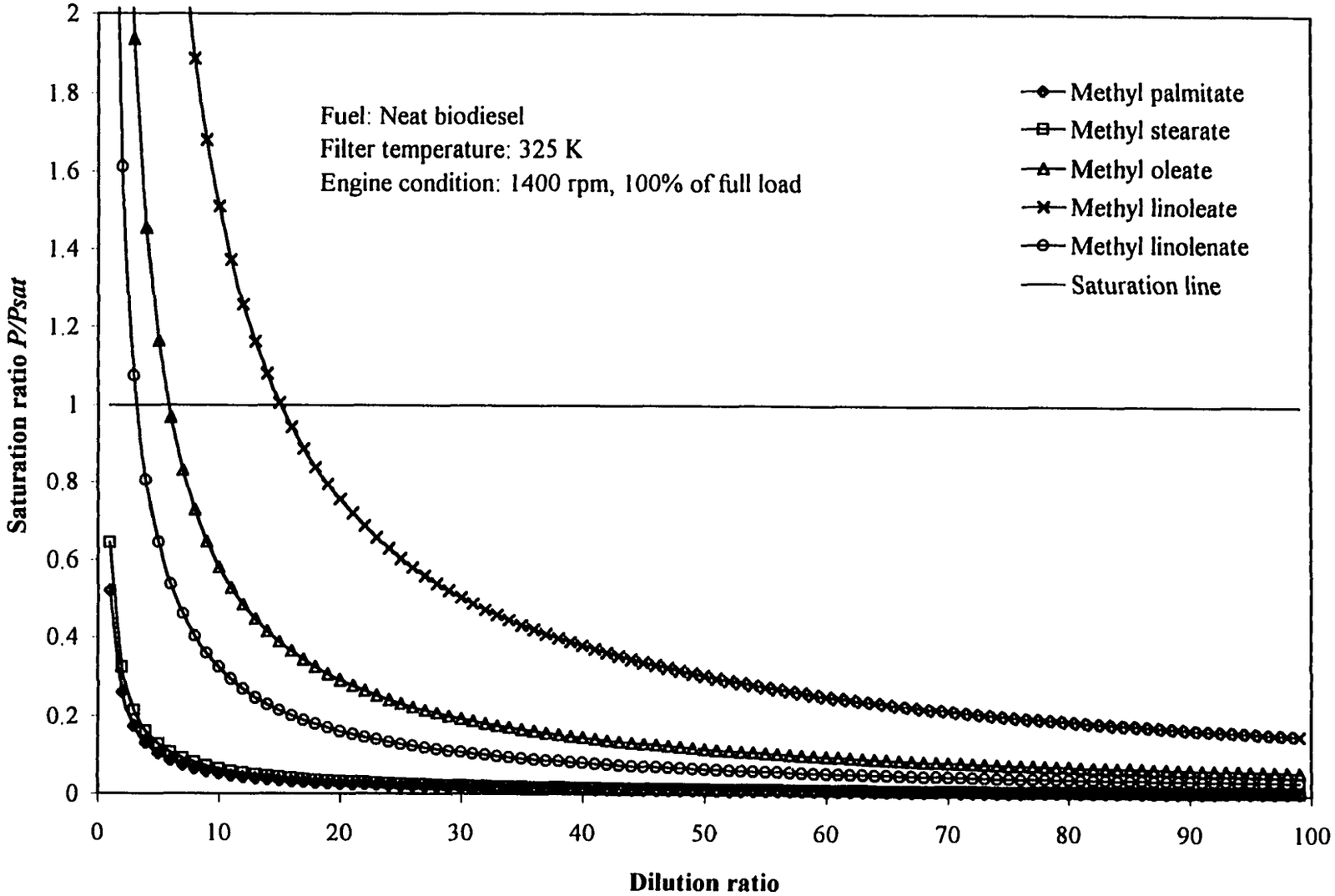

Figure 5.38 Effects of dilution ratio on saturation ratio of neat biodiesel at full-load engine condition

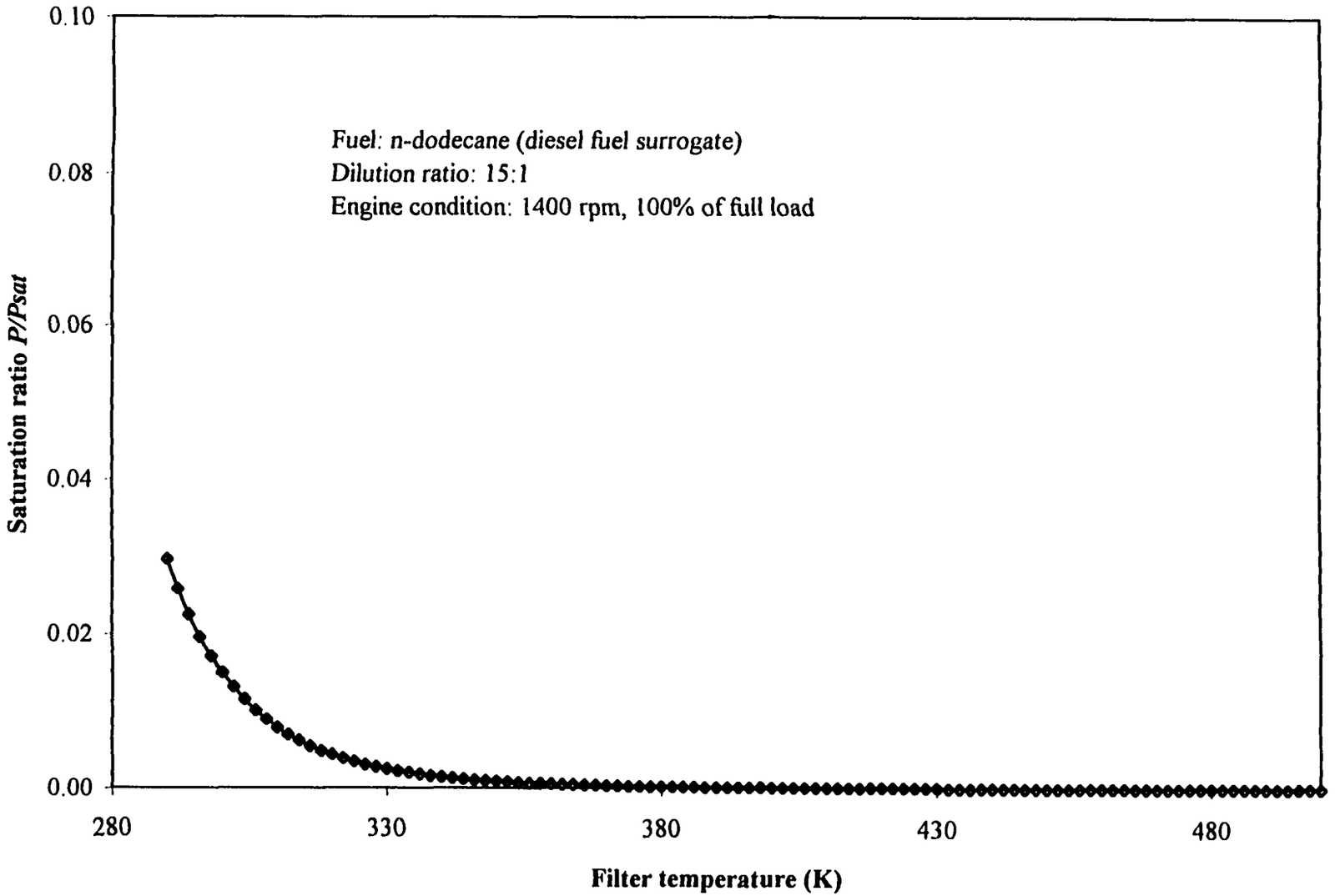

Figure 5.39 Effects of filter temperature on saturation ratio of n-dodecane at full-load engine condition

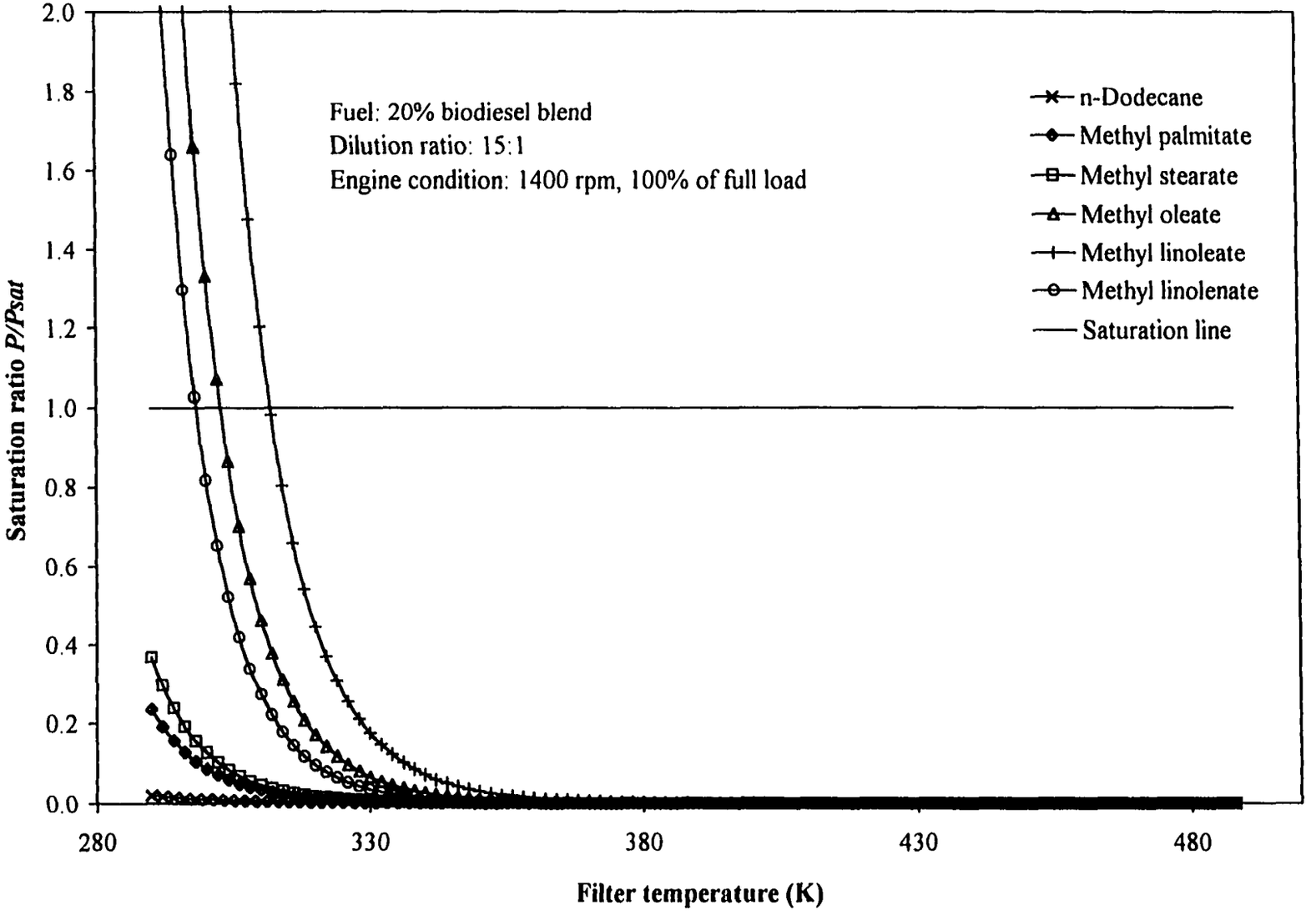

Figure 5.40 Effects of filter temperature on saturation ratio of 20% biodiesel blend at full-load engine condition

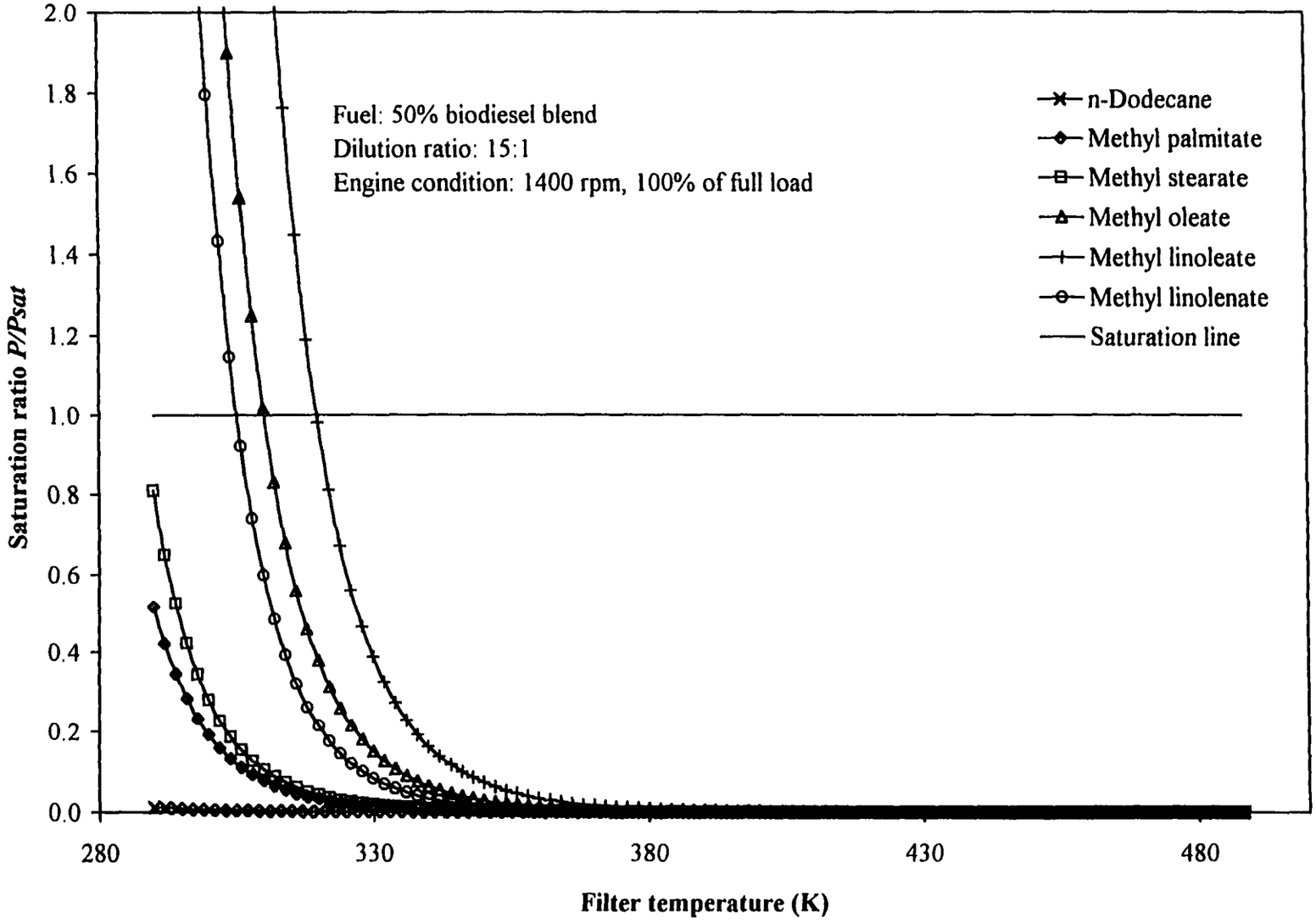

Figure 5.41 Effects of filter temperature on saturation ratio of 50% biodiesel blend at full-load engine condition

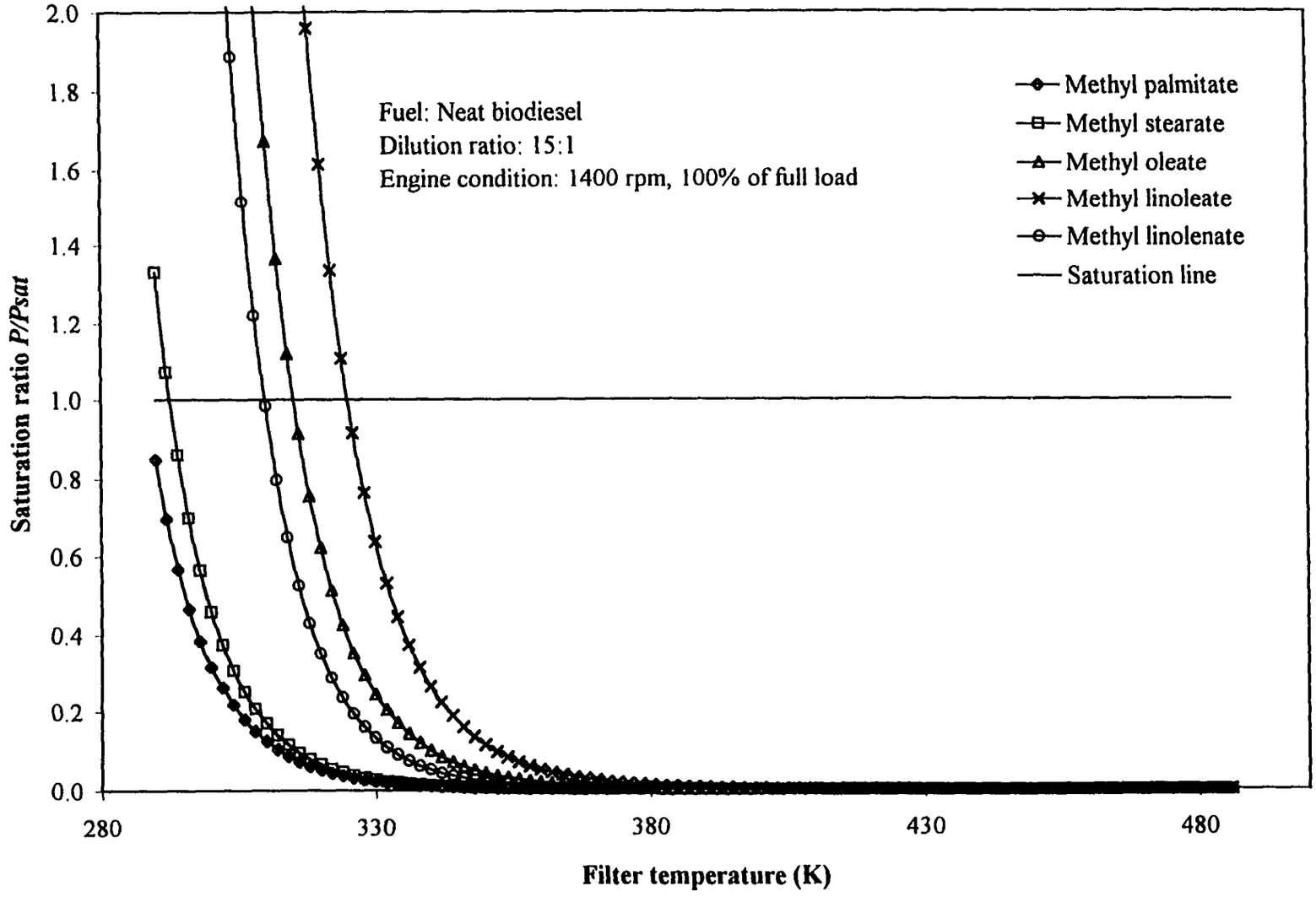

Figure 5.42 Effects of filter temperature on saturation ratio of neat biodiesel at full-load engine condition

by the condensation model shown in Table 5.1. The carbon particle concentrations in the raw exhaust gas are the average of the carbon particle emissions based on the engine tests as shown in Figure 5.2 and 5.8 for a 100% and 20% of full-load engine operating conditions, respectively.

5.2.2.2.1 Effects of dilution ratio on SOF formation due to adsorption. A comparison of the adsorbed SOF with variable dilution ratio and at a constant filter temperature of 325 K is shown in Figure 5.43. The engine condition was 1400 rpm and 100% of full-load. The adsorption curves in Figure 5.43 show the same influence of dilution ratio as the concentrations of total particulate and SOF shown in Figures 5.1 and 5.3. The decrease of adsorbed SOF was nonlinear, and a significant amount of adsorbed SOF was found even at high dilution ratios which was different from the results predicted by the condensation model. These observations were in general agreement with the solvent extraction results which showed that a substantial amount of SOF was present on the total particulates at high dilution ratio.

The predicted SOF concentration showed some differences from the measured data for fuel blends with a high fraction of No. 2 diesel fuel. This may be due to the assumption that n-dodecane was used to represent No. 2 diesel fuel. Actually, diesel fuel consists of many different compounds, and its fuel properties are different from n-dodecane. The soluble organic fraction on the particulates also has different properties from diesel fuel although, in this study, the SOF was assumed to have the same composition as the fuel. Mayer et al. [136] used a radioactive tracer technique to determine the contribution of engine oil to particulate matter. They found that about 16% to 80% (by wt.) of the extractable organic fraction of the total particulates was from the lubricant oil depending on engine speed and load. The lubricating oil typically consists of hydrocarbons with larger molecular weights than the compounds in diesel fuel. Its carbon number distribution is from C_{16} to C_{240} with a initial boiling point of about 670 K. The carbon number distribution in No. 2 diesel fuel is from C_{10} to C_{40} with an initial boiling point of 450 K. However, the boiling point of n-dodecane is 488 K which is close to the initial boiling point of diesel fuel. The lubricating oil and diesel fuel

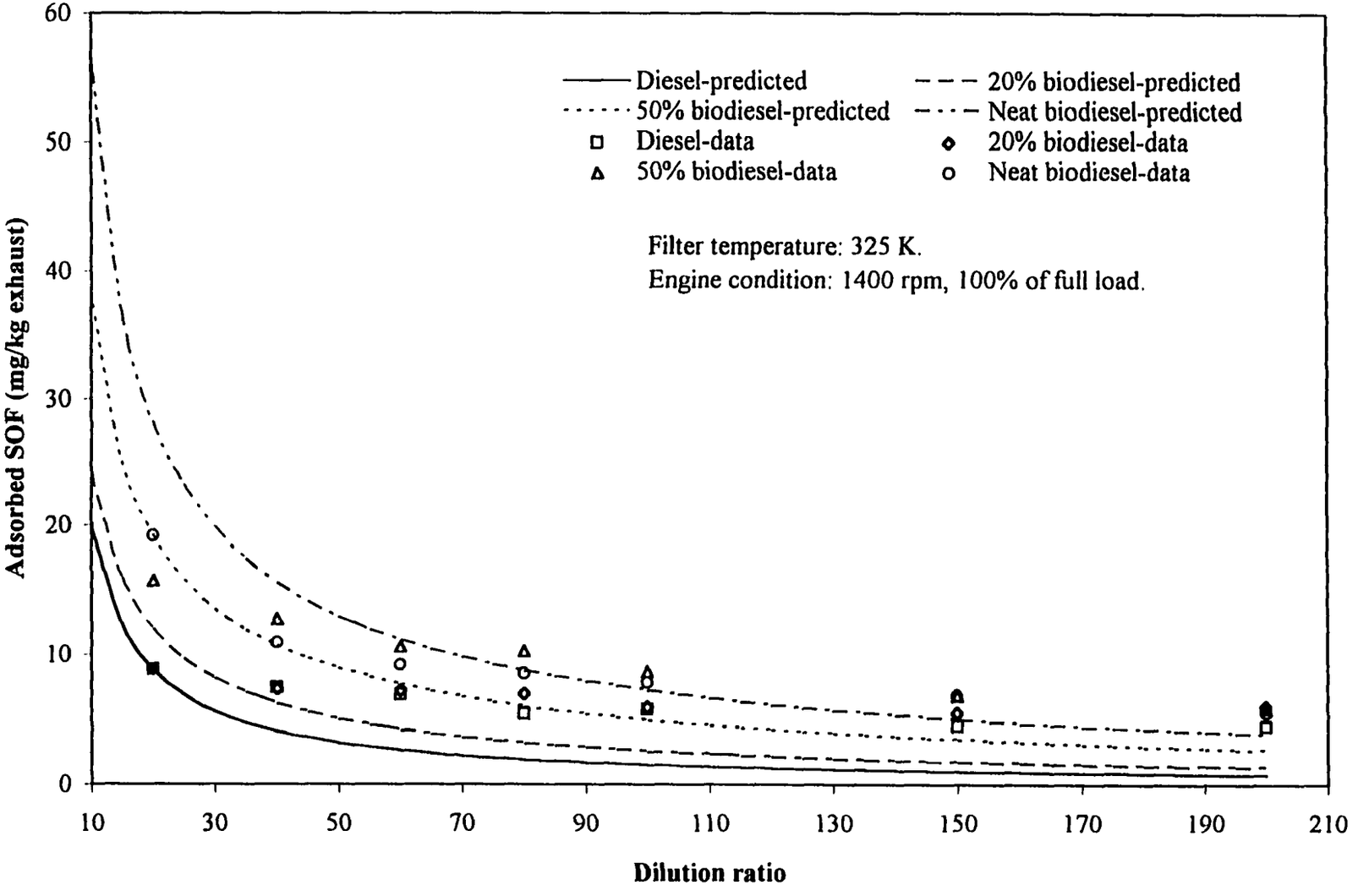

Figure 5.43 Comparison of adsorbed SOF between prediction and experiment with constant filter temperature at full-load engine condition

have higher boiling points and lower volatility than n-dodecane. Both lubricating oil and No. 2 diesel fuel will have higher saturation ratios compared with n-dodecane at the same operating condition. Since the adsorption process is a function of saturation ratio, more adsorbed hydrocarbons will collect on the carbon particle surface than would be predicted by n-dodecane. It should not have been surprising that the predicted adsorbed HC quantity would be low compared with the experimental results. When the fraction of biodiesel in the fuel blends increased, the predicted results were closer to the experimental data.

Another source of error with the adsorption model was that the adsorption energy of unburned hydrocarbons was estimated using a correlation based on n-alkane experimental data. For biodiesel blends which contained ester compounds, the estimated adsorption energy may be lower than their actual values.

The adsorption model gave low adsorbed SOF concentrations at high dilution ratio when compared with the experimental results. This may be attributable to the assumptions discussed above. The engine test results showed that, at high dilution ratio, the SOF levels from different fuels were very close. However, the results from the model showed a relatively large difference between these fuels.

Based on the predicted results, the adsorbed SOF increased with the biodiesel content in the fuel blends. The trends were generally consistent with the tested results except that the adsorption model predicted a relatively large difference of adsorbed SOF from fuel to fuel while the difference from the experimental results did not show too much.

Figure 5.44 shows the comparison between the results of the predicted adsorbed SOF concentrations and those measured experimentally at the 20% of full-load engine operating condition. The model correctly predicted the same trend for the formation of adsorbed SOF as that obtained from experiment when the dilution ratio was varied at a constant filter temperature of 325 K. The predicted quantity of adsorbed unburned hydrocarbons increased rapidly when the dilution ratio was decreased, especially at low dilution ratio. Although the adsorption curves for both engine operating conditions showed the same trend with varying dilution ratio, the quantity of adsorbed SOF at the light-load engine condition was significantly larger than at the full-load engine condition. This was because the concentration

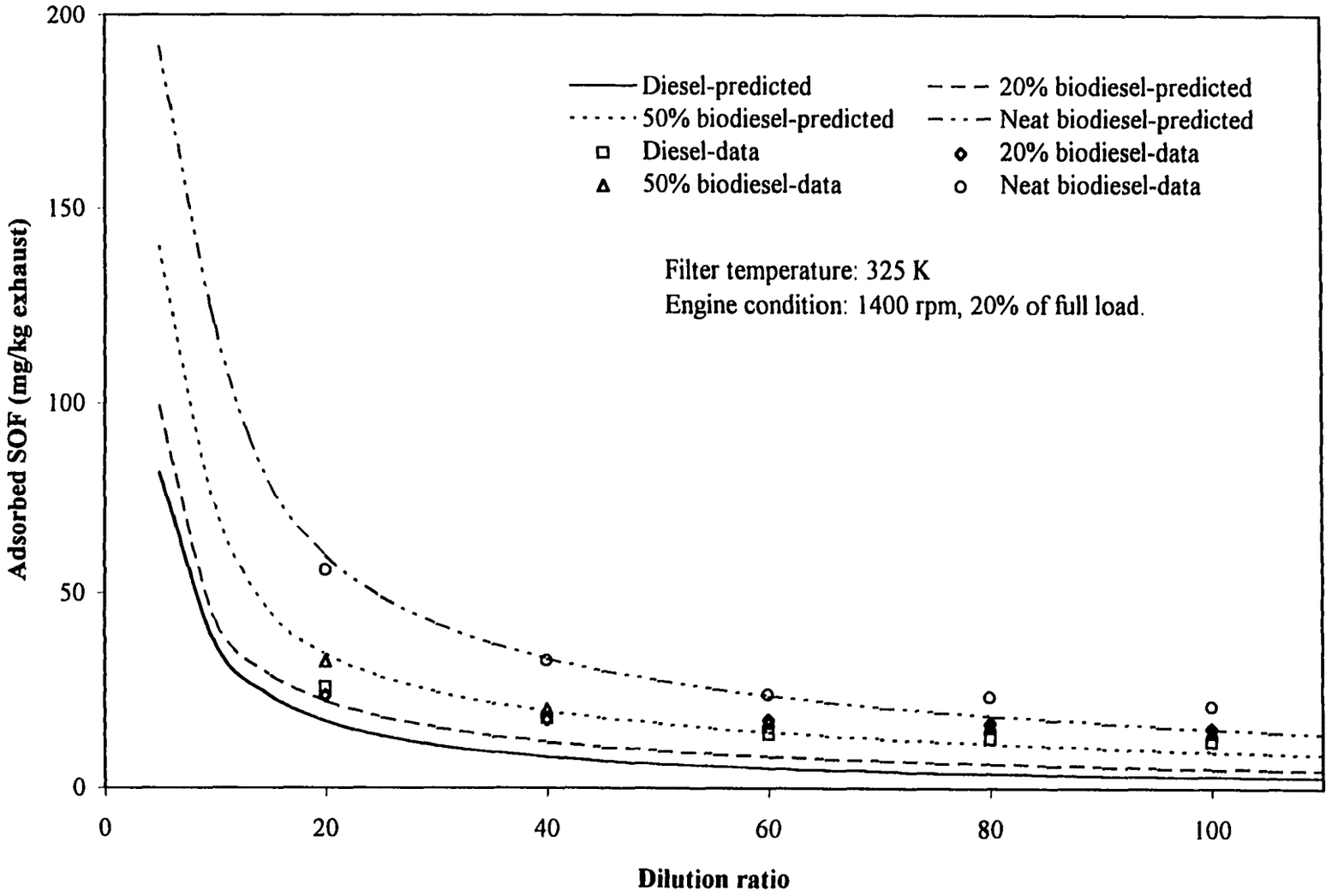

Figure 5.44 Comparison of adsorbed SOF between prediction and experiment with constant filter temperature at light-load engine condition

of unburned hydrocarbons in the engine exhaust gas was higher at the part load engine condition than at the full-load condition.

As at the high load condition, the predicted results of the adsorption model at the light-load engine condition showed a lower quantity of adsorbed SOF at high dilution ratio than that from experiment.

5.2.2.2.2 Effects of filter temperature on SOF formation due to adsorption. The predicted adsorbed SOF concentrations at the constant dilution ratio of 15:1 are shown in Figures 5.45 and 5.46 for the full and light-load engine conditions, respectively. The calculated values of the adsorbed SOF as the filter temperature is varied showed the same general trends as the total particulate and SOF measurements shown in Figures 5.9 and 5.10. The adsorption model predicts a nonlinear decrease in the adsorbed unburned hydrocarbons with increasing filter temperature. In addition, the adsorption model correctly predicts that a finite amount of unburned hydrocarbons should be present on the carbon particle surface at high filter temperature.

At the full-load engine condition, the predicted results were close to the experimental data at low filter temperatures. However, the experimental SOF concentrations for the 50% biodiesel blend and the neat biodiesel dropped quickly as the filter temperature increased compared with the predicted results. The model gave higher SOF levels than the measured values for these two fuels at high filter temperatures.

The SOF concentration predicted by the adsorption model was generally in agreement with the measured results at the 20% of full-load engine condition as shown in Figure 5.46. By studying the results predicted by the adsorption model, it is clear that the adsorption mechanism plays the dominant role during the SOF formation process in the dilution tunnel.

5.2.2.2.3 Effects of fuel components on SOF formation during dilution process. As discussed previously, fuel properties have a significant effect on the SOF formation during the dilution process. The fuel properties of biodiesel are different from those of diesel fuel, and the properties of each component in biodiesel may also be different. These different

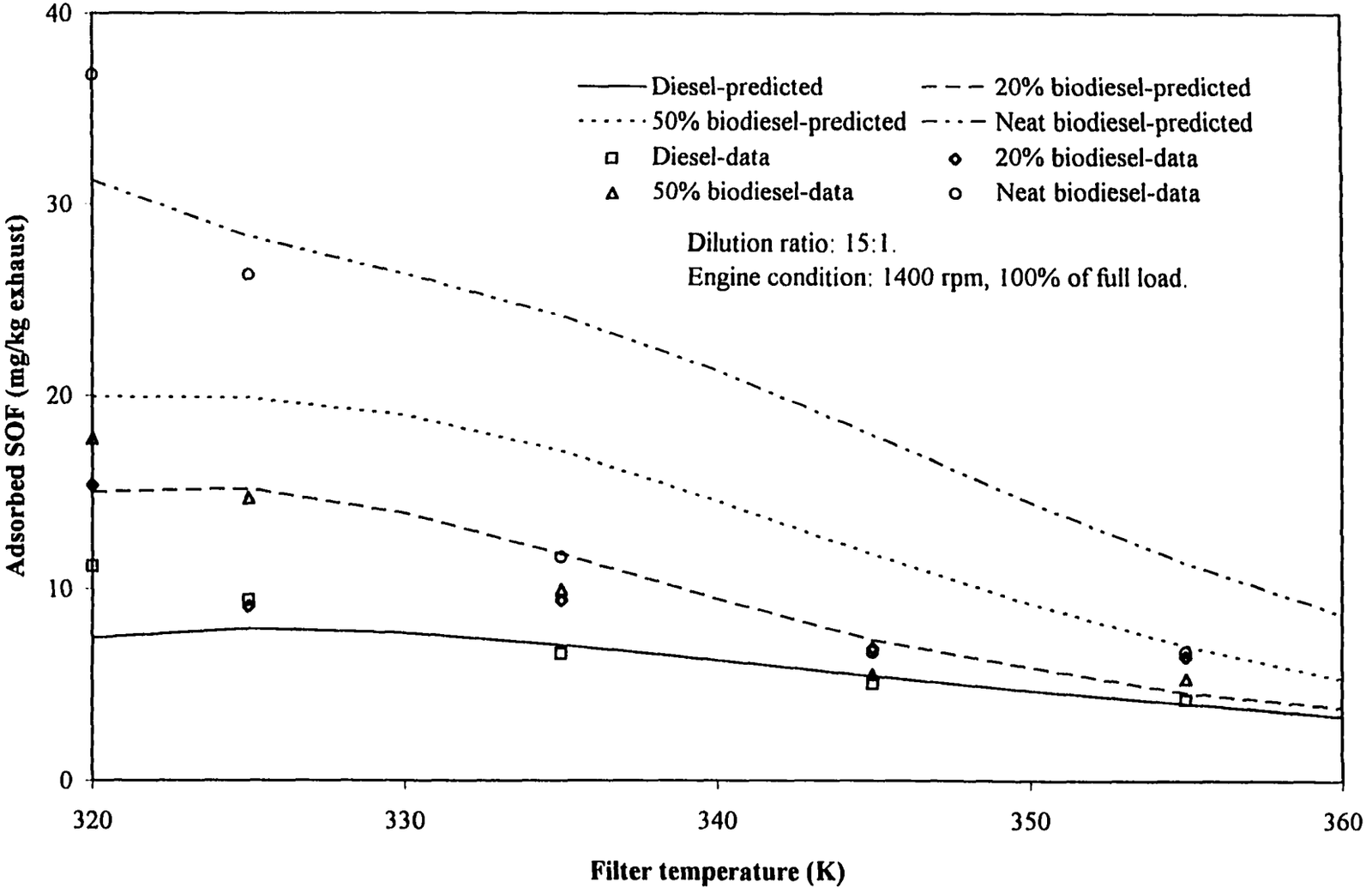

Figure 5.45 Comparison of adsorbed SOF between prediction and experiment with constant dilution ratio at full-load engine condition

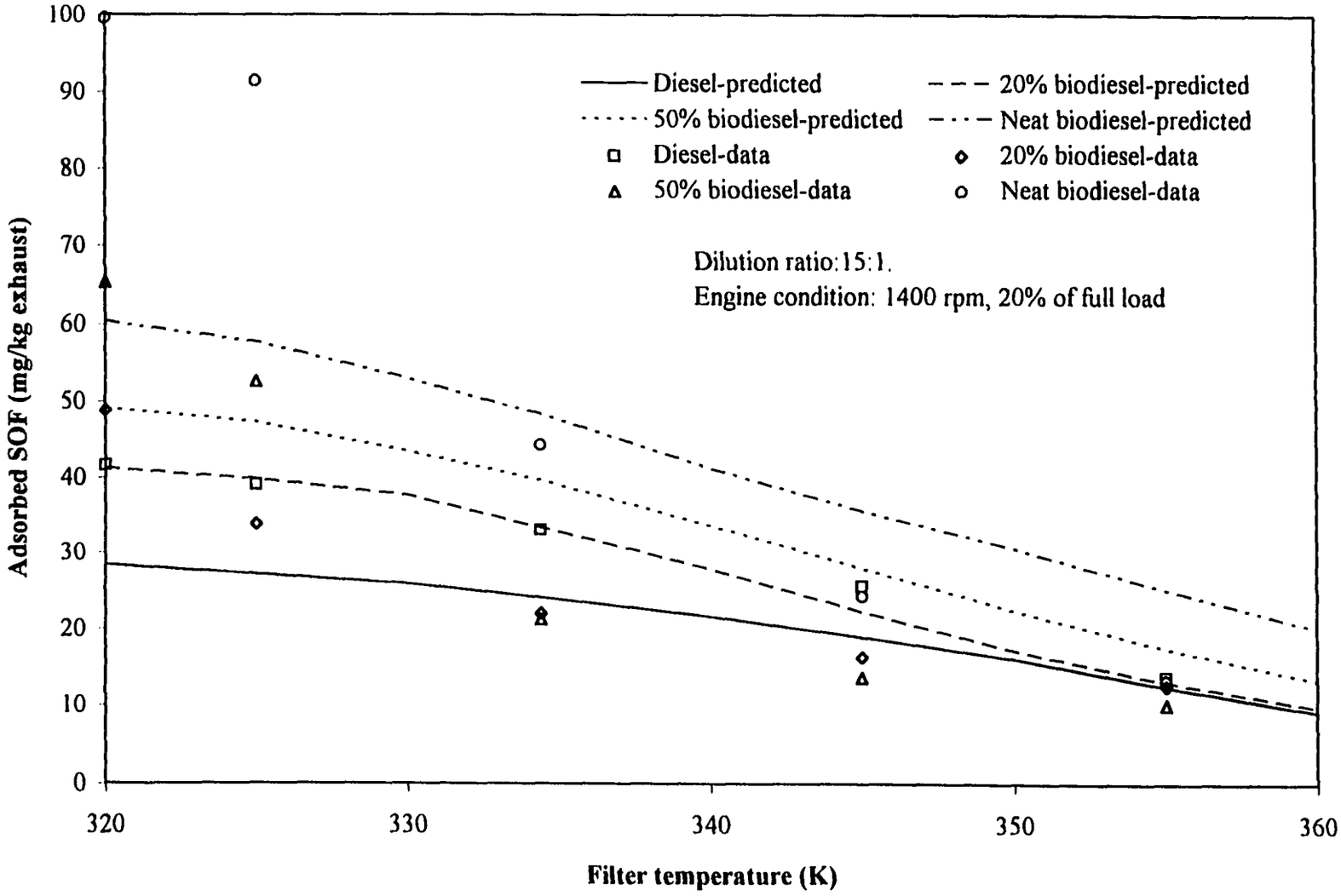

Figure 5.46 Comparison of adsorbed SOF between prediction and experiment with constant dilution ratio at light-load engine condition

properties will cause different adsorption results. Figures 5.47 to 5.49 illustrate the adsorbed amount of each component in the unburned hydrocarbons as the filter temperature is varied at the full-load engine operating condition. Although the diesel fuel content in the 20% biodiesel blend was the largest fraction, its adsorbed SOF concentration was much lower than the other components in the blends, such as methyl linoleate, methyl oleate, etc. The adsorption model based on the BET adsorption isotherm and the IAS multicomponent equation is a function of the saturation ratio, P/P_{sat}. Because each component in biodiesel has a lower saturated vapor pressure, higher boiling point, and lower volatility than diesel fuel, and the diesel fuel was assumed to be n-dodecane with a relatively high saturation pressure, the saturation ratios of the esters in the biodiesel would be much higher than diesel fuel during the dilution process. Therefore, a higher adsorbed concentration for each ester compound was not surprising. The adsorbed concentration of methyl linoleate was the highest among those compounds due to its high concentration in the biodiesel. As the biodiesel content in the fuel blends increased, the adsorbed quantities of each ester became large. At the part load engine condition, the adsorption results for the fuels showed the same trends as at the full-load engine condition.

5.2.3 Predicted results of HC concentration variation in heated sampling line

The two physical mechanisms, condensation and adsorption, appear to be the main factors that govern the change of the unburned hydrocarbon concentration when the HC sample is transported in the heated sampling line from the engine exhaust pipe to the flame ionization HC detector. When the HC sample is transported with the heated sampling line, no dilution air is added to the engine exhaust gas. Therefore, the dilution ratio is constant, and equal to 1:1. The quantity of liquefied unburned hydrocarbons due to condensation or adsorption is dependent on the HC sampling temperature and fuel properties. The unburned hydrocarbon concentration variation in the HC sampling line can be studied in detail using the condensation and adsorption models that were used to analyze the SOF formation during the engine exhaust gas dilution process. The input information for the calculations, such as the concentrations of solid carbon and unburned hydrocarbons, the composition of unburned hydrocarbons, etc., are the same as that used for the dilution process. The effects of

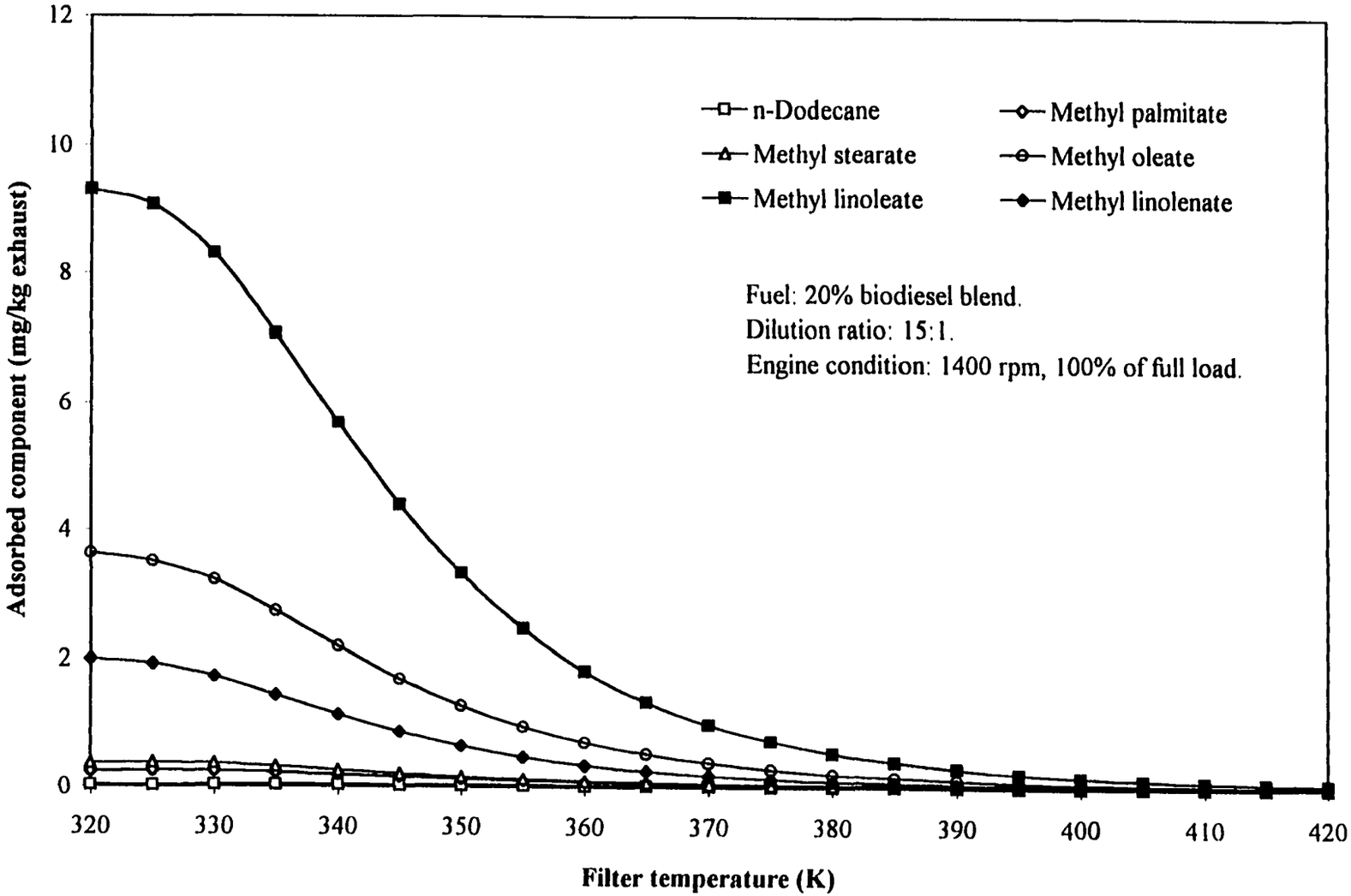

Figure 5.47 Effects of filter temperature on adsorption of each component for 20% biodiesel blend at full-load engine condition

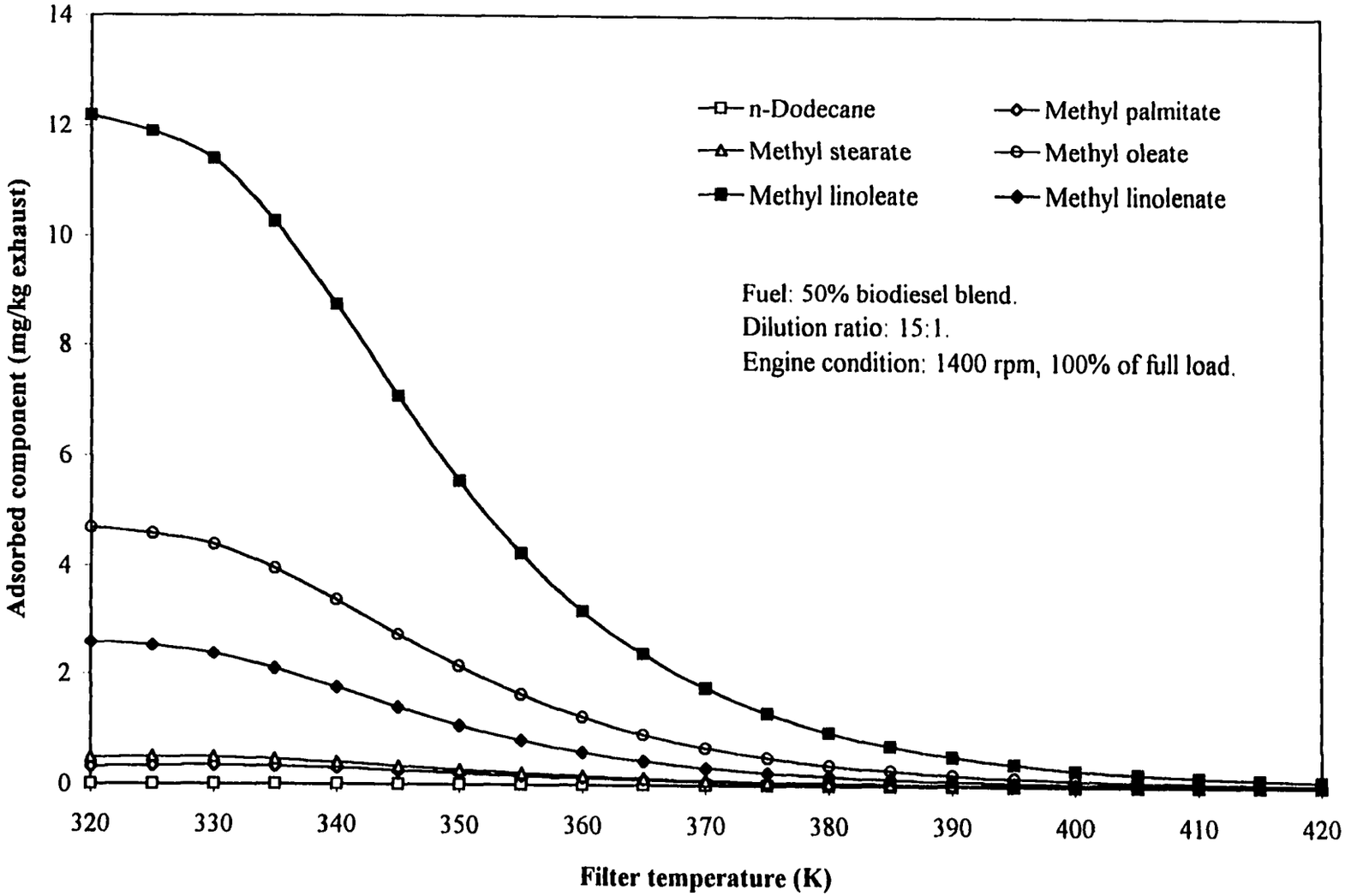

Figure 5.48 Effects of filter temperature on adsorption of each component for 50% biodiesel blend at full-load engine condition

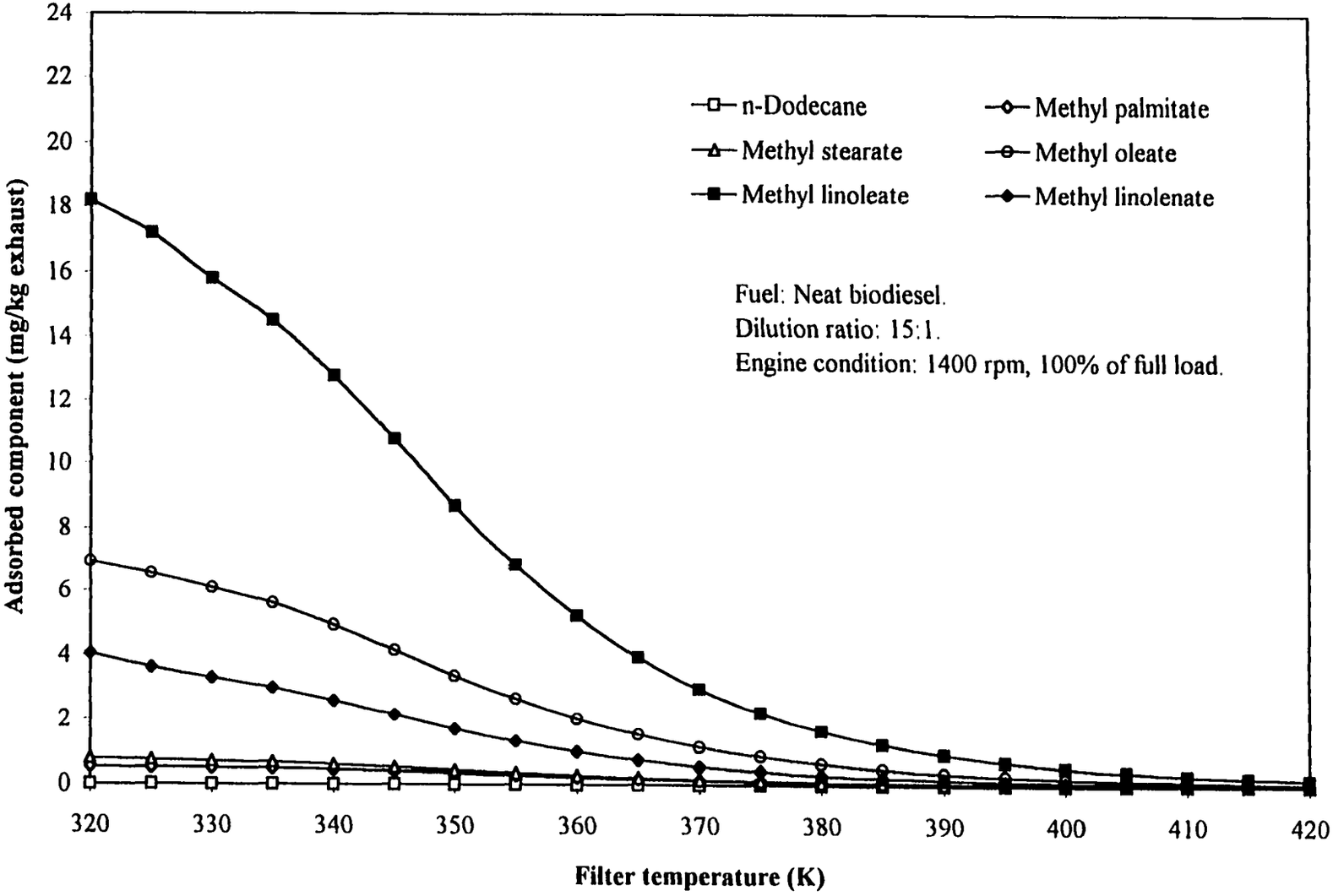

Figure 5.49 Effects of filter temperature on adsorption of each component for neat biodiesel at full-load engine condition

condensation and adsorption on the HC concentration change along the heated HC sampling line will be discussed in the following sections.

5.2.3.1 Effects of condensation on the HC concentration variation

Figures 5.50 to 5.53 are plots of the saturation ratio of various fuels as the sampling line temperature is varied at the full-load engine condition. The model shows that condensation took place only when the sampling line temperatures were lower than 352 and 360 K for the 50% blend and neat biodiesel, respectively. At the standard HC measurement temperature, 463 K (190 °C), no condensation of the unburned hydrocarbons could be found for any of the fuels.

When the HC concentration in the engine exhaust gas was increased at the light-load engine condition, condensation occurred only when the sampling line temperatures were lower than 355 and 365 K for the 50% blend and neat biodiesel, respectively, as shown in Figures 5.54 to 5.57. Based on the predicted results of the condensation model, it was not possible for any of the fuels to have vapor phase unburned hydrocarbons condensing on the sampling line wall or the carbon particle surface when the engine exhaust gas was transported with a heated sampling line at 463 K. The unburned hydrocarbon concentration should not be changed due to the condensation of vapor phase HC in the heated HC sampling line even for biodiesel fuels.

5.2.3.2 Effects of adsorption on HC concentration variation

Another possible mechanism that could change the unburned hydrocarbon concentration in the heated sampling line is adsorption. The adsorption can take place even at saturation ratios less than one. The compounds in biodiesel have lower saturation pressures than diesel fuel compounds at the same temperature. When biodiesel is used, especially with a high fraction of biodiesel in the fuel blends, the vapor phase unburned hydrocarbons in the exhaust gas will have a high saturation ratio and cause more unburned hydrocarbon adsorption.

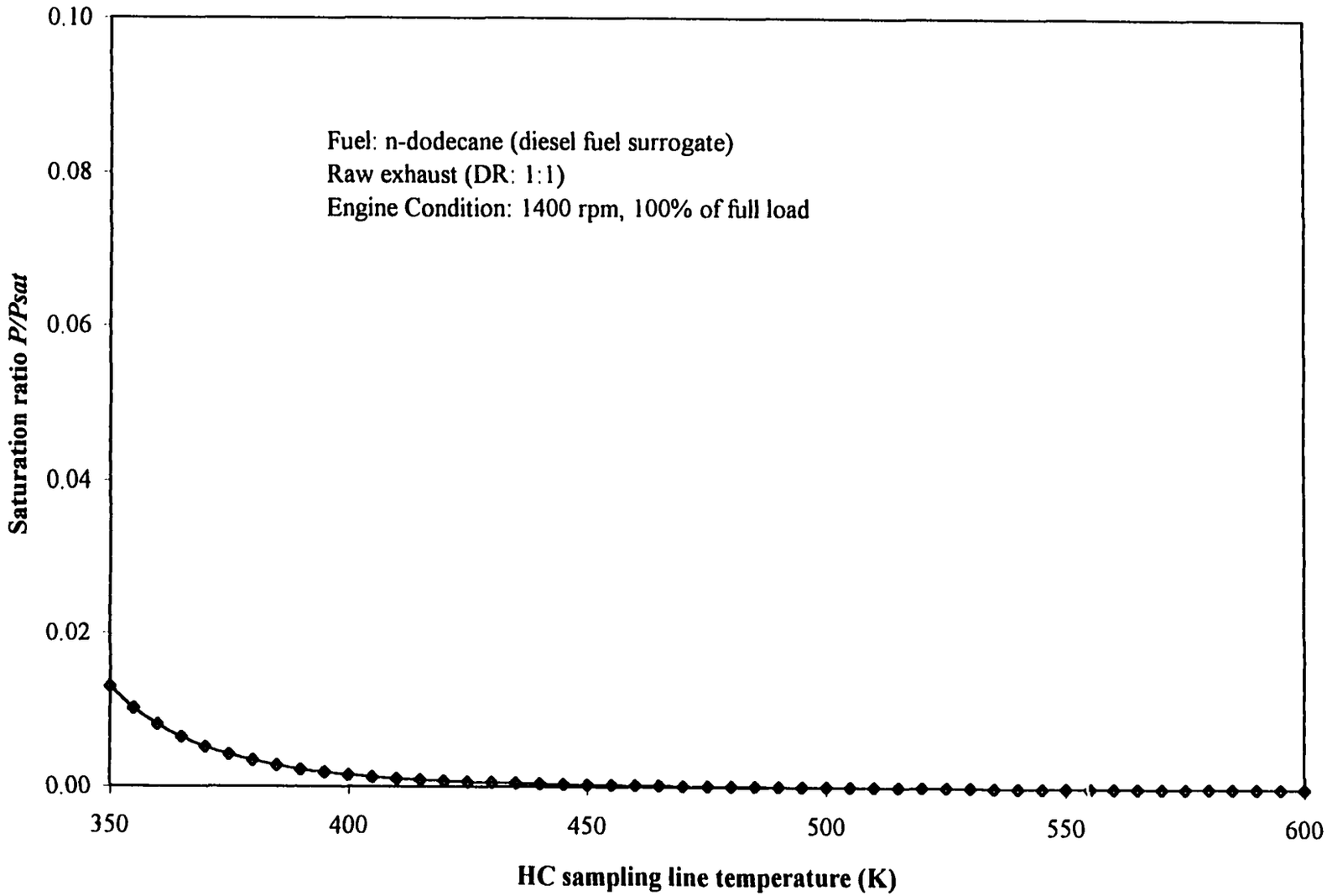

Figure 5.50 Effects of HC sampling line temperature on saturation ratio of n-dodecane at full-load engine condition

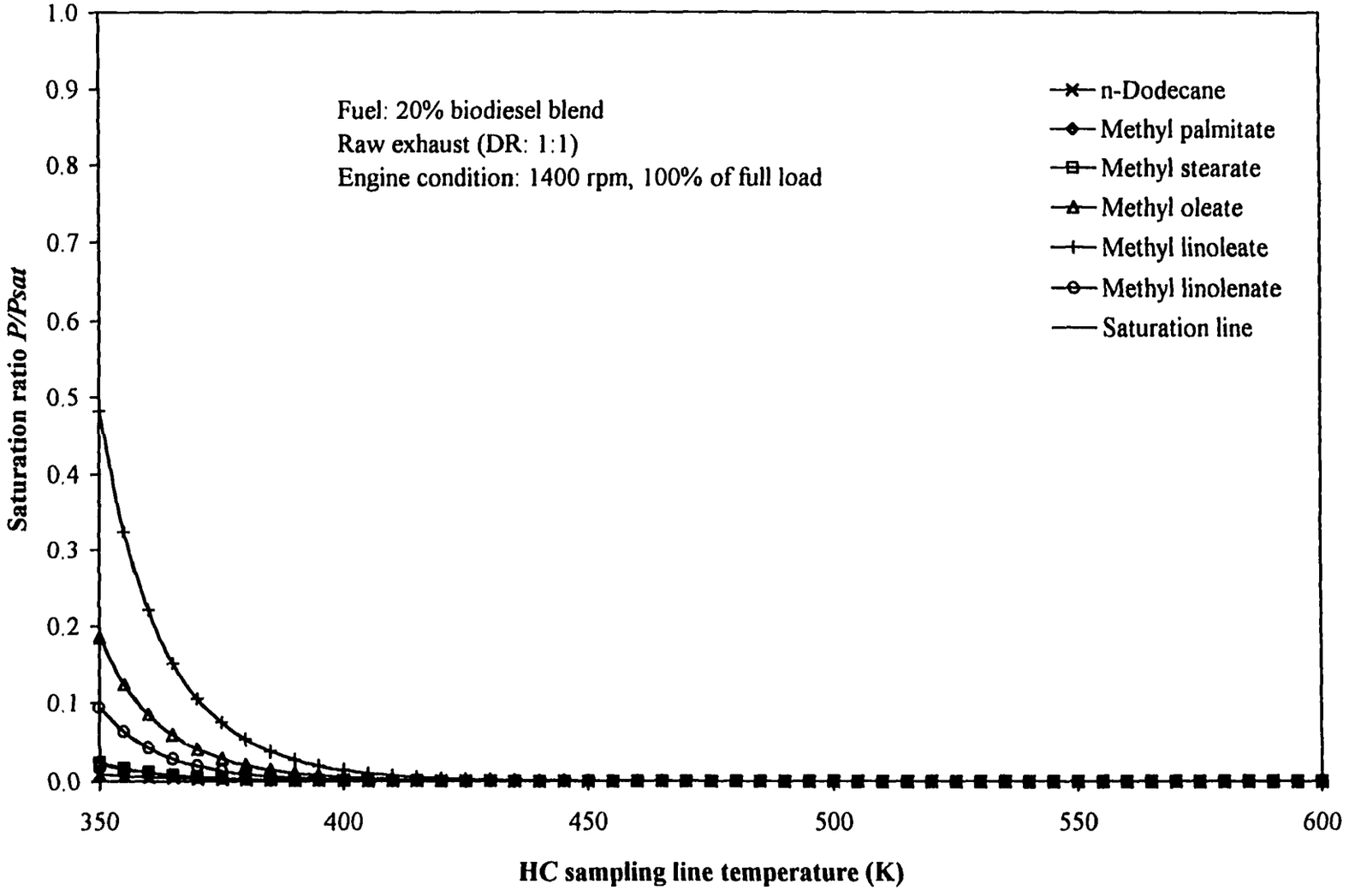

Figure 5.51 Effects of HC sampling line temperature on saturation ratio of 20% biodiesel blend at full-load engine condition

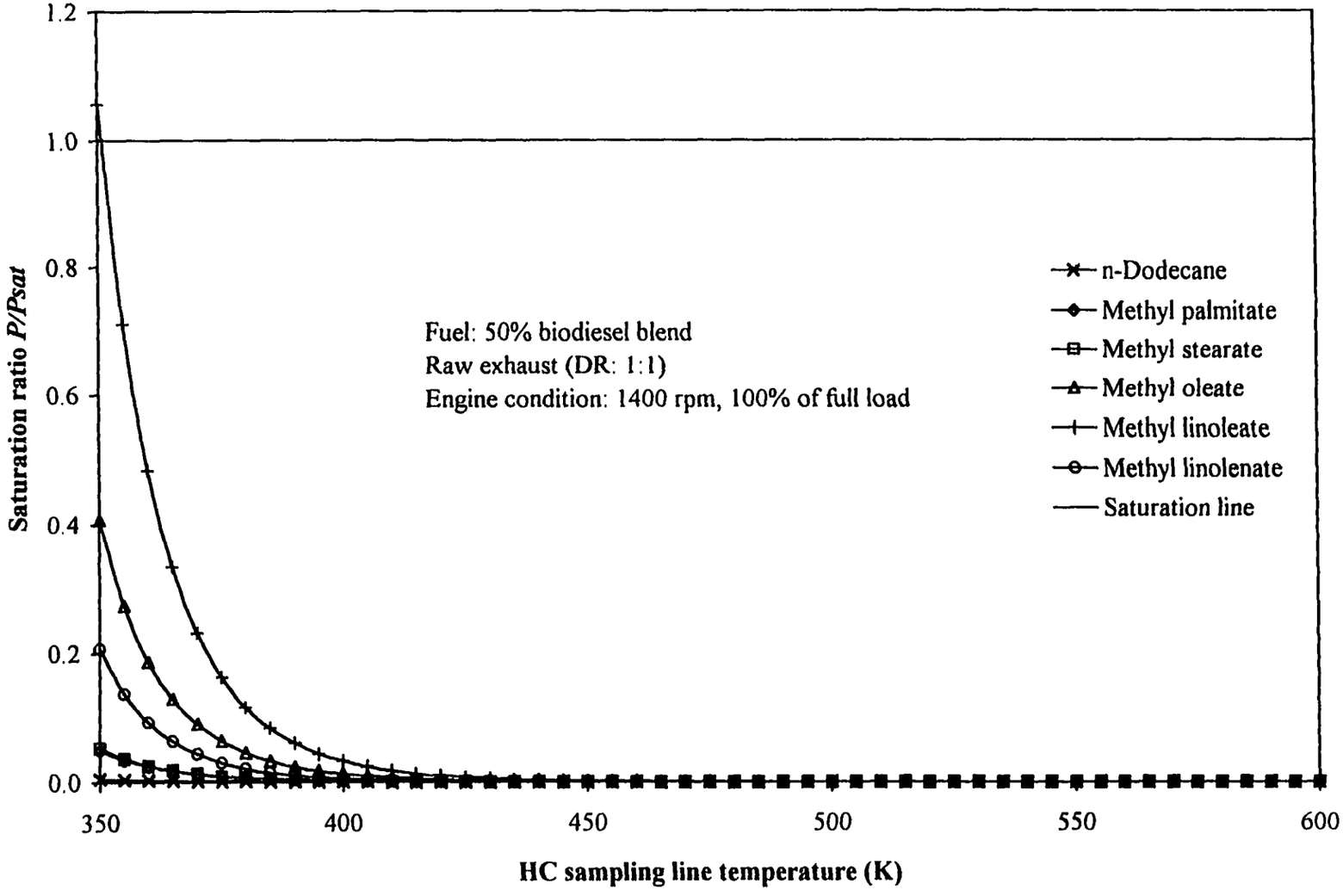

Figure 5.52 Effects of HC sampling line temperature on saturation ratio of 50% biodiesel blend at full-load engine condition

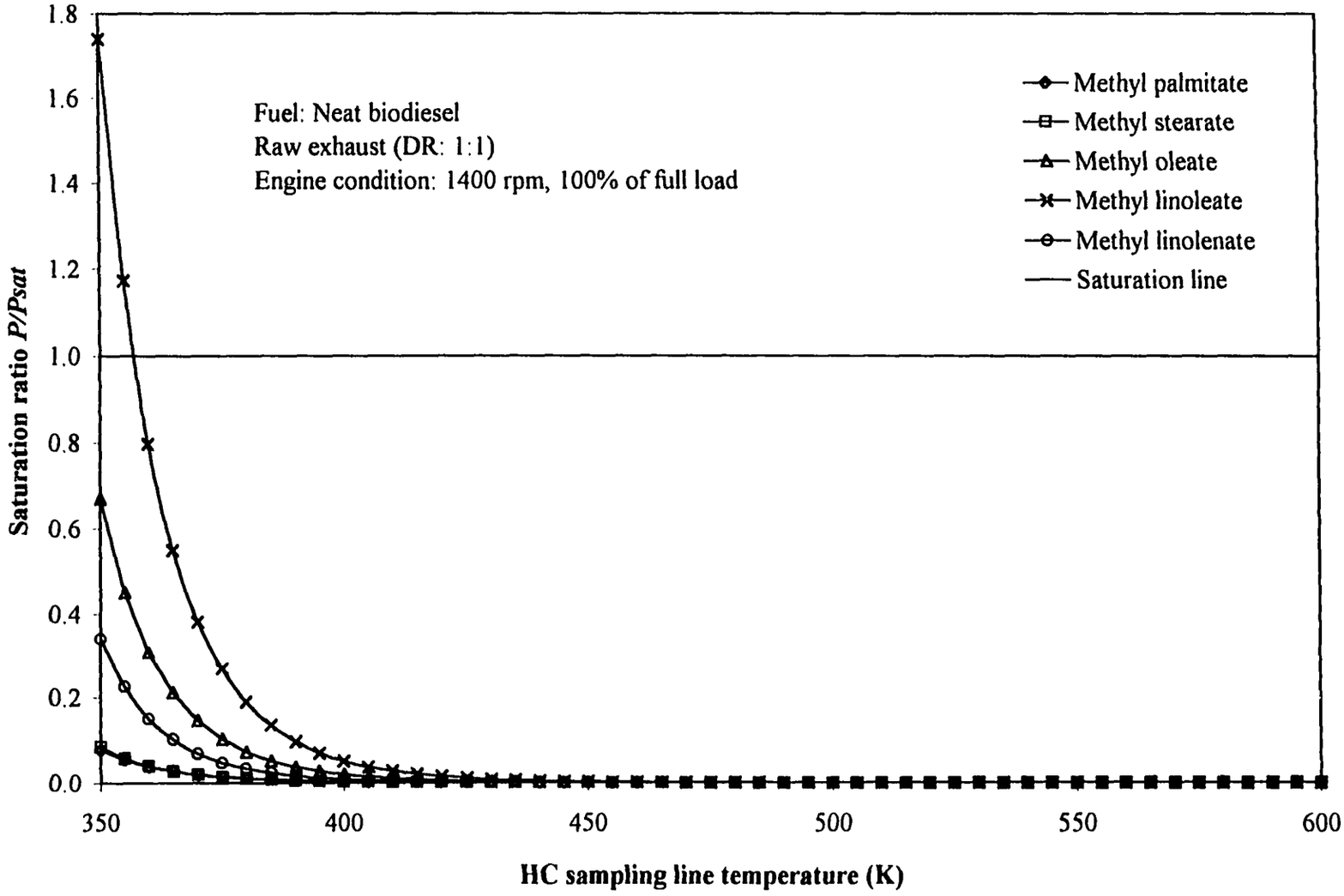

Figure 5.53 Effects of HC sampling line temperature on saturation ratio of neat biodiesel at full-load engine condition

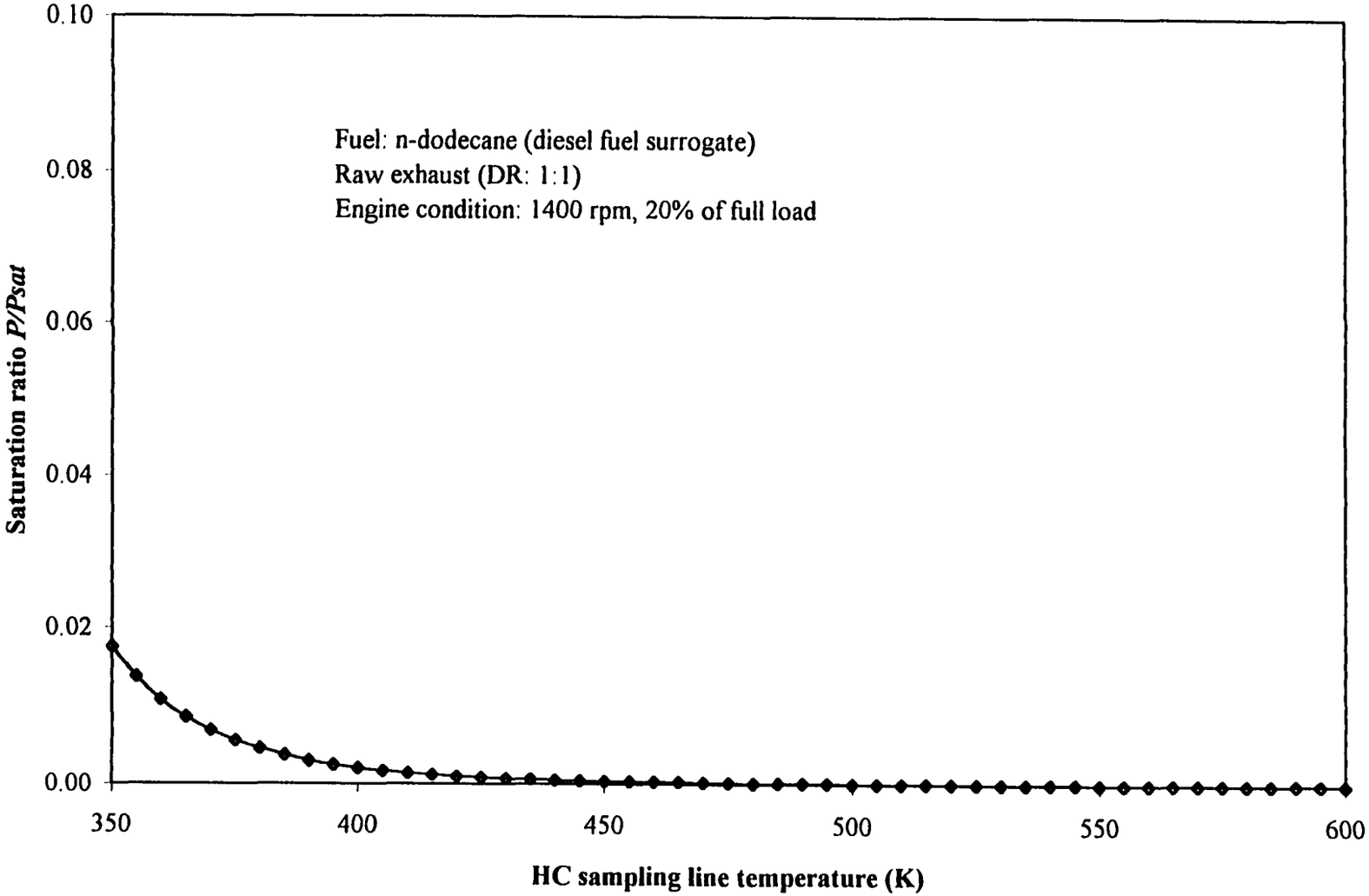

Figure 5.54 Effects of HC sampling line temperature on saturation ratio of n-dodecane at light-load engine condition

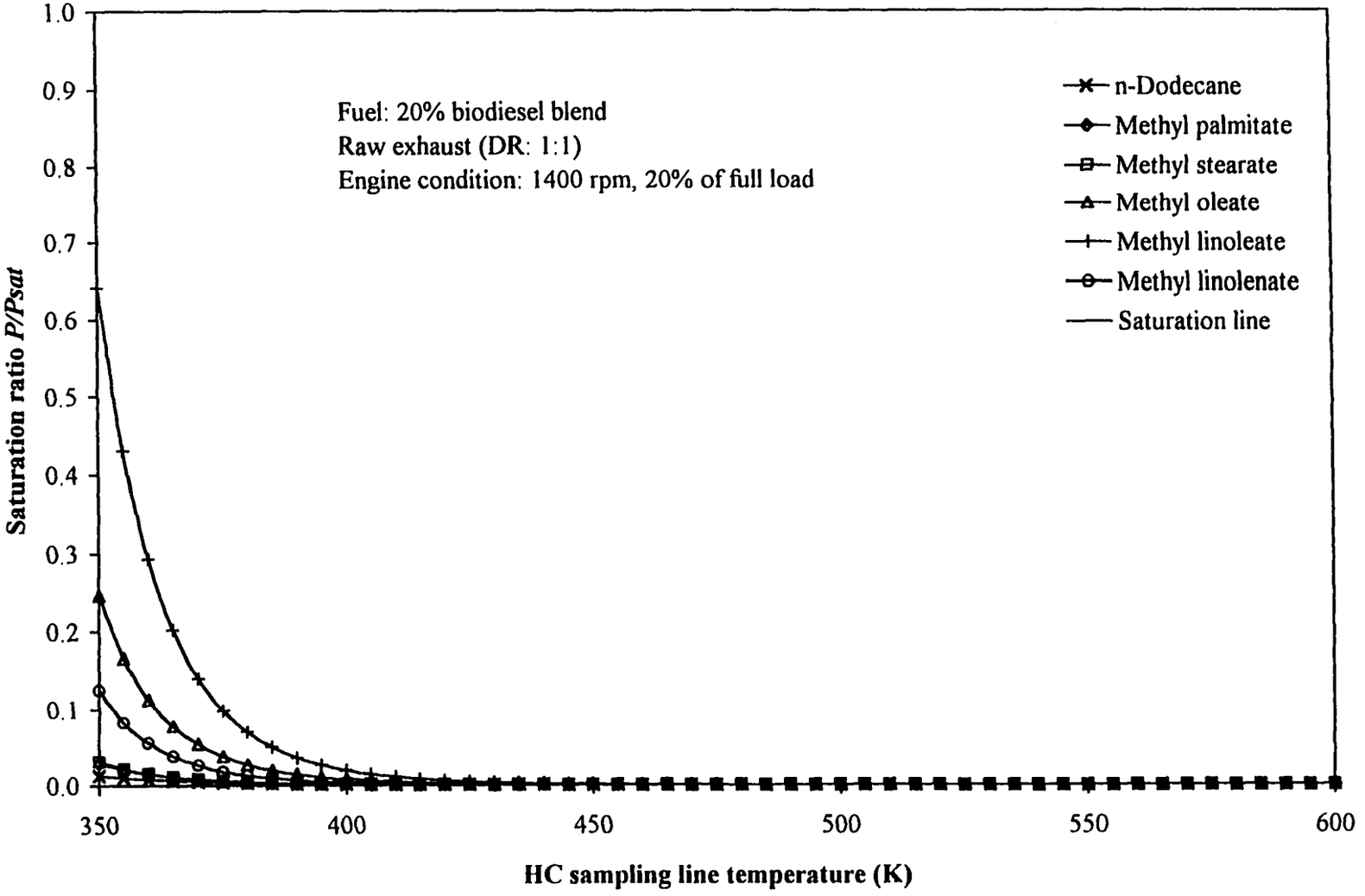

Figure 5.55 Effects of HC sampling line temperature on saturation ratio of 20% biodiesel blend at light-load engine condition

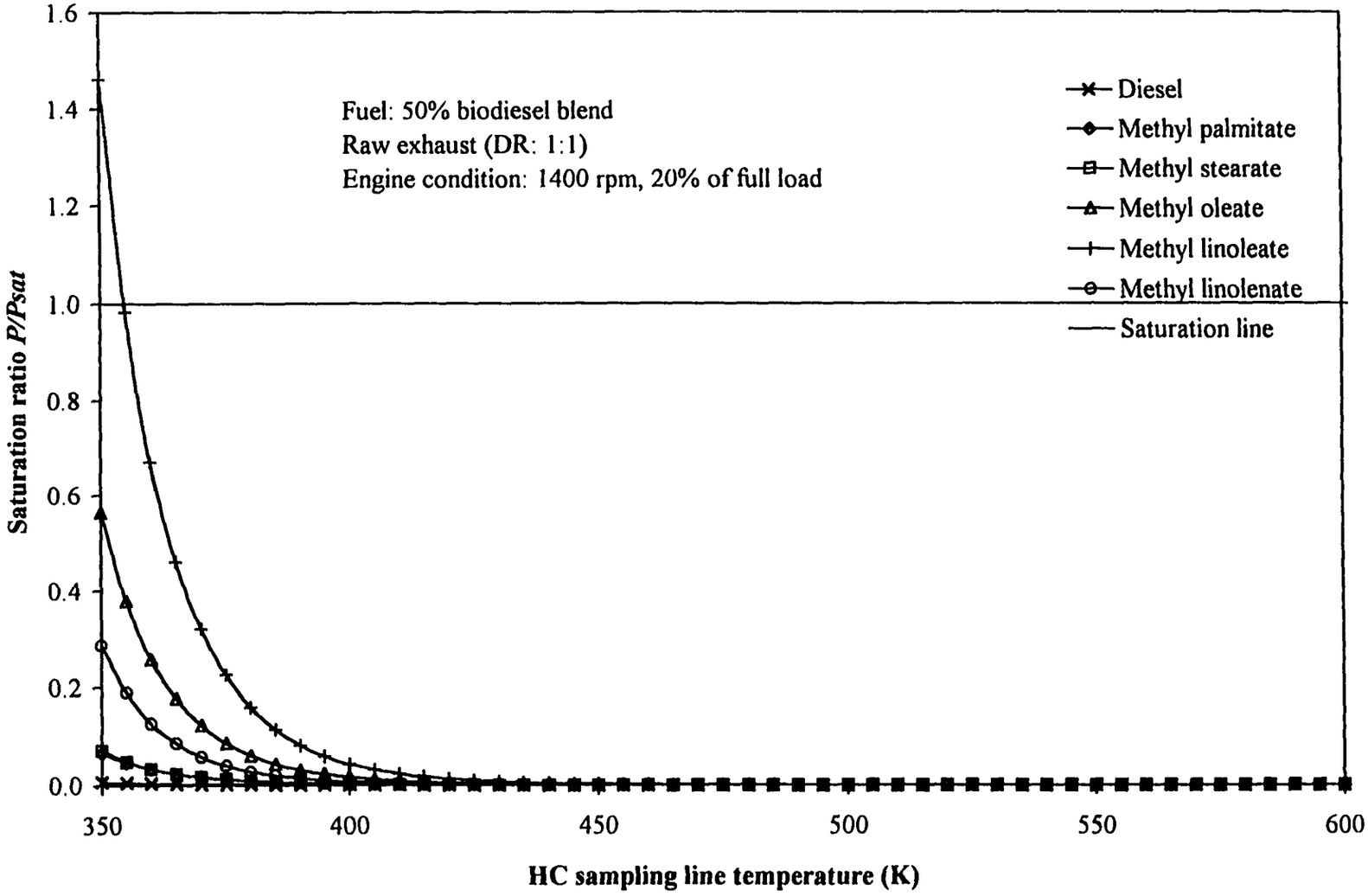

Figure 5.56 Effects of HC sampling line temperature on saturation ratio of 50% biodiesel blend at light-load engine condition

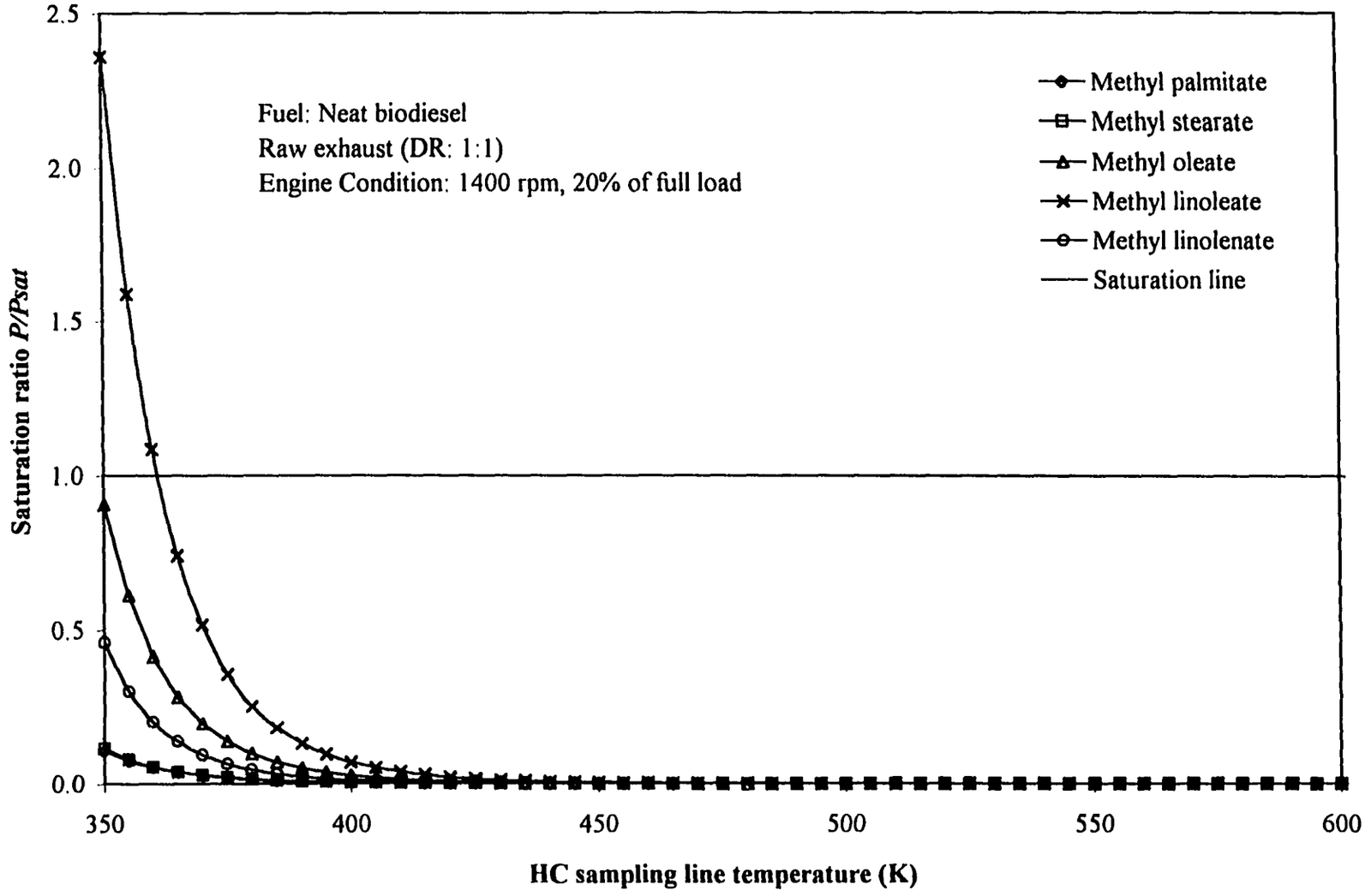

Figure 5.57 Effects of HC sampling line temperature on saturation ratio of neat biodiesel at full-load engine condition

Figures 5.58 to 5.61 show the adsorbed quantity of each component in the unburned hydrocarbons on the carbon particle surface as the HC sampling line temperature is varied. In all cases, only a small amount of SOF is formed at high temperature based on the adsorption model. The total adsorbed quantity at the standard HC sampling temperature of 463 K is shown in Figure 5.62 for the four fuels. The concentration of unburned hydrocarbons in the engine exhaust gas measured with the heated flame ionization detector is also shown in Figure 5.62. The adsorbed HC were only 1.3%, 2.4%, 5.1%, and 13.5% of the vapor phase HC concentration for diesel fuel, 20% biodiesel, 50% biodiesel, and neat biodiesel, respectively. The effect of unburned hydrocarbon adsorption in the heated HC sampling line becomes more significant as the fraction of biodiesel in the fuel blends increases.

On the other hand, if the HC sample temperature increases, the fraction of adsorbed unburned hydrocarbons in the vapor phase HC would be decreased. Table 5.2 illustrates the calculated amount of adsorbed HC as a fraction of the measured total HC concentration at 190, 250, and 300 °C. If the HC concentration at 300 °C is assumed to be the true value, the HC emission measurement errors due to the adsorption will be 26.1% and 2.7% when the sample temperature is at 190 and 250 °C for neat biodiesel, respectively.

Table 5.3 shows the corresponding results for the fractions of adsorbed unburned hydrocarbons in the measured vapor phase HC at 190, 250, and 300 °C at the 20% of full-load engine operating condition. Because the concentration of unburned hydrocarbons in the engine exhaust gas is higher at the part load engine condition than at the full-load engine condition, the quantity of adsorbed unburned hydrocarbons is higher at the light-load engine

Table 5.2 Calculated adsorbed HC fraction in the measured vapor HC concentration at full-load engine condition (%)

Temperature °C	Diesel	20% biodiesel	50% biodiesel	Neat biodiesel
190	1.3	2.4	5.11	13.5
250	0.1	0.2	0.6	1.4
300	0.1	0.1	0.1	0.3

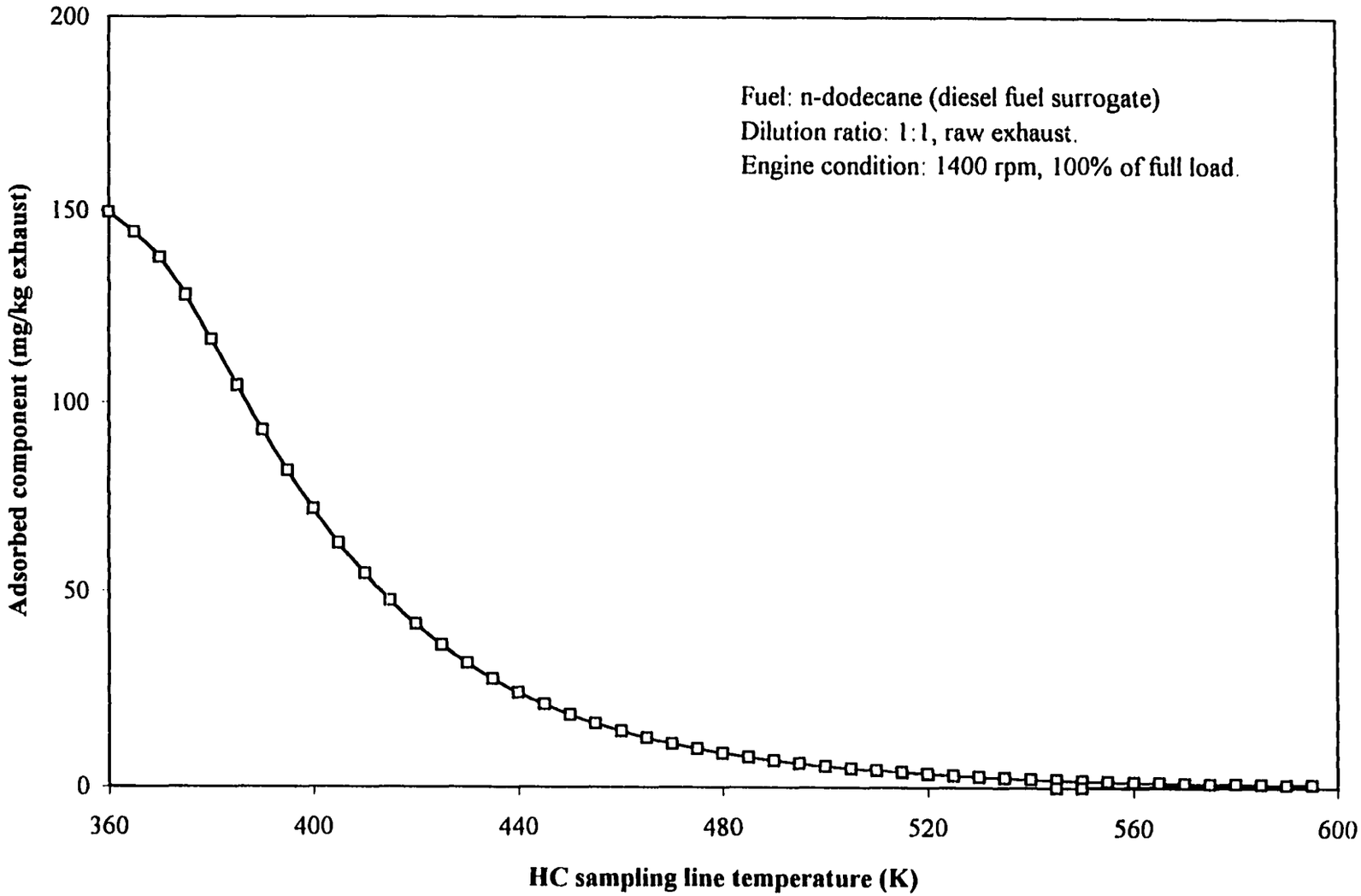

Figure 5.58 Effects of HC sampling line temperature on adsorbed individual component for n-dodecane at full-load engine condition

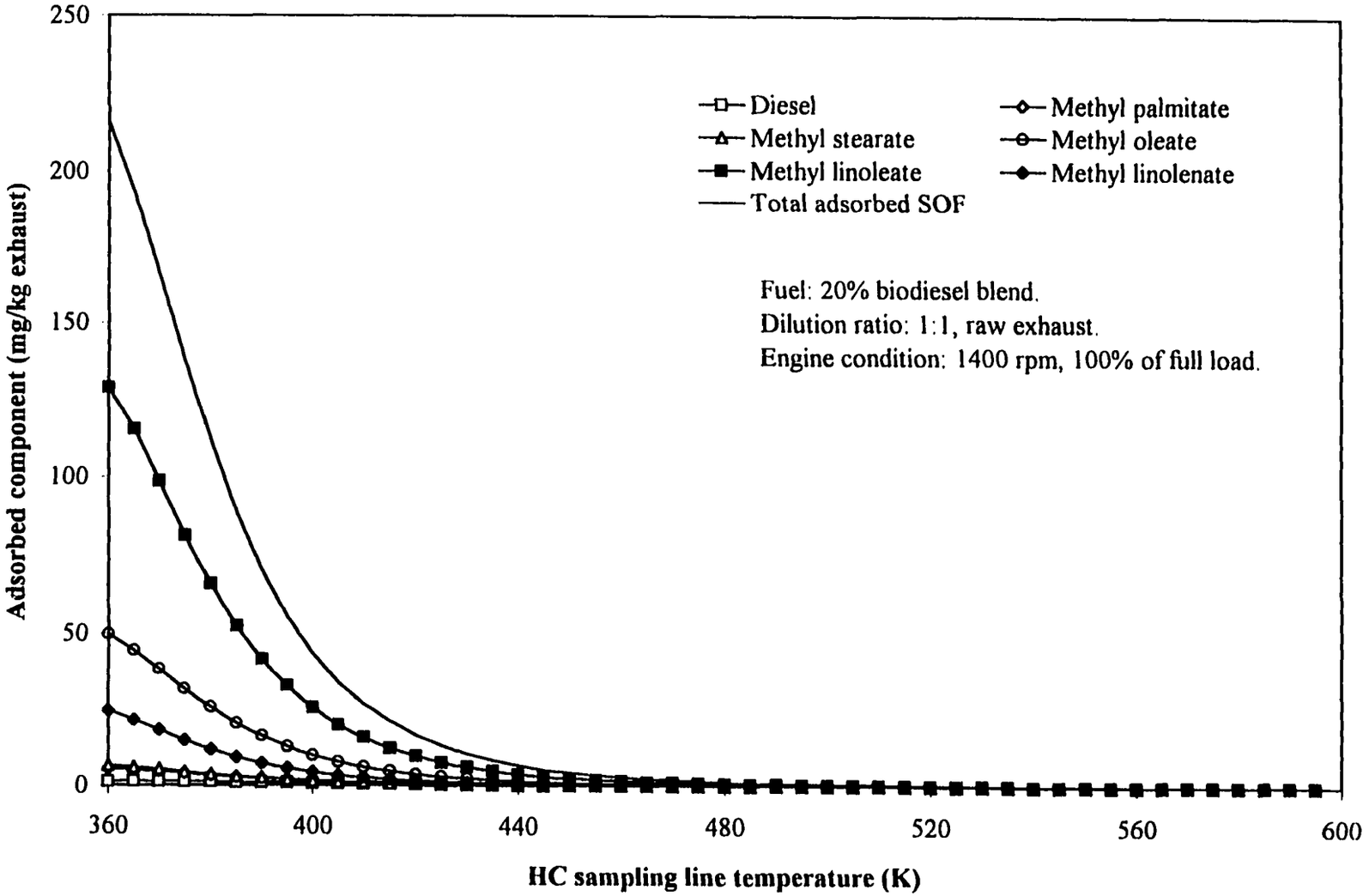

Figure 5.59 Effects of HC sampling temperature on adsorbed individual component for 20% biodiesel blend at full-load engine condition

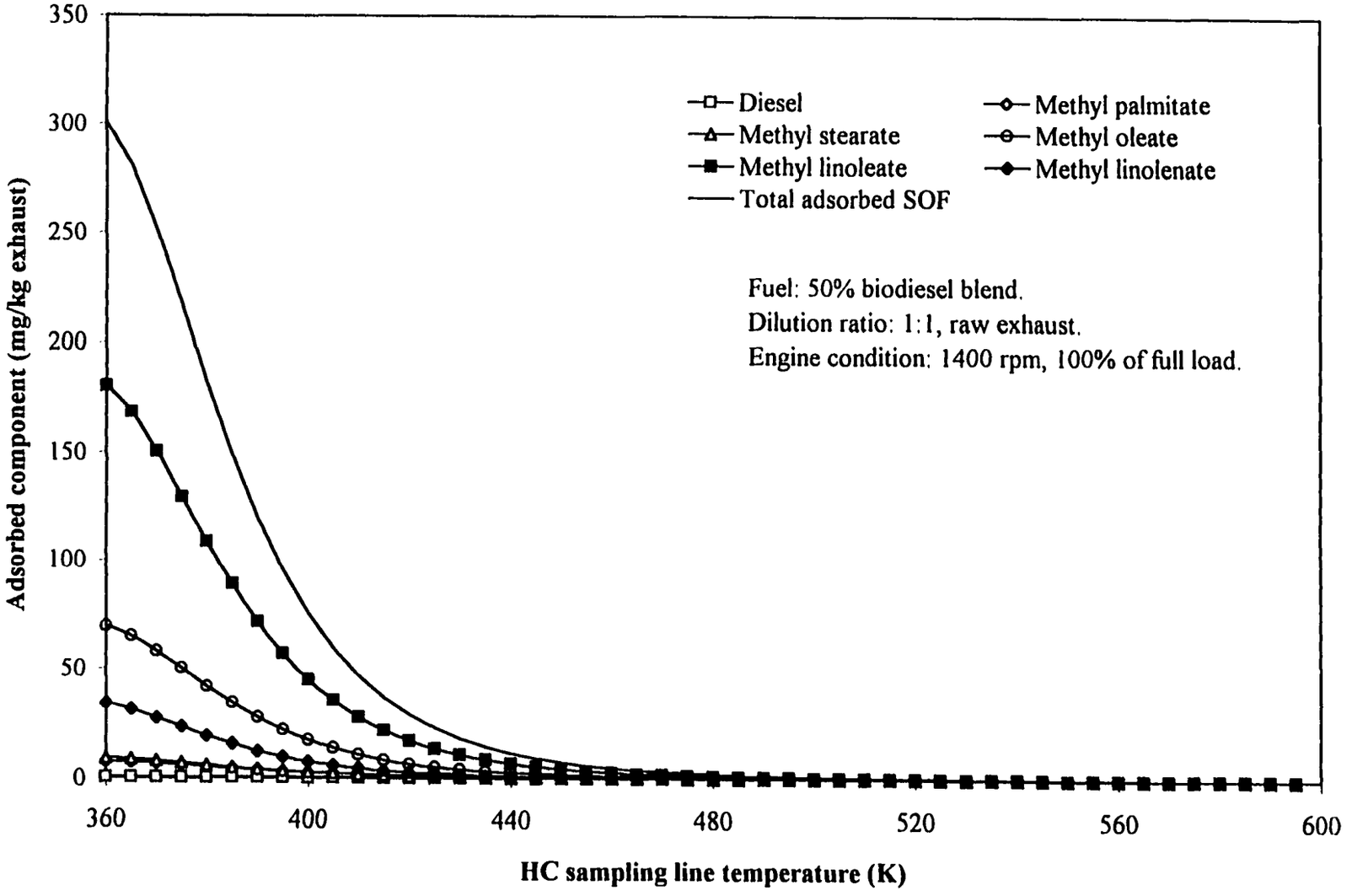

Figure 5.60 Effects of HC sampling line temperature on adsorbed individual component for 50% biodiesel blend at full-load engine condition

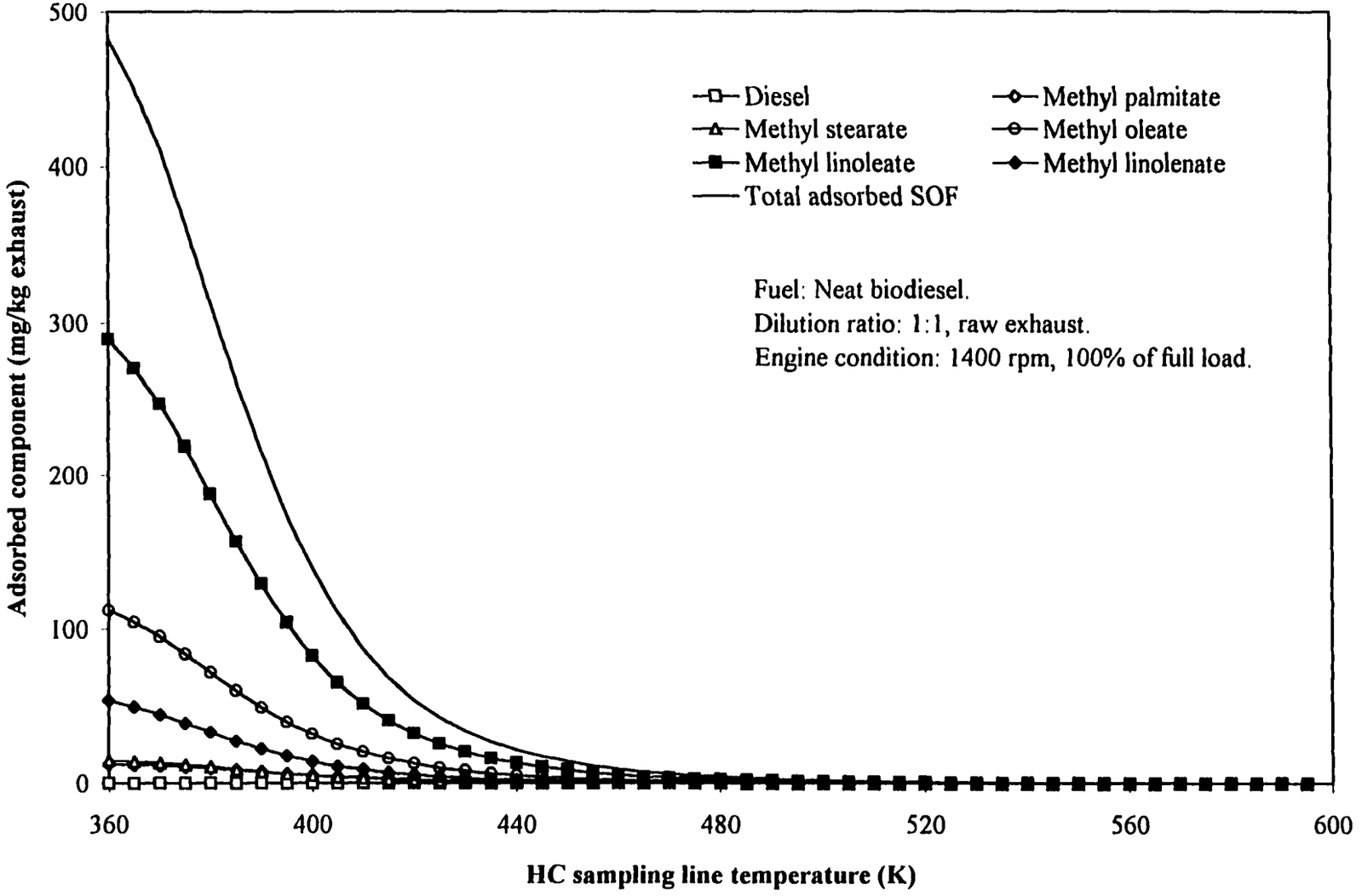

Figure 5.61 Effects of HC sampling line temperature on adsorbed individual component for neat biodiesel at full-load engine condition

condition. The adsorption effect is more severe than at the full-load engine condition. However, when the temperature of the HC sampling line is raised to 250 °C, the adsorption effect on the unburned hydrocarbons could be negligible.

Based on the above discussion, the adsorption of vapor phase hydrocarbons may significantly lower the measured HC concentration for fuels with a high fraction of biodiesel when the engine exhaust gas is transported with a heated sampling line at 190 °C. When a heated flame ionization detector that is heated to only 190 °C is used to measure the HC emissions for a diesel engine which is fueled with biodiesel blends, the measured results could be lower than the actual concentration in the engine exhaust gas.

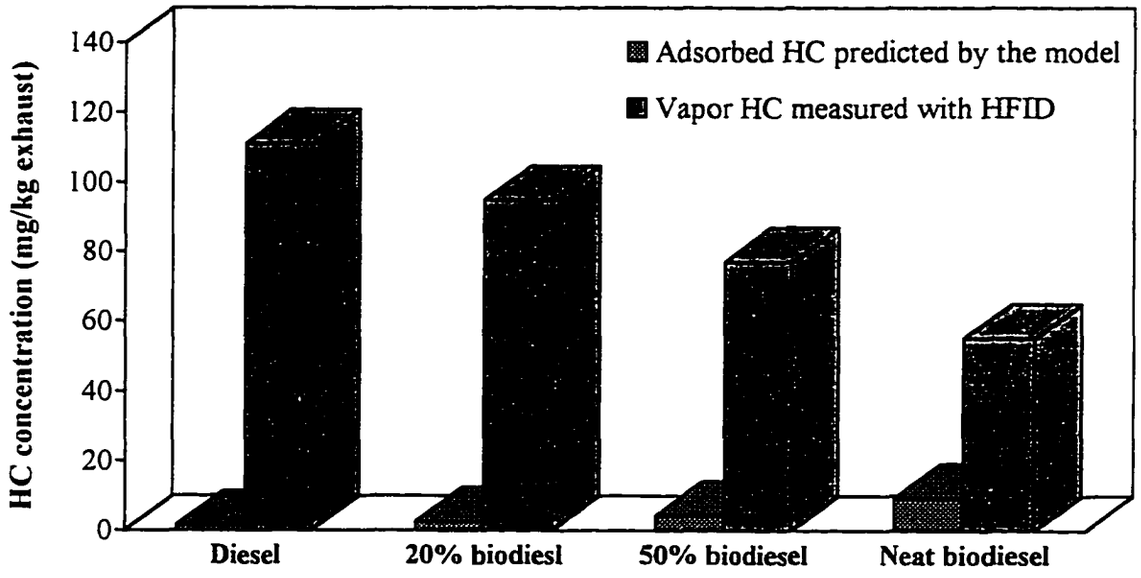

Figure 5.62 Vapor and liquid HC concentrations in raw exhaust gas at 463 K at full-load engine condition

Table 5.3 Calculated adsorbed HC fraction in the measured vapor HC concentration at light load engine condition (%)

Temperature °C	Diesel	20% biodiesel	50% biodiesel	Neat biodiesel
190	1.0	4.1	9.5	28.7
250	0.1	0.5	1.0	2.8
300	0.1	0.1	0.2	0.6

6. CONCLUSIONS

The objectives of this project were to study the effects of dilution tunnel conditions on biodiesel particulate emissions and the effects of HC sampling line temperature on the measurement of unburned hydrocarbon emissions from biodiesel-fueled engines. Models for adsorption and condensation were developed to predict and investigate the effects of dilution tunnel conditions and HC sampling line temperature on the measurement of particulate and HC emissions of biodiesel, and the model predictions were compared with experimental data to validate the models. The specific observations from the experiments and the results from comparison with the model predictions will be summarized in this chapter.

6.1 Conclusions

Comparison of the emissions between No. 2 diesel fuel and biodiesel blends, and comparison between experimental data and predictions of theoretical models were made at two engine operating conditions. Some conclusions can be drawn based on the experimental and theoretical studies.

1. Biodiesel and its blends with No. 2 diesel fuel can significantly lower total particulate and unburned hydrocarbon emissions compared with No. 2 diesel fuel at full-load engine condition.
2. Biodiesel and its blends with No. 2 diesel fuel produce higher total particulate matter than No. 2 diesel fuel at light-load engine condition. The high particulate emissions from biodiesel blends are caused by increase of SOF in the particulates.
3. Biodiesel produces a higher fraction of soluble organic fraction in its particulates than No. 2 diesel fuel for both full and light-load engine operating conditions. The SOF fractions of the neat biodiesel were 82.8% and 77.7% higher than for the baseline of No. 2 diesel fuel at full-load engine condition and a dilution ratio of 20:1 with a constant filter temperature of 325 K and a filter temperature of 320 K with a constant dilution ratio of 15:1, respectively.

4. Particulate matter was decreased for increasing dilution ratio at constant filter temperature due to the reduction in soluble organic fraction in the total particulates.
5. Particulate matter was decreased for increasing filter temperature at constant dilution ratio due to the reduction in soluble organic fraction in the total particulates.
6. Most of the unburned biodiesel is present as a condensed phase on the surface of the carbon particles following the exhaust gas dilution process, and only a small portion of the unburned biodiesel can be detected with the HFID in the vapor phase.
7. The vapor phase unburned hydrocarbon concentration in the engine exhaust gas is a function of the sampling line temperature. The concentration increases when the sampling line temperature is raised. When the sampling line temperature is above 250 °C, the change of unburned hydrocarbon concentration in the exhaust sample is very small.
8. Condensation of vapor phase unburned hydrocarbon could not explain the formation of soluble organic fraction in the particulates for diesel and biodiesel during the dilution process.
9. Condensation did not occur in the HC sampling line at and above the standard HC emission measurement temperature, 190 °C, for diesel and biodiesel.
10. Adsorption was the dominant mechanism that governs the formation of the soluble organic fraction for both diesel and biodiesel fuels during the dilution process.
11. At the standard HC sampling temperature, biodiesel adsorption can take place during the HC sample transport in the sampling line.
12. The multicomponent adsorption model developed here can be used to predict the total particulate formation during the dilution process, and the correct soluble fraction in the total particulates may be obtained if accurate basic information about fuel composition is available.

6.2 Recommendations for Future Work

Some modifications to the adsorption model are suggested based on the previous study. The purpose of the model modifications are to improve the capability of the model to

better predict the quantity of adsorbed unburned hydrocarbons on the diesel carbon particle surface. Some suggestions related to the experimental work will also be discussed.

1. More accurate energy of adsorption data for biodiesel, or esters, is needed. The energy of adsorption used in this study was calculated based on some correlations for n-alkanes. However, the molecular structure of biodiesel is different from n-alkanes. The neat biodiesel usually contains 12% oxygen by mass and includes some compounds with double bonds. If the energy of adsorption is determined based only on the carbon number in the compound, then the energy may be lower than actual energy of adsorption of biodiesel.
2. More accurate information about the molecular size of biodiesel is needed to improve the prediction capability of the adsorption model.
3. Because biodiesel shows a different chemical structure and physical properties from the diesel fuel, the specific surface area of the carbon particles produced by biodiesel during combustion may be different from the diesel fuel. Detailed information is needed to increase the accuracy of the model predictions.
4. During the biodiesel injection experiment, only a small HC concentration increase was observed when the concentration of unburned biodiesel was significantly increased. This phenomenon suggests that the typical the HFID does not respond correctly to the actual unburned biodiesel concentration in the engine exhaust gas. The reaction of HFID to unburned biodiesel should be studied in more detail.

APPENDIX A. SATURATION PRESSURE OF HYDROCARBON COMPOUNDS IN THE ENGINE EXHAUST GAS

The saturation pressure of each hydrocarbon component in the engine exhaust gas was determined using a correlation that was obtained by experimental data fitting. A general relationship between the saturation pressure (P_{sat}) and temperature (T) can be expressed as [106],

$$\log_{10}(P_{sat}) = \frac{\alpha}{T} + \beta \qquad \text{(A-1)}$$

where α and β are constants that depend on the substance and are determined by data fitting. Six different components were assumed to represent the unburned hydrocarbons in the engine exhaust gas to model the formation of soluble organic fraction in the total particulate matter. Tables A.1 to A.6 show experimentally determined saturation pressure data within a temperature range. The saturation pressure at other temperatures can be determined with the data fitting correlation (A-1). These tables also show a comparison between the experimental data and the calculated saturation pressure using the data fitting correlations.

Table A.1 Saturated vapor pressure data of n-dodecane [106, 107]

Temperature (K)	P_{sat} data (kPa)	P_{sat} Calculated (kPa)	Difference (kPa)	%
320.95	0.133	0.143	-0.010	-7.15
353.15	0.773	0.836	-0.063	-8.10
363.15	1.320	1.358	-0.038	-2.85
373.15	2.200	2.148	0.052	2.35
383.15	3.533	3.319	0.214	6.07
393.15	5.293	5.015	0.278	5.25
403.15	7.826	7.424	0.402	5.13
413.15	11.426	10.785	0.641	5.61
423.15	16.265	15.392	0.873	5.37
433.15	22.665	21.610	1.055	4.66
443.15	30.664	29.878	0.786	2.56
453.15	41.463	40.723	0.740	1.78
463.15	54.396	54.768	-0.373	-0.68
473.15	70.528	72.740	-2.213	-3.14
483.15	90.926	95.481	-4.555	-5.01
487.65	101.325	107.523	-6.198	-6.12
493.15	115.457	123.957	-8.500	-7.36

Regression equation is: $\mathrm{Log}_{10}(P_{sat}) = -2700.80/T + 7.5699$.

$R^2 = 0.9993$.

Table A.2 Saturated vapor pressure data of methyl palmitate [106, 107, 108]

Temperature (K)	P_{sat} data (kPa)	P_{sat} Calculated (kPa)	Difference (kPa)	%
407.45	0.133	0.136	-0.003	-2.16
421.15	0.267	0.271	-0.004	-1.39
435.15	0.533	0.522	0.011	1.99
439.95	0.667	0.648	0.018	2.76
445.15	0.800	0.815	-0.015	-1.82
450.15	1.067	1.010	0.057	5.37
457.15	1.333	1.353	-0.020	-1.50
475.15	2.666	2.761	-0.095	-3.55

Regression equation is: $\text{Log}_{10}(P_{sat}) = -3737.20/T + 8.3063$.

$R^2 = 0.9989$.

Table A.3 Saturated vapor pressure data of methyl stearate [106, 108]

Temperature (K)	P_{sat} data (kPa)	P_{sat} Calculated (kPa)	Difference (kPa)	%
442.55	0.267	0.273	-0.006	-2.18
457.75	0.533	0.546	-0.013	-2.44
462.55	0.667	0.673	-0.006	-0.95
466.75	0.800	0.806	-0.006	-0.76
471.95	1.067	1.003	0.064	6.03
477.25	1.267	1.246	0.021	1.63
478.95	1.360	1.335	0.025	1.83
481.55	1.480	1.482	-0.002	-0.12
485.25	1.720	1.715	0.005	0.27
489.75	2.040	2.044	-0.004	-0.18
495.45	2.533	2.539	-0.006	-0.26
500.45	3.080	3.060	0.020	0.65
502.55	3.346	3.306	0.040	1.21
503.85	3.466	3.466	0.000	-0.01
511.05	4.226	4.489	-0.263	-6.22
512.85	4.826	4.783	0.043	0.88

Regression equation is: $\mathrm{Log}_{10}(P_{sat}) = -4015.70/T + 8.5099.$

$R^2 = 0.9998.$

Table A.4 Saturated vapor pressure data of methyl oleate [106, 108]

Temperature (K)	P_{sat} data (kPa)	P_{sat} Calculated (kPa)	Difference (kPa)	%
428.72	0.139	0.141	-0.002	-1.38
435.92	0.205	0.206	-0.001	-0.35
442.71	0.292	0.291	0.001	0.47
443.33	0.300	0.300	0.000	0.07
448.61	0.392	0.389	0.003	0.74
450.66	0.431	0.430	0.001	0.27
458.52	0.630	0.625	0.005	0.87
465.00	0.843	0.842	0.001	0.15
467.89	0.968	0.959	0.009	0.92
471.61	1.133	1.132	0.001	0.11
475.61	1.353	1.348	0.005	0.34
479.11	1.566	1.568	-0.002	-0.13
482.08	1.766	1.779	-0.013	-0.74
485.22	2.005	2.030	-0.025	-1.24

Regression equation is: $\text{Log}_{10}(P_{sat}) = -4266.30/T + 9.0889$.

$R^2 = 0.9999$.

Table A.5 Saturated vapor pressure data of methyl linoleate [106, 108]

Temperature (K)	P_{sat} data (kPa)	P_{sat} Calculated (kPa)	Difference (kPa)	%
390.15	0.013	0.014	-0.001	-6.92
400.35	0.027	0.027	0.000	-1.53
411.35	0.053	0.052	0.001	2.17
418.15	0.080	0.077	0.003	3.83
427.15	0.133	0.126	0.007	5.34
439.65	0.267	0.243	0.024	9.11
455.55	0.533	0.529	0.004	0.69
466.15	0.800	0.864	-0.064	-8.05
473.05	1.067	1.175	-0.108	-10.16
479.15	1.333	1.531	-0.198	-14.86
488.15	2.666	2.234	0.432	16.20

Regression equation is: $\mathrm{Log}_{10}(P_{sat}) = -4266.30/T + 9.0889$.

$R^2 = 0.9972$.

Table A.6 Saturated vapor pressure data of methyl linolenate [106, 109]

Temperature (K)	P_{sat} data (kPa)	P_{sat} Calculated (kPa)	Difference (kPa)	%
391.55	0.013	0.014	-0.001	-4.26
401.65	0.027	0.027	0.000	-0.52
412.45	0.053	0.052	0.001	2.15
419.25	0.080	0.078	0.002	2.48
428.15	0.133	0.129	0.004	2.85
441.15	0.267	0.262	0.005	1.84
455.35	0.533	0.539	-0.006	-1.10
464.25	0.800	0.829	-0.029	-3.65

Regression equation is: $\text{Log}_{10}(P_{sat}) = -4439.80/T + 9.4820.$

$R^2 = 0.9996.$

APPENDIX B. CROSSECTIONAL AREA OF MOLECULES

The determination of the crossectional area of hydrocarbon molecules is discussed in this appendix. The molecular size of the unburned hydrocarbons determines the number of sites available on the carbon particle surface. The crossectional area of the molecules can be estimated with an equation developed by McClellan et al. [132] that is based on the assumptions of spherical shape of the molecule and hexagonal close packing.

$$A_m = 1.091\left(\frac{MW}{N_{AV}\rho}\right)^{2/3} \qquad \text{(B-1)}$$

where A_m = the crossectional area of molecule, cm^2.

MW = molecular weight.

$N_{AV} = 6.02205 \times 10^{23}$ mol^{-1}, Avagadro's number.

ρ = the density of adsorbate at liquid state, g/cm^3.

The calculated crossectional areas of unburned hydrocarbon molecules are shown in Table B.1. Because the density is a function of temperature, the crossectional area of the molecule may change with temperature due to its density change. The calculation of density is discussed in the Appendix C.

Table B.1 Crossectional area of molecules

Compound	Molecular weight	Density (g/cm^3)	Crossectional area ($Angs^2$)
$C_{12}H_{26}$	170.354	0.7487^{20a}	52.264
$C_{17}H_{34}O_2$	270.476	0.9239^{b}	67.453
$C_{19}H_{38}O_2$	298.532	0.8498^{40}	69.816
$C_{19}H_{36}O_2$	296.514	0.8739^{20}	68.217
$C_{19}H_{34}O_2$	294.496	0.8886^{18}	67.156
$C_{19}H_{32}O_2$	292.478	0.8962^{b}	72.519

[a]The superscript number indicates the temperature (°C) where the density was measured.
[b]Density was calculated with equation (C-1) at 20 °C.

APPENDIX C. DENSITY OF LIQUID UNBURNED HYDROCARBONS

The density of the liquid phase unburned hydrocarbons is a function of temperature. Its change with temperature can be determined with Grain's method [133].

The equation developed by Grain can be used to estimate the liquid density at different temperatures.

$$\rho = MW\,\rho_b\left(3-2\frac{T}{T_b}\right)^n \qquad \text{(C-1)}$$

where MW = molecular weight.

ρ_b = the molar density at boiling point, mol/cm^3.

T_b = the boiling point, K.

n = constant which is determined as following [133],

Compound	n
Alcohols	0.25
Hydrocarbons	0.29
Other organics	0.31

The density at the boiling point is determined as the inverse of the molar volume. The molar volume is calculated by summing the incremental values for every atom, chemical structure, and bond in the compounds based on Schroeder's method. Table C.1 shows the incremental values in this calculation.

Here is one example to show how Grain's method was used to find the density of n-dodecane at 52 °C. The basic information about n-dodecane is,

T_b = 489.45 K.

MW = 170.354.

The molar volume based on its molecular structure is,

Table C.1 Incremental values for estimating molar volume [133]

Molecular feature	Increment (cm^3/mol)	Molecular feature	Increment (cm^3/mol)
C	7	I	38.5
H	7	S	21
N	7	Rings	-7
O	7	Single bond	0
Br	31.5	Double bond	7
Cl	24.5	Triple bond	14
F	10.5		

$V_b = 12 \times 7$ (C) + 26×7 (H) = 266 cm^3/mol.

The molar density at its boiling point is,

$\rho_b = 1/V_b = 1/266 = 3.759 \times 10^{-3}$ mol/cm^3.

Because n-dodecane is a typical hydrocarbon compound, $n = 0.29$. So, the density of n-dodecane at 52 °C is,

$$\rho = 170.345 \times (3.759 \times 10^{-3}) \times [3 - 2 \times (52 + 273.15)/489.45]^{0.29}$$

$$= 0.7432 \text{ g/cm}^3$$

Table C.2 lists the boiling point of compounds in engine unburned hydrocarbons and other properties.

Table C.2 Properties of unburned hydrocarbons

Compound	Boiling point (K)	V_b (cm^3/mol)	ρ_b (mol/cm^3)	n
n-dodecane	489.45^{760a}	266	3.759×10^{-3}	0.29
Methyl palmitate	688.15^{747}	371	2.695×10^{-3}	0.31
Methyl stearate	715.15^{747}	413	2.421×10^{-3}	0.31
Methyl oleate	491.15^{20}	406	2.463×10^{-3}	0.31
Methyl linoleate	488.15^{20}	399	2.506×10^{-3}	0.31
Methyl linolenate	491.15^{18}	392	2.551×10^{-3}	0.31

[a]The superscript number with boiling point is the pressure where the boiling temperature is measured in mmHg.

APPENDIX D. DETERMINATION OF MOLECULAR WEIGHT OF RAW EXHAUST GAS

Because the undiluted engine raw exhaust gas consists of many chemical compounds, its molecular weight is an average of the molecular weights of the compounds in the mixture. If all the components in the exhaust gas are assumed to be ideal gases, the molecular weight of the undiluted exhaust gas can be calculated using the molecular weight and mole fraction of each component. An estimate of the composition of the exhaust gas can be obtained by assuming the combustion is a complete process, and that there is negligible water vapor in the air. Therefore, there will be only oxygen and nitrogen molecules in the air, and only carbon dioxide, water vapor, and nitrogen in the raw exhaust gas (for a stoichiometric mixture). The fuel contains carbon, hydrogen, and oxygen atoms with the general formula as $C_xH_yO_z$, and the air consists of oxygen and nitrogen molecules with a mole fraction of 0.21 and 0.79, respectively. At a stoichiometric fuel/air ratio condition, the complete combustion reaction is

$$C_xH_yO_z + \alpha(0.21O_2 + 0.79N_2) \rightarrow xCO_2 + y/2H_2O + \beta N_2 \qquad \text{(D-1)}$$

where $\alpha = 4.7619x + 1.1905y - 2.310z$.

$\beta = 3.7619x + 0.9405y - 1.8810z$.

If the combustion is under fuel lean conditions, excess air will be provided. The composition of the undiluted exhaust gas will contain oxygen from the excess air. Using a quantity called the *equivalence ratio*, ϕ, that is the ratio of the actual fuel/air ratio to the stoichiometric fuel/air ratio, the complete combustion reaction with excess air is

$$C_xH_yO_z + \alpha/\phi(0.21O_2 + 0.79N_2) \rightarrow xCO_2 + y/2H_2O + \kappa N_2 + \gamma O_2 \qquad \text{(D-2)}$$

where $\phi = \dfrac{F/A\big|_{actual}}{F/A\big|_{stoich.}} = \dfrac{F/A\big|_{actual}}{1/\alpha}$.

$\kappa = 0.79\alpha/\phi$.

$\gamma = 0.50z + 0.21\alpha/\phi - x - 0.25y$.

The mole fraction of each individual component in the undiluted exhaust gas for the excess air case is

$$y_{CO_2} = \frac{x}{n} \tag{D-3}$$

$$y_{H_2O} = \frac{y/2}{n} \tag{D-4}$$

$$y_{N_2} = \frac{\kappa}{n} \tag{D-5}$$

$$y_{O_2} = \frac{\gamma}{n} \tag{D-6}$$

where $n = x + y/2 + \kappa + \gamma = 0.25y + 0.50z + \alpha/\phi$, which is the total moles of exhaust gas.

and y_{CO_2}, y_{H_2O}, y_{N_2}, and y_{O_2} are the mole fractions for CO_2, H_2O, N_2, and O_2, respectively.

The average molecular weight of the raw exhaust gas can be found as

$$MW_{exh} = y_{CO_2}MW_{CO_2} + y_{CO_2}MW_{H_2O} + y_{N_2}MW_{N_2} + y_{O_2}MW_{O_2} \tag{D-7}$$

where Mw_{exh} = molecular weight of raw exhaust gas.

MW_{CO_2} = 44.01, CO_2 molecular weight.

MW_{H_2O} = 18.02, H_2O molecular weight.

MW_{N_2} = 28.01, N_2 molecular weight.

MW_{O_2} = 32.00, O_2 molecular weight.

APPENDIX E. ADSORPTION EQUILIBRIUM

An assumption used to develop the adsorption model and the condensation model was that all adsorption and condensation of vapor phase unburned hydrocarbons was at the equilibrium state. Before equilibrium was reached, the unburned hydrocarbons would be transferred from the bulk gas flow to the carbon particle surface by mass diffusion. It was necessary to check the equilibrium condition to determine whether or not equilibrium was reached when the engine exhaust gas was diluted in the dilution tunnel.

The mass transfer by diffusion is caused by a concentration gradient. The similarity between convection heat transfer and diffusion mass transfer is well known. A mass transfer coefficient that is similar to a heat transfer coefficient can be determined by assuming negligible viscous dissipation, no chemical reaction, and low mass transfer rate. The mass transfer rate can be expressed as,

$$m_a = h_m A_s (C_{a1} - C_{a2}) \qquad \text{(E-1)}$$

where m_a = diffusive mass transfer rate.

h_m = the mass transfer coefficient.

A_s = the area through which the transfer takes place.

C_{a1} and C_{a2} = concentrations in the bulk gas and on the surface, respectively.

Correlations for convection heat transfer can be used to determine the mass transfer coefficient based on the Reynolds number (*Re*), Prandtl number (*Pr*), Nusselt number (*Nu*), Sherwood number (*Sh*), and Schmidt number (*Sc*). The procedure to find the mass transfer rate used here was similar to the method discussed in reference [13].

The carbon particles in the engine exhaust gas are very small and they have a low density. The particle diameter of about 0.033 μm is the basis for the assumption of a specific area of 90 m^2/g as a sphere [95]. When the diluted exhaust gas moves down the dilution tunnel, the particles are assumed to move with the bulk gas at the same velocity that means

there is no slip between the carbon particles and the diluted exhaust gas. The Reynolds number of the carbon particles related to the bulk gas is nearly equal to zero ($Re \approx 0.0$).

For a sphere at low Re number, the Sherwood number can be determined with the following equation [137],

$$Sh = 2.0 + 0.60(Re)^{1/2}(Sc)^{1/3} = 2.0 \qquad \text{(E-2)}$$

where Sc: Schmidt number, $Sc = \mu/\rho D_{ab}$, and where D_{ab} is a mass diffusivity which can be calculated with Wilke-Lee correlation [137],

$$D_{ab} = \frac{(0.00107 - 0.000246\sqrt{1/MW_a + 1/MW_b})\,T^{1.5}\sqrt{1/MW_a + 1/MW_b}}{P\,(r_{ab})^2[f(kT/\varepsilon_{ab})]} \qquad \text{(E-3)}$$

where MW_a = molecular weight of substance a.

MW_b = molecular weight of substance b.

P = the absolute pressure, atm.

T = the absolute temperature, K.

$k = 1.3807 \times 10^{-23}$ J K^{-1}, Boltzmann constant.

r_{ab} = the molecular separation at collision, Å. $r_{ab} = (r_a + r_b)/2$.

ε_{ab} = the energy of molecular interaction. $\varepsilon_{ab} = \sqrt{\varepsilon_a \varepsilon_b}$.

$f(kT/\varepsilon_{ab})$ = the collision function determined with Figure E.1.

The values of r and ε for some substances are listed in Table E.1. The values also can be estimated from the component properties using the following relationships [137],

$$r = 1.18v^{1/3} \qquad \text{(E-4)}$$

$$\varepsilon/k = 1.21T_b \qquad \text{(E-5)}$$

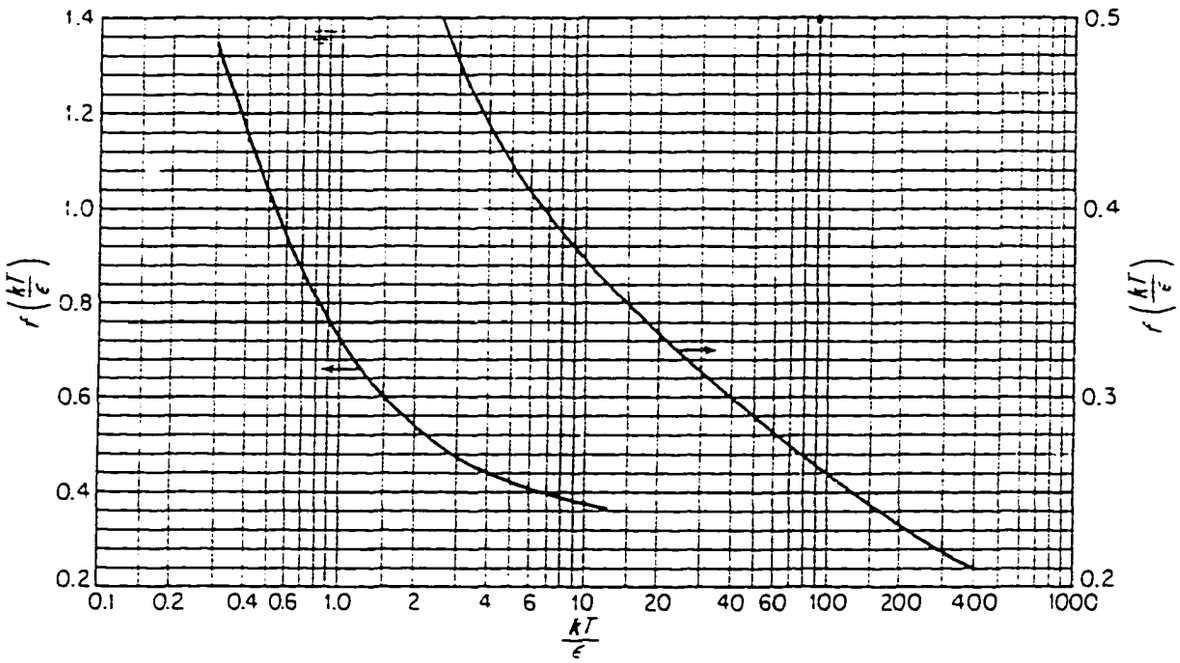

Figure E.1 Collision function for diffusion [137]

Table E.1 Force constants [137]

Gas	ε/k (K)	r (Å)
Air	97.0	3.617
H_2	33.3	2.968
N_2	91.46	3.681
CO_2	190.0	3.996
N_2O	220.0	3.879
NO	119.0	3.470
CH_4	136.5	3.882
O_2	113.2	3.433
CO	110.3	3.590

where v = molar volume at normal point, cm^3/mole which can be determined with Table E.2.

T_b = the normal boiling point, K.

The *Sh* number is defined as

$$Sh = \frac{h_{ab} d_p}{D_{ab}} \tag{E-6}$$

and the diffusion coefficient of substance *a* though *b* is

$$h_{ab} = \frac{Sh\, D_{ab}}{d_p} = 2.0 \frac{D_{ab}}{d_p} \tag{E-7}$$

The calculated coefficients of diffusion and other results for different fuels at 52 °C are shown in Table E.3.

To estimate the time required to reach the adsorption equilibrium, some assumptions are made:

- The adsorption is a rapid process compared with the mass transfer from the bulk gas to the particle surface.

Table E.2 Values for atomic volume calculation [137]

Atom in molecule	Atomic volume (cm^3/mol)
C	14.8
H	3.7
N	15.6
O	7.4
Oxygen in methyl esters	9.1
Oxygen in acids	12.0
Benzene ring	-15.0
Naphthalene ring	-30.0

Table E.3 Coefficient of diffusion

Fuel	*Sh*	D_{ab} (m^2/s)	h_m (m/s)
n-Dodecane	2.0	5.22×10^{-6}	316.36
20% biodiesel	2.0	6.82×10^{-6}	413.32
50% biodiesel	2.0	6.51×10^{-6}	394.69
Neat biodiesel	2.0	5.77×10^{-6}	349.87

- Carbon particles and unburned hydrocarbon molecules move together in the dilution tunnel.
- A linear adsorption isotherm due to the low unburned hydrocarbon concentration.
- Unburned hydrocarbon vapor at the surface of the particulate is in equilibrium with the amount of unburned hydrocarbon on the surface of the particulate.

Based on these assumptions, the unburned hydrocarbon concentration in the bulk gas can be expressed as [13],

$$\frac{d C_b}{dt} = h_{ab} A_{sol} C_{sol} (K_2 - C_b - \frac{C_b}{K_1}) \qquad \text{(E-8)}$$

where C_b = the concentration of unburned hydrocarbons in bulk gas, mg/m^3.

A_{sol} = the specific surface area of particulate, 90 m^2/g.

C_{sol} = the carbon particle concentration in the bulk gas, mg/m^3.

$K_1 = C_{sol}C_1$, $C_1 = 0.07096$ a constant [13].

$K_2 = C_{bi}/(C_{sol}C_1)$, C_{bi} is the initial concentration of unburned hydrocarbons in the bulk gas, mg/m^3.

After integration, the concentration of unburned hydrocarbons in the bulk gas is,

$$C_b = \frac{K_2}{1+1/K_1} + \frac{C_{bi}(1+1/K_1) - K_2}{1+1/K_1} e^{-t/T} \qquad \text{(E-9)}$$

where T is a time constant and $T = \dfrac{1}{h_{ab} A_{sol} C_{sol} (1+1/K_1)}$.

When the equilibrium is reached, $dC_b/dt = 0$, at $t = \infty$, $C_b = C_{beqm}$. The calculated equilibrium time during the engine exhaust gas diluted in the dilution tunnel used in this study was presented in Chapter 5.

REFERENCES

[1] Baumgard, K.J. and Johnson, J.H. The Effect of Low Sulfur and a Ceramic Particulate Filter on Diesel Exhaust Particles Size Distributions. SAE paper 920566, 1992.

[2] Brightwell, J., Fouillet, X., Cassano-Zoppi, A.L., Bernstein, D., Crawley, F., Duchosal, F., Gatz, R., Perczel, S., and Pfeifer, H. Tumours of the Respiratory Tract in Rats and Hamsters Following Chronic Inhalation of Engine Exhaust Emissions. J. Appl. Toxicol, 9, 1989, p23.

[3] Mauderly, J.L. Diesel Exhaust Environmental Toxicants-Human Exposures and Their Health Effects. Edited by Lippmann, M. Van Nostrand Reinhold, New York, 1992, p119.

[4] Johnson, J.H., Bagley, S.T., Gratz, L.D., and Leddy, D.G. A Review of Diesel Particulate Control Technology and Emissions. SAE paper 940233, 1994.

[5] Federal Register. Code of Federal Regulations CFR Title 40, Part 86, Subpart A. EPA, 1996.

[6] Goering, C.E., Schwab, A.W., Daugherty, M.J., Pryde, E.H., and Heakin, A.J. Fuel Properties of Eleven Vegetable Oils. Trans. of the ASAE Vol. 25(6), Nov. 1982, p1472.

[7] Bagby, M.O., Freedman, B., and Schwab, A.W. Seed Oils for Diesel Fuels: Sources and Properties. ASAE paper 87-1583, 1987.

[8] Wagner, L.E., Clark, S.J., and Schrock, M.D. Effects of Soybean Oil Esters on the Performance, Lubricating Oil, and Wear of Diesel Engines. SAE paper 841385, 1984.

[9] Freedman, B. and Pryde, E.H. Fatty Esters from Vegetable Oils for Use as a Diesel Fuel. Vegetable Oil Proceedings of the International Conference on Plant and Vegetable Oils as Fuels, Aug. 1982, p117.

[10] Zhang, Y. and Van Gerpen, J.H. Combustion Analysis of Esters of Soybean Oil in a Diesel Engine. SAE paper 960765, 1996.

[11] Chang, D.Y., Van Gerpen, J.H., Lee, I., Johnson, L., Hammond, E.G., and Marley, S. Fuel Properties and Emissions of Esters of Soybean Oil as Diesel Fuel. J. of Amer. Oil Chem. Soc. Vol. 73, No. 11, 1996.

[12] Johnson, J.E. Hydrocarbon Oxidation in a Diesel Catalytic Converter. M. Sc. Thesis University of Minnesota, 1993.

[13] Clerc, J.C. and Johnson, J.H. A Computer Heat Transfer and Hydrocarbon Adsorption Model for Predicting Diesel Particulate Emissions in Dilution Tunnels. SAE paper 821218, 1982.

[14] Plee, S.L. and MacDonald, J.S. Some Mechanisms Affecting the Mass of Diesel Exhaust Particulate Collected Following a Dilution Process. SAE paper 800186, 1980.

[15] Heywood, J.B. Internal Combustion Engine Fundamentals. McGraw-Hill, New York, 1988.

[16] Stone, R. Introduction to Internal Combustion Engines. 2nd edition Macmillan Press Ltd., London, 1992.

[17] McCarthy, C.I., Slodowske, W.J., Sienicki, E.J., and Jass, R.E. Diesel Fuel Property Effects on Exhaust Emissions from a Heavy-Duty Diesel Engine that Meet 1994 Emissions Requirements. SAE paper 922267, 1992.

[18] Miyamoto, N., Ogawa, H., Shibuya, M., and Suda, T. Description of Diesel Emissions by Individual Fuel Properties. SAE paper 922221, 1992.

[19] Ullman, T.L., Spreen, K.B., and Mason, R.L. Effects of Cetane Number, Aromatics, and Oxygenates on 1994 Heavy-Duty Diesel Engine Emissions. SAE paper 941020, 1994.

[20] Rosenthal, M.L. and Bendinsky, T. The Effects of Fuel Properties and Chemistry on the Emissions and Heat Release of Low-Emissions Heavy Duty Diesel Engines. SAE paper 932800, 1993.

[21] Zelenka, P., Kriegler, W., Herzog, P.L.,and Cartellieri, W.P. Ways toward the Clean Heavy-Duty Diesel. SAE paper 900602, 1990.

[22] Herzog, P.L., Burgler, L., Winklhofer, E., Zelenka, P., and Cartellieri, W. NO_x Reduction Strategies for DI Diesel Engines. SAE paper 920470, 1992.

[23] Federal Register. Code of Federal Regulations CFR Title 40, Part 86, Subpart B. EPA, 1996.

[24] Haynes, B.S. and Wagner, H.G. Soot Formation. Progress of Energy and Combustion Science 7, 1981.

[25] Luo, L. Pipho, M.J., Ambs, J.L., and Kittelson, D.B. Particle Growth and Oxidation in a Direct-Injection Diesel Engine. SAE paper 890580, 1989.

[26] Kamimoto, T. and Yagita, M. Particulate Formation and Flame Structure in Diesel Engines. SAE paper 890436, 1989.

[27] Graham, S.C., Homer, J.B., and Rosenfeld, J.L.J. The Formation and Coagulation of Soot Aerosols Generated by the Pyrolysis of Aromatic Hydrocarbons. Proc. Roy. Soc. Lond. A344, 1975.

[28] Vuk, C.T., Jones, M.A., and Johnson, J.H. The Measurement and Analysis of the Physical Character of Diesel Particulate Emissions. SAE paper 760131, 1976.

[29] Fujiwara, Y. and Fukazawa, S. Growth and Combustion of Soot Particulates in the Exhaust of diesel Engines. SAE paper 800984, 1980.

[30] Atkins, P.W. Physical Chemstry. 2nd edition, W. H. Freeman and Company, San Francisco, 1982.

[31] Adamson, A.W. Physical Chemistry of Surfaces. 3rd edition, John Wiley & Sons, Inc., New York, 1976.

[32] Amann, C.A. and Siegla, D.C. Diesel Particulates-What They Are and Why. Aerosol Sci. Technol., Vol. 1, 1982.

[33] Cautreels, W. and Van Cauwenberghe, K. Extraction of Organic Compounds from Airborne Particulate Matter. Water, Air, and Soil Pollution, Vol. 6, p103, 1976.

[34] Hill, H.H. Jr., Chan, K.W., and Karasek, F.W. Extraction of Organic Compounds from Airborne Particulate Matter for Gas Chromatographic Analysis. J. of Chromatography, Vol. 131, p245, 1977.

[35] Grosjean, W. Solvent Extraction and Organic Carbon Determination in Atmospheric Particulate Matter: The Organic Extraction-Organic Carbon Analyzer Technique . Analytical Chemistry, Vol. 47, p797.

[36] Halsall, R., McMillan, M.L., and Schwartz, B.J. An Improved Method for Determining the Hydrocarbon Fraction of Diesel Particulates by Vacuum Oven Sublimation. SAE paper 872136, 1987.

[37] Shimpi, S.A. and Yu, Y. Determination of a Reliable and Efficient Diesel Particulate Hydrocarbon Extraction Process. SAE paper 811183, 1981.

[38] Andrews, G.E., Abdelhalim, S., Abbass, M.K., Asadi-Aghdam, H.R., Williams, P.T., and Bartle, K.D. The Role of Exhaust Pipe and In Cylinder Deposits on Diesel Particulate Composition. SAE paper 921648, 1992.

[39] Cuthbertson, R.D., Stinton, H.C., and Wheeler, R.W. The Use of a Thermogravimetric Analyzer for the Investigation of Particulates and Hydrocarbons in Diesel Engine Exhaust. SAE paper 790814, 1979.

[40] Draper, W.M., Hartmann, H., Kittelson, D.B., Watts, W.F., and Baumgard, Jr., K.J. Impact of a Ceramic Trap and Manganese Fuel Additive on the Biological Activity and Chemical Composition of Exhaust Particles from Diesel Engines Used in Underground Mines. SAE paper 871621, 1987.

[41] Cautreels, W. and Van Cauwenberghe, K. Experiments on the Distribution of Organic Pollutants Between Airborne Particulate Matter and the Corresponding Gas Phase. Atmospheric Envir., Vol. 12, p1133, 1976.

[42] Karasek, F.W., Denney, D.W., Chan, K.W., and Clement, R.E. Analysis of Complex Organic Mixtures on Airborne Particulate Matter. Analytical Chemistry, Vol. 50, p82.

[43] Information Report: 1979 Progress of the Chemical Characterization Panel of the Composition of Diesel Exhaust Project and results of Particulate Extraction Round-Robin. CRC Report No. 516. Coordinating Research council, Inc. 219 Perimeter Center Parkway, Altlanta, Georgia, March 1980.

[44] Funkenbusch, E.F., Leddy, D.G., and Johnson, J.H. The Characterization of the Soluble Organic Fraction of Diesel Particulate Matter. SAE paper 790418, 1979.

[45] Lipkea, W.H., Johnson, J.H., and Vuk, C.T. The Physical and Chemical Character of Diesel Particulate Emissions-Measurement Techniques and Fundamental Considerations. SAE paper 780108, 1978.

[46] Springer, K.J. Low-Emission Diesel Fuel for 1991 - 1994. J. of Engineering for Gas Turbines and Power, Vol. 111, p361, July, 1989.

[47] Wall, J.C., Shimpi, S.A., and Yu, M.L. Fuel Sulfur Reduction for Control of Diesel Particulate Emissions. SAE paper 872139, 1987.

[48] Opris, C.N., Gratz, L.D., Bagley, S.T., Baumgard, K.J., Leddy, D.G., and Johnson, J.H. The Effects of Fuel Sulfur Concentration on Regulated and Unregulated Heavy-Duty Diesel Emissions. SAE paper 930730, 1993.

[49] Cowley, L.T., Doyon, J., and Stradling, R.J. The Influence of Composition and Properties of Diesel Fuel on Particulate Emissions from Heavy-Duty Engines. SAE paper 932732, 1993.

[50] Bertioli, C., Del Giacomo, N., Iorio, B., and Prati, M.V. The Influence of Fuel Composition on Particulate emissions of DI diesel Engines. SAE paper 932733, 1993.

[51] Quick, G.R. An In Depth Look at Farm Fuel Alternatives. Power Farming Magazine 89(2), p10, 1980.

[52] Krawczyk, T. Biodiesel - Alternative Fuel Makes Inroads but Hurdles Remain. INFORM Vol. 7, No. 8, p800, 1996.

[53] deMan, J.M. Chemical and Physical Properties of Fatty Acids. Fatty Acids in Foods and Their Health Implications. Edited by Chow, C.K., Marcel Dekker, Inc., New York, p17, 1992.

[54] Van Gerpen, J.H., Hammond, E.G., Johnson, L.A., Marley, S.J., Yu, L., Lee, I., and Monyem, A. Determining the Influence of Contaminants on Biodiesel Properties. Final Report Prepared for The Iowa Energy Center, 94-09-1, 1996.

[55] Freedman, B., Bagby, M.O., Callahan, T.J., and Ryan, T.W. Cetane Numbers of Fatty Esters, Fatty Alcohols and Triglycerides Determined in a Constant Volume Combustion Bomb. SAE paper 900343, 1990.

[56] Goering, C.E., Schwab, A.W., Daugherty, M.J., Pryde, E.H., and Heakin, A.J. Fuel Properties of Eleven Vegetable Oils. Tran. of the ASAE, Vol. 25(6), p142, Nov., 1982.

[57] Bagby, M.O. and Freedman, B. Seed Oils for Diesel Fuels: Sources and Properties. ASAE paper 871583, 1987.

[58] Braun, D.E. and Stephenson, K.Q. Alternative Fuel Blend and Diesel Engine Tests. Vegetable Oil Fuels - Proceeding of the International Conference on Plant and Vegetable Oils as Fuels, p294, Aug., 1982.

[59] Mazed, M.A., Summers, J.D., and Batchelder, D.G. Peanut, Soybean and Cottonseed Oil as Diesel Fuels. Tran. of the ASAE, Vol. 28(5), p1375, 1985.

[60] Mazed, M.A., Summers, J.D., and Batchelder, D.G. Diesel Engine-Diesel/Vegetable Oil Short Term Performance Tests. ASAE paper 851058, 1985.

[61] Ishii, Y. and Takeuchi, R. Vegetable Oils and Their Effect on Farm Engine Performance. Tran. of the ASAE, Vol. 30(1), p2, 1987.

[62] Hemmerlein, N., Korte, V., Richter, H., and Schroder, G. Performance, Exhaust Emissions, and Durability of Modern Diesel Engines Running on rapeseed Oil. SAE paper 910848, 1991.

[63] Ryan, T.W., Callahan, T.J., and Dodge, L.G. Characterization of Vegetable Oils for Use as Fuels in Diesel Engines. Vegetable Oil Fuels - Proceeding of the International Conference on Plant and Vegetable Oils as Fuels, p70, Aug., 1982.

[64] Tahir, A.R., Lapp, H.M., and Buchanan, L.C. Sunflower Oil as a Fuel for Compression Ignition Engines. Vegetable Oil Fuels - Proceeding of the International Conference on Plant and Vegetable Oils as Fuels, p82, Aug., 1982.

[65] Fort, E.F. and Blumberg, P.N. Performance and Durability of a Turbocharged Diesel Engine Fueled with Cottonseed Oil Blends. Vegetable Oil Fuels - Proceedings of the International Conference on Plant and Vegetable Oils as Fuels, p374, Aug., 1982.

[66] Schlick, M.L., Hanna, M.A., and Schinstock, J.L. Soybean and Sunflower Oil Performance in a Diesel Engine. Trans. of the ASAE, Vol. 31(5), Sept., 1988.

[67] Ryan III, T.W. and Callahan, T.J. The Effects on the Vegetable Oil Properties on Injection and Combustion in Two Different Diesel Engines. JAOCS, Vol. 61(10), p1610, 1984.

[68] Rewolinski, C. and Shaffer, D.L. Sunflower Oil Diesel Fuel; Lubrication System Contamination. JAOCS, Vol. 67(7), p1120, 1985.

[69] Crookes, R.J, Nazha, M.A.A., and Kiannejad, F. Single and Multi Cylinder Diesel-Engine Tests with Vegetable Oil Emulsions. SAE paper 922230, 1992.

[70] Goering, C.E., Schwab, A.W., Campion, R.M., and Pryde, E.H. Soyoil-ethanol Microemulsions as Diesel Fuel. Tran. of the ASAE, Vol. 26(6), p1602, 1983.

[71] Chang, D.Y. and Van Gerpen, J.H. Fuel Properties and Engine Performance for Biodiesel Prepared from Modified Feedstocks. SAE paper 971684, 1997.

[72] Peterson, C.L., Feldman, M., Korus, R., and Auld, D.L. Batch Type Transesterification Process for Winter Rape Oil. Applied Engineering in Agriculture, Vol. 7(6), p711, Nov., 1991.

[73] Vander G.L. Characterization of Vegetable Oil Combustion. Process to Manufacture Ethyl Ester of Rape Oil. First Biomass Conference of the Americas: Energy, Environment , Agriculture, and Industry Proceedings, Vol. II, p815, Aug., 1993.

[74] Wagner, L.E., Clark, S.J., and Schrock, M.D. Effects of Soybean Oil Esters on the Performance, Lubricating Oil, and Wear of Diesel Engines. SAE paper 841385, 1984.

[75] Last, R.J., Kruger, M., and Durnholz, M. Emissions and Performance Characteristics of a 4-Stroke , Direct Injection Diesel Engine Fueled with Blends of Biodiesel and Low Sulfur Diesel Fuel. SAE paper 950054, 1995.

[76] McDonald, J., Purcell, D.L., McClure, B.T., and Kittelson, D.B. Emission Characteristics of Soy Methyl Ester Fuels in an IDI Compression Ignition Engine. SAE paper 950400, 1995.

[77] Graboski, M.S., Ross, J.D., and McCormick, R.L. Transient Emissions from No. 2 Diesel and Biodiesel Blends in a DDC Series 60 Engine. SAE paper 961166, 1996.

[78] Schmidt, K. and Van Gerpen, J.H. The Effect of Biodiesel Fuel Composition on Diesel Combustion and Emissions. SAE paper 961086, 1996.

[79] Freedman B., Bagby, M.O., Callahan, T.J., and Ryan, III, T.W. Cetane Numbers of Fatty Esters, Fatty Alcohols and Triglycerides Determined in a Constant Volume Combustion Bomb. SAE paper 900343, 1990.

[80] Harrington, K. Chemical and Physical Properties of Vegetable Oil Esters and Their Effect on Diesel Fuel Performance. Biomass Vol. 9, p1, 1986.

[81] Alfuso, S., Auriemma, M., Police, G., and Prati, M.V. The Effect of Methyl-Ester of Rapeseed Oil on Combustion and Emissions of DI Diesel Engines. SAE paper 932801, 1993.

[82] Choi, C.Y., Bower, G.R., and Reitz, R.D. Effects of Biodiesel Blended Fuels and Multiple Injections on D.I. Diesel Engine Emissions. SAE paper 970218, 1997.

[83] Abbass, M.K., Andrews, G.E., Williams, P.T., and Bartle, K.D. Diesel Particulate Composition Changes Along an Air Cooled Exhaust Pipe and Dilution Tunnel. SAE paper 890789, 1989.

[84] Gross, G.P., MacDonald, J.S., and Shahed, S.M. Informational Report on the Measurement of Diesel Particulate Emissions. In Coordinating Research Council Report No. 522, 1982.

[85] Perez, J.M., Jass, R.E., and Leddy, D.G. Chemical Methods for the Measurement of Unregulated Diesel Emissions. In Coordinating Research Council Report No. 551, 1987.

[86] Harrington, J.A. and Yetter, R.A. Application of a Mini-Dilution Tube in the Study of Fuel Effects on stratified Charge Engine Emissions and Combustion. SAE paper 811198, 1981.

[87] Suzuki, J. Development of Dilution Mini-Tunnel and Its Availability for Measuring Diesel Exhaust Particulate Matter. SAE paper 851547, 1985.

[88] Hirakouchi, N., Fukano, I., and shoji, T. Measurement of Diesel Exhaust Emissions with MinioDilution Tunnel. SAE paper 890181, 1989.

[89] Heden, P., Eriksson, C., and Gustavsson, L. A Simplified Dilution Tunnel System Intended for Heavy-Duty Diesel Development. SAE paper 861279, 1986.

[90] Murray, B.C. Development of a Transient Diesel Exhaust Emissions Measurement System. M.S. Thesis, Iowa State University, 1989.

[91] Amann, C.A., Stivender, D.L., Plee, S.L., and MacDonald, J.S. Some Rudiments of Diesel Particulate Emissions. SAE paper 800251, 1980.

[92] MacDonald, J.S., Plee, S.L., D'Arcy, J.B., and Schreck, R.M. Experimental Measurements of the Independent Effects of Dilution Ratio and Filter Temperature on Diesel Exhaust Particulate Samples. SAE paper 800185, 1980.

[93] Frisch, L.E., Johnson, J.H., and Leddy, D.G. Effect of Fuels and Dilution Ratio on Diesel Particulate Emissions SAE paper 790417, 1979.

[94] Kittelson, D.B. and Johnson J.H. Variability in Particle Emission Measurements in the Heavy Duty Transient Test. SAE paper 910738, 1991.

[95] Barris, M.A. Mass Transfer Processes Affecting the Nature of Diesel Exhaust Aerosols. M.S. Thesis, University of Minnesota, 1981.

[96] Khatri, N.J., Johnson, J.H., and Leddy, D.G. The Characterization of the Hydrocarbon and Sulfate Fractions of Diesel Particulate Matter. SAE paper 780111, 1978.

[97] Andrews, G.E., Abdelhalim, S.M., and Williams, P.T. Characterization of Diesel Particulate Emissions of Two IDI Diesel Engines Using Diesel and Kerosene Fuels. SAE paper 961231, 1996.

[98] Hurn, R.W. and Marshall, W.F. Techniques for Diesel Emissions Measurement. SAE paper 680418, 1968.

[99] Fosseen, D. Identification of Elements Found in Increased Soluble Fraction of Particulate Emissions with a Methyl Soyate Blend. Final report to the National Biodiesel Board, Contract No. 219-3, Fosseen Manufacturing and Development, Radcliffe, IA, 1995.

[100] Callendar, Engineering, 126, p594, 1928.

[101] Antoine, C. and Acad, C.R. Sci., Paris 107, p681, 1888.

[102] Montgomery, A.H. Vapor Pressure Equations. MS Thesis, Iowa State University, 1952.

[103] Majer, V., Svoboda, V. and Pick, J. Heats of Vaporization of Fluids. Studies in Modern Thermodynamics 9, Elservier, Science Publishers, Amsterdam, The Netherlands, 1989.

[104] Cragoe, C.S. International critical Tables. Vol. 3, McGraw-Hill, New York, 1928.

[105] Yaws, C.L. Handbook of Vapor Pressure. Gulf Publishing Company, Houston, Texas, 1994.

[106] CRC Handbook of Chemistry and Physics. 74th Edition, CRC Press, Inc., Boca Raton, Florida, 1994.

[107] Jordan, T.E. Vapor Pressure of Organic Compounds. Interscience Publishers, Inc., New York, 1954.

[108] Boublik, T, Fried, V., and Hala, E. The Vapor Pressure of Pure Substances, Physical Sciences Data 17. 2nd Revised Edition, Elsevier Science Publishers B.V., Amsterdam, Netherlands, 1984.

[109] Fatty Acids Their Chemistry, Properties, Production, and Uses Part One. 2nd Edition, Edited by Markley, K., Interscience Publishers, Inc., New York, 1968.

[110] Tien, C. Adsorption Calculations and Modeling. Butterworth-Heinemann, Newton, MA, 1994.

[111] Atkins, P.W. Physical Chemistry. 2nd Edition, Oxford University Press, London, UK, 1982.

[112] Oscik, J. and Cooper, I.L. Adsorption. Ellis Horwood Limited, England, 1982.

[113] Funkenbusch, E.F., Ledy, D.G., and Johnson, J.H. The Characterization of the Soluble Organic Fraction of Diesel Particulate Matter. SAE paper 790418, 1979.

[114] Ahmad, T., Plee, S.L., and Myers, J.P. Effects of Intake-Air Composition on Gas Phase and Particulate Bound HC Emissions from Diesel Engines. SAE paper 811196, 1981.

[115] Mayers, A.L. and Prausnitz, J.M. Thermodynamics of Mixed-Gas Adsorption. J. AIChE Vol. 11, p121, 1965.

[116] Suwanayuen, S. and Danner, R.P. J. AIChE Vol. 26, p68, 1980.

[117] Grant, R.J. and Meanes, M. Ind. Eng. Chem. Fund. Vol. 5, p490, 1966.

[118] Radke, C.J. and Prausnitz, J.M. J. AIChE Vol. 18, p761, 1972.

[119] Freundlich, H. Colloid and Capillary Chemistry. Methuen, London, 1926.

[120] Langmuir, I. J. Am. Chem. Soc. Vol. 40, p1361, 1918.

[121] Brunauer, S.P. The Adsorption of Gases and Vapors. Vol. 1, Princeton University Press, Princeton, New Jersey, 1945.

[122] Adamson, A.W. Physical Chemistry of Surfaces. 3rd Edition John Wiley & Sons. Inc., New York, 1976.

[123] Brunauer, S.P., Emmett, H, and Teller, E. J. of Am. Chem. Soc. Vol. 60, p309, 1938.

[124] Harkins, W.D. and Jura, G. J. Am. Chem. Soc. Vol. 66, p1366, 1944.

[125] Jura, G. and Harkins, W.D. J. Am. Chem. Soc. Vol. 68, p1941, 1946.

[126] Ruthven, D.M. Nature Phys. Sci. Vol. 232, p70, 1971.

[127] Ponec, V., Knor, Z., and Cerny, S. Adsorption on Solids. Butterworth & Co., London, England, 1974.

[128] Valenzuela, D.P. and Myers, A.L. Adsorption Equilibrium Data Handbook. Prentice Hall, New Jersey, 1989.

[129] Riddick, J.A., Bunger, W.B., and Sakano, T.K. Organic Solvents Physical Properties and Methods of Purification. 4th Edition, John Wiley & Sons, New York, 1986.

[130] Schaeffer, W.D., Polley, M.H., Smith, W.R. The Nature of Carbon Black Surfaces as Revealed by Adsorption Studies. J. of Phys. Colloids Chem. Vol. 54, p227, 1950.

[131] Avgul, N.N. and Kiselev, A.V. Physical Adsorption of Gases and Vapors on Graphitized Carbon Blacks. Chemistry and Physics of Carbon Vol. 6, Edited by Philip, L. and Walker, Jr., Marcel Dekker, Inc., New York, 1970.

[132] McClellan, A.L. and Harnsberger, H.F. Cross-sectional Areas of Molecules Adsorbed on Solid Surfaces. J. of Colloid. and Interface Sci. Vol. 23, p577, 1967.

[133] Lyman, W.J., Reehl, W.F., and Rosenblatt, D.H. Handbook of Chemical Property Estimation Methods. American Chemical Society, Washington, DC, 1990.

[134] Zhang, Y. Emissions and Combustion of Fatty Acid Esters of Soybean Oil in a Diesel Engine. M.S. Thesis, Iowa State University, 1994.

[135] Jiang, Q. Prediction of Diesel Engine Particulate Emission during Transient Cycles. Ph. D. Dissertation, Iowa State University, 1991.

[136] Mayer, W.J., Lechman, D.C., and Hilden, D.L. The Contribution of Engine Oil to Diesel Exhaust Particulate Emissions. SAE paper 800256, 1980.

[137] Treybal, R.E. Mass-Transfer Operations. McGraw Hill Book Company, New, York, 1968.

ACKNOWLEDGMENTS

There have been many people who greatly assisted me through my graduate work. I would like to especially thank Dr. Jon H. Van Gerpen for all his help, guidance, and encouragement during my research. I would also like to thank the other members of my committee, Dr. Howard N. Shapiro, Dr. Gerald M. Colver, Dr. Stephen J. Marley, and Dr. Earl G. Hammond.

A very special thanks also goes to James Dautremont for his technical support and assistance.

I gratefully appreciate the friendship and support of my office colleagues Seref Soylu, Abdul Monyem, Mustafa Canakci, and Mustafa Ertunc during my research.

I would lastly like to thank my wife Haiyan and my lovely son Franklin for all of their love and support that I received during my graduate work.